Preferred Degradation of the Cell Division Protein FtsZ by ADEP-activated ClpP Protease and its use in understanding Divisome Progression

Dissertation

der Mathematisch-Naturwissenschaftlichen Fakultät

der Eberhard Karls Universität Tübingen

zur Erlangung des Grades eines

Doktors der Naturwissenschaften

(Dr. rer. nat.)

vorgelegt von

Nadine Silber

aus Stuttgart Bad Cannstatt

Tübingen

2022

Gedruckt mit Genehmigung der Mathematisch-Naturwissenschaftlichen Fakultät der Eberhard Karls Universität Tübingen.

Tag der mündlichen Qualifikation:	01.08.2022
Dekan:	Prof. Dr. Thilo Stehle
1. Berichterstatter/-in:	Dr. Peter Sass
2. Berichterstatter/-in:	Prof. Dr. Friedrich Götz

Table of contents

Abbreviations

µg	microgram
µM	micromolar
AMR	antimicrobial resistance
Å	angstrom
ATP	adenosine triphosphate
approx.	approximately
C terminus	carboxy terminus
C-terminal	carboxy-terminal
CTD	carboxy terminal domain
CTL	carboxy terminal linker
CTT	carboxy terminal tail
CTV	carboxy terminal variable region
CFU	colony forming unit
DNA	deoxyribonucleic acid
DEAE-dextran	diethylaminoethyl-dextran
DMSO	dimethyl sulfoxide
DTT	dithiothreitol
e.g.	for example (lat.: *exempli gratia*)
Fig.	figure
Fig. S	supplementery figure
FRAP	fluorescence recovery after photobleaching
FITC-casein	fluorescein isothiocyanate-casein
GDP	guanosine-5'-diphosphate
GTP	guanosine-5'-triphosphate
GTPγS	guanosine-5'-[gamma-thio]triphosphate
eGFP	enhanced green fluorescent protein
h	hour
HCl	hydrochloric acid
His	histidine
IDSA	Infectious Disease Society of America
i.e.	that is to say (lat.: id est)
KCl	potassium chloride
K	potassium
Mg	magnesium
$MgCl_2$	magnesium chloride

MIC	minimal inhibitory concentration
min	minute
ml	milliliter
mM	millimolar
Movie S	supplementery movie
MRSA	methicillin-resistant *Staphylococcus aureus*
nm	nanometer
N terminus	amino terminus
N-terminal	amino-terminal
NTD	amino-terminal domain
NTP	amino-terminal peptide
PDB	protein data bank
PONR	point of no return
PASTA	penicillin-binding protein and serine threonine kinase associated
R-state	relaxed state
sec	second
SEDS	shape, elongation, division and sporulation
Suc-LY-AMC	N-succinyl-Leu-Tyr-7-amino-4-methylcoumarin
SDS-Page	sodium dodecyl sulphate–polyacrylamide gel electrophoresis
Tris	tris(hydroxymethyl)aminomethan
T-state	tensed state
VRE	vancomycin-resistant enterococci
WHO	World Health Organization

Zusammenfassung

Die Zellteilung ist ein lebenswichtiger Prozess und in den meisten Bakterien steht hierbei das essenzielle Zellteilungsprotein FtsZ im Mittelpunkt des Geschehens. FtsZ ist ein GTP-hydrolysierendes Protein, das Nukleotid-abhängig einzelsträngige Polymere bildet, die sich wiederum über laterale Interaktionen bündeln und schließlich den sogenannten Z-Ring an der zukünftigen Zellteilungsebene aufbauen. Hier dient der Z-Ring als Gerüst für weitere Proteine, die zusammen mit FtsZ das sogenannte Divisom bilden. Während der letzten Jahre wurde die bakterielle Zellteilung verstärkt untersucht, da diese als vielversprechendes Angriffsziel für neue Antibiotika gilt. In diesem Zusammenhang zeigte sich, dass Acyldepsipeptid-Antibiotika (ADEPs) einen schnellen proteolytischen Abbau von zellulärem FtsZ in Bakterien verursachen. Hierbei interagiert ADEP jedoch nicht direkt mit FtsZ, sondern bindet und aktiviert die bakterielle ClpP Peptidase, was schließlich zum unkontrollierten Abbau von naszierenden Peptiden am Ribosom führt und interessanterweise auch zum Abbau von FtsZ. FtsZ ist bisher das erste und einzige gefaltete bakterielle Protein, dessen Abbau durch ADEP-aktiviertes ClpP (ADEP-ClpP) sowohl *in vitro* als auch *in vivo* bestätigt wurde. Die vorliegende Arbeit untersucht daher die Frage, weshalb FtsZ ein präferiertes Zielsubstrat für den Abbau durch ADEP-ClpP darstellt. Betrachtet man die Struktur von FtsZ, zeigt sich, dass es sich um ein insgesamt globuläres Protein handelt, welches einen flexiblen, unstrukturierten C-Terminus trägt, der für die Interaktion mit anderen Zellteilungsproteinen wichtig ist. In diesem Kontext würde der C-Terminus also eine sehr vulnerable Zielstruktur für den Abbau durch ADEP-ClpP darstellen. Es zeigte sich jedoch, dass der C-Terminus nicht als präferierter Angriffspunkt für ADEP-ClpP dient, sondern der kurze N-Terminus von FtsZ die präferierte Zielstruktur darstellt und außerdem, dass ADEP-ClpP die N-terminale Domäne von FtsZ entfaltet. Dies stellt eine Funktion von ClpP dar, die unter natürlichen Bedingungen zwingend auf assoziierte Chaperonen angewiesen ist, die Substrate ATP-abhängig entfaltet und in die proteolytische ClpP-Kammer einschleusen. Es zeigte sich hierbei, dass die Hydrophobizität des N-Terminus wichtig für die Entfaltung von FtsZ durch ADEP-ClpP ist. Vermutlich basiert die Entfaltung auf hydrophoben Wechselwirkungen zwischen dem hydrophoben N-Terminus und den ebenfalls hydrophoben Regionen am Rand der Eintrittspore der ClpP-Kammer. Die Entfaltung und der Abbau von FtsZ wurden interessanterweise durch Bindung von GTP bzw. GTPγS (einem nicht hydrolysierbarem GTP-Derivat, das die Polymerisation von FtsZ inhibiert) verhindert. Diese Nukleotid-basierte Stabilisierung der N-terminalen Domäne lieferte neue Einblicke bezüglich der Stabilität von FtsZ. So konnten wir zeigen, dass die Nukleotidbindung die Stabilität von FtsZ erhöht, wodurch der N-terminale Abbau durch ADEP-ClpP verhindert wurde. Weiterführende Untersuchungen des Abbaus bei erhöhten Konzentrationen von ADEP und ClpP identifizierten den C-Terminus von FtsZ als einen zusätzlichen Angriffspunkt. Dies deutet auf

ein erweitertes Zielspektrum des ADEP-ClpP Komplexes unter diesen Bedingungen hin. Somit liefern diese Ergebnisse die molekulare Erklärung zu vorausgehenden Ganzzellstudien, in denen beobachtet wurde, dass stäbchenförmige *Bacillus subtilis* Zellen, in Abhängigkeit der ADEP Konzentration, unterschiedliche Phänotypen ausbilden. Bei niedrigen Konzentrationen von ADEP wachsen die Zellen zu extrem langen Filamenten heran, was deutlich auf eine Inhibierung der Zellteilung hinweist, wohingegen die Biomasseproduktion und andere zelluläre Prozesse weitestgehend unbeeinflusst bleiben. Unter diesen Bedingungen ist vermutlich der präferierte Abbau von FtsZ für die Ausbildung des charakteristischen Phänotyps verantwortlich. Bei hohen Konzentrationen von ADEP bleibt das filamentöse Wachstum hingegen aus und die Zellen zeigen eine veränderte, unregelmäßige Zellform, was auf schwerwiegendere Zellschädigungen hindeutet und nicht nur durch einen präferierten Abbau von FtsZ zu erklären ist. Unter diesen Bedingungen ist das Zielspektrum von ADEP-ClpP offenbar erweitert und zusätzliche Proteine, neben FtsZ, werden in der Zelle abgebaut.

Die hier beschriebenen verschiedenen Phänotypen deuten auf den schnellen Abbau des zytoplasmatischen FtsZ-Pools bei niedrigen ADEP Konzentrationen hin. Auf dieser Grundlage zogen wir in Erwägung, ADEP als Instrument zur Untersuchung der Zellteilung zu verwenden, um die Ausbildung und das Fortschreiten des Z-Rings und des Divisoms zu untersuchen. Der Z-Ring ist eine sehr dynamische Struktur, welche die Zellteilungsebene umläuft und den Teilungsprozess vorantreibt. Diese Dynamik basiert auf dem ständigen Einbau von FtsZ an einem Ende des Polymers, während vom anderen Ende FtsZ-Einheiten dissoziieren. Dadurch entsteht eine Abhängigkeit der FtsZ-Dynamik vom zytoplasmatischen FtsZ-Pool. Durch Zeitraffer-Fluoreszenzmikroskopie beobachteten wir, dass Z-Ringe im Frühstadium zerfielen, sobald der zelluläre FtsZ-Pool durch ADEP-ClpP deutlich reduziert war. Im Gegensatz dazu blieben Z-Ringe im Spätstadium unbeeinflusst und führten zur Vollendung der Zellteilung, sobald das späte Zellteilungsprotein PBP2b am Septum lokalisierte. Dieses Ergebnis deutet auf ein Zwei-Stufen-Modell hin: (i) in der frühen Phase des Z-Ring-Aufbaus ist der zytoplasmatische FtsZ-Pool und damit die Dynamik der Z-Ringe von wesentlicher Bedeutung für den Fortlauf der Zellteilung. (ii) In der späten Phase wird der zytoplasmatische FtsZ-Pool entbehrlich und das Fortschreiten des Divisoms wird vermutlich durch andere Proteine wie Peptidoglykan-Synthasen gesteuert und vorangetrieben.

Zusammenfassend trägt diese Arbeit zum besseren Verständnis des Wirkmechanismus von ADEP bei und charakterisiert darüber hinaus strukturelle und physikochemischen Eigenschaften von FtsZ, die das zentrale Zellteilungsprotein zu einem präferierten Substrat für den Abbau durch ADEP-ClpP machen. Des Weiteren validiert diese Arbeit ADEP als molekulares Werkzeug zur Untersuchung der bakteriellen Zellteilung und wir lieferten dadurch neue Einblicke in die grundlegenden Prinzipien während dieses Prozesses.

Summary

Cell division is a vital process for bacteria and therefore requires the precise coordination in terms of timing and spacing. FtsZ polymerizes in a nucleotide-dependent manner into protofilaments that form higher ordered structures via lateral interactions, thereby assembling the so called Z-ring at the future division site. Here, the Z-ring serves as a scaffold for other cell division proteins to adhere to, together assembling the so-called divisome. During the past years, cell division has gained considerable attention as it represents a promising target for antibiotic interference. Since FtsZ is highly conserved among bacteria and acts as a central player during cell division, the protein emerged to be of particular interest. In this context, cellular FtsZ is rapidly depleted when cells were treated with acyldepsipeptide antibiotics (ADEP). Importantly, ADEP does not directly bind to FtsZ but displays an unusual mechanism. ADEPs bind to the bacterial ClpP peptidase thereby inhibiting all natural functions of ClpP and furthermore activating it for the degradation of nascent peptides at the ribosome and, interestingly, for the untimely proteolysis of FtsZ. To date, FtsZ is the first and only folded bacterial protein that was shown to be degraded by ADEP-activated ClpP (ADEP-ClpP) *in vitro* as well as *in vivo,* whereas other tested proteins resist degradation.

In this thesis, we unraveled the structural and physicochemical features of FtsZ that make it a preferred and especially vulnerable target for ADEP-ClpP. A closer look at the structure of FtsZ shows that it is a globular protein with a disordered C terminus that protrudes from the core domain and is important for the interaction with other cell division proteins. Therefore, the C terminus of FtsZ would represent a very likely target structure for the attack by ADEP-ClpP. Surprisingly, we showed that the flexible C terminus of FtsZ is not the preferred target site, but revealed that the short N-terminus of FtsZ is preferably targeted by ADEP-ClpP. Furthermore, we showed that N-terminal attack of FtsZ by ADEP-ClpP leads to N-terminal unfolding of the protein. To date, ClpP has never been shown to degrade a folded protein without the help of a cognate energy-driven ATPase. In this context, it emerged that the hydrophobicity of the N terminus is decisive for the degradation of FtsZ and we suggest that N-terminal unfolding of FtsZ is driven by means of hydrophobic interactions between the hydrophobic N terminus of FtsZ and the hydrophobic rim of the entrance pore of the ClpP barrel. Furthermore, we demonstrated that unfolding and degradation of FtsZ is prevented upon binding of either GTP or GTPγS (the latter represents a non-hydrolyzable derivative of GTP that inhibits FtsZ polymerization). These results imply that nucleotide-devoid FtsZ may be characterized by a rather loose protein fold, and that ADEP-ClpP is therefore capable of N-terminally unfolding and degrading FtsZ. Further investigations of the degradation process at elevated concentrations of ADEP/ClpP revealed that the C terminus of FtsZ becomes an additional

target, suggesting a broadening of the target spectrum of ADEP-ClpP at increased concentrations.

Therefore, our results elaborate the molecular basis for the earlier observed distinct phenotypes of *Bacillus subtilis* cells that were treated with different concentrations of ADEP. In this context, at low inhibitory concentrations of ADEP, cells proceed biomass production and other cellular processes, while cell division is abrogated due to the degradation of FtsZ. This results in a filamentous growth of rod-shaped *B. subtilis* cells. We suggest that under these conditions, ADEP-ClpP preferably targets and degrades FtsZ due to the here described characteristics of FtsZ that make this protein an especially attractive and vulnerable substrate for ADEP-ClpP. In contrast, when cells are treated with high concentrations of ADEP, biomass production ceases and cells display an uneven cell morphology indicating that severe additional damage has occurred to the cells. Hence, we propose that under these conditions, the target spectrum of ADEP-ClpP is broadened and other putative protein targets are degraded in addition to FtsZ. The different phenotypes described here indicated that at low ADEP concentrations the cytoplasmic FtsZ pool is rapidly depleted. This allowed us to further use ADEP as a tool to study the molecular principles of Z-ring assembly and progression. The Z-ring represents a highly dynamic structure that treadmills around the division plane, thereby guiding peptidoglycan synthesis in order to build the septal cell wall. The dynamic treadmilling motion of FtsZ filaments results from the constant incorporation of FtsZ monomers at one end, while depolymerization occurs from the opposite end. Hence, FtsZ dynamics strictly rely on a cytoplasmic FtsZ pool that ensures the constant supply with new monomers. By employing time-lapse fluorescence microscopy we investigated the fate of different stages of the Z-ring upon the depletion of the cytoplasmic FtsZ pool at low inhibitory concentrations of ADEP. We observed that the initiation of Z-ring formation was inhibited and that established early-stage Z-rings disintegrated under these conditions. However, Z-rings that had already entered a later stage finalized septum formation and cell division. Therefore, a two-step model of Z-ring assembly and progression is suggested: (i) During the early stages of cell division, the cytoplasmic FtsZ pool is required for Z-ring assembly, and Z-ring dynamics are important to drive the assembly of the early divisome. However, (ii) at the later stage, Z-ring dynamics are less important and the divisome finalizes cell division independent of the depletion of the cytoplasmic FtsZ pool.

In summary, this work contributes to a better understanding of the mechanism of action of ADEP and characterizes the structural and physicochemical features of FtsZ that make the central cell division protein a preferred target for the degradation by ADEP-ClpP. Furthermore, this work validates ADEP as a molecular tool to study bacterial cell division, and we provided new insights into the principles of cell division.

List of publications and personal contributions

Publication 1:

Nadine Silber[1], Stefan Pan[1], Sina Schäkermann[2], Christian Mayer[1], Heike Brötz-Oesterhelt[#,1] , Peter Sass[#,1,3]. 2020. Cell division protein FtsZ is unfolded for N-terminal degradation by antibiotic-activated ClpP. ***mBio***, Vol. 11, No. 3, DOI: 10.1128/mBio.01006-20

The initial study concept was conceived by Peter Sass and Heike Brötz-Oesterhelt. I was further involved in the conception of the project, and I designed experiments together with Peter Sass. Plasmids that were used in this study were mainly generated by me and by Lutz Alfter and Janette Alford during their internship under my guidance. Exceptions were plasmids pETftsZbs$_{11\text{-}382,}$ pETftsZbs$_{L272E}$, pETstrep-ftsZ-his$_{6,}$ pETclpPsa and pETclpPsa that were generated by Peter Sass, and plasmid pNP90 that was provided by Leendert Hamoen (University of Amsterdam, Netherlands). MS analysis was performed by Peter Sass and Sina Schäkermann. Western Blot analysis with *B. subtilis* strains 2014 and 2020 were performed by Peter Sass. All other experiments including protein degradation assays, GTPase activity tests, Western Blot analysis, CD spectrometry and N-terminal Edman sequencing were conducted by me, and I purified all proteins that were used for this study. Initial data evaluation and interpretation was performed by me and Peter Sass, and data was further discussed with all authors. Stefan Pan particularly supported evaluation of the densitometry data. Peter Sass and I designed and prepared all figures and tables in close cooperation. I visualized all crystal structures of the FtsZ protein with exception of figure 7. Furthermore, I generated all graphs under the guidance of Peter Sass. Peter Sass drafted the manuscript with my assistance regarding the material and methods part. As all authors I was involved in editing the manuscript. Furthermore, I conducted all experiments that were requested during the revision process and finalized the manuscript together with Peter Sass.

Publication 2:

Nadine Silber *,[1], Cruz L Matos de Opitz*,[1], Christian Mayer*,[1], Peter Sass [1,4]. 2020. Cell division protein FtsZ: from structure and mechanism to antibiotic target. **Future Microbiology**, Vol. 15, No. 9, DOI: 10.2217/fmb-2019-0348

The review was drafted in shared parts by Cruz L. Matos de Opitz, Christian Mayer and me. In particular, I drafted the first part of the manuscript regarding structure and abundance of FtsZ, its functional regions as well as the section dealing with Z-ring assembly and force generation. After consultation with Peter Sass I prepared figure 1 and the corresponding figure legend. Peter Sass outlined, edited and finalized the manuscript.

Publication 3

Nadine Silber*,[1], Christian Mayer*,[1], Cruz L Matos de Opitz[1], Peter Sass[1,3]. 2021. Progression of the late-stage divisome is unaffected by the depletion of the cytoplasmic FtsZ pool. ***Communications Biology,*** Vol. 4, No. 270, Doi: 10.1038/s42003-021-01789-9.

The initial study concept and experimental design was conceived by Peter Sass, Christian Mayer and me. Microscopy experiments were jointly conducted by Christian Mayer and me with support by Cruz L. Matos de Opitz under the guidance of Peter Sass. I performed the FtsZ degradation assay depicted in figure 1b. Data was discussed and interpreted by all authors. Furthermore, figures 2 and 3 as well as supplementary videos S1, S2 and S3 were jointly prepared by Christian Mayer and me. Data evaluation for figure 3b was mainly conducted by me with support from Christian Mayer and Cruz L. Matos de Opitz. Figure 2 and 3 were arranged and finalized by Peter Sass and me. I also prepared supplementary video S4 in assistance with Cruz L Matos de Opitz. All authors edited and finalized the manuscript.

[1] Department of Microbial Bioactive Compounds, Interfaculty Institute of Microbiology & Infection Medicine, University of Tübingen, Auf der Morgenstelle 28, Tübingen 72076, Germany
[2] Applied Microbiology, Ruhr University Bochum, Bochum, Germany
[3] Cluster of Excellence-Controlling Microbes to Fight Infections, Tübingen, Germany
[4] German Center for Infection Research (DZIF), partner site Tübingen, Tübingen 72076, Germany
* shared first authorship
[#] shared senior authorship

1 Introduction

1.1 Bacterial cell growth and division

“The dream of every cell is to become two cells.” – This quotation originates from the French biologist François Jacob and poetically describes cell division as a fundamental process for all living organisms. Bacteria have evolved various strategies to make their dream come true: apart from budding and multiple offspring formation, the most prevalent and best studied propagation mechanism is binary fission (Angert, 2005). The process of binary fission relies on the division of a mother cell into two identical daughter cells. In the context of cell division, the bacterial cell cycle starts with the birth of a cell, followed by the replication of the genetic material, and ends after septum formation with the separation of the two progeny (Cooper et al., 1968; Wang et al., 2009). Rod-shaped bacteria such as *Bacillus subtilis* or *Escherichia coli,* which reproduce by binary fission, grow until they approximately reach double their length before dividing in the middle of the cell (Donachie, 1968; Donachie et al., 1976). During cytokinesis, processes such as septum formation, cell separation, and the duplication of the genetic material occur in an astonishingly precise manner in terms of timing and spacing. This requires a range of cellular events conducted by multi-protein machineries. In the context of cell growth, supramolecular complexes termed as elongasome and divisome accomplish the integration of newly synthesized peptidoglycan into the lateral and the septal cell wall, respectively.

The elongasome is only found in rod-shaped bacteria and is controlled by the actin-homologous MreB proteins, which are involved in the control of cell morphogenesis. These proteins were originally identified by mutations that resulted in the loss of cell shape (Normark, 1969; Wachi et al., 1987, 1989). *B. subtilis* has three MreB isoforms that colocalize (Carballido-López et al., 2006; Kawai et al., 2009 a): MreB (in an operon together with MreC and MreD), Mbl (MreB-like) (Abhayawardhane et al., 1995) and MreBH (MreB-homolog). During cell elongation, MreB proteins form dynamic helical structures (Jones et al., 2001; Defeu Soufo et al., 2004; Figge et al., 2004) or at least dynamic patches that move circumferentially around the cell (Garner et al., 2011; Julia et al., 2011), thereby coordinating other proteins of the elongasome. For example, MreBH interacts with LytE, an autolysin involved in the cell wall metabolism through the hydrolysis of peptidoglycan, and supports its correct localization (Carballido-López et al., 2006). MreB and Mbl, in contrast, are involved in the organization of the synthesis of peptidoglycan at the lateral cell wall by interacting with cell wall synthesizing proteins (Kawai et al., 2009 a). In this regard, potential interaction partners of MreB (Errington et al., 2017) include different Penicillin-binding proteins (PBPs) (Kawai et al., 2009 b) as well as RodA (Julia et al., 2011), the latter belonging to the SEDS family of

proteins that are involved in shape, elongation, division and sporulation (Henriques et al., 1998; Meeske et al., 2016). In *B. subtilis*, RodA and PBP2a are thought to act jointly in a subcomplex polymerizing the lateral cell wall (Cho et al., 2016; Meeske et al., 2016; Emami et al., 2017) by incorporating the peptidoglycan precursor lipid II into the existing cell wall. In addition to the synthesis of lateral cell wall by the elongasome, the septal cell wall is produced by the divisome which eventually leads to the division of one cell into two daughter cells.

1.2 Division site selection and divisome assembly

The divisome consists of a diverse set of proteins (Silber et al., 2020 a) and in most bacteria its assembly at the prospective site of cell division is initiated by the major cell division protein FtsZ. To do so, FtsZ polymerizes into filaments in which monomers are arranged in a head-to-tail manner. These filaments establish higher ordered structures via lateral interactions, thereby building the so-called Z-ring at the future division site of the bacterial cell. As the Z-ring serves as a scaffold for other cell division proteins to adhere to, FtsZ localization and accurate Z-ring assembly needs to be tightly controlled. In *B. subtilis* division site selection is maintained by two negatively acting regulatory systems: The nucleoid occlusion (Noc) system and the Min system. The Noc system depends on the Noc protein (Wu et al., 2004), a DNA binding protein that prevents divisome assembly in close vicinity to the nucleoid. Recent data revealed Noc to function as a barrier that does not directly interact with FtsZ to prevent its polymerization, but rather prevents the migration of FtsZ filaments away from the division site (Yu et al., 2021). Mid-cell localization of the Z-ring is furthermore assured by the Min system (Bramkamp et al., 2008), which prevents the localization of FtsZ and thus divisome assembly at the cell poles of the bacterial cell (Blasios et al., 2013). The Min system includes the cytoplasmic protein MinC and the membrane-associated protein MinD, which together form a complex at the cell poles. The localization of MinCD depends on DivVIA and MinJ (Bernhardt et al., 2005; Patrick et al., 2008). In this context, MinJ is responsible to recruit MinCD to DivVIA, which was shown to preferentially localize to curved membranes (Lenarcic et al., 2009). Within this complex, MinC is regarded to function as the effector of the system, inhibiting the polymerization of FtsZ by direct protein-protein interaction (Hu et al., 1999; Scheffers, 2008). Upon precise spatio-temporal Z-ring assembly at mid-cell, additional cell division proteins are recruited in a time-dependent hierarchical order. In *B. subtilis,* assembly of the divisome was shown to occur mostly in two steps. During the first step, the major cell division protein FtsZ and other “early divisomal proteins” localize to mid-cell after approx. 20% of a full cell cycle has elapsed. With a slight delay, the “late divisomal proteins” responsible for septal cell wall synthesis arrive at mid-cell after 45-60% of a full cell cycle (Gamba et al., 2009) (Fig. 1).

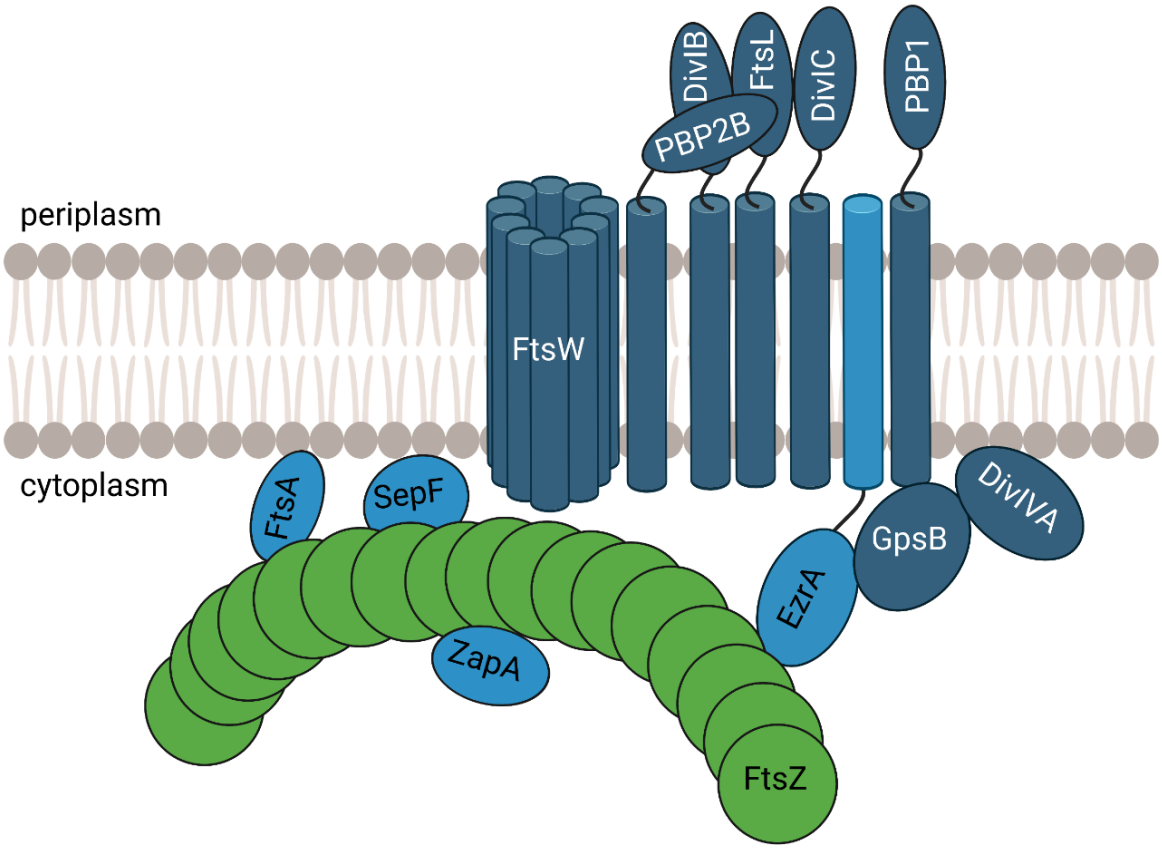

Fig. 1: Schematic representation of the core components of the *B. subtilis* divisome including "early" and "late" cell division proteins. In *B. subtilis*, assembly of the core divisome follows two steps: During the first step, the early cell division proteins including FtsZ (green), FtsA, EzrA, ZapA, and SepF (all in light blue) localize at mid-cell on the inner side of the cell membrane. FtsZ initiates cell division by polymerizing into a ring-like structure that marks the future division plane and serves as a scaffold for other cell division proteins to adhere to. The FtsZ-ring is indicated by one protofilament which consists of single FtsZ monomers. Early cell division proteins arrive at mid-cell with a time delay of 20% of a full cell cycle that starts with a newly born cell and ends with the finalization of septum formation. The second step during divisome assembly comprises mid-cell localization of late cell division proteins including GpsB, FtsL, DivIB, FtsW, PBP2b, and DivIVA (all in dark blue) that arrive at the divisome with a time delay of around 60% of the cell cycle (Gamba et al., 2009). The figure was adapted from Gamba et al., 2009 and modified using BioRender software.

In addition to FtsZ, early divisomal proteins in *B. subtilis* include amongst others FtsA, EzrA, ZapA, and SepF (Gamba et al., 2009), which all assemble at the inner side of the cytoplasmic membrane (Fig. 1). FtsA is a membrane targeting protein that arrives at mid-cell shortly after FtsZ and anchors the Z-ring to the membrane by interaction with the C terminus of FtsZ (Wang et al., 1997 b; Jensen et al., 2005). The membrane anchoring function of FtsA is supported by SepF (Hamoen et al., 2006) as the overexpression of SepF alleviated cell division defects in

an *ftsA* deletion strain (Ishikawa et al., 2006). Furthermore, SepF has been shown to promote FtsZ protofilament formation and filament bundling *in vitro* by directly interacting with the C terminus of FtsZ (Singh et al., 2008; Gündoğdu et al., 2011; Król et al., 2012), suggesting a dual function of SepF. Polymerization and bundling of FtsZ is further promoted by ZapA, a non-essential but widely conserved Z-ring-associated protein (Gueiros-Filho et al., 2002). In contrast to SepF and ZapA, EzrA functions as a negative modulator, which prevents the polymerization of FtsZ by direct interaction with its C terminus (Haeusser et al., 2004, 2007; Singh et al., 2007), thus regulating Z-ring formation and contributing to its dynamics. For example, EzrA is not only found at mid-cell, but is also shown to localize to the cell poles during exponential growth, where it prevents extra Z-ring formation (Levin et al., 1999; Haeusser et al., 2004). Upon the arrival of early divisomal proteins at mid-cell, the late divisomal proteins, which are mostly involved in peptidoglycan synthesis, follow in a delayed step.

The late divisomal proteins include GpsB, FtsL, DivIB, DivIC, PBP2b, FtsW and DivIVA (Gamba et al., 2009). As these late-stage proteins, with the exception of GpsB and DivIVA, are membrane spanning proteins with their major domains on the outside of the cytoplasmic membrane, they are together considered as the “outer ring” of the divisome (Harry et al., 1993; Katis et al., 1997; Sievers et al., 2000). Bacterial two-hybrid analyses revealed the interaction of FtsL with PBP2b, DivIB, and DivIC (Daniel et al., 1998, 2006). As a consequence, the assembly of the late-stage divisomal proteins PBP2b, FtsL, DivIC, DivIB and FtsW is interdependent and happens in a non-sequential manner, meaning that the depletion of any of these proteins prevents the assembly of all others (Daniel et al., 1998, 2000 a; Sievers et al., 2000; Errington et al., 2003; Gamba et al., 2016). For example, deletion of *pbp2b,* which encodes for a protein involved in cross-linking of peptidoglycan strands, leads to elongation and eventually lysis of *B. subtilis* cells (Daniel et al., 2000 b). Synthesis of peptidoglycan to build the septal cell wall is furthermore supported by FtsW, which belongs to the SEDS family of proteins (Gamba et al., 2016; Meeske et al., 2016). FtsW is described to contain 10 transmembrane segments (Gérard et al., 2002) and was recently suggested to be a peptidoglycan synthase in the Gram-positive bacteria *Staphylococcus aureus* and *Streptococcus thermophiles.* Here, FtsW together with its cognate class B PBP were shown to be involved in polymerizing the septal cell wall (Taguchi et al., 2019). In *E. coli*, FtsW is furthermore described to act as a flippase that transports the peptidoglycan precursor lipid II from the cytosol across the membrane (Mohammadi et al., 2011), where it is then incorporated into the growing cell wall. The late-stage divisomal proteins GpsB and DivIVA are cytoplasmic proteins and therefore not assigned to the outer ring of the divisome. DivIVA is a late divisomal protein localizing to mid-cell (Gamba et al., 2009) where it acts to prevent further Z-ring

formation by retaining MinCD at the new cell poles (Marston et al., 1999). To do so, DivIVA specifically binds to curved membranes and thus localizes to the cell poles (Lenarcic et al., 2009). Here, DivIVA together with MinCD forms an oligomeric network structure, thereby preventing the polymerization of FtsZ in the pole region (Marston et al., 1999; Stahlberg et al., 2004; Scheffers, 2008; Blasios et al., 2013). GpsB is involved in cell elongation as well as cell division interacting with both, MreC and EzrA (Claessen et al., 2008). During the cell cycle, GpsB is furthermore involved in shuttling PBP1 between the lateral and the septal cell wall (Ishino et al., 1980; Pedersen et al., 1999; Scheffers et al., 2004; Claessen et al., 2008). In this context, PBP2 (Den Blaauwen et al., 2003; van der Ploeg et al., 2013) and PBP5 (Potluri et al., 2010) in *E. coli*, were also found to participate in both, the divisome and the elongasome. The contribution to both supramolecular complexes indicates a common evolutionary past, and indeed, it is assumed that the elongasome has evolved from the divisome (Szwedziak et al., 2013).

Taken together, precise localization and assembly of the divisome is a fundamental process that is implemented by the interplay of a diverse set of proteins. Within the divisome, FtsZ is the major player and pacemaker protein. Its assembly into the Z-ring initiates cell division by marking the future division site and by serving as the scaffold for other cell division proteins. Importantly, the Z-ring does not represent a rigid scaffold, but rather a highly dynamic structure that is assumed to guide the peptidoglycan synthesizing enzymes around the division plane, thereby being considered as the driving force during cell division (Bisson-Filho et al., 2017). Understanding the dynamic nature of the Z-ring requires a detailed functional and structural insight into the major cell division protein FtsZ, which is provided in the following sections.

1.3 Structure and function of FtsZ

Filamentation temperature sensitive mutant Z (FtsZ) was discovered in 1980 (Lutkenhaus et al., 1980) by screening mutants of *E. coli* that grew into filaments at a non-permissive temperature of 42 °C (van de Putte et al., 1964; Hirota et al., 1968; Walker et al., 1975). Later on, FtsZ was described as an essential cell division protein in most bacteria. FtsZ is highly conserved in the domains of Bacteria and Archaea with only few exceptions, such as the phylum of Chlamydiae that for example completely lack the *ftsZ* gene (Stephens et al., 1998; Vaughan et al., 2004). FtsZ is the prokaryotic homolog of tubulin (Erickson, 1997) and together the two proteins were categorized as a distinct family of guanosine-triphosphate (GTP) - hydrolyzing enzymes, sharing a very similar structure. Both proteins consist of two folding domains, namely the N-terminal domain (NTD) and the C-terminal domain (CTD) that are connected via a central helix (Fig. 2A). The NTD harbors the nucleotide binding site with the

highly conserved and glycine-rich tubulin signature motif, characterized by the sequence pattern GGGTG[S/T]G (Nogales et al., 1998). The CTD contains an elongated flexible C terminus that protrudes the globular core domain of FtsZ and is largely disordered, therefore being not resolved in crystal structures. Nevertheless, the extreme C terminus of FtsZ has an important function in the interaction with a variety of other proteins and thus serves as a central hub (Buske et al., 2012; Pazos et al., 2013).

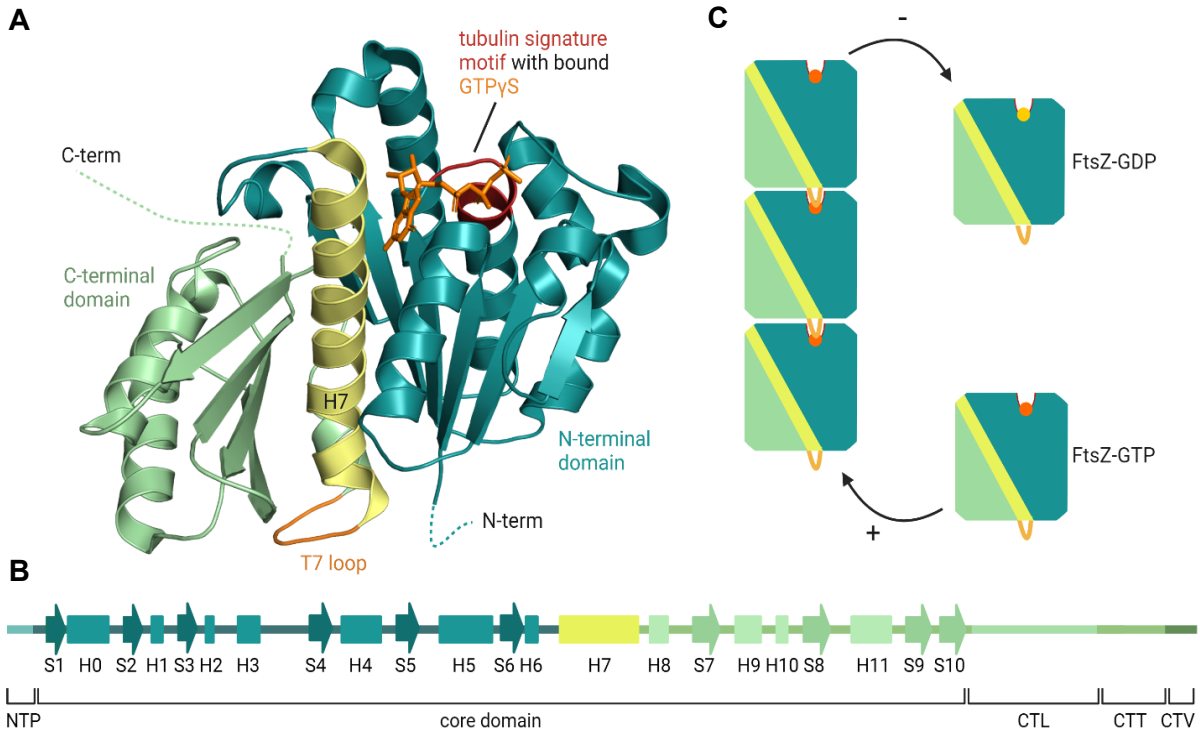

Fig. 2: Structure and assembly of *B. subtilis* FtsZ. (A) Crystal structure of *B. subtilis* FtsZ (BsFtsZ; residues 12-316, PDB: 2RHO), with bound GTPγS (in orange) which is a non-hydrolyzable GTP-analog (Raymond et al., 2009). The N-terminal domain is colored in cyan, the C-terminal domain is colored in light green. The two domains are connected via the central helix H7 (in yellow). The termini are depicted as dotted lines as they are not solved in the crystal structure. The tubulin signature motif, which is located on loop T4, is marked in red. (B) Functional regions of FtsZ: the five functional regions of FtsZ are indicated by different colors in the secondary structure representation of the FtsZ protein. (NTP: N-terminal peptide; CTL: C-terminal linker; CTT: C-terminal tail; CTV: C-terminal variable region). Arrows that are labelled with S1-S10 represent β-sheets. Boxes that are labelled with H0-H11 represent α-helices. (C) Schematic model of the directed growth of FtsZ filaments. In particular, the T7 loop (orange) is exposed to the surrounding at the growing end of a filament, where new guanosine-triphosphate (GTP) -bound FtsZ monomers are added (GTP in orange; the growing end is indicated with the arrow and the plus). Two adjacent monomers form the active site for GTP hydrolysis at their interface. Depolymerization of guanosine-diphosphate (GDP) -bound FtsZ monomers (GDP in yellow; depolymerization indicated with the arrow and the minus) takes place at the opposite end of the filament. Constant growing and shrinking of FtsZ filaments result in the so-called “treadmilling” dynamic.

In general, FtsZ can be further divided into five distinct functional regions: The N-terminal peptide (NTP), the core domain, the disordered C-terminal highly variable linker (CTL), the C-terminal tail (CTT), and the C-terminal variable region (CTV) (Fig. 2B). Among the Firmicutes, the NTP has not been assigned any function so far and is only poorly conserved. The FtsZ core region, defined to start with a widely conserved isoleucine at position 14 in *B. subtilis* FtsZ (BsFtsZ) (Vaughan et al., 2004), is responsible for nucleotide binding and hydrolysis. In this context, binding of a nucleotide is conferred by loops T1-4 (of which loop T4 carries the tubulin signature motif), loop T5 and T6, and helix H7, all establishing contacts to GTP (Nogales et al., 1998). The hydrolysis of a bound nucleotide moreover relies on the T7 loop of another FtsZ monomer, which needs to be inserted into the nucleotide binding pocket, to complete the active site (de Boer et al., 1992; Scheffers et al., 2002). The extended flexible C terminus of FtsZ comprises the CTL that connects the FtsZ core with the CTT and the CTV regions. The CTL, also designated as a “spacer”, is a highly variable region regarding its length as well as its amino acid sequence. The CTL of BsFtsZ and FtsZ from *E. coli* (EcFtsZ) comprises 51 and 54 amino acids, respectively. In other organisms, however, it can be up to 330 amino acids long (Vaughan et al., 2004). The truncation of the CTL in BsFtsZ has severe effects on GTPase activity. In this regard, an FtsZ protein lacking the CTL region (FtsZΔCTL) shows decreased GTPase activity and is thus impaired in polymerization as well as filament bundling. This results in an elevated critical concentration that has to be exceeded for the polymerization of FtsZ (Buske et al., 2013). Interestingly, the exchange of the amino acid sequence of the CTL seems to be less critical, as the exchange with another CTL or the scrambling of the amino acid sequence had no effect on FtsZ polymerization behavior. Hence, functionality of FtsZ does not depend on a defined amino acid sequence of the CTL but on its length, which appears to be a critical feature for correct FtsZ functionality. In this context, the length of the CTL was suggested to be important to define a distinct distance of FtsZ to the membrane during its interaction with membrane anchoring proteins (Buske et al., 2013; Gardner et al., 2013). Furthermore, the CTL was recently shown to be responsible for keeping a defined distance between single FtsZ filaments, and changes in its length had an impact on inter-filament spacing. Keeping a defined distance between the filaments is thought to be important to prevent sticking of filaments to each other, thereby ensuring proper Z-ring dynamics (Huecas et al., 2017). The CTT together with the CTV is designated the “grappling hook peptide” (Buske et al., 2013), functioning as a central hub that interacts with various proteins associated with cell division. Divisomal proteins that have been shown to interact with the C-terminal region of FtsZ include amongst others EzrA (Levin et al., 1999; Singh et al., 2007), SepF (Król et al., 2012), FtsA (Wang et al., 1997 b; Ma et al., 1999), and ZapA (Gueiros-Filho et al., 2002). In this regard, the CTT is described to constitute as “landing pad” possessing two highly conserved residues (prolin and phenylalanine) that have been shown

to be important for the interaction with FtsA (Ma et al., 1999; Yan et al., 2000). In contrast, the CTV is a highly variable region that lacks conserved residues but has been shown to support lateral interactions between BsFtsZ filaments *in vitro*. Lateral interaction between filaments are here mediated through the positively charged CTV that allows for electrostatic interactions (Buske et al., 2012).

The here described features of the distinct regions, which either mediate the interaction with other proteins or contribute to the dynamic behavior of FtsZ, already give a hint on the pivotal role of FtsZ during cell division. FtsZ dynamics include the interaction between single FtsZ subunits at the longitudinal interface as well as the lateral interaction between polymerized filaments, thereby constituting the molecular basis for Z-ring assembly and initiation of cell division.

1.4 FtsZ dynamics – from filament formation to treadmilling Z-rings

FtsZ is a GTPase that self-assembles into protofilaments in a nucleotide-dependent manner (Mukherjee et al., 1998). Within this head-to-tail assembly of FtsZ subunits, the active site for GTP hydrolysis is formed at the interface of two adjacent monomers (Fig. 2C). In this regard, the upper subunit provides the T7 synergy loop that is inserted into the nucleotide binding site of the lower subunit (Scheffers et al., 2002). The addition of new GTP-bound FtsZ monomers to a growing filament occurs at the bottom site where the T7 loop is exposed to the surrounding. After GTP-hydrolysis, depolymerization of guanosine-diphosphate (GDP) -bound FtsZ subunits occurs at the opposite end of the filament (Du et al., 2018). The constant incorporation of new subunits at the growing end of a filament and the depolymerization of FtsZ subunits at the shrinking end results in a dynamic filament whose motion resembles a treadmilling-like mechanism. Interestingly, the crystal structure of FtsZ from *S. aureus* (SaFtsZ) was found to undergo a conformational transition from a closed monomeric to an opened oligomeric structure. More precisely, in the open structure of SaFtsZ, the angle between the CTD and the NTD is increased, thereby opening a gap between the two domains which is designated as the interdomain cleft. In contrast, the interdomain cleft was shown to be closed in crystal structures of monomeric SaFtsZ (Wagstaff et al., 2017).

The polymerization of FtsZ depends on a defined minimal concentration, which is termed as the critical concentration. Below this critical concentration, FtsZ polymers assemble barely, whereas above this concentration polymers are the dominant species in a reaction. For EcFtsZ and BsFtsZ the critical concentration for polymerization *in vitro* is around 1-2.5 µM depending on the buffer conditions (Mukherjee et al., 1998, 1999; Blasios et al., 2013). In the presence of GTP, FtsZ polymerizes into single-stranded, straight filaments, while incubation with GDP

results in shorter and curved filaments as well as mini-rings. The addition of crowding agents such as DEAE-dextran (diethylaminoethyl-dextran) support the assembly of higher ordered structures. In this context, GTP-bound FtsZ forms thick bundles and sheets of filaments *in vitro*, and GDP-bound FtsZ assembles into tubes (Lu et al., 2000). The assembly of such higher ordered structures is supported by lateral interactions between filaments mediated by the flexible C terminus of FtsZ (Huecas et al., 2008). The curvature of GDP-bound filaments relies on a nucleotide-dependent conformational switch of the FtsZ T3 loop. In GTP-bound filaments, the T3 loop adopts a tensed state (T-state), which is shifted into a relaxed state (R-state) upon GTP hydrolysis (Díaz et al., 2001; Li et al., 2013). The GDP-related form of FtsZ weakens longitudinal interactions between adjacent monomers and results in bending of the filament. With respect to cell division, bending of FtsZ filaments based on GTP hydrolysis is thought to exert an inward force on the membrane, thereby supporting membrane invagination (Li et al., 2013). Furthermore, hydrolysis of GTP to GDP leads to the destabilization of the FtsZ filament and facilitates the depolymerization at the shrinking end (Scheffers et al., 2000; Huecas et al., 2004).

To initiate cell division, dynamic filaments of FtsZ condense into the Z-ring at the future divison site. Based on the directed growth of the filaments, the Z-ring treadmills around the lateral axis of the cell (Fig. 3) (Bisson-Filho et al., 2017). Within a filament that polymerizes at steady-state, single FtsZ molecules have been shown to be stationary (Niu et al., 2008). As a consequence, the Z-ring is permanently rearranging itself with a half-time of 8-30 seconds (Stricker et al., 2002; Anderson et al., 2004). To ensure a constant supply of available FtsZ monomers, around 70% of cellular FtsZ is not incorporated into filaments, but is available as a cytoplasmic pool (Stricker et al., 2002).

The dynamic motion of FtsZ itself and its ability to assemble into ring-related structures is intrinsic and hence independent of modulatory proteins. In this regard, FtsZ attached to an artificial C-terminal membrane anchor assembled into contractile Z-rings in liposomes (Osawa et al., 2008, 2009). A recently published study showed related findings with fluorescently labelled FtsZ that assembled dynamic Z-ring precursors in a *sepF/zapA/ezrA*-depleted strain of *B. subtilis*. Nevertheless, these Z-ring precursors did not condense into a distinct and functional Z-ring. Thus, FtsZ modulators are crucial for the assembly of a functional Z-ring and its correct localization (Squyres et al., 2021). Of note, treadmilling of FtsZ has been suggested to drive PBP2b around the division plane and thus guides peptidoglycan synthesis at the septal cell wall in *B. subtilis* (Bisson-Filho et al., 2017). In their study, the authors investigated treadmilling dynamics by making use of the compound PC190723, which was earlier shown to interfere with FtsZ, thereby inhibiting cell division.

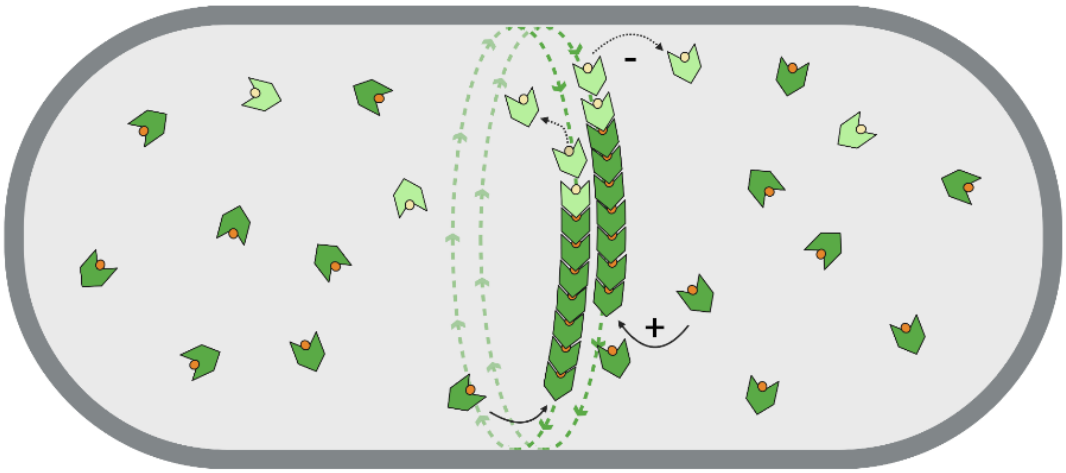

Fig. 3: FtsZ assembles into a dynamic, ring-like structure (Z-ring) at the future division site. The Z-ring (indicated as a green dotted line) is a highly dynamic structure that moves around the division plane and consists of FtsZ polymers interacting laterally. This directed, circulating motion around mid-cell is called treadmilling and relies on the addition of GTP-bound FtsZ-monomers (dark green; GTP in orange) at the growing (+) end of an FtsZ filament and the depolymerization of GDP-bound monomers (light green; GDP in yellow) at the opposite end (-) of the filament. Growing and shrinking of FtsZ filaments is indicated with arrows. The figure was created using BioRender software.

1.5 Targeting bacterial cell division with antimicrobial compounds

In recent years, the process of cell division has attracted considerable attention because of its high potential as a novel target for antimicrobial agents. To date, no clinically applied antibiotic interferes with bacterial cell division, although there are already anticancer drugs in clinical application, such as the vinca alkaloids (Jordan et al., 1991) and the taxanes (Schiff et al., 1980; Rowinsky et al., 1992; Jordan et al., 1993) that target tubulin, the eukaryotic homolog of FtsZ. Since FtsZ is the key protein of cell division and is furthermore virtually ubiquitous in bacteria, it in particular represents an auspicious antibiotic target. Most of the cell division inhibitors known so far, act by direct binding to FtsZ (Silber et al., 2020 a), thereby modulating its GTPase activity and its dynamic assembly properties. More specifically, most compounds target the nucleotide binding site or the region of the T7 loop of FtsZ. Since these regions are also conserved in tubulin, cross-targeting of such agents poses a challenging problem in terms of clinical application. Therefore, alternative binding sites with a higher selectivity for antimicrobial agents or even other mechanisms to interrupt cell division were investigated intensively during the past years. In this context, for example, the interdomain cleft of FtsZ emerged to be an interesting target site for antimicrobial interference, as this region has only low sequence and structural similarity to tubulin (Pradhan et al., 2021).

1.5.1 PC190723 inhibits cell division by interfering with FtsZ

In recent years, the compound PC190723 has been used in several studies to investigate FtsZ dynamics in bacteria (Bisson-Filho et al., 2017; Monteiro et al., 2018; Whitley et al., 2021). With a minimal inhibitory concentration (MIC) in the range of 0.5 – 1 µg/ml, the benzamide derivative shows promising antimicrobial activity against Gram-positive bacteria including pathogenic methicillin-resistant *S. aureus* (MRSA) (Haydon et al., 2008). The treatment with PC190723 or derivatives thereof results in the inhibition of cell division due to perturbed FtsZ localization. This causes rod-shaped *B. subtilis* cells to grow into filaments (Fig. 4A-E) (Adams et al., 2011) and spherical *S. aureus* cells to enlarge (Haydon et al., 2008). The compound was shown to bind to the open-cleft conformation of FtsZ, which in BsFtsZ and SaFtsZ is predominantly found in polymers. In contrast, FtsZ monomers adapt a closed cleft to which PC190723 cannot bind (Artola et al., 2017). More precisely, the compound directly binds the interdomain cleft that is formed between helix H7, the T7 loop and the beta-sheets in the C-terminal domain of the FtsZ structure (Fig. 4F).

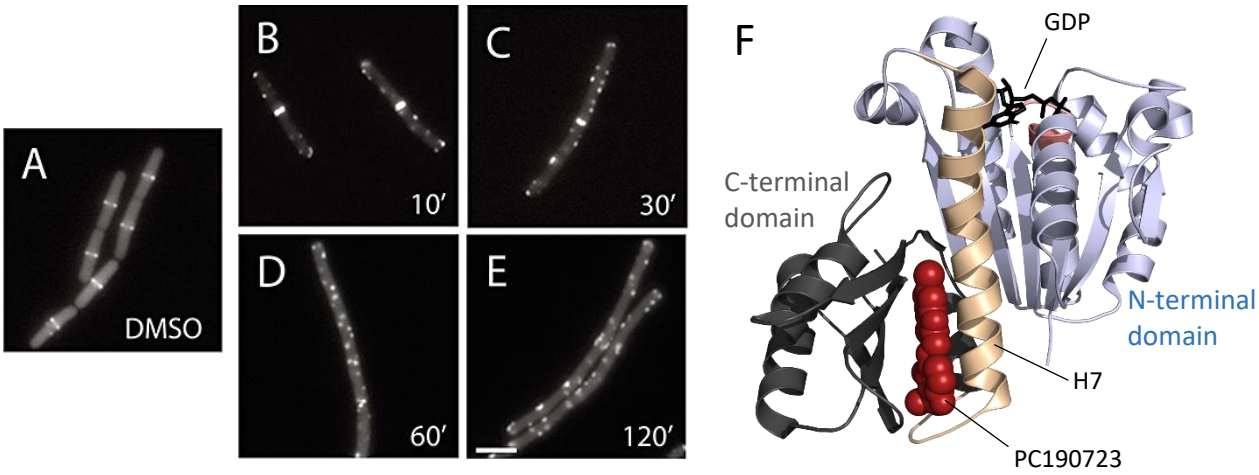

Fig. 4: PC190723 acts by binding to the interdomain cleft of FtsZ resulting in an immediate block in cell division. (A-E) Localization of GFP-FtsZ in *B. subtilis* strain 2020 in (A) the absence of the compound and after (B) 10 min, (C) 30 min, (D) 60 min, (E) 120 min treatment with 2 µg/ml of the PC190723-analog 8j. While FtsZ correctly assembled into Z-rings in the DMSO control (A), treatment with 8j resulted in mislocalization of FtsZ (B-E) that formed distinct foci distributed throughout the cell, finally leading to a halt in cell division. Scale bar, 3 µm. Images adapted from Adams et al., 2011, reprinted with kind permission from WILEY. (F) Crystal structure of PC190723-, GDP- bound *S. aureus* FtsZ; PDB: 3VOB (Matsui et al., 2012). The NTD of FtsZ is colored in light blue and includes the tubulin signature motif (salmon) and bound GDP (black); the CTD of FtsZ is colored in dark grey. The two domains are connected via the central helix H7 (beige). The compound PC190723 binds to the open conformation of the interdomain cleft in FtsZ filaments, which is formed by helix H7, the T7 loop and the four beta-sheets of the CDT.

Binding of PC190723 to the open conformation of the interdomain cleft thus stabilizes FtsZ filaments and halts FtsZ dynamics (Andreu et al., 2010; Elsen et al., 2012), finally abrogating cell division (Haydon et al., 2008; Matsui et al., 2012). Noteworthy, PC190723 had no effect on tubulin *in vitro* and was furthermore the first FtsZ-targeting compound with proven *in vivo* efficacy (Haydon et al., 2008). Moreover, the compound and different derivatives thereof showed a synergistic effect in combination with cefurocime, cefdinir and imipenem, thereby re-sensitizing MRSA to those β-lactam antibiotics (Tan et al., 2012; Kaul et al., 2015; Lui et al., 2019). Unfortunately, due to its unfavorable drug-like and pharmacokinetic properties, clinical development of PC190723 has been limited. However, several approaches have been made with new derivatives of PC190723, which may represent promising drug candidates for future therapeutic use (Kaul et al., 2013, 2015; Stokes et al., 2013; Kumar et al., 2021). In this context, the novel prodrug TXA709 (product TXA707) revealed improved pharmacokinetic properties, as well as an increased *in vivo* efficacy against staphylococci compared with PC190723 and other derivatives thereof, representing a promising lead compound with respect to the development of a new antibiotic treatment strategy by inhibiting bacterial cell division (Kaul et al., 2015).

1.5.2 ADEP antibiotics inhibit bacterial cell division by inducing the ClpP-mediated degradation of FtsZ

The vast majority of cell division inhibitors known to date act by direct binding to FtsZ, e.g., PC190723, thereby affecting its dynamic assembly properties (Silber et al., 2020 a). In contrast, a new class of acyldepsipeptide antibiotics (ADEPs) revealed a new mode of action that is not based on direct interaction with FtsZ, but nevertheless affects cell division and FtsZ in an unprecedented manner. ADEP antibiotics have proven antimicrobial activity against a broad range of Gram-positive bacteria including MRSA and vancomycin-resistant *Enterococcus faecium* (VRE) (Brötz-Oesterhelt et al., 2005). The compound was originally isolated from the bioactive extract A54556 produced by *Streptomyces hawaiiensis* NRRL 15010. Six closely related components have been identified from this extract (Michel et al., 1985), of which ADEP1 (formerly known as factor A) revealed the highest activity. ADEP1 served as the precursor for a series of congeners that were synthesized by *Bayer HealthCare AG* in a structure optimization program amongst others yielding ADEP2 and ADEP4 with improved activity against Gram-positive bacteria (Brötz-Oesterhelt et al., 2005; Malik et al., 2020).

ADEP antibiotics act by dysregulation of the bacterial Clp protease (Brötz-Oesterhelt et al., 2005), which is widely conserved and involved in protein homeostasis, protein quality control, developmental processes and virulence (Msadek et al., 1998; Kock et al., 2004). The Clp protease consists of a proteolytic core ClpP and associated Clp-ATPases for substrate binding and unfolding. In this regard, ClpP monomers assemble into two stacked heptameric rings that are commonly flanked by hexameric rings of cognate Clp-ATPases on both sides. Proteolytic activity of ClpP strictly depends on this direct association with the ClpATPases that recognize, unfold and thread substrates into the proteolytic ClpP-barrel (Malik et al., 2017). ADEPs bind to the proteolytic core ClpP of the protease, leading to the following consequence: First, ADEPs compete with Clp-ATPases for the same binding site on ClpP, abrogating ClpP-Clp-ATPase interactions and thereby blocking all natural functions of the Clp protease (Fig. 5; I. Inhibition). Second, ADEP activates the otherwise dormant ClpP core for the degradation of nascent polypeptides at the ribosome as well as the loosely folded model protein casein (Fig. 5; II. Activation) (Brötz-Oesterhelt et al., 2005; Kirstein et al., 2009).

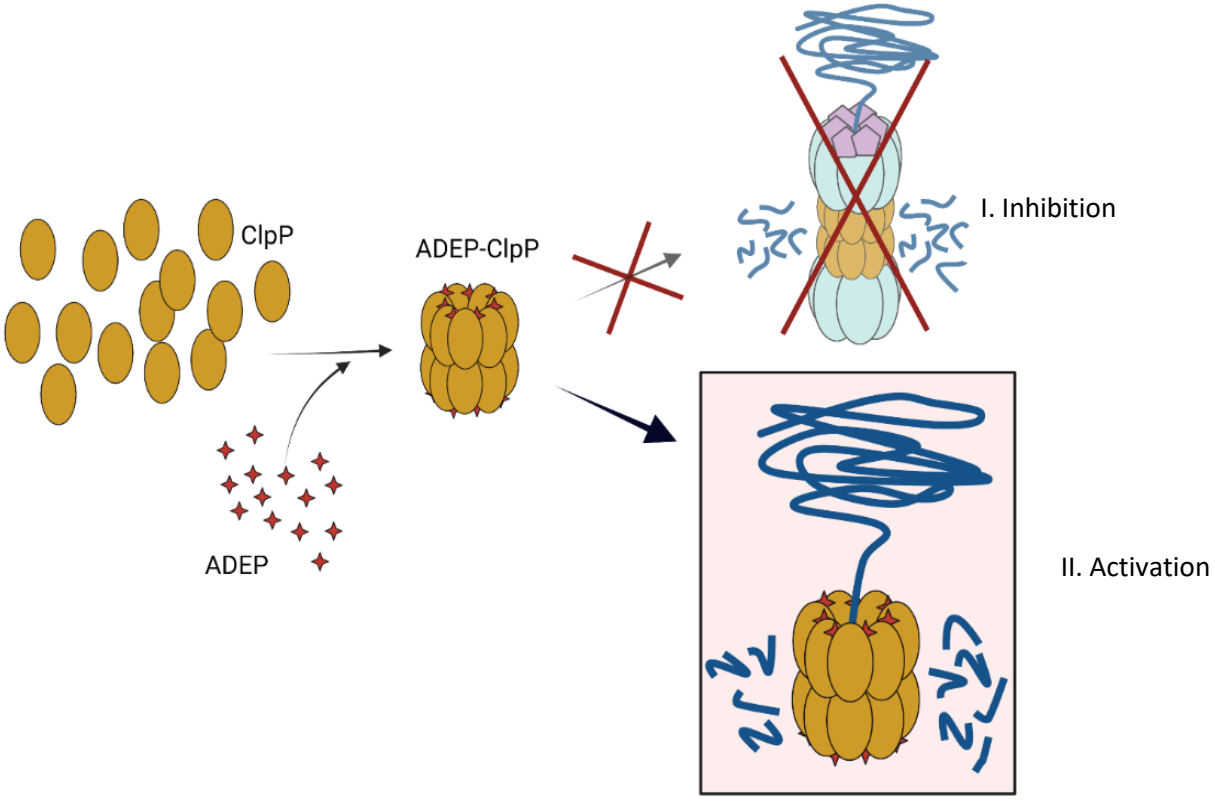

Fig. 5: ADEP inhibits natural functions of the Clp protease and activates the ClpP core for uncontrolled proteolysis. Schematic overview of the dual mode of action of the antibiotic acyldepsipeptide (ADEP). By binding to the interface of two ClpP monomers, ADEP antibiotics lead to the I.) inhibition of all natural functions of the Clp protease; and II.) activation of the dormant core ClpP for the degradation of nascent polypeptides at the ribosome as well as the loosely folded model protein casein (Brötz-Oesterhelt et al., 2005; Kirstein et al., 2009; Lee et al., 2010; Li et al., 2010). The figure was adapted from Malik et al., 2017 and modified using BioRender software.

Further studies showed that ADEP-binding to ClpP triggers a conformational change of the ClpP N-terminal segments that results in the opening of the usually tightly closed entrance pore to the proteolytic chamber of the ClpP core (Lee et al., 2010; Li et al., 2010), now allowing for entry of non-native substrates (Brötz-Oesterhelt et al., 2005; Kirstein et al., 2009). One would think that such unleashed proteolytic activity may have broad and severe consequences for the bacterial cell. However, dependent on the applied ADEP concentration, two distinct phenotypes could be distinguished: higher concentrations of ADEP (>5x MIC) resulted in a clear inhibition of *B. subtilis* growth and a severe decline in the number of colony forming units (CFU), whereas at lower concentrations close to the MIC (approx. 2-3x MIC), surprisingly, *B. subtilis* cells grew into long filaments that reached a length of up to 200 µm (Fig. 6A-C) (Sass et al., 2011), clearly indicating a distinct interference with bacterial cell division.

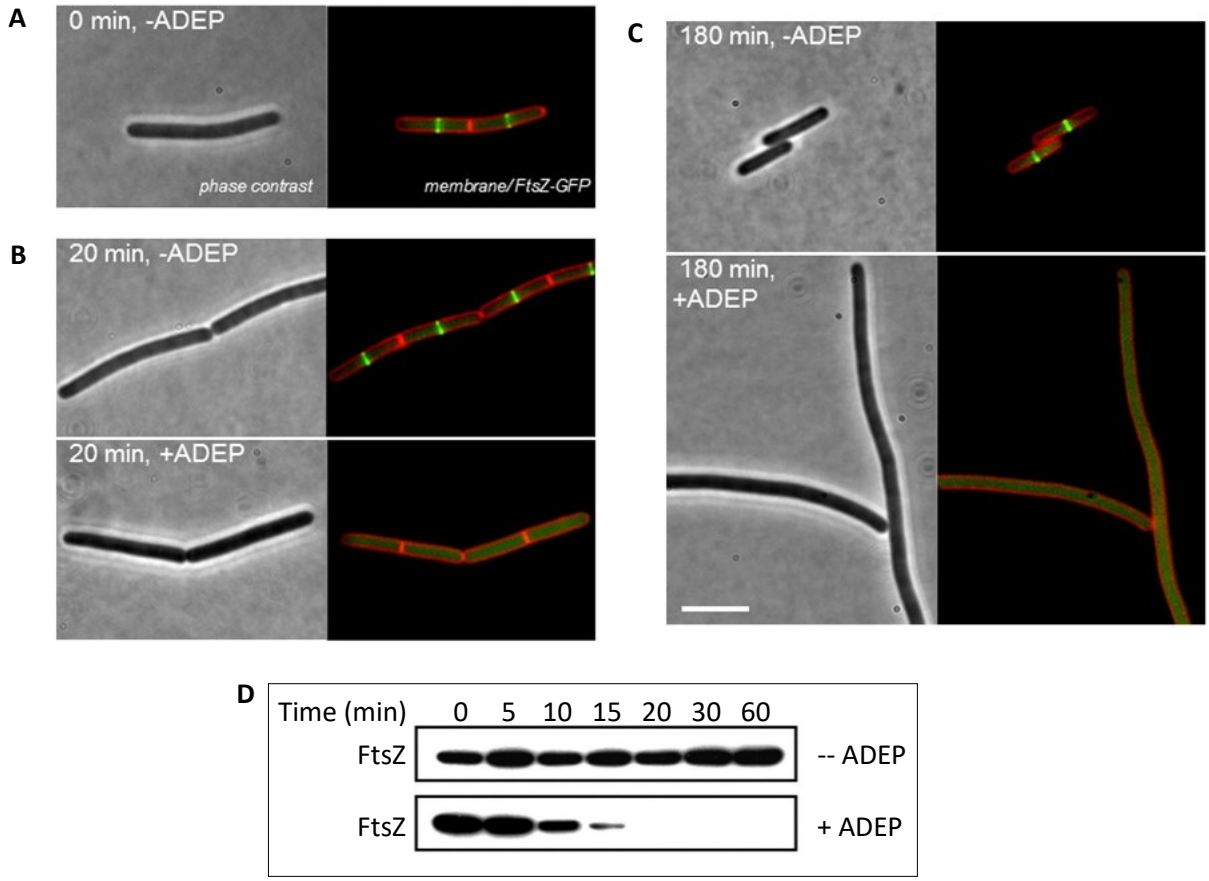

Fig. 6: Micrographs of *B. subtilis* cells show the delocalization of GFP-tagged FtsZ in presence of 0.25 µg/ml ADEP. (A) In the absence of ADEP, *B. subtilis* cells showed mid-cell localization of GTP-tagged FtsZ and normal Z-ring formation during unperturbed cell division**.** (B+C) At ADEP concentrations close to the MIC, Z-ring assembly was inhibited and cells grew into long filaments. Scale bar, 5 µm. Membranes were stained with FM5-95 (red). (D) Western blot analysis showed a decreased abundance of FtsZ in ADEP-treated *B. subtilis* cells over time, while the level of FtsZ in untreated cells remained unaffected. Micrographs and western blot images were reprinted with permission from Sass et al., 2011.

It could be shown, that ADEP-activated ClpP led to fast degradation of FtsZ *in vitro* as well as in whole cells (Fig. 6D). Furthermore, FtsZ appeared to be a preferred target for ADEP-ClpP, since other exemplary protein substrates were not degraded (Sass et al., 2011; Silber et al., 2020 b). Remarkably, to date, no other bacterial protein has been identified as a substrate for ADEP-activated ClpP *in vitro* as well as *in vivo*, raising the questions on the particular reasons for the observed preference of ADEP-ClpP for FtsZ.

2 Research objectives

FtsZ is the central player during cell division in most bacteria and therefore represents a promising target for antibiotic interference. Most of the known compounds, e.g. PC190723, interfere with the process of cell division by directly interacting with FtsZ. However, the antibiotic ADEP reveals a unique mode of action inducing a ClpP-mediated degradation of FtsZ. Interestingly, FtsZ appears to be preferentially targeted and degraded by ADEP-activated ClpP, both *in vitro* and in living cells. Noteworthy, no other bacterial protein with a comparable vulnerability against ADEP-activated ClpP is known to date. Nevertheless, the molecular rationale behind FtsZ being a preferred target for ADEP-ClpP is still unclear.

Therefore, the first objective of this work was to identify structural features of FtsZ that confer its vulnerability to ADEP-ClpP. Hence, the interaction site of FtsZ for ADEP-ClpP should be determined. To this end, the degradation of different FtsZ mutant proteins (including N- and C-terminal truncations) should be investigated *in vitro* and compared to the degradation of wild-type FtsZ. In addition, the molecular and physicochemical reasons for the interaction of ADEP-ClpP with FtsZ should be examined by analyzing the degradation of different FtsZ mutant proteins with various amino acid substitutions. After the identification of the interaction site of FtsZ and the determination of critical features, the identified region was meant to be evaluated for a broader application. Therefore, the interaction site of FtsZ for ADEP-ClpP should be transferred to other putative protein targets and investigated with respect to degradation by ADEP-activated ClpP. Another aim of this work was to characterize the course of FtsZ degradation with respect to the FtsZ structure and fold. For this purpose, the earliest degradation bands of FtsZ, resulting from the degradation by ADEP-ClpP, should be N-terminally sequenced by Edman degradation.

It has been shown that treatment of *B. subtilis* with low concentrations of ADEP, close to the MIC, results in the degradation of FtsZ and eventually leads to an extremely filamentous growth of rod-shaped cells. However, treatment with high concentrations of the antibiotic, several times the MIC, leads to cessation of biomass production that is accompanied by a drop in the number of CFU indicating additional damage to the cell. Therefore, another goal of this work was to understand the molecular basis for the two distinct phenotypes at low versus high ADEP concentrations. To investigate this, different ADEP and ClpP concentrations should be evaluated *in vitro* and characterized with respect to the degradation of FtsZ.

FtsZ is a GTPase that polymerizes into higher ordered structures in a nucleotide-dependent manner and thereby assembles the Z-ring in the course of cell division. In this context, this work further aimed to investigate the impact of nucleotide binding and filament formation with

respect to the degradation efficiency of FtsZ by ADEP-ClpP *in vitro*. For this purpose, different polymerization-deficient mutant FtsZ proteins should be incubated with nucleotides and subsequently analyzed in terms of degradation.

Another objective of this work was to analyze the cellular effect of ADEP on FtsZ and Z-ring formation in living cells. To this end, ADEP treatment should be followed in a *B. subtilis* strain expressing fluorescently-labelled FtsZ using time-lapse fluorescence microscopy. Due to the preferred degradation of FtsZ at low ADEP concentrations, ADEP was meant to be further used as a tool to gain a better understanding of the molecular principles of cell division and its dependence on FtsZ.

3 Summary of Results

3.1 Cell division protein FtsZ is unfolded for N-terminal degradation by antibiotic-activated ClpP

3.1.1 ADEP-activated ClpP preferentially targets the short N terminus of FtsZ

FtsZ is described as the central cell division protein in the vast majority of bacteria and has been shown to be rapidly degraded by ADEP-activated ClpP in *in vitro* assays as well as *in vivo*. In this respect, ADEP concentrations close to the MIC result in filamentous growth of rod-shaped *B. subtilis* cells and swelling of spherical *S. aureus* cells due to the inhibition of cell division despite ongoing biomass production (Sass et al., 2011). Furthermore, no other folded bacterial protein has yet been confirmed for degradation by ADEP-activated ClpP *in vitro* and in living cells, together suggesting that FtsZ may be a preferential target of ADEP-activated ClpP. To answer the question, whether FtsZ is indeed a preferential target, we followed up a study from 2013, in which Conlon and colleagues postulated several further proteins to be targeted by ADEP-activated ClpP in *S. aureus.* These proteins were identified by proteomic analyses of an MRSA culture that was grown to stationary phase and treated with high concentrations of ADEP (10x MIC) over a period of 24 h. Among the proteins which abundance decreased most during ADEP treatment, Conlon and colleagues postulated elongation factor Tu (EF-Tu), fructose-bisphosphate aldolase (FbaA), and pyruvate kinase (PykA), in addition to FtsZ (Conlon et al., 2013).

We therefore investigated the degradation of FbaA in exponentially growing *B. subtilis* and *S. aureus* cultures when treated with low inhibitory concentrations of ADEP. Interestingly, our data did not reveal degradation of FbaA in *B. subtilis* or *S. aureus* when cells were treated with ADEP concentrations close to the MIC (0.25 µg/ml for *B. subtilis*; 1 µg/ml for *S. aureus*). However, under the same conditions, FtsZ was completely depleted (Publication 1, Fig. 1A). To further examine this result, we studied the degradation of BsEF-Tu, BsFbaA and BsPykA by ADEP-ClpP *in vitro*. We could show that all proteins resisted degradation in a time range in which equimolar concentrations of ADEP and ClpP (each 1.5 µM) completely degraded FtsZ (Publication 1, Fig. 1B). These data indicated that FtsZ represents a preferred target for ADEP-activated ClpP in *B. subtilis and S. aureus* under the evaluated conditions. In order to unravel the molecular reason for the preferred degradation of FtsZ, we sought to identify and further characterize structural features of FtsZ that are prone to degradation by ADEP-ClpP. The structure of BsFtsZ reveals a short N terminus of 13 amino acids followed by the globular FtsZ core region including the nucleotide binding site, as well as a long, disordered C terminus that protrudes the globular core domain and comprises 67 residues. Due to its flexibility and length, it was tempting to speculate that the disordered C terminus might be easily accessed

by ADEP-activated ClpP. To test this hypothesis, we constructed various BsFtsZ mutant proteins lacking different portions of the C terminus. The degradation of the mutant proteins was investigated in *in vitro* assays applying equimolar concentrations of ADEP and ClpP (each 1.5 µM) and were then compared to the degradation of full-length FtsZ ($BsFtsZ_{1-382}$). However, unexpectedly, the truncation of the C terminus had no notable effect on the degradation efficiency of FtsZ by ADEP-ClpP. However, when we tested FtsZ mutant proteins lacking the short N terminus, a clear delay in degradation efficiency was observed in relation to the wild-type protein (Publication 1, Fig 1E+F). These results unexpectedly revealed that ADEP-activated ClpP preferentially targets the short N terminus of FtsZ.

3.1.2 Hydrophobicity of the FtsZ N terminus is important for degradation

Investigating the physicochemical properties of the extreme N terminus of FtsZ revealed that it contains four hydrophobic amino acids, which contribute to an overall hydrophobicity in this region (Publication 1, Fig. 2A). In order to examine, whether this might be a critical feature for preferred attack by ADEP-ClpP, we exchanged the hydrophobic amino acids within the N terminus with either glycine or serine, yielding two mutant proteins ($BsFtsZ_{mutG}$ and $BsFtsZ_{mutS}$, respectively). These mutant proteins were characterized by a less hydrophobic N terminus compared to the native N terminus (Publication 1, Fig. 2B). Both mutant proteins showed delayed degradation at equimolar concentrations of ADEP and ClpP (each 1.5 µM). To exclude that a specific amino acid sequence is critical for N-terminal attack of FtsZ by ADEP-ClpP, we scrambled the order of the hydrophobic amino acids in the N-terminal region, yielding the FtsZ mutant protein $BsFtsZ_{FLLI}$. Here, the hydrophobic nature of the N terminus was maintained while the amino acid sequence was altered (Publication 1, Fig. 2B). Importantly, the degradation of $BsFtsZ_{FLLI}$ was similar to the degradation of wild-type FtsZ ($BsFtsZ_{1-382}$), indicating that it is not a specific amino acid sequence at the extreme N terminus, but the overall hydrophobic nature that triggers N-terminal attack of FtsZ by ADEP-ClpP.

3.1.3 The N terminus of FtsZ does not act as a universal degradation tag for ADEP-activated ClpP

Based on our results, that the short N terminus of FtsZ is preferably targeted by ADEP-ClpP, we wondered whether the N terminus of FtsZ might function as a degradation tag determining proteins for proteolysis by ADEP-ClpP. In this context, the SsrA tag in *E. coli,* for example, marks proteins for proteolysis by ClpXP and ClpAP (Gottesman et al., 1998). To examine our hypothesis, we fused the N terminus of FtsZ (comprising the first 10 amino acids) to the Spx protein resulting in $FtsZ_{1-10}$-Spx. Spx in *B. subtilis* is known to be a physiological substrate for

ClpXP (Nakano et al., 2002, 2003), but is not degraded by ADEP-activated ClpP (Kirstein et al., 2009). Furthermore, we attached the N terminus of FtsZ to both termini of the enhanced green fluorescent protein (eGFP), yielding the proteins $FtsZ_{1\text{-}10}$-eGFP and eGFP-$FtsZ_{10\text{-}1}$. In this context, eGFP served as model substrate that was earlier shown to resist degradation by ADEP-activated ClpP *in vitro* (Sass et al., 2011). Our results showed that none of the recombinant proteins was degraded by ADEP-ClpP *in vitro*, even though samples were incubated for a prolonged time period of 16-20 h, which was enough to result in full degradation of FtsZ (Publication 1, Fig. 3A). To further investigate whether degradation of protein substrates might be triggered by the attachment of the entire FtsZ protein, we fused FtsZ to the N terminus of eGFP, yielding $FtsZ_{eGFP}$. Although the FtsZ part of this fusion protein was degraded, the GFP portion remained intact when incubated with ADEP-ClpP. As a consequence, degradation products with a slightly higher molecular weight than eGFP accumulated on SDS-Page (Publication 1, Fig. 3B). These results proved that neither attaching the short N terminus nor fusing the whole FtsZ protein to potential targets, could trigger degradation of these proteins, thereby revealing that the N terminus of FtsZ does not act as a universal degradation tag for ADEP-ClpP.

3.1.4 FtsZ cleavage extends into the folded N-terminal domain

We have shown that the N terminus of FtsZ is preferably targeted by ADEP-activated ClpP. N-terminal attack of FtsZ was furthermore confirmed by N-terminal Edman sequencing of the two largest degradation products visible on SDS-Page (Publication 1, Fig. 4B). In this context, the sequencing results showed cleavage of FtsZ up to amino acid positions 28 and 49, located at the end of helix H0 and H1, respectively. Both identified cleavage sites are located within the fold of the NTD of FtsZ (Publication 1, Fig. 4C), thereby confirming that N-terminal degradation of FtsZ extends into the folded structure of the protein. Since the folded FtsZ protein cannot access the proteolytic chamber of ClpP, we hypothesized that N-terminal degradation of FtsZ requires unfolding of the protein prior to degradation. To date, ClpP has never been shown to degrade a folded protein in the absence of a cognate, energy-driven ATPase. Therefore, it could be speculated that the truncation of the N terminus of FtsZ might intrinsically destabilize the protein, possibly leading to self-unfolding. However, we could show that the truncation of the N terminus of FtsZ ($BsFtsZ_{11\text{-}382}$) does not affect folding and functionality of the mutant protein. In this regard, we demonstrated that the GTPase activity of $BsFtsZ_{11\text{-}382}$ is not affected compared to the activity of $BsFtsZ_{1\text{-}382}$ (Publication 1, Fig. S1). Furthermore, circular dichroism (CD) spectrometry data of $BsFtsZ_{11\text{-}382}$ and $BsFtsZ_{1\text{-}382}$ (in presence and absence of different nucleotides) appeared to be superimposable revealing the same folding state of the proteins (Publication 1, Fig. 4A). In addition, the degradation of

$BsFtsZ_{11-382}$ by ADEP-ClpP was clearly delayed in relation to the degradation of $BsFtsZ_{1-382}$. Together, these results make the possibility of self-unfolding of FtsZ very unlikely. Indeed, our results suggest that ADEP-ClpP is capable of destabilizing the folding of FtsZ during N-terminal attack, thereby allowing for ongoing protein degradation in the absence of an energy-driven ATPase. To further confirm this, we next investigated the degradation of FtsZ by ADEP-ClpP upon increasing the stability of the FtsZ fold.

3.1.5 Nucleotide binding prevents N-terminal degradation by stabilizing FtsZ

Since the NTD of FtsZ includes the nucleotide binding site, we investigated the stability of the FtsZ fold in the presence of nucleotides. The crystal structure of nucleotide-bound FtsZ revealed several non-covalent contacts between FtsZ and the bound nucleotide (Raymond et al., 2009). These contacts are either established in close vicinity to helix H1 or indirectly stabilize helix H0 (Publication 1, Fig. 5A). Since we had found that cleavage of FtsZ by ADEP-ClpP extends into the folded NTD of FtsZ and had identified cleavage sites in close vicinity to helices H0 and H1, we wondered whether it might be possible that the sole binding of a nucleotide may stabilize these two helices, thereby preventing N-terminal unfolding and degradation of FtsZ by ADEP-ClpP. To examine this, we incubated FtsZ ($BsFtsZ_{1-382}$ and $BsFtsZ_{1-315}$) with GTP and performed subsequent degradation assays with ADEP-ClpP. Indeed, we found FtsZ to resist degradation when pre-incubated with GTP, whereas FtsZ without GTP was clearly degraded. In addition, we also showed that FtsZ resists degradation when pre-incubated with GDP (Publication 1, Fig. 5B). Upon GTP-binding, FtsZ polymerizes in a head-to-tail manner thereby forming single-stranded dynamic protofilaments. These filaments grow at one end by the incorporation of new GTP-bound FtsZ subunits and, after GTP-hydrolysis, shrink at the opposite end by the depolymerization of GDP-bound FtsZ subunits. Within a filament, the N terminus of FtsZ, which we revealed as the preferred target site for ADEP-ClpP, is presumably buried between two adjacent FtsZ monomers (Publication 1, Fig. 5A). Hence, it might be also possible that the degradation of FtsZ is prevented due to a steric hindrance since the N terminus of polymerized FtsZ may be hardly accessible for ADEP-ClpP. To study this, we made use of the non-hydrolyzable GTP-analog GTPγS, which binds to FtsZ but does not induce polymerization of larger filaments (Scheffers et al., 2000), thus presumably mostly generating nucleotide-bound monomeric FtsZ. Degradation assays of GTPγS-bound FtsZ revealed that binding of the non-hydrolyzable nucleotide had the same effect as GTP and GDP and rendered FtsZ virtually resistant against ADEP-ClpP under the conditions tested (Publication 1, Fig. 5B). To further explore these results, we constructed a polymerization-deficient FtsZ mutant protein. In this context, the amino acid substitution from leucine to glutamic acid at position 272 in FtsZ from *E. coli* was

earlier reported to result in a protein that binds GTP but does not form polymers. This mutation is located at the interface of adjacent monomers thereby disturbing the head-to-tail association in FtsZ polymers (Li et al., 2013). We could show that the exchange of leucine to glutamic acid in BsFtsZ (yielding $BsFtsZ_{L272E}$) indeed resulted in a decreased GTPase activity of the protein (Publication 1, Fig. S2) thereby suggesting hampered polymerization. The degradation assay of $BsFtsZ_{L272E}$ confirmed our results regarding GTPγS, since the degradation by ADEP-ClpP was inhibited when $BsFtsZ_{L272E}$ was incubated with either GTP, GDP or GTPγS.

Taken together, our results revealed that nucleotide binding of either GTP, GDP or GTPγS renders FtsZ resistant against N-terminal degradation by ADEP-ClpP at equimolar concentrations of ADEP and ClpP. Hence, binding of the nucleotide alone prevents FtsZ from degradation by ADEP-ClpP rather than steric hindrance due to FtsZ polymerization. Obviously, nucleotide binding stabilizes the N-terminal fold of FtsZ, thereby preventing attack and subsequent degradation by ADEP-ClpP. Furthermore, these results confirm that ADEP-ClpP indeed is capable of N-terminally unfolding FtsZ in the absence of an energy-driven ATPase.

3.1.6 The C terminus of FtsZ is increasingly degraded at higher concentrations of ADEP-ClpP

Considering that the N terminus of FtsZ is preferably attacked by ADEP-ClpP and that N-terminal degradation is prevented by nucleotide binding, a degradation product of nucleotide-bound FtsZ was not to be expected in degradation assays. Nevertheless, in the case of the degradation of nucleotide-bound $BsFtsZ_{1\text{-}382}$ as well as $BsFtsZ_{L272E}$, a faint band appeared on SDS-Page for samples representing 2 h of incubation of FtsZ with ADEP-ClpP (Publication 1, Fig. 5B). Since nucleotides were present in the assay in a 250-fold surplus over FtsZ (1 mM GTP and 4 µM FtsZ were used in the assay), and the faint degradation product was not observed for the C-terminally truncated mutant protein $BsFtsZ_{1\text{-}315}$, N-terminal degradation appeared rather unlikely for nucleotide-bound $BsFtsZ_{1\text{-}382}$ and $BsFtsZ_{L272E}$. Rather, these results hinted at weak C-terminal degradation of FtsZ by ADEP-ClpP. Indeed, a weak C-terminally truncated degradation product was confirmed for nucleotide-bound $BsFtsZ_{1\text{-}382}$ via Western Blot analysis using anti-His_6 antibodies (Publication 1, Fig. S6). However, C-terminal attack did not result in complete degradation of FtsZ, but only in the truncation of the flexible, disordered C terminus, which was visible on SDS-Page by a minor band shift of the full-length protein $BsFtsZ_{1\text{-}382}$. In order to further characterize this observation, we tested whether C-terminal degradation of FtsZ could be further stimulated by increasing concentrations of ADEP. To this end, we raised the molar ratio of ADEP over ClpP by a factor

of 2.5 (1.5 µM of ClpP with 3.75 µM of ADEP) and additionally increased the overall amount of ADEP and ClpP (2.5 µM of ClpP with 6.25 µM of ADEP). When degrading $BsFtsZ_{1-382}$ in the presence of nucleotides, elevated concentrations of ADEP over ClpP (1.5 µM ClpP + 3.75 µM ADEP) resulted in pronounced C-terminal degradation products, that appeared even stronger at higher concentrations of ADEP and ClpP (2.5 µM ClpP + 6.25 µM ADEP) (Publication 1, Fig. 6A). To further examine C-terminal degradation at different molar ratios of ADEP and ClpP, the degradation of $BsFtsZ_{1-382}$, $BsFtsZ_{11-382}$, as well as $BsFtsZ_{1-315}$ was investigated by applying a constant ClpP concentration of 1.5 µM, while stepwise increasing the ADEP level from 0 µM to 7.25 µM (Publication 1, Fig. 6B). The degradation of $BsFtsZ_{1-382}$ as well as $BsFtsZ_{1-315}$ readily started at equimolar concentrations of ADEP and ClpP, whereas degradation of $BsFtsZ_{11-382}$ was hardly detectable under these conditions, thereby again highlighting the importance of the N terminus for the preferred degradation. Increasing the molar ratio of ADEP over ClpP generally resulted in an enhanced degradation efficiency. Noteworthy, $BsFtsZ_{11-382}$ was also increasingly degraded, suggesting enhanced C-terminal degradation at increasing ADEP levels. However, the degradation efficiency of all tested proteins stagnated when a molar ratio of 1:2.5 (1.5 µM ClpP and 3.75 µM ADEP) was reached. The here observed increased efficiency of substrate degradation by ADEP-ClpP was further confirmed by our related results using the fluorogenic dipeptide Suc-LY-AMC (N-succinyl-Leu-Tyr-7-amino-4-methylcoumarin) and the fluorogenic protein FITC-casein (fluorescein isothiocyanate-casein) as model substrates in *in vitro* ADEP-ClpP degradation assays. For both substrates, the degradation was enhanced at a molar ratio of 1:2.5 (using either 1.5 µM ClpP with 3.75 µM ADEP or 2.5 µM ClpP with 6.25 µM ADEP) compared to equimolar concentrations of ADEP and ClpP (Publication 1, Fig. 6E). In order to examine the impact of the increased degradation efficiency of ADEP-activated ClpP on other proteins, we investigated the degradation of BsEF-Tu, BsFbaA, and BsPykA using 2.5 µM ClpP with 6.25 µM ADEP. Our results showed that BsEF-Tu and BsPykA remained unaffected in *in vitro* degradation assays under these conditions, whereas the amount of BsFbaA slightly decreased. Of note, $BsFtsZ_{1-382}$ was completely degraded under the evaluated conditions (Publication 1, Fig. 6C). However, when we further investigated the degradation of FbaA in *B. subtilis* and *S. aureus* cells using high levels of ADEP (>10x MIC), we did not observe degradation of FbaA. In contrast, as a control, FtsZ was fully degraded in both *B. subtilis* and *S. aureus* cells when treated with high concentrations of ADEP. Of note, it may be the case that FbaA was not stably folded after protein purification and was thus more prone to degradation by ADEP-ClpP in our *in vitro* assay. Furthermore, we cannot exclude that in cells, the pool of FbaA is either replenished constantly and quickly enough or that the protein fold of FbaA is stabilized by secondary factors thereby preventing degradation by ADEP-activated ClpP.

Summarized, at elevated concentrations of ADEP and ClpP, the C terminus of FtsZ becomes an additional target of ADEP-activated ClpP due to an increased peptidolytic and proteolytic efficiency of ADEP-ClpP. Hence, these results suggest a broadening of the substrate spectrum at higher concentrations of ADEP and ClpP and therefore might reflect the degradation of protein substrates other than FtsZ in ADEP-treated bacterial cells.

3.2 Progression of the late-stage divisome is unaffected by the depletion of the cytoplasmic FtsZ pool

FtsZ is regarded as the pacemaker of cell division. However, it remained elusive whether the main driving force during cell division is generated by GTP hydrolysis of FtsZ (Li et al., 2007; Coltharp et al., 2017) or whether septal cell wall synthesis drives cytokinesis (Coltharp et al., 2016, 2017). We have shown that FtsZ is a preferred target protein for degradation by ADEP-activated ClpP (Sass et al., 2011; Silber et al., 2020 b). Therefore, we considered to use ADEP as a tool to deplete the cytoplasmic FtsZ pool and then follow the fate of the divisome under these conditions to investigate the role of FtsZ for divisome assembly and progression during the course of cell division in *B. subtilis*. To this end, we performed time-lapse studies with *B. subtilis* strain 2020 (Stokes et al., 2005) that expresses an additional GFP-FtsZ fusion protein under a xylose inducible promoter. This allowed us to follow the fate of the Z-ring and divisome progression upon the depletion of the cytoplasmic pool of FtsZ during ADEP treatment. To do so, we defined 3 stages of Z-ring progression: (i) early stage Z-rings, (ii) intermediate stage Z-rings, and (iii) late-stage Z-rings (Publication 3, Fig. 2b). Early stage Z-rings, which had just started to assemble, showed a low and sometimes diffuse fluorescence signal at mid-cell. Intermediate stage Z-rings were more progressed and already formed a clearly visible ring at mid-cell. These Z-rings were in a transition phase between early and late-stage Z-rings. Late-stage Z-rings showed a clear and strong signal at mid-cell, visible either as a ring or a dot, dependent on the progression of Z-ring constriction (Publication 3, Fig. 2b). To explore the role of the cytoplasmic FtsZ pool in Z-ring and divisome progression, we followed the fate of Z-rings at these different stages during ADEP treatment with respect to disintegration versus progression and finalization of cell division. We showed that filamentation concentrations of ADEP resulted in the disintegration of all observed early stage Z-rings. Furthermore, the assembly of new Z-rings was inhibited, most probably due to a drop of the cellular concentration of FtsZ below the critical concentration that is needed for polymerization. Z-rings in the intermediate phase showed a heterogenous behavior, and approx. two-thirds of the Z-rings disintegrated, whereas approx. one-third of the intermediate Z-rings constricted and finalized cell division. Moreover, all late-stage Z-rings finalized

cytokinesis, appearing to be unaffected by ADEP-treatment and thus the depletion of the cytoplasmic pool of FtsZ (Publication 3, Fig.2 a+b; Fig. S1+2; Movie S1-3). Since the late-stage divisomes successfully finished cytokinesis even in the presence of ADEP, we further investigated the fate of late-stage divisome proteins during ADEP treatment via time-lapse microscopy using the *B. subtilis* strain CM03, concomitantly expressing mCherry-FtsZ as well as GFP-PBP2b (Publication 3, Fig. 3). As expected, early stage Z-rings, which then disintegrated upon ADEP treatment, showed either weak and diffuse, or no signals for GFP-PBP2b. In contrast, after Z-rings had entered the intermediate stage, increasing amounts of GFP-PBP2b were present at mid-cell. From these Z-rings, approx. 81% finalized cell division while only 19% disintegrated. As soon as Z-rings entered the later stage, substantial amounts of GFP-PBP2b were detected at mid-cell, and all cells constricted and finalized cell septum formation (Publication 3, Fig. 3; Fig. S3; Movie S4). Obviously, as soon as substantial amounts of late-stage divisome proteins (here PBP2b) localized at mid-cell, divisome progression remained unaffected by the depletion of the cytoplasmic FtsZ pool.

In conclusion, our data suggests a two-step model of FtsZ-ring assembly and progression. During the first step, the FtsZ cytoplasmic pool is necessary for Z-ring initiation and septal constriction initiation, indicating that FtsZ dynamics is critical during this step. However, later-stage divisome progression is unaffected by the depletion of the cytoplasmic FtsZ pool and progression might be driven by other triggers such as the late-stage divisome protein PBP2b.

4 Discussion

4.1 FtsZ is especially vulnerable to degradation by ADEP-activated ClpP

Under physiological conditions, proteolytic activity of ClpP strictly depends on energy-driven ATPases that, together with adapter proteins, recognize and unfold substrates to guide them into the proteolytic chamber of the ClpP barrel (Frees et al., 2007; Malik et al., 2017). The antibiotic ADEP overcomes this tight control mechanism proving potency against a broad range of Gram-positive bacteria including threatening pathogens such as VRE and MRSA (Brötz-Oesterhelt et al., 2005). ADEP binding to ClpP results in the inhibition of all natural functions of ClpP, and at the same time activates ClpP for uncontrolled proteolysis of nascent peptides emerging from the ribosome (Brötz-Oesterhelt et al., 2005; Kirstein et al., 2009). Interestingly, the important cell division protein FtsZ also appears to be degraded (Sass et al., 2011). Indeed, this is the first time that ClpP has been found to degrade a folded bacterial protein without the help of a cognate energy-driven ATPase. So far, FtsZ had not been reported to be intrinsically unstable or loosely folded (Löwe et al., 1998; Nogales et al., 1998). Nevertheless, our results suggest that FtsZ is a particularly vulnerable target for ADEP-activated ClpP and we showed that the essential cell division protein is rapidly degraded *in vitro* as well as *in vivo* (Silber et al., 2020 b). In contrast, several other tested proteins including physiological Clp substrates such as MecA, MscA, Spx or ComK resist degradation by ADEP-ClpP (Kirstein et al., 2009; Sass et al., 2011; Silber et al., 2020 b). In a study by Conlon and colleagues, proteomic analysis of *S. aureus* cells treated with high concentrations of ADEP for an extended period of time revealed decreased abundance of multiple proteins in addition to FtsZ (Conlon et al., 2013). In their study, the authors postulated the proteins FbaA, PykA, and EF-Tu to be also targets for ADEP-ClpP. However, our *in vivo* data showed that FbaA resisted degradation when cells were treated with low concentrations of ADEP, whereas FtsZ was completely degraded in both, *S. aureus* and *B. subtilis*. Furthermore, our *in vitro* degradation assays showed that FbaA, PykA as well as EF-Tu resisted degradation by ADEP-ClpP, while FtsZ was completely degraded under the same conditions (Silber et al., 2020 b). Hence, our data clearly show that FtsZ appears to be exceptionally prone to degradation by ADEP-ClpP compared to other potential protein targets, currently marking it as the preferred folded protein target of ADEP-activated ClpP.

Prior to this work, it was unclear why FtsZ appears to be preferentially attacked and degraded by ADEP-ClpP. However, the data presented in this thesis, provide a molecular rationale for its increased vulnerability against degradation by ADEP-ClpP and gives novel insight into the role of the structural features of FtsZ in ADEP-dependent degradation.

The structure of FtsZ comprises a short N terminus followed by a conserved core domain that harbors the nucleotide binding site, and it ends with a long, disordered C terminus that protrudes the globular core (Löwe et al., 1998). During the past years, the role of the C terminus has been extensively studied *in vitro* as well as *in vivo* and was revealed to be a critical determinant for FtsZ dynamics as well as Z-ring assembly (Buske et al., 2012, 2013, 2015; Gardner et al., 2013; Sundararajan et al., 2019; Cohan et al., 2020). In this regard, the C terminus was described to act as a central hub (Pazos et al., 2013) that interacts with various cell division proteins, such as FtsA (Jensen et al., 2005). Furthermore, it has been shown to be critical for lateral interactions required for the assembly of higher ordered structures that are a prerequisite for establishing the Z-ring (Buske et al., 2012, 2013). Since the extended C terminus of BsFtsZ comprises 67 amino acids, it may be assumed to be an easily accessible target that could readily diffuse into the entrance pore of the ADEP-ClpP barrel in order to be degraded. Thus, the degradation of the extreme C terminus of FtsZ alone would have severe effects on FtsZ functionality and would most likely effectively disturb cell division. On this account, we first hypothesized that the extended C terminus of FtsZ may be the preferred target site for ADEP-activated ClpP. Therefore, it was particularly surprising that we did not observe impaired degradation of C-terminally truncated FtsZ mutant proteins ($BsFtsZ_{1-364}$ and $BsFtsZ_{1-315}$) when compared to the degradation of $BsFtsZ_{1-382}$. In contrast, we identified the short N terminus of BsFtsZ to be the preferred target site for ADEP-activated ClpP. In this regard, the degradation of N-terminally truncated FtsZ mutant proteins showed a significant delay in degradation compared to full-length FtsZ, clearly indicating N-terminal rather than C-terminal attack of the protein (Publication 1, Fig. 1F). N-terminal degradation of FtsZ was furthermore confirmed by sequencing the two largest degradation products visible on SDS-Page using Edman degradation. The results obtained here showed that cleavage of FtsZ by ADEP-ClpP extends into the N-terminal fold, temporarily halting within helix H0 and H1 (Publication 1, Fig. 4B+C). The short, structurally unsolved portion of the N terminus of FtsZ, which to date has not been assigned any function in the domain of Firmicutes, comprises merely 10 amino acids. As an extended polypeptide chain, this would correspond to a length of 36 Å according to the Pauling model (Pauling et al., 1951). However, the minimal distance that an extended polypeptide chain needs to span to allow for degradation by ADEP-ClpP would be at least ~40 Å, measured from the top of the ClpP barrel (Glu53) to the catalytic residue serine (S97), which is part of the catalytic triad (calculated from crystal structure PDB: 3KTK using PyMOL; see Fig. 7). This would mean that, for degradation, either the entire N-terminal domain of FtsZ needs to enter the ClpP barrel or the N-terminal domain of FtsZ is unfolded prior to degradation. Although the diameter of the entrance pore of the ClpP tetradecamer increases from ~1.8 nm to ~2.7 nm upon ADEP binding (Lee et al., 2010), this would still not be sufficient for the entry of the folded N-terminal domain which has a diameter

of approx. 4 nm at its narrowest part (calculated from crystal structure PDB: 2Rho using PyMOL). Hence, unfolding of the N-terminal domain of FtsZ prior to degradation of the cell division protein FtsZ by ADEP-ClpP appeared to be required (Fig. 7). In this context, the question arises of how ADEP-activated ClpP might be capable to unfold the N-terminal domain of FtsZ. To give an answer to this question, we investigated the physicochemical properties of FtsZ and found that the short N terminus is characterized by an overall hydrophobicity which is essentially mediated by four amino acids. Since the exchange of these amino acids with less hydrophobic ones had resulted in delayed degradation, we could demonstrate that the hydrophobicity of this region is crucial for N-terminal attack of FtsZ by ADEP-ClpP (Publication 1, Fig. 2). In this regard it is important to note that the rim of the entrance pore as well as the surface of the degradation chamber on the inner side of the ClpP barrel, are also lined with hydrophobic residues (Wang et al., 1997 a; Sowole et al., 2013). Thus, hydrophobic interactions between the N terminus of FtsZ and the outer rim of ClpP might play a pivotal role in N-terminal attack and subsequent unfolding of FtsZ by ADEP-ClpP. The hydrophobic effect is one of the main driving forces in protein folding and describes the energetic preference of hydrophobic residues to cluster together (Camilloni et al., 2016). In doing so, proteins burry hydrophobic residues on the inside, thereby avoiding water contact. Furthermore, hydrophobic interactions play an important role in protein-protein association (Young et al., 1994; Tsai et al., 1997 a; b) and may trigger the assembly of supramolecular complexes (Garcia-Seisdedos et al., 2017). Considering this, hydrophobic interactions between FtsZ and ADEP-ClpP might facilitate the unfolding of the N-terminal domain of FtsZ. More precisely, we propose that the attraction between the surface-exposed N-terminal hydrophobic region of FtsZ and the hydrophobic rim of the ClpP barrel might initially support a docking event. Hydrophobic interactions between the FtsZ N terminus and the ClpP entrance pore might be extended after docking, reaching into the inside of the hydrophobic ClpP chamber. The sum of hydrophobic interactions between ADEP-ClpP and FtsZ may lead to a weakening of intramolecular contacts within the N-terminal domain of FtsZ, which could eventually result in its destabilization and subsequent unfolding (see Fig. 7). Thus, ADEP-ClpP might unfold the N-terminal domain of FtsZ by rather “holding tightly” via hydrophobic interactions instead of actively pulling (Silber et al., 2020 b).

The hypothesis of N-terminal unfolding of FtsZ is further supported by our finding, that nucleotide binding prevents N-terminal degradation of FtsZ by ADEP-ClpP. This result indicates that the N-terminal fold of FtsZ is stabilized upon nucleotide binding thereby preventing unfolding of the protein. In this context, several contacts are established between FtsZ and a bound nucleotide, i.e., seven segments of FtsZ (loop T1-T6 and helix H7) are described to be involved in nucleotide binding (Nogales et al., 1998). Specifically, several non-

covalent contacts are established directly with loop T1, which is in close vicinity to helix H0, and in addition contacts with loop T4 indirectly stabilize helix H1 (Publication 1, Fig. 5A, zoom window). We therefore suggest that intrinsic interactions in a nucleotide bound FtsZ-monomer are stronger than the established hydrophobic interactions between FtsZ and the ADEP-ClpP complex. As a result, N-terminal unfolding and degradation of FtsZ by ADEP-ClpP is prevented. Of note, a stabilization of the FtsZ fold, mediated by nucleotide binding, was also suggested for EcFtsZ (Andreu et al., 2002). Here, upon increasing denaturing conditions, two unfolding steps were observed by Andreu and colleagues. In their study, circular dichroism (CD) spectrometry data revealed that the first unfolding step of FtsZ coincided with the release of the nucleotide, and the authors suggested that formation of the secondary structure of the N-terminal domain depends on nucleotide binding that stabilized the EcFtsZ fold (Andreu et al., 2002). Related results were also obtained from another group who suggested an intermediate state of EcFtsZ during thermal denaturation. This intermediate state already adapted at a relative low temperature of 30 °C (Santra et al., 2003) and might indicate the unfolding of the N-terminal domain due to a rather low stability. Furthermore, a recently published study revealed that nucleotide binding to SaFtsZ supports the correct folding of the protein. By performing nuclear magnetic resonance (NMR) as well as CD spectrometry, SaFtsZ was found to adapt an unfolded state *in vitro* under certain buffer conditions. Here, the folding of FtsZ could be either induced by addition of nucleotide, increasing glycerol-/ ion-concentrations, or by increasing osmolytes in the buffer (Huecas et al., 2020). Although our own CD spectrometry data proved the integrity of the BsFtsZ secondary structure in the absence and presence of nucleotides in our assays (Publication 1, Fig 4A), the collective results from our group and others clearly indicate that nucleotide binding to FtsZ increases protein stability compared to apo-FtsZ.

Based on the data presented in this thesis, we suggest that the N-terminal domain of FtsZ inherits a more loosely fold that is unfolded and degraded by ADEP-activated ClpP during N-terminal attack. However, unfolding and degradation of the N-terminal domain is prevented by nucleotide binding, due to a more stabilized fold of the N-terminal domain of FtsZ.

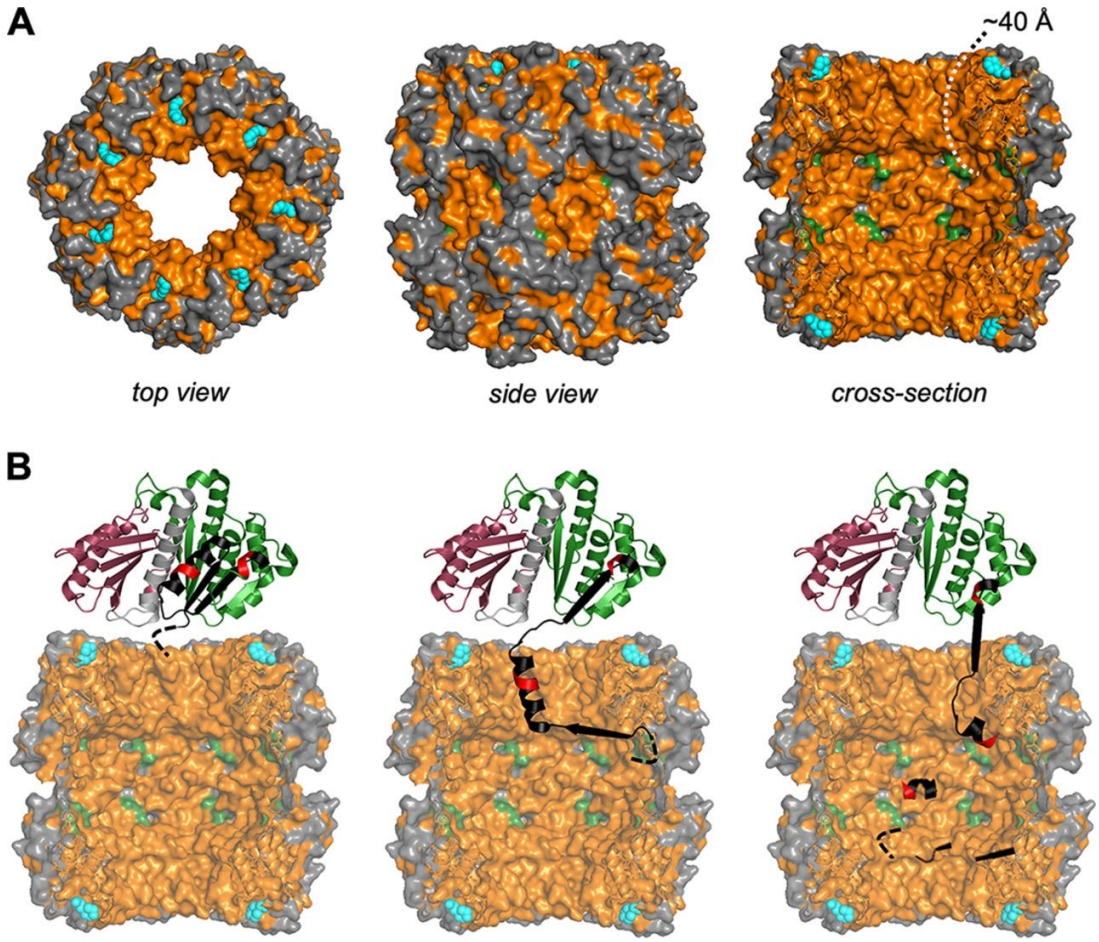

Fig. 7: Proposed model for N-terminal degradation of FtsZ by ADEP-activated ClpP. (A) Depicted is a top view (left), a side view (middle) and a cross-section (right) of the crystal structure of the ADEP-bound *B. subtilis* ClpP tetradecamer (PDB entry: 3KTK). Hydrophobic regions are colored in orange; catalytic residues that are buried in the ClpP barrel are colored in green; bound ADEP is colored in cyan. The first 17 N-terminal residues of each ClpP monomer that cluster around the entrance pore of the ClpP barrel are not solved in the crystal structure but include several hydrophobic residues (Lee et al., 2010). In order to reach the catalytic triads within the ClpP barrel, a distance of ~40 Å needs to be spanned. (B) The FtsZ N terminus is preferably targeted by ADEP-ClpP due to its overall hydrophobicity that supports docking with the hydrophobic entrance pore of the ClpP barrel. Unfolding of the N-terminal domain may then be triggered by means of hydrophobic interactions. Hydrophobic interactions could potentially extend further into the ClpP chamber and might be strong enough to weaken intrinsic contacts in the N-terminal FtsZ fold, leading to its destabilization and unfolding. Noteworthy, we have shown that nucleotide binding prevents N-terminal degradation presumably by stabilizing the fold of the N-terminal domain of FtsZ. The figure was adapted from Silber et al., 2020 b.

4.2 High versus low ADEP concentrations result in distinct phenotypes of *B. subtilis* and reveal a broadened target spectrum of ADEP-ClpP

Rod-shaped *B. subtilis* cells display two distinct phenotypes when treated with different concentrations of ADEP. In this regard, at low inhibitory concentrations (2-3x MIC), also referred to as “filamentation concentrations of ADEP”, *B. subtilis* cells grow into extremely long filaments reaching a length up to 200 µm. Under these conditions, biomass production and other cellular processes proceed while cell division is abrogated (Sass et al., 2011). In contrast, at high concentrations of ADEP (10x MIC), cells quickly cease biomass production remaining shorter and furthermore displaying an uneven cell morphology (Sass et al., 2011; Mayer et al., 2019). These two distinct phenotypes suggest different cascades of events that are triggered at different concentrations of the antibiotic. In this context, the results obtained during this thesis provide insights into the molecular basis for the observed phenotypes at high versus low ADEP concentrations.

The prominent filamentous phenotype of rod-shaped cells that were grown at low concentrations of ADEP result from the inhibition of cell division due to the degradation of FtsZ, while biomass production proceeds (Sass et al., 2011). And we have shown here that FtsZ represents a preferred target for ADEP-ClpP in comparison to other putative protein substrates (Sass et al., 2011; Silber et al., 2020 b). As ADEP stabilizes the ClpP oligomer in its extended active conformation (Lee et al., 2010; Malik et al., 2017), all ADEP molecules might be in complex with ClpP when filamentation concentrations of ADEP are applied. On a cellular level, it might be well feasible that low inhibitory concentrations of ADEP are not sufficient to completely saturate all ClpPs within the cell. Of note, ADEP treatment was even shown to result in an elevated cellular level of its target ClpP (Brötz-Oesterhelt et al., 2005; Malik et al., 2020). The expression of ClpP was furthermore shown to be induced under several stress conditions (Gerth et al., 1998). Hence, during the course of treatment, the ADEP level more or less remains constant while the level of ClpP even increases. In this context, it is important to note that the active sites of ClpP are allosterically activated by ADEP binding, inducing a conformational switch that controls accessibility as well as activity of the catalytic sites (Gersch et al., 2015). Solved crystal structures of ADEP-bound ClpP tetradecamers are well saturated with ADEP and all binding sites are occupied (Lee et al., 2010; Li et al., 2010; Schmitz et al., 2014; Brown Gandt et al., 2018; Wong et al., 2018). Consequently, all catalytic triads are allosterically activated resulting in an extended conformation of the ClpP barrel in which the entrance pore is enlarged from a diameter of ~1.8 nm to ~2.7 nm (Lee et al., 2010). However, at low ADEP concentrations, ClpP barrels may not be saturated, and thus not fully activated, resulting in a preferred attack and subsequent degradation of FtsZ at its hydrophobic N terminus. Hence, under these conditions and despite a potential inhibition of

the natural functions of ClpP, metabolic pathways and biomass production may sufficiently proceed while cell division is abrogated due to the preferred degradation of FtsZ by ADEP-ClpP, finally resulting in considerable filamentation of the bacterial cells.

In contrast, when high concentrations of ADEP are applied, *B. subtilis* cells remain short and reveal an uneven cell morphology including bulging and bending (Mayer et al., 2019). The lack of the filamentous phenotype as well as the disturbed cell morphology indicates that under these conditions, severe damage has occurred to the cells. As hypothesized by Mayer and colleagues, this suggests that several other proteins, in addition to FtsZ, were targeted by ADEP-activated ClpP. Moreover, under these conditions, ClpP most likely digests all nascent polypeptides emerging from the ribosome (Kirstein et al., 2009), presumably having a detrimental effect on the cell metabolism. In contrast, at low inhibitory concentrations of ADEP, degradation of nascent peptides at the ribosome might be limited due to the restricted degradative capacity of ADEP-ClpP, explaining why metabolic pathways are maintained and cell growth proceeds. As mentioned earlier, at high ADEP concentrations, cells lack the filamentous phenotype displaying an unenven cell morphoplogy (Mayer et al., 2019). In this context, phenotypes of bending and bulging were also observed in connection with the depletion or mutation of proteins involved in cell wall synthesis and cell division in *B. subtilis* (Popham et al., 1996; Kawai et al., 2009 b; Peters et al., 2016). The degradation of other target proteins, additionally to FtsZ, was also suggested by Conlon and colleagues when they evaluated proteomic data of *S. aureus* cells that were treated with high concentrations of ADEP for a pro-longed time period (Conlon et al., 2016). In their study, more than 400 presumed targets for ADEP-activated ClpP in *S. aureus* have been proposed. We picked three of the proteins (FbaA, PykA, EF-Tu) that Conlon and colleagues listed among those with the most significant decrease in abundance to investigate their degradation. We observed no degradation of FbaA in both, *S. aureus* and *B. subtilis* after 2 h treatment using high concentrations of ADEP whereas FtsZ was completely degraded under the same conditions. *In vitro* degradation assays using FbaA from *B. subtilis* as a substrate, only revealed a slight reduction of the FbaA protein band on SDS-Page. This effect seemed negligible when compared to the degradation of FtsZ. *In vitro* degradation of BsEF-Tu and BsPykA, was not observed (Publication 1, Fig. 1A+B). In this context, it is noteworthy that Conlon and colleagues took samples for proteomic analysis from cultures that were grown to stationary phase and then treated with high ADEP concentrations for an extended time period of 24 h (Conlon et al., 2013). During stationary phase, cells experience stress conditions such as starvation or the accumulation of harmful metabolites which was shown to result in the degradation of several proteins (Michalik et al., 2009). Therefore, with regard to the results obtained by proteomic analysis from Conlon and colleagues, decreased abundance of

proteins might not exclusively relate to degradation by ADEP-activated ClpP, since protein degradation could also be facilitated by other staphylococcal proteases under these conditions. For example, in a recent study, several proteins such as MurG, HemA, or HtrA were identified as substrates for the FtsH protease (Liu et al., 2017) which, however, were also listed as potential ADEP-ClpP substrates in *S. aureus* (Conlon et al., 2013). Thus, FtsZ indeed is a preferred target for ADEP-ClpP, and under the conditions tested, its degradation is not comparable to that of FbaA. However, the phenotype of cells treated with high concentrations of ADEP clearly shows that there are other protein targets for ADEP-ClpP (additionally to FtsZ) in the cell. The idea of other ADEP-ClpP targets than FtsZ is furthermore supported by our finding that the degradation of the model substrates FITC-casein and Suc-LY-AMC could be further increased when using elevated concentrations of ADEP over ClpP. (Publication 1, Fig. 6E). Moreover, we have shown that the C terminus of FtsZ becomes an additional target for ADEP-ClpP at elevated concentrations of ADEP and ClpP (Publication 1, Fig. 6A). Therefore, we suggest that at elevated ADEP concentrations, a saturated ClpP oligomer might gain its maximum destructive capacity. This is further supported by the finding that the stepwise increase of ADEP over ClpP in our *in vitro* degradation experiments revealed that the degradation efficiency stagnates above a molar ratio of 2.5:1 (ADEP:ClpP), indicating that ClpP is fully activated under these conditions and has reached its maximum degradation capacity (Publication 1, Fig. 6B). Under these circumstances the entrance pore is probably enlarged to its full extend, thereby allowing additional target substrates, such as the C terminus of FtsZ, to enter the proteolytic chamber. As the C terminus of FtsZ does not have a distinct hydrophobic nature (Publication 1, Fig. 2A), C-terminal targeting is most probably not mediated by hydrophobic attraction and interaction, but could be conferred by simple diffusion of the extended C terminus through the widened pore of the ClpP barrel. In this context, peptides and intrinsically disordered proteins in the cell might be degraded indiscriminately and in accordance to this, ADEP-ClpP has been shown to degrade nascent polypeptides emerging from the ribosome (Kirstein et al., 2009). Interestingly, C-terminal degradation of FtsZ by ADEP-ClpP does not lead to unfolding and degradation of the entire protein but results only in the shortening of the C terminus (Publication 1, Fig. 6A). It might be speculated that the C-terminal domain of FtsZ possesses a more stable fold compared to the N-terminal domain. However, alternatively, ADEP-ClpP may not be capable to hold the C terminus tight due to its hydrophilicity and therefore cannot C-terminally unfold the protein. The results obtained during this study together with the observed phenotype of *B. subtilis* cells strongly support the hypothesis of additional substrates for ADEP-ClpP at high concentrations of ADEP. Under these conditions, ADEP-ClpP rapidly depletes the cellular FtsZ pool and also effectively degrades peptides emerging from the ribosome. Moreover, ADEP-ClpP may be activated to its full extend, degrading other putative protein targets in addition to FtsZ. The

concomitant inhibition of the natural functions of Clp may further aggravate the effect of ADEP treatment. Usually, ClpP is involved in protein homeostasis, protein quality control, developmental processes as well as virulence (Msadek et al., 1998; Kock et al., 2004). Hence, protein homeostasis is additionally disturbed during ADEP treatment, which could have otherwise relieved protein stress.

To sum this up, the treatment of *B. subtilis* with high concentrations of ADEP presumably unleashes the full destructive power of ADEP-ClpP, resulting in a broadened target spectrum which finally causes serious damage to the cells and rapid killing. In contrast, when low ADEP concentrations are applied, ClpP might be not activated to its full extend. This leads, first and foremost, to the preferred degradation of FtsZ resulting in the depletion of the cytoplasmic FtsZ pool. Hence, under these conditions, Z-ring assembly and cell division are inhibited while biomass production proceeds and cells grow into considerably long filaments. Importantly, filamentation concentrations of ADEP (2-3x MIC) suffice to kill the bacterial cells (Brötz-Oesterhelt et al., 2005; Sass et al., 2011; Mayer et al., 2019) which seems to mostly rely on the depletion of the cytoplasmic FtsZ pool. This aspect will be further discussed in the following section.

4.3 Bacterial killing by the depletion of FtsZ

The antibacterial effects of ADEP at different concentrations were recently investigated on a single cell level. In this context, time-lapse as well as fluorescence microscopy were used to follow morphological changes that finally lead to bacterial killing (Mayer et al., 2019). High ADEP concentrations were shown to lead to the rapid cessation of biomass production and *B. subtilis* cells revealed an uneven cell morphology (Sass et al., 2011; Mayer et al., 2019). This phenotype already indicates that due to the broadened target spectrum of ADEP-ClpP, severe damage has occurred to the cells (as discussed in the previous paragraph). In this regard, the degradation of other essential protein targets (in addition to FtsZ) as well as the degradation of peptides emerging from the ribosome, accompanied with the inhibition of physiological functions of ClpP, result in a drop in CFU and effectively cause bacterial cell death. Thus, time-kill experiments showed that *S. aureus* cells which were treated with high concentrations of ADEP (96x MIC/84 µg/ml) for a short period of time (10 min) were eradicated within 24 h (Mayer et al., 2019). This was also the case when cells were treated with low concentrations of ADEP (2x MIC/1 µg/ml) for an extended period of time (8 h). Interestingly, intermediate concentrations of ADEP (16x MIC/ 8 µg/ml) that were applied for an intermediate period of time (1 h) did not results in bacterial killing. Further investigations revealed that the bactericidal effect of ADEP strictly depends on the exposure time as well as the applied

concentration (Mayer et al., 2019). In this context it was shown that both high ADEP concentrations applied for a short period of time as well as low ADEP concentrations applied for an extended period of time result in cell death, whereas the intermediate situation remarkably is not effective in killing cells (Mayer et al., 2019).

Continuing studies on a single cell level revealed that *B. subtilis* cells that were treated with low concentrations of ADEP (2x MIC/0.125 µg/ml) for 4 have a remarkably high potential to recover and in this context all cells were shown to re-initiate Z-ring formation when shifted into ADEP-free medium (Mayer et al., 2019). Under these conditions, cells proceed biomass production and grow into long filaments during ADEP treatment (Sass et al., 2011). Remarkably, metabolic pathways were shown to be unaffected under these conditions and the syntheses of DNA, RNA, proteins as well as cell wall proceeds (Sass et al., 2011). However, when ADEP was applied for an extended period of time, cells gradually lost their potential to recover and after an exposure time of 6 h only 40% of the cells recovered and re-initiated Z-ring formation (Mayer et al., 2019). Furthermore, Mayer et al. could show that pro-longed treatment with low concentrations of ADEP, from which only 40% of cells recovered, resulted in an aberrant nucleoid morphology (Mayer et al., 2019). We have demonstrated that FtsZ is preferentially targeted by ADEP-ClpP eventually leading to the depletion of the cytoplasmic FtsZ pool (Sass et al., 2011; Silber et al., 2020 b, 2021). Hence, the question arises whether the depletion of the cytoplasmic FtsZ pool alone is sufficient to trigger an abnormal nucleoid morphology and to finally kill bacterial cells after an extended period of time. To answer this question Mayer and colleagues argued that after an extended halt of cell division, cells have entered a state of terminal cell cycle arrest (Mayer et al., 2019). This state is reached when cells have passed the so-called “point of no return” (Arjes et al., 2014). The point of no return was earlier described in a study investigating FtsZ-deprived *B. subtilis* strains (Arjes et al., 2014). In their study, Arjes and co-workers found that during the down-regulation of *ftsZ*, *B. subtilis* remained metabolically active for a certain period of time, while cell division was inhibited. This observation is consistent with findings of our group, showing that cells maintain cellular processes (Sass et al., 2011) at filamentation concentrations of ADEP at which the cytoplasmic FtsZ pool is depleted, thereby remaining viable for at least 4 hours (Mayer et al., 2019; Silber et al., 2021). Furthermore, Arjes and colleagues demonstrated that after a pro-longed period of *ftsZ* depletion, cells have passed the point of no return and lost their potential to recover when shifted to permissive conditions (Arjes et al., 2014). In line with these results, Mayer and colleagues demonstrated that the recovery potential of *B. subtilis* cells is remarkably high when shifted into ADEP-free medium. However, after a pro-longed exposure time, 60% of the cells lost the potential to recover and failed to re-initiate Z-ring formation when shifted into ADEP-free medium. Moreover, these cells had mis-segregated

nucleoids (Mayer et al., 2019). In accordance with this finding, a study from 2016 showed an abnormal high number of unsegregated nucleoids in *E. coli* cells that were deprived of *ftsZ* (Sánchez-Gorostiaga et al., 2016). The authors of this study argued that impaired nucleoid segregation occured due to impaired FtsK-localization due to the absence of FtsZ. Since FtsK displays a linker between nucleoid segregation and cell division in *E. coli* (Yu et al., 1998; Bigot et al., 2005), the segregation of nucleoids may be affected by the loss of FtsZ. In *B. subtilis* chromosome segregation and cell division are also linked, here via SpoIIIE and SftA (Biller et al., 2009; Kaimer et al., 2009). Hence, such interconnection of FtsZ with proteins required for chromosome segregation supports the hypothesis that the ADEP-triggered depletion of FtsZ may be sufficient to further trigger aberrant nucleoid morphology and the entry into a quiescent state from which bacteria cannot recover. However, loss of the recovery potential due to entry into a terminal cell cycle arrest accompanied by abnormal nucleoid morphology was not the only effect under these conditions. Mayer and colleagues furthermore observed that pro-longed treatment periods with low concentrations of ADEP led to defects in the cell envelope and thus to cell lysis of a high number of filaments (Mayer et al., 2019). Since a single *B. subtilis* filament consist of a consortium of multiple cells that are not separated by septa, Mayer and colleagues argued that the loss of cell wall integrity at one position is highly destructive and affects the entire filament (Mayer et al., 2019). Similar observations of lysis prone phenotypes were also made for *B. subtilis* (Beall et al., 1991) and *E. coli* (Sánchez-Gorostiaga et al., 2016) filaments that were deprived of FtsZ by genetic down-regulation. In addition, effects of pro-longed ADEP treatment at filamentation concentrations may also be aggravated due to the inhibition of natural functions of ClpP. Although ClpP is not essential in *B. subtilis* under moderate growth conditions, it may still affect the cell's ability to counteract the ADEP-induced perturbation of the cellular protein content. In mycobacteria, where ClpP is essential for survival, mycobacterial killing by ADEP even solely relies on the inhibition of natural functions of the Clp machinery, and ClpP is not activated for degradation of FtsZ in these species (Famulla et al., 2016). However, in *B. subtilis* ClpP is critical during growth at elevated temperatures and under stress conditions and mutants are impaired in competence development, motility and sporulation (Gerth et al., 1998; Msadek et al., 1998). In this context, the Clp machinery in *B. subtilis* is involved in the degradation of major proteins such as the global transcriptional regulator Spx or the competence transcription factor ComK and further has been shown to be critical for bulk protein turnover (Kock et al., 2004). In this study, we have shown that neither ComK nor Spx were targeted by ADEP-ClpP *in vitro* (Silber et al., 2020 b). Our data clearly show that FtsZ is preferentially degraded by ADEP-ClpP compared to other potential protein targets. At filamentation concentrations of ADEP, this results in the inhibition of cell division due to the rapid depletion of the cytoplasmic FtsZ pool (Sass et al., 2011; Silber et al., 2021). The depletion of the cytoplasmic FtsZ pool triggers multiple,

detrimental downstream effects including an aberrant nucleoid morphology and causes a terminal cell cycle arrest when cell division was inhibited for an extended period of time. Since cells are not able to recover from this state, pro-longed exposure time at filamentation concentrations of ADEP eventually leads to cell death (Mayer et al., 2019). With regard to a potential therapeutic use, the high potential of bacteria to recover from ADEP treatment needs to be considered by adjusting both exposure time and dosage. However, since *B. subtilis* remains metabolically active at filamentation concentrations of ADEP for at least 4 h while cell division is inhibited due to the depletion of the cytoplasmic FtsZ pool, the antibiotic can be used as a tool to study the mechanism of cell division.

4.4 Cell division inhibitors as promising antibiotics and tools to study divisome assembly and progression

Since cell division is an essential process in bacteria, it has emerged as a promising pathway for antibiotic intervention in recent years. Since FtsZ is virtually ubiquitous in bacteria, it in particular represents a promising target for the inhibition of cell division. To date, no clinically applied antibiotic targets bacterial cell division, although there are already anticancer drugs in clinical application, such as the vinca alkaloids and the taxanes, that target tubulin, the eukaryotic homolog of FtsZ (Schiff et al., 1980; Jordan et al., 1993). Most of the FtsZ-targeting compounds known so far directly interfere with FtsZ by targeting its nucleotide binding site or by binding the region of the T7 synergy loop, thereby modulating FtsZ dynamics (see Table 1 in Silber et al., 2020a). However, the most challenging problem in regard to antibiotics that target FtsZ, is presumably the high structural similarity to its eukaryotic homolog tubulin. In this context the nucleotide binding site, for example, includes the tubulin signature motif, a highly conserved sequence pattern in FtsZ and tubulin (Nogales et al., 1998), making cross-targeting a major risk. In line with this, cytotoxicity in human cells is a challenging problem and compounds such as sanguinarine (Beuria et al., 2005; Lopus et al., 2006), viriditoxin (Noh et al., 2017; Su et al., 2020) or plumpagin (de Paiva et al., 2003; Acharya et al., 2008) that have antimicrobial activity, reveal pharmacological side effects. Remarkably, the antibiotics ADEP and PC190723 have shown promise in inhibiting cell division by affecting FtsZ without having the problem of cross-targeting tubulin. In this context, PC190723 directly binds to the interdomain cleft of FtsZ which is formed by Helix H7, the T7 loop and the four beta-sheets of the C-terminal domain. By binding to the interdomain cleft, PC190723 stabilizes FtsZ filaments and halts FtsZ treadmilling (Haydon et al., 2008; Bisson-Filho et al., 2017). Since tubulin lacks the interdomain cleft (Kusuma et al., 2019), PC190723 does not interfere with tubulin *in vitro* (Haydon et al., 2008). Hence, this region represents a promising drug binding pocket with a

high selectivity for FtsZ and was therefore recently referred to as the achilles heel of FtsZ (Kusuma et al., 2019; Pradhan et al., 2021). In general, the interdomain cleft is not highly conserved across different bacterial species and varies regarding its amino acid composition, size, and accessibility (Kusuma et al., 2019; Pradhan et al., 2021). This heterogeneity might pose a challenge with respect to the development of broad-spectrum antibiotics that target the interdomain cleft, but allows for the development of highly selective compounds. Unlike all other FtsZ-targeting antibiotics known so far, the mode of action of ADEP displays a different and novel mechanism by activating the ClpP peptidase for uncontrolled proteolysis. Although ADEP deregulates ClpP, we could show that ADEP treatment first and foremost led to the preferred degradation of FtsZ and a subsequent depletion of the cytoplasmic FtsZ pool (Silber et al., 2020 b, 2021). Remarkably, ADEP does not directly target FtsZ, however, it triggers the ClpP-mediated degradation of FtsZ, thereby inhibiting cell division in an unprecedented manner. The depletion of the cytoplasmic FtsZ pool by ADEP-activated ClpP leads to the abrogation of FtsZ dynamics, which causes the inhibition of cell division and eventually results in cell death as discussed in the previous chapter. Interestingly, the effect of ADEP appeared to be multifaceted and we presented different cascades of events that are triggered by different ADEP levels present in the cell. In this context, both high concentrations applied for a short period of time as well as low concentrations of ADEP applied for a pro-longed time period were shown to result in cell death (Mayer et al., 2019). With regard to pharmacodynamic properties, these results underlined the unique mode of action of ADEP and its high potential for clinical application, since usually killing by antimicrobial drugs either depends on exposure time or on concentration (Levison, 2004). Although ADEP was also shown to deregulate human mitochondrial ClpP *in vitro* (Lowth et al., 2012), cytotoxicity was only observed when ADEP levels were 100 - 1000 times higher than the bacterial MIC (Brötz-Oesterhelt et al., 2005; Arvanitis et al., 2016; Wong et al., 2018). ADEPs have proven promising activity against Gram-positive bacteria, including life-threatening pathogens such as MRSA or VRE, with an MIC in the range of 0.01 – 0.05 µg/ml (Brötz-Oesterhelt et al., 2005). The compound PC190723 was also shown to be active against Gram-positive bacteria and revealed an MIC in the range of 0.5 – 1 µg/ml against staphylococci, including MRSA (Haydon et al., 2008). Noteworthy, PC190723 was the first compound that was reported to have *in vivo* efficacy. In this regard, 100% of mice that were challenged with a lethal dose of *S. aureus* survived after the intravenous application of PC190723 (Haydon et al., 2008). However, spontaneous resistance against PC190723 in *S. aureus* was observed to occur with a frequency of 2×10^{-8}. Furthermore, PC190723 was found to have poor pharmacokinetic properties and thus never entered clinical application. The optimization of PC190723, however, yielded compounds 1 and 2 that revealed improved antimicrobial activities and pharmacokinetic properties (Stokes et al., 2013), thereby representing promising lead structures. Other derivatives of PC190723,

i.e., TXA541, TXA709, and compound 9, showed increased efficacy against staphylococci and decreased cytotoxicity. Moreover, compound 9 revealed activity against mycobacteria (Kaul et al., 2013, 2015; Hu et al., 2017). In addition, PC190723 and derivatives thereof were shown to re-sensitize MRSA to β-lactam antibiotics showing a synergistic effect when combined with imipenem, cefdinir or cefuroxime (Tan et al., 2012; Kaul et al., 2016; Lui et al., 2019). It was furthermore shown that the combination of cefdinir and TXA709 not only had a synergistic effect but also reduced the resistance frequency in MRSA (Kaul et al., 2016), highlighting the potential for combination therapy with derivatives of PC190723. Promising antibiotic activity was also observed for ADEP, however, spontaneous ADEP-resistant mutants of different Firmicutes were observed *in vitro* and occured with a rate of 10^{-6}. Of note, all isolates carried a mutation in the *clpP* gene (Malik et al., 2020). In the majority of the selected ADEP-resistant isolates, mutations in ClpP either affected the catalytic activity or tetradecamer formation of ClpP. All mutations seemed to result in a Clp machinery that was out-of-function. This was also the case when ADEP binding sites were mutated, as mutations here also abrogated the interaction with the Clp-ATPases (Malik et al., 2020). ClpP is not essential under moderate conditions under which ADEP resistant mutants were selected. However, retaining the full activity of ClpP might be of greater importance during host infection and thus the resistance rate might be lower under these circumstances. The combination of ADEP with other antibiotics was particularly recommended (Brötz-Oesterhelt et al., 2021). In this context, a recent study showed that the combination of ADEP4 with linezolid and oxacillin is highly effective against MRSA (Mroue et al., 2019). Furthermore, in combination with rifampicin, ADEP4 not only eradicated a variety of *S. aureus* strains including USA300 but also eradicated a staphylococcal biofilm *in vitro* as well as in a mouse model (Conlon et al., 2013). Biofilms pose a major health concern during antibacterial therapy as they are enriched with so-called persister cells. Persisters are dormant cells with down-regulated vital processes that are regarded as the main reason for antibiotic resistance during bacterial infections (Lewis, 2007). It has been shown that the entry into the dormant state coincides with a drop in the cellular ATP level, thereby presumably also decreasing the activity of potential drug targets (Conlon et al., 2016). Remarkably, ADEP antibiotics act via an ATP-independent ClpP over-activation mechanism and thus can exert antimicrobial activity against persisters even though their vital processes are down-regulated. Therefore, ADEP represents a promising antibiotic for clinical application interfering with bacterial cell division via an unprecedented mode of action. In this thesis, we have demonstrated that FtsZ is a highly vulnerable target for degradation by ADEP-activated ClpP (Sass et al., 2011; Silber et al., 2020 b) and that, when applied at filamentation concentrations, ADEP triggers the depletion of the cytoplasmic FtsZ pool (Sass et al., 2011; Mayer et al., 2019; Silber et al., 2021). Under these conditions cell division is inhibited, while cellular processes proceed for several hours (Sass et al., 2011; Mayer et al., 2019).

Furthermore, cells appeared to have a remarkably high potential to recover when shifted into ADEP-free medium (Mayer et al., 2019). Together, these results establish the antibiotic as a suitable tool to study the mechanism of cell division in Gram-positive bacteria. In addition, the high potential to recover from ADEP treatment furthermore allows to use ADEP as a switch between the inhibition of cell division and normal growth (Mayer, 2020). Following the idea of using ADEP as a tool, it may not only be used to study cell division in living cells, but could also represent an interesting tool to investigate structural features of FtsZ. In this context, an *in vitro* assay with ADEP and ClpP could be used to investigate distinct features of FtsZ from different organisms. Interestingly, ADEP-activated ClpP from *B. subtilis* was shown to degrade FtsZ from different organisms including *B. subtilis* (Sass et al., 2011), *S. aureus* (Silber et al., 2020 b), *E. coli* (unpublished data), as well as *Mycobacterium tuberculosis* (Famulla et al., 2016). Since CD spectrometry data that were obtained during guanidinium chloride unfolding of *Methanococcus jannaschii* FtsZ (MjFtsZ) revealed a higher stability of MjFtsZ compared to EcFtsZ (Andreu et al., 2002), an *in vitro* degradation assay with ADEP-ClpP might help to investigate the different stabilities of FtsZ from various organisms with respect to unfolding and degradation. These results may provide novel insight into the general folding state and the stability of the essential cell division protein FtsZ. The compound PC190723 was also shown to be a suitable tool for studying cell division in Gram-positive bacteria (Bisson-Filho et al., 2017; Monteiro et al., 2018; Whitley et al., 2021). Since treatment with PC190723 results in a rapid arrest of FtsZ treadmilling (Bisson-Filho et al., 2017) the compound was used to investigate distinct stages during cell division (Monteiro et al., 2018; Whitley et al., 2021).

In this thesis, we used filamentation concentrations of ADEP to deplete the cytoplasmic FtsZ pool of *B. subtilis.* The depletion of the cytoplasmic FtsZ pool under these conditions eventually resulted in the inhibition of cell division due to the abrogation of FtsZ dynamics. Similar to PC190723, ADEP abrogated FtsZ dynamics without the need of genetic manipulation. However, PC190723 was shown to stabilize FtsZ (Haydon et al., 2008; Bisson-Filho et al., 2017) filaments that remain in the cell. In contrast, at filamentation concentrations of ADEP, FtsZ was preferably degraded and the drop of the cellular level of FtsZ resulted in the halt of FtsZ dynamics. This allowed us to study Z-ring assembly and progression in dependence of the cytoplasmic FtsZ pool. In this work, we successfully validated the antibiotic ADEP as a tool to study cell division and thereby gained novel insights into the principles of cytokinesis (see next chapter).

4.5 Depletion of the cytoplasmic FtsZ pool differently affects early- and late-stage divisomes

Cell division in bacteria is mainly orchestrated by FtsZ. Driven by GTP consumption, FtsZ polymerizes into protofilaments that build higher ordered structures via lateral interactions (Sundararajan et al., 2017), eventually assembling the Z-ring at the future division site. FtsZ is the first protein to localize to mid-cell initiating divisome assembly and serving as a scaffold for other proteins to adhere to. In the course of cell division, assembly of the divisome proceeds and the Z-ring constricts in order to build the septal cell wall. Although bacterial cell division has been studied intensively since the discovery of FtsZ in 1980 (Lutkenhaus et al., 1980), it remained enigmatic how bacteria generate the force to constrict the cell membrane during cytokinesis and this issue has been the subject of intense debate during the past years. Principally, it was assumed that the force is generated either by peptidoglycan synthesis (Li et al., 2007, 2013; Coltharp et al., 2016, 2017) or by GTP hydrolysis. In the latter case, FtsZ and its dynamic treadmilling motion was proposed to be the main driving force, capable of exerting a mechanical force on the membrane originating from its GTP-hydrolyzing properties (Li et al., 2007, 2013; Coltharp et al., 2017). Indeed, when the C terminus of FtsZ was fused to an amphipathic helix that functioned as a membrane anchor, GTP-consuming FtsZ was sufficient to invaginate liposomes in the absence of other divisome proteins (Osawa et al., 2008, 2009). However, the situation in cells may be different in comparison to the *in vitro* situation. Indeed, a study from 2016 suggested that FtsZ alone is not able to invaginate the membrane of an *E. coli* cell (Daley et al., 2016). In their study, the authors found cell constriction to be dependent on the presence of FtsN, which in *E. coli* represents the allosteric activator for peptidoglycan synthesis (Weiss, 2015; Daley et al., 2016). In 2017, two independent studies revealed that in rod-shaped *E. coli* and *B. subtilis* cells, treadmilling of FtsZ filaments guides enzymes of the cell wall synthesis machinery around the division plane. Even though, it was suggested that FtsZ treadmilling and peptidoglycan synthesis are coupled (Bisson-Filho et al., 2017; Yang et al., 2017), it remained elusive whether the dynamic motion of FtsZ was required throughout the complete cell division process. The Z-ring is highly dynamic and rearranges quickly (Stricker et al., 2002; Anderson et al., 2004), and its directed growth strictly relies on the constant exchange of FtsZ monomers with the cytoplasmic pool (Qin et al., 1998; Erickson et al., 2010). In this thesis, we have shown that filamentation concentrations of ADEP trigger the ClpP-mediated untimely degradation of FtsZ, thereby inhibiting cell division. Under these conditions, biomass production proceeds and cellular processes are maintained (Sass et al., 2011). As a result, cells remain viable for at least 4 h and grow into long filaments (Sass et al., 2011; Mayer et al., 2019). Since FtsZ represents an especially vulnerable target for ADEP-ClpP that is preferably attacked and degraded in bacterial cells, resulting in the depletion of

the cytoplasmic FtsZ pool within minutes (Sass et al., 2011; Mayer et al., 2019; Silber et al., 2021), we set out to employ the antibiotic ADEP as a tool to investigate the role of the cytoplasmic pool of FtsZ. The cytoplasmic FtsZ pool is required for Z-ring dynamics in the assembly and progression of the Z-ring and the divisome during the process of cell division. In the context of divisome assembly, a study from 2009 revealed that divisome assembly in *B. subtilis* follows to steps (Gamba et al., 2009). In this context, proteins have been categorized as either early or late divisome proteins, the latter including enzymes that are involved in synthesizing the septal cell wall (e.g. PBP2b) (Gamba et al., 2009). Related results were obtained by the group of Ethan Garner, who suggested that the *B. subtilis* divisome consists of two subcomplexes. In this regard, one subcomplex comprises stationary cytoplasmic proteins that directly bind to FtsZ within a treadmilling filament (Squyres et al., 2021) The FtsZ-binding proteins FtsA, EzrA, SepF and ZapA, that represent early divisome proteins (Gamba et al., 2009), have been shown to bundle treadmilling FtsZ filaments, thereby supporting the condensation of FtsZ bundles into the Z-ring (Squyres et al., 2021). Furthermore, this condensation event was revealed to be critical to build the Z-ring and to initiate cell division (Squyres et al., 2021). The second subcomplex includes peptidoglycan-synthesizing enzymes that move around the division plane alongside with treadmilling FtsZ filaments (Squyres et al., 2021). In this thesis, we investigated whether distinct phases during cell division depend equally on the cytoplasmic FtsZ pool. Our results showed that ADEP treatment prevents the formation of new Z-rings and furthermore lead to the disintegration of all early stage Z-rings. Since the dynamic motion of the Z-ring at steady-state strictly depends on the constant exchange of FtsZ monomers with the cytoplasmic pool (Anderson et al., 2004; Erickson et al., 2010), depletion of the FtsZ pool eventually resulted in the decomposition of early stage Z-rings, corroborating the importance of FtsZ dynamics in Z-ring formation. Moreover, we observed that the formation of new Z-rings was suppressed which is the direct consequence of reduced cellular FtsZ levels below the critical concentration, that is required for polymerization of FtsZ (Mukherjee et al., 1998, 1999). In contrast, all Z-rings that were in a progressed phase constricted and finalized septum formation, eventually dividing the mother cell into two daughter cells. These Z-rings appeared to be unaffected by the depletion of the cytoplasmic FtsZ pool, indicating that during this later stage of cell division, divsome progression may be driven by other triggers, but does not seem to depend on the cytoplasmic FtsZ pool and FtsZ dynamics. To further investigate this, we localized the peptidoglycan synthase PBP2b as a cellular marker for the late-stage divisome. Our data shows that the localization of substantial amounts of PBP2b at mid-cell coincides with cells that finalized cell division. In line with these results, our data furthermore revealed, that progressed Z-rings (indicated by the arrival of the late-stage divsiome protein PBP2b) are unaffected by the depletion of the cytoplasmic FtsZ pool. In contrast, during early phases of divisome assembly,

when no clear foci of fluorescently labelled PBP2b were observed to be localized at mid-cell (Silber et al., 2021), early divisomes disintegrated upon ADEP treatment, indicating that divisome assembly presumably strictly relies on FtsZ dynamics. Our results were further corroborated by Whitley and colleagues in a recent study that investigated the role of FtsZ treadmilling by making use of the compound PC190723. Their data showed that a halt of FtsZ treadmilling does not affect septal cell wall synthesis when it was once initiated. The authors suggested that FtsZ treadmilling is needed to condense FtsZ filaments into a distinct Z-ring at mid-cell, and that FtsZ treadmilling is important to initiate cell constriction. However, in consistence with our findings, Whitley and colleagues revealed that FtsZ treadmilling becomes dispensable after constriction initiation (Whitley et al., 2021). Similar results were also obtained in spherical *S. aureus* cells using PC190723, where the arrival of the putative lipid II flippase MurJ at the division site coincided with an FtsZ treadmilling independent step of cytokinesis (Monteiro et al., 2018).

Our results presented here, support a two step-model of divisome assembly and progression (Fig. 8): During the first step, Z-ring formation and dynamics strictly rely on the cytoplasmic FtsZ pool. In this phase, a certain level of the FtsZ pool is needed to initiate Z-ring assembly at mid-cell. Furthermore, during the first step, the FtsZ pool ensures a constant supply with FtsZ monomers to maintain Z-ring dynamics which is critical during this phase. However, during the second step, which is initiated by the arrival of late-stage divisome proteins, the cytoplasmic FtsZ pool becomes dispensable. During this phase, divisome progression does not rely on the cytoplasmic FtsZ pool and Z-ring dynamics but may be driven by late-stage triggers, such as peptidoglycan synthases that finalize septum formation (Silber et al., 2021). The result in this study therefore revealed a step during cell division in *B. subtilis* that is independent of FtsZ dynamics, and successfully established the antibiotic ADEP as a novel tool to investgate the mechanism of cell division in Gram-positive bacteria.

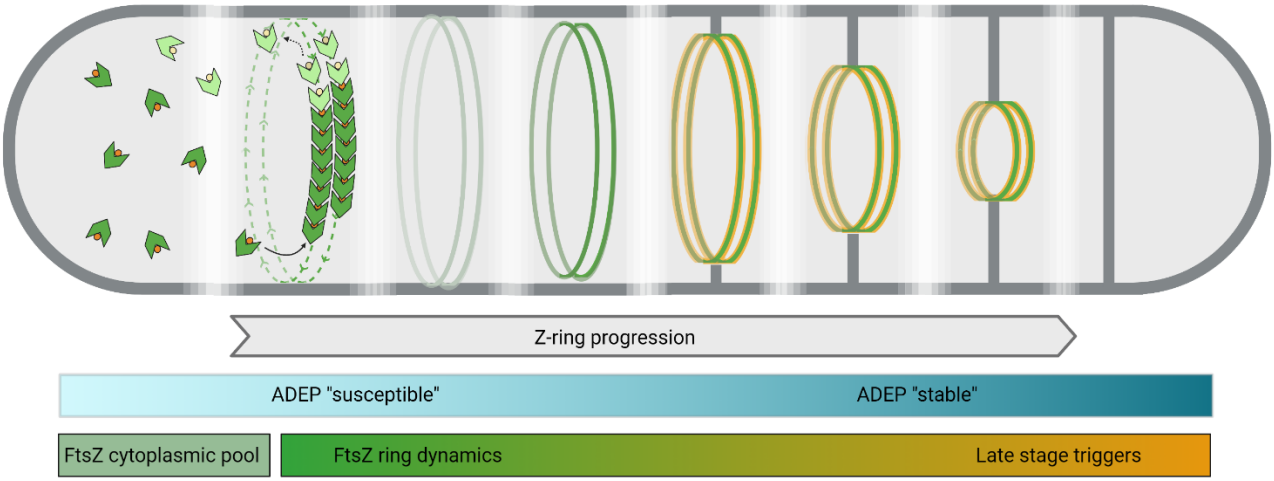

Fig. 8: Z-ring assembly and progression follows a two-step model. ADEP treatment with concentrations close to the MIC results in the rapid depletion of cytoplasmic FtsZ (Sass et al., 2011; Mayer et al., 2019; Silber et al., 2020 b). Our data show that early Z-rings (in green) disintegrate upon ADEP treatment, whereas progressed Z-rings (framed orange) are unaffected by ADEP treatment and finalize septum formation and cell division. Hence, our data suggest a two-step model: during the first step, initiation of Z-ring formation and assembly of the early divisome strictly rely on FtsZ dynamics. In this phase, Z-rings disintegrate upon ADEP-treatment due to the depletion of the cytoplasmic FtsZ pool that is required for FtsZ dynamics. During the second step, Z-ring dynamics becomes less important and the divisome finalizes cell division independent of the depletion of cytoplasmic FtsZ pool. During this phase, cell division might be driven by other triggers such as peptidoglycan synthases that arrive at the division site. The figure was adapted from Silber et al., 2021 and modified using BioRender software.

5 References

Abhayawardhane, Y.; Stewart, G. C., 1995: *Bacillus subtilis* possesses a second determinant with extensive sequence similarity to the *Escherichia coli mreB* morphogene. *Journal of bacteriology*., **177**, 765–773.

Acharya, B. R.; Bhattacharyya, B.; Chakrabarti, G., 2008: The natural naphthoquinone plumbagin exhibits antiproliferative activity and disrupts the microtubule network through tubulin binding. *Biochemistry*., **47**, 7838–7845.

Adams, D. W.; Wu, L. J.; Czaplewski, L. G.; Errington, J., 2011: Multiple effects of benzamid antibiotics on FtsZ function. *Molecular microbiology*., **80**, 68–84.

Anderson, D. E.; Gueiros-Filho, F. J.; Erickson, H. P., 2004: Assembly dynamics of FtsZ rings in *Bacillus subtilis* and *Escherichia coli* and effects of FtsZ-regulating proteins. *Journal of bacteriology*., **186**, 5775–5781.

Andreu, J. M.; Oliva, M. A.; Monasterio, O., 2002: Reversible unfolding of FtsZ cell division proteins from archaea and bacteria: comparison with eukaryotic tubulin folding and assembly. *Journal of Biological Chemistry*., **277**, 43262–43270.

Andreu, J. M.; Schaffner-Barbero, C.; Huecas, S.; Alonso, D.; Lopez-Rodriguez, M. L.; Ruiz-Avila, L. B.; Núñez-Ramírez, R.; Llorca, O.; Martín-Galiano, A. J., 2010: The antibacterial cell divisioninhibitor PC190723 is an FtsZ polymer-stabilizing agent that induces filament assembly and condensation. *The Journal of biological chemistry*., **285**, 14239–14246.

Angert, E. R., 2005: Alternatives to binary fission in bacteria. *Nature Reviews Microbiology*., **3**, 214–224.

Arjes, H. A.; Kriel, A.; Sorto, N. A.; Shaw, J. T.; Wang, J. D.; Levin, P. A., 2014: Failsafe mechanisms couple division and DNA replication in bacteria. *Current Biology*., **24**, 2149-2155.

Artola, M.; Ruíz-Avila, L. B.; Ramírez-Aportela, E.; Martínez, R. F.; Araujo-Bazán, L.; Vázquez-Villa, H.; Martín-Fontecha, M.; Oliva, M. A.; Martín-Galiano, A. J.; Chacón, P.; López-Rodríguez,M. L.; Andreu, J. M.; Huecas, S., 2017: The structural assembly switch of cell division protein FtsZ probed with fluorescent allosteric inhibitors. *Chemical Science*., **8**,1525–1534.

Arvanitis, M.; Li, G.; Li, D. D.; Cotnoir, D.; Ganley-Leal, L.; Carney, D. W.; Sello, J. K.; Mylonakis, E., 2016: A conformationally constrained cyclic acyldepsipeptide is highly effective in mice infected with methicillin-susceptible and -resistant *Staphylococcus aureus*. *PloS one*., **11**, e0153912.

Beall, B.; Lutkenhaus, J., 1991: FtsZ in *Bacillus subtilis* is required for vegetative septation and for asymmetric septation during sporulation. *Genes & development*., **5**, 447–455.

Bernhardt, T. G.; de Boer, P. A. J., 2005: SlmA, a nucleoid-associated, FtsZ binding protein required for blocking septal ring assembly over chromosomes in *E. coli. Molecular cell*., **18**, 555–564.

Beuria, T. K.; Santra, M. K.; Panda, D., 2005: Sanguinarine blocks cytokinesis in bacteria by inhibiting FtsZ assembly and bundling. *Biochemistry*., **44**, 16584–16593.

Bigot, S.; Saleh, O. A.; Lesterlin, C.; Pages, C.; El Karoui, M.; Dennis, C.; Grigoriev, M.; Allemand, J. F.; Barre, F. X.; Cornet, F., 2005: KOPS: DNA motifs that control *E. coli* chromosome segregation by orienting the FtsK translocase. *The EMBO journal*., **24**, 3770–3780.

Biller, S. J.; Burkholder, W. F., 2009: The *Bacillus subtilis* SftA (YtpS) and SpoIIIE DNA translocases play distinct roles in growing cells to ensure faithful chromosome partitioning. *Molecular Microbiology*., **74**, 790–809.

Bisson-Filho, A. W.; Hsu, Y. P.; Squyres, G. R.; Kuru, E.; Wu, F.; Jukes, C.; Sun, Y.; Dekker, C.; Holden, S.; VanNieuwenhze, M. S.; Brun, Y. V; Garner, E. C., 2017: Treadmilling by FtsZfilaments drives peptidoglycan synthesis and bacterial cell division. *Science*., **355**, 739 LP – 743.

Blasios, V.; Bisson-Filho, A. W.; Castellen, P.; Nogueira, M. L. C.; Bettini, J.; Portugal, R. V; Zeri, A. C. M.; Gueiros-Filho, F. J., 2013: Genetic and biochemical characterization of the MinC-FtsZ interaction in *Bacillus subtilis*. *PLOS ONE*., **8**, e60690.

Bramkamp, M.; Emmins, R.; Weston, L.; Donovan, C.; Daniel, R. A.; Errington, J., 2008: A novel component of the division-site selection system of *Bacillus subtilis* and a new mode of action for the division inhibitor MinCD. *Molecular Microbiology*., **70**, 1556–1569.

Brötz-Oesterhelt, H.; Beyer, D.; Kroll, H. P.; Endermann, R.; Ladel, C.; Schroeder, W.; Hinzen, B.; Raddatz, S.; Paulsen, H.; Henninger, K.; Bandow, J. E.; Sahl, H. G.; Labischinski, H., 2005: Dysregulation of bacterial proteolytic machinery by a new class of antibiotics. *Nature medicine*., **11**, 1082–1087.

Brötz-Oesterhelt, H.; Vorbach, A., 2021: Reprogramming of the caseinolytic protease by ADEP antibiotics: molecular mechanism, cellular consequences, therapeutic potential. *Frontiers in molecular biosciences*., **8**, 690902.

Brown Gandt, A.; Griffith, E. C.; Lister, I. M.; Billings, L. L.; Han, A.; Tangallapally, R.; Zhao, Y.; Singh, A. P.; Lee, R. E.; LaFleur, M. D., 2018: *In vivo* and *in vitro* effects of a ClpP-activating antibiotic against vancomycin-resistant enterococci. *Antimicrobial Agents and Chemotherapy*., **62**, e00424-18.

Buske, P. J.; Levin, P. A., 2012: Extreme C terminus of bacterial cytoskeletal protein FtsZ plays fundamental role in assembly independent of modulatory proteins. *The Journal of biological chemistry*., **287**, 10945–10957.

Buske, P. J.; Levin, P. A., 2013: A flexible C-terminal linker is required for proper FtsZ assembly *in vitro* and cytokinetic ring formation *in vivo*. *Molecular microbiology*., **89**, 249–263.

Buske, P. J.; Mittal, A.; Pappu, R. V; Levin, P. A., 2015: An intrinsically disordered linker plays a critical role in bacterial cell division. *Seminars in cell & developmental biology*., **37**, 3–10.

Camilloni, C.; Bonetti, D.; Morrone, A.; Giri, R.; Dobson, C. M.; Brunori, M.; Gianni, S.; Vendruscolo, M., 2016: Towards a structural biology of the hydrophobic effect in protein folding. *Scientific Reports*., **6**, 28285.

Carballido-López, R.; Formstone, A.; Li, Y.; Ehrlich, S. D.; Noirot, P.; Errington, J., 2006: Actin homolog MreBH governs cell morphogenesis by localization of the cell wall hydrolase LytE. *Developmental Cell*., **11**, 399–409.

Cho, H.; Wivagg, C. N.; Kapoor, M.; Barry, Z.; Rohs, P. D. A.; Suh, H.; Marto, J. A.; Garner, E. C.; Bernhardt, T. G., 2016: Bacterial cell wall biogenesis is mediated by SEDS and PBP polymerase families functioning semi-autonomously. *Nature Microbiology*., **1**, 16172.

Claessen, D.; Emmins, R.; Hamoen, L. W.; Daniel, R. A.; Errington, J.; Edwards, D. H., 2008: Control of the cell elongation-division cycle by shuttling of PBP1 protein in *Bacillus subtilis*. *Molecular microbiology*., **68**, 1029–1046.

Cohan, M. C.; Eddelbuettel, A. M. P.; Levin, P. A.; Pappu, R. V, 2020: Dissecting the functional contributions of the intrinsically disordered C-terminal tail of *Bacillus subtilis* FtsZ. *Journal of Molecular Biology*., **432**, 3205–3221.

Coltharp, C.; Buss, J.; Plumer, T. M.; Xiao, J., 2016: Defining the rate-limiting processes of bacterial cytokinesis. *Proceedings of the National Academy of Sciences*., **113**, E1044 LP-E1053.

Coltharp, C.; Xiao, J., 2017: Beyond force generation: Why is a dynamic ring of FtsZ polymers essential for bacterial cytokinesis? *BioEssays : news and reviews in molecular, cellular and developmental biology*., **39**, 1–11.

Conlon; Nakayasu; Fleck; LaFleur; Isabella; Coleman; Leonard; Smith; Adkins; Lewis, 2013: Activated ClpP kills persisters and eradicates a chronic biofilm infection. *Nature*., **503**, 365–370.

Conlon, B. P.; Rowe, S. E.; Gandt, A. B.; Nuxoll, A. S.; Donegan, N. P.; Zalis, E. A.; Clair, G.; Adkins, J. N.; Cheung, A. L.; Lewis, K., 2016: Persister formation in *Staphylococcus aureus* is associated with ATP depletion. *Nature microbiology*., **1**.

Cooper, S.; Helmstetter, C. E., 1968: Chromosome replication and the division cycle of *Escherichia coli* B/r. *Journal of Molecular Biology*., **31**, 519–540.

Daley, D. O.; Skoglund, U.; Söderström, B., 2016: FtsZ does not initiate membrane constriction at the onset of division. *Scientific Reports*., **6**, 33138.

Daniel, R. A.; Harry, E. J.; Katis, V. L.; Wake, R. G.; Errington, J., 1998: Characterization of the essential cell division gene *ftsL* (*yllD*) of *Bacillus subtilis* and its role in the assembly of the division apparatus. *Molecular Microbiology*., **29**, 593–604.

Daniel, R. A.; Errington, J., 2000a: Intrinsic instability of the essential cell division protein FtsL of *Bacillus subtilis* and a role for DivIB protein in FtsL turnover. *Molecular microbiology*., **36**, 278–289.

Daniel, R. A.; Harry, E. J.; Errington, J., 2000b: Role of penicillin-binding protein PBP 2B in assembly and functioning of the division machinery of *Bacillus subtilis*. *Molecular microbiology*., **35**, 299–311.

Daniel, R. A.; Noirot-Gros, M. F.; Noirot, P.; Errington, J., 2006: Multiple interactions between the transmembrane division proteins of *Bacillus subtilis* and the role of FtsL instability in divisome assembly. *Journal of Bacteriology*., **188**, 7396 LP – 7404.

de Boer, P.; Crossley, R.; Rothfield, L., 1992: The essential bacterial cell-division protein FtsZ is a GTPase. *Nature*., **359**, 254–256.

de Paiva, S. R.; Figueiredo, M. R.; Aragão, T. V.; Kaplan, M. A. C., 2003: Antimicrobial activity *in vitro* of plumbagin isolated from Plumbago species. *Memorias do Instituto Oswaldo Cruz*., **98**, 959–961.

Defeu Soufo, H. J.; Graumann, P. L., 2004: Dynamic movement of actin-like proteins within bacterial cells. *EMBO reports*., **5**, 789–794.

Den Blaauwen, T.; Aarsman, M. E. G.; Vischer, N. O. E.; Nanninga, N., 2003: Penicillin-binding protein PBP2 of *Escherichia coli* localizes preferentially in the lateral wall and at mid-cell in comparison with the old cell pole. *Molecular microbiology*., **47**, 539–547.

Díaz, J. F.; Kralicek, A.; Mingorance, J.; Palacios, J. M.; Vicente, M.; Andreu, J. M., 2001: Activation of cell division protein FtsZ. Control of switch loop T3 conformation by the nucleotide gamma-phosphate. *The Journal of biological chemistry*., **276**, 17307-17315.

Donachie, W. D., 1968: Relationship between cell size and time of initiation of DNA replication. *Nature*., **219**, 1077–1079.

Donachie, W. D.; Begg, K. J.; Vicente, M., 1976: Cell length, cell growth and cell division. *Nature*., **264**, 328–333.

Du, S.; Pichoff, S.; Kruse, K.; Lutkenhaus, J., 2018: FtsZ filaments have the opposite kinetic polarity of microtubules. *Proceedings of the National Academy of Sciences*., **115**, 10768 LP – 10773.

Elsen, N. L.; Lu, J.; Parthasarathy, G.; Reid, J. C.; Sharma, S.; Soisson, S. M.; Lumb, K. J., 2012: Mechanism of action of the cell-division inhibitor PC190723: modulation of FtsZ assembly cooperativity. *Journal of the American Chemical Society*., **134**, 12342–12345.

Emami, K.; Guyet, A.; Kawai, Y.; Devi, J.; Wu, L. J.; Allenby, N.; Daniel, R. A.; Errington, J., 2017: RodA as the missing glycosyltransferase in *Bacillus subtilis* and antibiotic discovery for the peptidoglycan polymerase pathway. *Nature Microbiology*., **2**, 16253.

Erickson, H. P., 1997: FtsZ, a tubulin homologue in prokaryote cell division. *Trends in Cell Biology*., **7**, 362–367.

Erickson, H. P.; Anderson, D. E.; Osawa, M., 2010: FtsZ in bacterial cytokinesis: cytoskeleton and force generator all in one. *Microbiology and Molecular Biology Reviews*., **74**, 504 LP–528.

Errington, J.; Daniel, R. A.; Scheffers, D. J., 2003: Cytokinesis in bacteria. *Microbiology and molecular biology reviews : MMBR*., **67**, 52–65, table of contents.

Errington, J.; Wu, L. J., 2017: Cell cycle machinery in *Bacillus subtilis*. *Sub-cellular biochemistry*., **84**, 67–101.

Famulla; Sass; Malik; Akopian; Kandror; Alber; Hinzen; Ruebsamen-Schaeff; Kalscheuer; Goldberg; Brötz-Oesterhelt, 2016: Acyldepsipeptide antibiotics kill mycobacteria by preventing the physiological functions of the ClpP1P2 protease. *Molecular microbiology*., **101**, 194 – 209.

Figge, R. M.; Divakaruni, A. V; Gober, J. W., 2004: MreB, the cell shape-determining bacterial actin homologue, co-ordinates cell wall morphogenesis in *Caulobacter crescentus*. *Molecular Microbiology*., **51**, 1321–1332.

Frees, D.; Savijoki, K.; Varmanen, P.; Ingmer, H., 2007: Clp ATPases and ClpP proteolytic complexes regulate vital biological processes in low GC, Gram-positive bacteria. *Molecular Microbiology*., **63**, 1285–1295.

Gamba, P.; Veening, J. W.; Saunders, N. J.; Hamoen, L. W.; Daniel, R. A., 2009: Two-step assembly dynamics of the *Bacillus subtilis* divisome. *Journal of Bacteriology*., Vol. 191pp. 4186 LP–4194.

Gamba, P.; Hamoen, L. W.; Daniel, R. A., 2016: Cooperative recruitment of FtsW to the division site of *Bacillus subtilis*. *Frontiers in Microbiology*.

Garcia-Seisdedos, H.; Empereur-Mot, C.; Elad, N.; Levy, E. D., 2017: Proteins evolve on the edge of supramolecular self-assembly. *Nature*., **548**, 244–247.

Gardner, K. A. J. A.; Moore, D. A.; Erickson, H. P., 2013: The C-terminal linker of *Escherichia coli* FtsZ functions as an intrinsically disordered peptide. *Molecular microbiology*., **89**, 264–275.

Garner, E. C.; Bernard, R.; Wang, W.; Zhuang, X.; Rudner, D. Z.; Mitchison, T., 2011: Coupled, circumferential motions of the cell wall synthesis machinery and MreB filaments in *B. subtilis*. *Science (New York, N.Y.)*., **333**, 222–225.

Gérard, P.; Vernet, T.; Zapun, A., 2002: Membrane topology of the *Streptococcus pneumoniae* FtsW division protein. *Journal of bacteriology*., **184**, 1925–1931.

Gersch, M.; Famulla, K.; Dahmen, M.; Göbl, C.; Malik, I.; Richter, K.; Korotkov, V. S.; Sass, P.; Rübsamen-Schaeff, H.; Madl, T.; Brötz-Oesterhelt, H.; Sieber, S. A., 2015: AAA+ chaperones and acyldepsipeptides activate the ClpP protease via conformational control. *Nature Communications*., **6**, 6320.

Gerth, U.; Krüger, E.; Derré, I.; Msadek, T.; Hecker, M., 1998: Stress induction of the *Bacillus subtilis clpP* gene encoding a homologue of the proteolytic component of the Clp protease and the involvement of ClpP and ClpX in stress tolerance. *Molecular Microbiology*., **28**, 787–802.

Gottesman, S.; Roche, E.; Zhou, Y.; Sauer, R. T., 1998: The ClpXP and ClpAP proteases degrade proteins with carboxy-terminal peptide tails added by the SsrA-tagging system. *Genes & development*., **12**, 1338–1347.

Gueiros-Filho, F. J.; Losick, R., 2002: A widely conserved bacterial cell division protein that promotes assembly of the tubulin-like protein FtsZ. *Genes & development*., **16**, 2544–2556.

Gündoğdu, M. E.; Kawai, Y.; Pavlendova, N.; Ogasawara, N.; Errington, J.; Scheffers, D. J.; Hamoen, L. W., 2011: Large ring polymers align FtsZ polymers for normal septum formation. *The EMBO Journal*., **30**, 617–626.

Haeusser, D. P.; Schwartz, R. L.; Smith, A. M.; Oates, M. E.; Levin, P. A., 2004: EzrA prevents aberrant cell division by modulating assembly of the cytoskeletal protein FtsZ. *Molecular microbiology*., **52**, 801–814.

Haeusser, D. P.; Garza, A. C.; Buscher, A. Z.; Levin, P. A., 2007: The division inhibitor EzrA contains a seven-residue patch required for maintaining the dynamic nature of the medial FtsZ ring. *Journal of Bacteriology*., **189**, 9001 LP – 9010.

Hamoen, L. W.; Meile, J. C.; de Jong, W.; Noirot, P.; Errington, J., 2006: SepF, a novel FtsZ-interacting protein required for a late step in cell division. *Molecular microbiology*., **59**, 989–999.

Harry, E. J.; Stewart, B. J.; Wake, R. G., 1993: Characterization of mutations in *divIB* of *Bacillus subtilis* and cellular localization of the DivIB protein. *Molecular microbiology*., **7**, 611–621.

Haydon, D. J.; Stokes, N. R.; Ure, R.; Galbraith, G.; Bennett, J. M.; Brown, D. R.; Baker, P. J.; Barynin, V. V; Rice, D. W.; Sedelnikova, S. E.; Heal, J. R.; Sheridan, J. M.; Aiwale, S. T.; Chauhan, P. K.; Srivastava, A.; Taneja, A.; Collins, I.; Errington, J.; Czaplewski, L. G., 2008: An inhibitor of FtsZ with potent and selective anti-staphylococcal activity. *Science (New York, N.Y.)*., **321**, 1673–1675.

Henriques, A. O.; Glaser, P.; Piggot, P. J.; Moran, C. P. J., 1998: Control of cell shape and elongation by the *rodA* gene in *Bacillus subtilis*. *Molecular microbiology*., **28**, 235–247.

Hirota, Y.; Ryter, A.; Jacob, F., 1968: Thermosensitive mutants of *E. coli* affected in the processes of DNA synthesis and cellular division. *Cold Spring Harbor symposia on quantitative biology*., **33**, 677–693.

Hu, Z.; Mukherjee, A.; Pichoff, S.; Lutkenhaus, J., 1999: The MinC component of the division site selection system in *Escherichia coli* interacts with FtsZ to prevent polymerization. *Proceedings of the National Academy of Sciences*., **96**, 14819 LP – 14824.

Hu, Z.; Zhang, S.; Zhou, W.; Ma, X.; Xiang, G., 2017: Synthesis and antibacterial activity of 3-benzylamide derivatives as FtsZ inhibitors. *Bioorganic & Medicinal Chemistry Letters*., **27**, 1854–1858.

Huecas, S.; Andreu, J. M., 2004: Polymerization of nucleotide-free, GDP- and GTP-bound cell division protein FtsZ: GDP makes the difference. *FEBS letters*., **569**, 43–48.

Huecas, S.; Llorca, O.; Boskovic, J.; Martín-Benito, J.; Valpuesta, J. M.; Andreu, J. M., 2008: Energetics and geometry of FtsZ polymers: nucleated self-assembly of single protofilaments. *Biophysical journal*. 2007/11/16., **94**, 1796–1806.

Huecas, S.; Ramirez-Aportela, E.; Vergonos, A.; Nunez-Ramirez, R.; Llorca, O.; Diaz, J. F.; Juan-Rodriguez, D.; Oliva, M. A.; Castellen, P.; Andreu, J. M., 2017: Self-organization of FtsZ polymers in solution reveals spacer role of the disordered C-terminal tail. *Biophysical journal*., **113**, 1831–1844.

Huecas, S.; Canosa-Valls, A. J.; Araújo-Bazán, L.; Ruiz, F. M.; Laurents, D. V; Fernández-Tornero, C.; Andreu, J. M., 2020: Nucleotide-induced folding of cell division protein FtsZ from *Staphylococcus aureus*. *The FEBS Journal*., **287**, 4048–4067.

Ishikawa, S.; Kawai, Y.; Hiramatsu, K.; Kuwano, M.; Ogasawara, N., 2006: A new FtsZ-interacting protein, YlmF, complements the activity of FtsA during progression of cell division in *Bacillus subtilis*. *Molecular Microbiology*., **60**, 1364–1380.

Ishino, F.; Mitsui, K.; Tamaki, S.; Matsuhashi, M., 1980: Dual enzyme activities of cell wall peptidoglycan synthesis, peptidoglycan transglycosylase and penicillin-sensitive transpeptidase, in purified preparations of *Escherichia coli* penicillin-binding protein 1A. *Biochemical and biophysical research communications*., **97**, 287–293.

Jensen, S. O.; Thompson, L. S.; Harry, E. J., 2005: Cell division in *Bacillus subtilis*: FtsZ and FtsA association is Z-ring independent, and FtsA is required for efficient midcell Z-ring assembly. *Journal of Bacteriology*., **187**, 6536 LP – 6544.

Jones, L. J. F.; Carballido-López, R.; Errington, J., 2001: Control of cell shape in bacteria: helical, actin-like filaments in *Bacillus subtilis*. *Cell*., **104**, 913–922.

Jordan, M. A.; Thrower, D.; Wilson, L., 1991: Mechanism of inhibition of cell proliferation by Vinca alkaloids. *Cancer research*., **51**, 2212–2222.

Jordan, M. A.; Toso, R. J.; Thrower, D.; Wilson, L., 1993: Mechanism of mitotic block and inhibition of cell proliferation by taxol at low concentrations. *Proceedings of the National Academy of Sciences of the United States of America*., **90**, 9552–9556.

Julia, D. E.; Arnaud, C.; H., C. A.; Vincent, F.; Roland, W. S.; Rut, C. L., 2011: Processive movement of MreB-associated cell wall biosynthetic complexes in bacteria. *Science*., **333**, 225–228.

Kaimer, C.; González-Pastor, J. E.; Graumann, P. L., 2009: SpoIIIE and a novel type of DNA translocase, SftA, couple chromosome segregation with cell division in *Bacillus subtilis*. *Molecular Microbiology*., **74**, 810–825.

Katis, V. L.; Harry, E. J.; Wake, R. G., 1997: The *Bacillus subtilis* division protein DivIC is a highly abundant membrane-bound protein that localizes to the division site. *Molecular microbiology*., **26**, 1047–1055.

Kaul, M.; Mark, L.; Zhang, Y.; Parhi, A. K.; LaVoie, E. J.; Pilch, D. S., 2013: Pharmacokinetics and *in vivo* antistaphylococcal efficacy of TXY541, a 1-methylpiperidine-4-carboxamide prodrug of PC190723. *Biochemical Pharmacology*., **86**, 1699–1707.

Kaul, M.; Mark, L.; Zhang, Y.; Parhi, A. K.; Lyu, Y. L.; Pawlak, J.; Saravolatz, S.; Saravolatz, L. D.; Weinstein, M. P.; LaVoie, E. J.; Pilch, D. S., 2015: TXA709, an FtsZ-targeting benzamide prodrug with improved pharmacokinetics and enhanced *in vivo* efficacy against methicillin-resistant *Staphylococcus aureus*. *Antimicrobial Agents and Chemotherapy*., **59**, 4845 LP – 4855.

Kaul, M.; Mark, L.; Parhi, A. K.; LaVoie, E. J.; Pilch, D. S., 2016: Combining the FtsZ-targeting prodrug TXA709 and the cephalosporin cefdinir confers synergy and reduces the frequency of resistance in methicillin-resistant Staphylococcus aureus. *Antimicrobial agents and chemotherapy*., **60**, 4290–4296.

Kawai, Y.; Asai, K.; Errington, J., 2009a: Partial functional redundancy of MreB isoforms, MreB, Mbl and MreBH, in cell morphogenesis of *Bacillus subtilis*. *Molecular Microbiology*., **73**, 719–731.

Kawai, Y.; Daniel, R. A.; Errington, J., 2009b: Regulation of cell wall morphogenesis in *Bacillus subtilis* by recruitment of PBP1 to the MreB helix. *Molecular microbiology*., **71**, 1131–1144.

Kirstein; Hoffmann; Lilie; Schmidt; Rübsamen-Waigmann; Brötz-Oesterhelt; Mogk; Turgay, 2009: The antibiotic ADEP reprogrammes ClpP, switching it from a regulated to an uncontrolled protease. *EMBO molecular medicine*., **1**, 37–49.

Kock, H.; Gerth, U.; Hecker, M., 2004: The ClpP peptidase is the major determinant of bulk protein turnover in *Bacillus subtilis*. *Journal of bacteriology*., **186**, 5856–5864.

Król, E.; van Kessel, S. P.; van Bezouwen, L. S.; Kumar, N.; Boekema, E. J.; Scheffers, D. J. 2012: *Bacillus subtilis* SepF binds to the C-terminus of FtsZ. *PLOS ONE*., **7**, e43293.

Kumar, M.; Mathur, T.; Barman, T. K.; Chaira, T.; Kumar, R.; Joshi, V.; Pandya, M.; Sharma, L.; Fujii, K.; Bandgar, M.; Jadhav, B.; Bambal, R.; Upadhyay, D.; Masuda, N.; Verma, A. K.; Bhatnagar, P. K., 2021: Novel FtsZ inhibitor with potent activity against *Staphylococcus aureus*. *Journal of Antimicrobial Chemotherapy*., **76**, 2867–2874.

Kusuma, K. D.; Griffith, R.; Harry, E. J.; Bottomley, A. L.; Ung, A. T., 2019: *In silico* analysis of FtsZ crystal structures towards a new target for antibiotics. *Australian Journal of Chemistry*., **72**, 184–193.

Lee, B. G.; Park, E. Y.; Lee, K. E.; Jeon, H.; Sung, K. H.; Paulsen, H.; Rübsamen-Schaeff, H.; Brötz-Oesterhelt, H.; Song, H. K., 2010: Structures of ClpP in complex with acyldepsipeptide antibiotics reveal its activation mechanism. *Nature Structural & Molecular Biology*., **17**, 471–478.

Lenarcic, R.; Halbedel, S.; Visser, L.; Shaw, M.; Wu, L. J.; Errington, J.; Marenduzzo, D.; Hamoen, L. W., 2009: Localisation of DivIVA by targeting to negatively curved membranes. *The EMBO Journal*., **28**, 2272–2282.

Levin, P. A.; Kurtser, I. G.; Grossman, A. D., 1999: Identification and characterization of a negative regulator of FtsZ ring formation in *Bacillus subtilis*. *Proceedings of the National Academy of Sciences*., **96**, 9642 LP – 9647.

Levison, M. E., 2004: Pharmacodynamics of antimicrobial drugs. *Infectious Disease Clinics*., **18**, 451–465.

Lewis, K., 2007: Persister cells, dormancy and infectious disease. *Nature Reviews Microbiology*., **5**, 48–56.

Li, D. H. S.; Chung, Y. S.; Gloyd, M.; Joseph, E.; Ghirlando, R.; Wright, G. D.; Cheng, Y. Q.; Maurizi, M. R.; Guarné, A.; Ortega, J., 2010: Acyldepsipeptide antibiotics induce the formation of a structured axial channel in ClpP: a model for the ClpX/ClpA-bound state of ClpP. *Chemistry & Biology*., **17**, 959–969.

Li, Y.; Hsin, J.; Zhao, L.; Cheng, Y.; Shang, W.; Huang, K. C.; Wang, H. W.; Ye, S., 2013: FtsZ protofilaments use a hinge-opening mechanism for constrictive force generation. *Science (New York, N.Y.)*., **341**, 392–395.

Li, Z.; Trimble, M. J.; Brun, Y. V; Jensen, G. J., 2007: The structure of FtsZ filaments *in vivo* suggests a force-generating role in cell division. *The EMBO journal*., **26**, 4694–4708.

Liu, Q.; Hu, M.; Yeo, W. S.; He, L.; Li, T.; Zhu, Y.; Meng, H.; Wang, Y.; Lee, H.; Liu, X.; Li, M.; Bae, T., 2017: Rewiring of the FtsH regulatory network by a single nucleotide change in *saeS* of *Staphylococcus aureus*. *Scientific Reports*., **7**, 8456.

Lopus, M.; Panda, D., 2006: The benzophenanthridine alkaloid sanguinarine perturbs microtubule assembly dynamics through tubulin binding. A possible mechanism for its antiproliferative activity. *The FEBS journal*., **273**, 2139–2150.

Löwe, J.; Amos, L. A., 1998: Crystal structure of the bacterial cell-division protein FtsZ. *Nature*., **391**.

Lowth, B. R.; Kirstein-Miles, J.; Saiyed, T.; Brötz-Oesterhelt, H.; Morimoto, R. I.; Truscott, K. N.; Dougan, D. A., 2012: Substrate recognition and processing by a Walker B mutant of the human mitochondrial AAA+ protein CLPX. *Journal of structural biology*., **179**, 193–201.

Lu, C.; Reedy, M.; Erickson, H. P., 2000: Straight and curved conformations of FtsZ are regulated by GTP hydrolysis. *Journal of Bacteriology*., **182**, 164 LP – 170.

Lui, H. K.; Gao, W.; Cheung, K. C.; Jin, W. Bin; Sun, N.; Kan, J. W. Y.; Wong, I. L. K.; Chiou, J.; Lin, D.; Chan, E. W. C.; Leung, Y. C.; Chan, T. H.; Chen, S.; Chan, K. F.; Wong, K. Y., 2019: Boosting the efficacy of anti-MRSA β-lactam antibiotics via an easily accessible, non-cytotoxic and orally bioavailable FtsZ inhibitor. *European journal of medicinal chemistry*., **163**, 95–115.

Lutkenhaus, J. F.; Wolf-Watz, H.; Donachie, W. D., 1980: Organization of genes in the *ftsA-envA* region of the *Escherichia coli* genetic map and identification of a new *fts* locus (*ftsZ*). *Journal of bacteriology*., **142**, 615–620.

Ma, X.; Margolin, W., 1999: Genetic and functional analyses of the conserved C-terminal core domain of *Escherichia coli* FtsZ. *Journal of Bacteriology*., **181**, 7531 LP – 7544.

Malik, I. T.; Brötz-Oesterhelt, H., 2017: Conformational control of the bacterial Clp protease by natural product antibiotics. *Natural product reports*., **34**, 815–831.

Malik, I. T.; Pereira, R.; Vielberg, M. T.; Mayer, C.; Straetener, J.; Thomy, D.; Famulla, K.; Castro,H.; Sass, P.; Groll, M.; Brötz-Oesterhelt, H., 2020: Functional characterisation of ClpP mutations conferring resistance to acyldepsipeptide antibiotics in Firmicutes. *ChemBioChem*., **21**, 1997–2012.

Marston, A. L.; Errington, J., 1999: Selection of the midcell division site in *Bacillus subtilis* through MinD-dependent polar localization and activation of MinC. *Molecular microbiology*., **33**, 84–96.

Matsui, T.; Yamane, J.; Mogi, N.; Yamaguchi, H.; Takemoto, H.; Yao, M.; Tanaka, I., 2012: Structural reorganization of the bacterial cell-division protein FtsZ from *Staphylococcus aureus*. *Acta crystallographica. Section D, Biological crystallography*., **68**, 1175–1188.

Mayer, C.; Sass, P.; Brötz-Oesterhelt, H., 2019: Consequences of dosing and timing on the antibacterial effects of ADEP antibiotics. *International Journal of Medical Microbiology*., **309**, 151329.

Mayer, C., 2020: Cellular effects and resistance mechanism of ADEP antibiotics in *Bacillus subtilis* and *Staphylococcus aureus*.

Meeske, A. J.; Riley, E. P.; Robins, W. P.; Uehara, T.; Mekalanos, J. J.; Kahne, D.; Walker, S.; Kruse, A. C.; Bernhardt, T. G.; Rudner, D. Z., 2016: SEDS proteins are a widespread family of bacterial cell wall polymerases. *Nature*., **537**, 634–638.

Michalik, S.; Liebeke, M.; Zühlke, D.; Lalk, M.; Bernhardt, J.; Gerth, U.; Hecker, M., 2009: Proteolysis during long-term glucose starvation in *Staphylococcus aureus* COL. *PROTEOMICS*., **9**, 4468–4477.

Michel, K. H.; Kastner, R. E., 1985: A54556 antibiotics and process for production thereof. *US Patent*., **4492650**.

Mohammadi, T.; van Dam, V.; Sijbrandi, R.; Vernet, T.; Zapun, A.; Bouhss, A.; Diepeveen-de Bruin, M.; Nguyen-Distèche, M.; de Kruijff, B.; Breukink, E., 2011: Identification of FtsW as a transporter of lipid-linked cell wall precursors across the membrane. *The EMBO journal*., **30**, 1425–1432.

Monteiro, J. M.; Pereira, A. R.; Reichmann, N. T.; Saraiva, B. M.; Fernandes, P. B.; Veiga, H.; Tavares, A. C.; Santos, M.; Ferreira, M. T.; Macário, V.; VanNieuwenhze, M. S.; Filipe, S. R.; Pinho, M. G., 2018: Peptidoglycan synthesis drives an FtsZ-treadmilling-independent step of cytokinesis. *Nature*., **554**, 528–532.

Mroue, N.; Arya, A.; Brown Gandt, A.; Russell, C.; Han, A.; Gavrish, E.; LaFleur, M., 2019: Pharmacodynamics of ClpP-activating antibiotic combinations against Gram-positive pathogens. *Antimicrobial agents and chemotherapy*., **64**.

Msadek, T.; Dartois, V.; Kunst, F.; Herbaud, M. L.; Denizot, F.; Rapoport, G., 1998: ClpP of *Bacillus subtilis* is required for competence development, motility, degradative enzyme synthesis, growth at high temperature and sporulation. *Molecular Microbiology*., **27**, 899–914.

Mukherjee, A.; Lutkenhaus, J., 1998: Dynamic assembly of FtsZ regulated by GTP hydrolysis. *The EMBO journal*., **17**, 462–469.

Mukherjee, A.; Lutkenhaus, J., 1999: Analysis of FtsZ assembly by light scattering and determination of the role of divalent metal cations. *Journal of Bacteriology*., **181**, 823 LP–832.

Nakano, S.; Zheng, G.; Nakano, M. M.; Zuber, P., 2002: Multiple pathways of Spx (YjbD) proteolysis in *Bacillus subtilis*. *Journal of Bacteriology*., **184**, 3664 LP – 3670.

Nakano, S.; Küster-Schöck, E.; Grossman, A. D.; Zuber, P., 2003: Spx-dependent global transcriptional control is induced by thiol-specific oxidative stress in *Bacillus subtilis*. *Proceedings of the National Academy of Sciences*., **100**, 13603 LP – 13608.

Niu, L.; Yu, J., 2008: Investigating intracellular dynamics of FtsZ cytoskeleton with photoactivation single-molecule tracking. *Biophysical Journal*., **95**, 2009–2016.

Nogales, E.; Downing, K. H.; Amos, L. A.; Löwe, J., 1998: Tubulin and FtsZ form a distinct family of GTPases. *Nature Structural Biology*., **5**, 451–458.

Noh, T. H.; Sen, L.; Hong, J.; Lee, J. H.; Moon, H. R.; Jung, J. H., 2017: Antibacterial activities of viriditoxin congeners and synthetic analogues against fish pathogens. *Bioorganic & Medicinal Chemistry Letters*., **27**, 4970–4974.

Normark, S., 1969: Mutation in *Escherichia coli* K-12 mediating spherelike envelopes and changes tolerance to ultraviolet irradiation and some antibiotics. *Journal of bacteriology*., **98**, 1274–1277.

Osawa, M.; Anderson, D. E.; Erickson, H. P., 2008: Reconstitution of contractile FtsZ rings in liposomes. *Science (New York, N.Y.)*., **320**, 792–794.

Osawa, M.; Anderson, D. E.; Erickson, H. P., 2009: Curved FtsZ protofilaments generate bending forces on liposome membranes. *The EMBO journal*., **28**, 3476–3484.

Patrick, J. E.; Kearns, D. B., 2008: MinJ (YvjD) is a topological determinant of cell division in *Bacillus subtilis*. *Molecular Microbiology*., **70**, 1166–1179.

Pauling, L.; Corey, R. B.; Branson, H. R., 1951: The structure of proteins: Two hydrogen-bonded helical configurations of the polypeptide chain. *Proceedings of the National Academy of Sciences*., **37**, 205 LP – 211.

Pazos, M.; Natale, P.; Vicente, M., 2013: A specific role for the ZipA protein in cell division: stabilization of the FtsZ protein. *The Journal of biological chemistry*., **288**, 3219–3226.

Pedersen, L. B.; Angert, E. R.; Setlow, P., 1999: Septal localization of penicillin-binding protein 1 in *Bacillus subtilis*. *Journal of bacteriology*., **181**, 3201–3211.

Peters, J. M.; Colavin, A.; Shi, H.; Czarny, T. L.; Larson, M. H.; Wong, S.; Hawkins, J. S.; Lu, C. H. S.; Koo, B. M.; Marta, E.; Shiver, A. L.; Whitehead, E. H.; Weissman, J. S.; Brown, E. D.; Qi, L. S.; Huang, K. C.; Gross, C. A., 2016: A comprehensive, CRISPR-based functional analysis of essential genes in bacteria. *Cell*., **165**, 1493 – 1506.

Popham, D. L.; Setlow, P., 1996: Phenotypes of *Bacillus subtilis* mutants lacking multiple class A high-molecular-weight penicillin-binding proteins. *Journal of Bacteriology*., **178**, 2079–2085.

Potluri, L.; Karczmarek, A.; Verheul, J.; Piette, A.; Wilkin, J. M.; Werth, N.; Banzhaf, M.; Vollmer, W.; Young, K. D.; Nguyen-Distèche, M.; den Blaauwen, T., 2010: Septal and lateral wall localization of PBP5, the major D,D-carboxypeptidase of *Escherichia coli*, requires substrate recognition and membrane attachment. *Molecular microbiology*., **77**, 300–323.

Pradhan, P.; Margolin, W.; Beuria, T. K., 2021: Targeting the achilles heel of FtsZ: the interdomain cleft. *Frontiers in microbiology*., **12**, 732796.

Qin, S.; William, M., 1998: FtsZ dynamics during the division cycle of live *Escherichia coli* cells. *Journal of Bacteriology*., **180**, 2050–2056.

Raymond, A.; Lovell, S.; Lorimer, D.; Walchli, J.; Mixon, M.; Wallace, E.; Thompkins, K.; Archer, K.; Burgin, A.; Stewart, L., 2009: Combined protein construct and synthetic gene engineering for heterologous protein expression and crystallization using Gene Composer. *BMC biotechnology*., **9**, 37.

Rowinsky, E. K.; Onetto, N.; Canetta, R. M.; Arbuck, S. G., 1992: Taxol: the first of the taxanes, an important new class of antitumor agents. *Seminars in oncology*., **19**, 646–662.

Sánchez-Gorostiaga, A.; Palacios, P.; Martínez-Arteaga, R.; Sánchez, M.; Casanova, M.; Vicente, M., 2016: Life without division: Physiology of *Escherichia coli* FtsZ-deprived filaments. *mBio*., **7**.

Santra, M. K.; Panda, D., 2003: Detection of an intermediate during unfolding of bacterial cell division protein FtsZ: loss of functional properties precedes the global unfolding of FtsZ. *Journal of Biological Chemistry*., **278**, 21336–21343.

Sass; Josten; Famulla; Schiffer; Sahl; Hamoen; Brötz-Oesterhelt, 2011: Antibiotic acyldepsipeptides activate ClpP peptidase to degrade the cell division protein FtsZ. *Proceedings of the National Academy of Sciences*., **108**, 17474 LP – 17479.

Scheffers, D. J.; den Blaauwen, T.; Driessen, A. J., 2000: Non-hydrolysable GTP-gamma-S stabilizes the FtsZ polymer in a GDP-bound state. *Molecular microbiology*., **35**, 1211–1219.

Scheffers, D. J.; de Wit, J. G.; den Blaauwen, T.; Driessen, A. J. M., 2002: GTP hydrolysis of cell division protein FtsZ: evidence that the active site is formed by the association of monomers. *Biochemistry*., **41**, 521–529.

Scheffers, D. J.; Errington, J., 2004: PBP1 is a component of the *Bacillus subtilis* cell division machinery. *Journal of bacteriology*., **186**, 5153–5156.

Scheffers, D. J., 2008: The effect of MinC on FtsZ polymerization is pH dependent and can be counteracted by ZapA. *FEBS Letters*., **582**, 2601–2608.

Schiff, P. B.; Horwitz, S. B., 1980: Taxol stabilizes microtubules in mouse fibroblast cells. *Proceedings of the National Academy of Sciences of the United States of America*., **77**, 1561–1565.

Schmitz, K. R.; Carney, D. W.; Sello, J. K.; Sauer, R. T., 2014: Crystal structure of *Mycobacterium tuberculosis* ClpP1P2 suggests a model for peptidase activation by AAA+ partner binding and substrate delivery. *Proceedings of the National Academy of Sciences*., **111**, E4587 LP-E4595.

Sievers, J.; Errington, J., 2000: The *Bacillus subtilis* cell division protein FtsL localizes to sites of septation and interacts with DivIC. *Molecular Microbiology*., **36**, 846–855.

Silber; Matos; Mayer; Sass, 2020a: Cell division protein FtsZ: from structure and mechanism to antibiotic target. *Future Microbiology*., **15**, 801–831.

Silber; Pan; Schäkermann; Mayer; Brötz-Oesterhelt; Sass, 2020b: Cell division protein FtsZ is unfolded for N-terminal degradation by antibiotic-activated ClpP. *mBio*., **11**, e01006-20.

Silber, N.; Mayer, C.; Matos de Opitz, C. L.; Sass, P., 2021: Progression of the late-stage divisome is unaffected by the depletion of the cytoplasmic FtsZ pool. *Communications Biology*., **4**, 270.

Singh, J. K.; Makde, R. D.; Kumar, V.; Panda, D., 2007: A membrane protein, EzrA, regulates assembly dynamics of FtsZ by interacting with the C-terminal tail of FtsZ. *Biochemistry*., **46**, 11013–11022.

Singh, J. K.; Makde, R. D.; Kumar, V.; Panda, D., 2008: SepF increases the assembly and bundling of FtsZ polymers and stabilizes FtsZ protofilaments by binding along its length. *Journal of Biological Chemistry*., **283**, 31116–31124.

Sowole, M. A.; Alexopoulos, J. A.; Cheng, Y. Q.; Ortega, J.; Konermann, L., 2013: Activation of ClpP protease by ADEP antibiotics: insights from hydrogen exchange mass spectrometry. *Journal of Molecular Biology*., **425**, 4508–4519.

Squyres, G. R.; Holmes, M. J.; Barger, S. R.; Pennycook, B. R.; Ryan, J.; Yan, V. T.; Garner, E.C., 2021: Single-molecule imaging reveals that Z-ring condensation is essential for cell division in *Bacillus subtilis*. *Nature Microbiology*.

Stahlberg, H.; Kutejová, E.; Muchová, K.; Gregorini, M.; Lustig, A.; Müller, S. A.; Olivieri, V.; Engel, A.; Wilkinson, A. J.; Barák, I., 2004: Oligomeric structure of the *Bacillus subtilis* cell division protein DivIVA determined by transmission electron microscopy. *Molecular microbiology*., **52**, 1281–1290.

Stephens, R. S.; Kalman, S.; Lammel, C.; Fan, J.; Marathe, R.; Aravind, L.; Mitchell, W.; Olinger, L.; Tatusov, R. L.; Zhao, Q.; Koonin, E. V; Davis, R. W., 1998: Genome sequence of an obligate intracellular pathogen of humans: *Chlamydia trachomatis*. *Science (New York, N.Y.)*., **282**, 754–759.

Stokes, N. R.; Sievers, J.; Barker, S.; Bennett, J. M.; Brown, D. R.; Collins, I.; Errington, V. M.; Foulger, D.; Hall, M.; Halsey, R.; Johnson, H.; Rose, V.; Thomaides, H. B.; Haydon, D. J.; Czaplewski, L. G.; Errington, J., 2005: Novel inhibitors of bacterial cytokinesis identified by a cell-based antibiotic screening assay. *Journal of Biological Chemistry*., **280**, 39709–39715.

Stokes, N. R.; Baker, N.; Bennett, J. M.; Berry, J.; Collins, I.; Czaplewski, L. G.; Logan, A.; Macdonald, R.; Macleod, L.; Peasley, H.; Mitchell, J. P.; Nayal, N.; Yadav, A.; Srivastava, A.; Haydon, D. J., 2013: An improved small-molecule inhibitor of FtsZ with superior *in vitro* potency, drug-like properties, and *in vivo* efficacy. *Antimicrobial agents and chemotherapy*., **57**, 317–325.

Stricker, J.; Maddox, P.; Salmon, E. D.; Erickson, H. P., 2002: Rapid assembly dynamics of the *Escherichia coli* FtsZ-ring demonstrated by fluorescence recovery after photobleaching. *Proceedings of the National Academy of Sciences of the United States of America*., **99**, 3171–3175.

Su, M.; Zhao, C.; Li, D.; Cao, J.; Ju, Z.; Kim, E. L.; Jung, Y. S.; Jung, J. H., 2020: Viriditoxin stabilizes microtubule polymers in SK-OV-3 cells and exhibits antimitotic and antimetastatic potential. *Marine Drugs*.

Sundararajan, K.; Goley, E. D., 2017: The intrinsically disordered C-terminal linker of FtsZ regulates protofilament dynamics and superstructure *in vitro*. *Journal of Biological Chemistry*., **292**, 20509–20527.

Sundararajan, K.; Barrows, J. M.; Goley, E. D., 2019: Determinants of FtsZ C-terminal linker-dependent regulation of cell wall metabolism in *Caulobacter crescentus*. *bioRxiv*., 632075.

Szwedziak, P.; Löwe, J., 2013: Do the divisome and elongasome share a common evolutionary past? *Current Opinion in Microbiology*., **16**, 745–751.

Taguchi, A.; Welsh, M. A.; Marmont, L. S.; Lee, W.; Sjodt, M.; Kruse, A. C.; Kahne, D.; Bernhardt, T. G.; Walker, S., 2019: FtsW is a peptidoglycan polymerase that is functional only in complex with its cognate penicillin-binding protein. *Nature microbiology*., **4**, 587–594.

Tan, C. M.; Therien, A. G.; Lu, J.; Lee, S. H.; Caron, A.; Gill, C. J.; Lebeau-Jacob, C.; Benton-Perdomo, L.; Monteiro, J. M.; Pereira, P. M.; Elsen, N. L.; Wu, J.; Deschamps, K.; Petcu, M.; Wong, S.; Daigneault, E.; Kramer, S.; Liang, L.; Maxwell, E. et al., 2012: Restoring methicillin-resistant *Staphylococcus aureus* susceptibility to β-lactam antibiotics. *Science translational medicine*., **4**, 126ra35.

Tsai, C. J.; Lin, S. L.; Wolfson, H. J.; Nussinov, R., 1997a: Studies of protein-protein interfaces: a statistical analysis of the hydrophobic effect. *Protein science : a publication of the Protein Society*., **6**, 53–64.

Tsai, C. J.; Xu, D.; Nussinov, R., 1997b: Structural motifs at protein-protein interfaces: protein cores versus two-state and three-state model complexes. *Protein science : a publication of the Protein Society*., **6**, 1793–1805.

van de Putte, P.; van Dillewijn, J.; Rörsch, A., 1964: The selection of mutants of *Escherichia coli* with impaired cell division at elevated temperature. *Mutation Research/Fundamental and Molecular Mechanisms of Mutagenesis*., **1**, 121–128.

van der Ploeg, R.; Verheul, J.; Vischer, N. O. E.; Alexeeva, S.; Hoogendoorn, E.; Postma, M.; Banzhaf, M.; Vollmer, W.; den Blaauwen, T., 2013: Colocalization and interaction between elongasome and divisome during a preparative cell division phase in *Escherichia coli*. *Molecular Microbiology*., **87**, 1074–1087.

Vaughan, S.; Wickstead, B.; Gull, K.; Addinall, S. G., 2004: Molecular evolution of FtsZ protein sequences encoded within the genomes of archaea, bacteria, and eukaryota. *Journal of Molecular Evolution*., **58**, 19–29.

Wachi, M.; Doi, M.; Tamaki, S.; Park, W.; Nakajima-Iijima, S.; Matsuhashi, M., 1987: Mutant isolation and molecular cloning of *mre* genes, which determine cell shape, sensitivity to mecillinam, and amount of penicillin-binding proteins in *Escherichia coli*. *Journal of bacteriology*., **169**, 4935–4940.

Wachi, M.; Doi, M.; Okada, Y.; Matsuhashi, M., 1989: New *mre* genes *mreC* and *mreD*, responsible for formation of the rod shape of *Escherichia coli* cells. *Journal of bacteriology*., **171**, 6511–6516.

Wagstaff, J. M.; Tsim, M.; Oliva, M. A.; García-Sanchez, A.; Kureisaite-Ciziene, D.; Andreu, J. M.; Löwe, J., 2017: A polymerization-associated structural switch in FtsZ that enables treadmilling of model filaments. *mBio*., **8**.

Walker, J. R.; Kovarik, A.; Allen, J. S.; Gustafson, R. A., 1975: Regulation of bacterial cell division: temperature-sensitive mutants of *Escherichia coli* that are defective in septum formation. *Journal of Bacteriology*., **123**, 693 LP – 703.

Wang, J.; Hartling, J. A.; Flanagan, J. M., 1997a: The structure of ClpP at 2.3 Å resolution suggests a model for ATP-dependent proteolysis. *Cell*., **91**, 447–456.

Wang, J. D.; Levin, P. A., 2009: Metabolism, cell growth and the bacterial cell cycle. *Nature reviews. Microbiology*., **7**, 822–827.

Wang, X.; Huang, J.; Mukherjee, A.; Cao, C.; Lutkenhaus, J., 1997b: Analysis of the interaction of FtsZ with itself, GTP, and FtsA. *Journal of Bacteriology*., **179**, 5551 LP – 5559.

Weiss, D. S., 2015: Last but not least: new insights into how FtsN triggers constriction during *Escherichia coli* cell division. *Molecular microbiology*., **95**, 903–909.

Whitley, K. D.; Jukes, C.; Tregidgo, N.; Karinou, E.; Almada, P.; Cesbron, Y.; Henriques, R.; Dekker, C.; Holden, S., 2021: FtsZ treadmilling is essential for Z-ring condensation and septal constriction initiation in *Bacillus subtilis* cell division. *Nature Communications*., **12**, 2448.

Wong, K. S.; Mabanglo, M. F.; Seraphim, T. V; Mollica, A.; Mao, Y. Q.; Rizzolo, K.; Leung, E.; Moutaoufik, M. T.; Hoell, L.; Phanse, S.; Goodreid, J.; Barbosa, L. R. S.; Ramos, C. H. I.; Babu, M.; Mennella, V.; Batey, R. A.; Schimmer, A. D.; Houry, W. A., 2018: Acyldepsipeptide analogs dysregulate human mitochondrial ClpP protease activity and cause apoptotic cell death. *Cell Chemical Biology*., **25**, 1017-1030.e9.

Wu, L. J.; Errington, J., 2004: Coordination of cell division and chromosome segregation by a nucleoid occlusion protein in *Bacillus subtilis*. *Cell*., **117**, 915–925.

Yan, K.; Pearce, K. H.; Payne, D. J., 2000: A conserved residue at the extreme C-terminus of FtsZ is critical for the FtsA-FtsZ interaction in *Staphylococcus aureus*. *Biochemical and biophysical research communications*., **270**, 387–392.

Yang, X.; Lyu, Z.; Miguel, A.; McQuillen, R.; Huang, K. C.; Xiao, J., 2017: GTPase activity–coupled treadmilling of the bacterial tubulin FtsZ organizes septal cell wall synthesis. *Science*., **355**, 744 LP – 747.

Young, L.; Jernigan, R. L.; Covell, D. G., 1994: A role for surface hydrophobicity in protein-protein recognition. *Protein science : a publication of the Protein Society*., **3**, 717–729.

Yu, X. C.; Weihe, E. K.; Margolin, W., 1998: Role of the C terminus of FtsK in *Escherichia col*i chromosome segregation. *Journal of bacteriology*., **180**, 6424–6428.

Yu, Y., Zhou, J., Gueiros-Filho, F. J., Kearns, D. B., & Jacobson, S. C. (2021). Noc corrals migration of FtsZ Protofilaments during cytokinesis in *Bacillus subtilis*. *MBio*, *12*(1), e02964-20

6 Appendix

6.1 Publication 1

AMERICAN SOCIETY FOR MICROBIOLOGY | mBio®

RESEARCH ARTICLE
Molecular Biology and Physiology

Cell Division Protein FtsZ Is Unfolded for N-Terminal Degradation by Antibiotic-Activated ClpP

Nadine Silber,[a] Stefan Pan,[a] Sina Schäkermann,[b] Christian Mayer,[a] Heike Brötz-Oesterhelt,[a,c] Peter Sass[a,c]

[a]Department of Microbial Bioactive Compounds, Interfaculty Institute of Microbiology and Infection Medicine, University of Tuebingen, Tuebingen, Germany
[b]Applied Microbiology, Ruhr University Bochum, Bochum, Germany
[c]Cluster of Excellence-Controlling Microbes to Fight Infections, Tuebingen, Germany

Heike Brötz-Oesterhelt and Peter Sass share senior authorship.

ABSTRACT Antibiotic acyldepsipeptides (ADEPs) deregulate ClpP, the proteolytic core of the bacterial Clp protease, thereby inhibiting its native functions and concomitantly activating it for uncontrolled proteolysis of nonnative substrates. Importantly, although ADEP-activated ClpP is assumed to target multiple polypeptide and protein substrates in the bacterial cell, not all proteins seem equally susceptible. In *Bacillus subtilis*, the cell division protein FtsZ emerged to be particularly sensitive to degradation by ADEP-activated ClpP at low inhibitory ADEP concentrations. In fact, FtsZ is the only bacterial protein that has been confirmed to be degraded *in vitro* as well as within bacterial cells so far. However, the molecular reason for this preferred degradation remained elusive. Here, we report the unexpected finding that ADEP-activated ClpP alone, in the absence of any Clp-ATPase, leads to an unfolding and subsequent degradation of the N-terminal domain of FtsZ, which can be prevented by the stabilization of the FtsZ fold via nucleotide binding. At elevated antibiotic concentrations, importantly, the C terminus of FtsZ is notably targeted for degradation in addition to the N terminus. Our results show that different target structures are more or less accessible to ClpP, depending on the ADEP level present. Moreover, our data assign a Clp-ATPase-independent protein unfolding capability to the ClpP core of the bacterial Clp protease and suggest that the protein fold of FtsZ may be more flexible than previously anticipated.

IMPORTANCE Acyldepsipeptide (ADEP) antibiotics effectively kill multidrug-resistant Gram-positive pathogens, including vancomycin-resistant enterococcus, penicillin-resistant *Streptococcus pneumoniae* (PRSP), and methicillin-resistant *Staphylococcus aureus* (MRSA). The antibacterial activity of ADEP depends on a new mechanism of action, i.e., the deregulation of bacterial protease ClpP that leads to bacterial self-digestion. Our data allow new insights into the mode of ADEP action by providing a molecular explanation for the distinct bacterial phenotypes observed at low versus high ADEP concentrations. In addition, we show that ClpP alone, in the absence of any unfoldase or energy-consuming system, and only activated by the small molecule antibiotic ADEP, leads to the unfolding of the cell division protein FtsZ.

KEYWORDS ADEP, antibiotics, acyldepsipeptides, guanosine nucleotides, protein unfolding, cytokinesis, Clp protease, Clp-ATPases

Antibiotic acyldepsipeptides (ADEPs) kill Gram-positive bacteria, including human pathogens, by deregulating the bacterial protease Clp (1–4). The Clp protease is conserved across most bacterial species, where it is naturally involved in protein homeostasis and regulatory proteolysis. Clp is important for maintaining vital cellular functions particularly under stress conditions and directs developmen-

Citation Silber N, Pan S, Schäkermann S, Mayer C, Brötz-Oesterhelt H, Sass P. 2020. Cell division protein FtsZ is unfolded for N-terminal degradation by antibiotic-activated ClpP. mBio 11:e01006-20. https://doi.org/10.1128/mBio.01006-20.

Editor Lotte Søgaard-Andersen, Max Planck Institute for Terrestrial Microbiology

Address correspondence to Heike Brötz-Oesterhelt, heike.broetz-oesterhelt@uni-tuebingen.de, or Peter Sass, peter.sass@uni-tuebingen.de.

Received 21 April 2020
Accepted 26 May 2020
Published 30 June 2020

tal processes like cell differentiation, genetic competence, and virulence (5, 6). Thus, Clp protease has emerged as a novel target for antibiotic action and virulence inhibition (7–9).

Clp protease constitutes a macromolecular complex that is composed of a proteolytic core, ClpP, that associates with specific hexameric unfoldases, the Clp-ATPases, and accessory adaptor proteins (8, 10). ClpP forms a tetradecameric, barrel-shaped structure with the proteolytic chamber secluded within the assembled complex. The cognate Clp-ATPases interact with the ClpP tetradecamer via distinct hydrophobic pockets at both sides of the barrel (11). Substrate access to the proteolytic chamber is strictly controlled by the partner Clp-ATPases, which recognize the respective protein substrates, unfold them in an ATP-dependent manner, and thread the unfolded polypeptide chains through the apical and distal entrance pores of the ClpP barrel (12). It is important to note that ClpP is capable of degrading peptides on its own, but not fully folded proteins, and strictly depends on ATP-driven Clp-ATPases for proteolytic activation in the natural context (10, 12).

ADEP antibiotics compete with the Clp-ATPases for the same binding sites on ClpP, which results in a dual mechanism of action; by binding to the hydrophobic pockets of ClpP, ADEPs abrogate the interaction of ClpP with its partner Clp-ATPases, thereby preventing all cellular functions of Clp in general and regulatory proteolysis (13). This is sufficient to kill mycobacteria (14, 15), which rely on a functional Clp system for viability (16). However, in most bacterial species, including *Bacillus subtilis* or *Staphylococcus aureus*, Clp is not essential for growth, and thus, mere Clp inhibition is not sufficient to kill bacteria under normal growth conditions. In such species, a ClpP activation mechanism leads to bacterial killing; ADEP binding supports the oligomerization process of ClpP (13) and locks the catalytic triads in an active conformation via allosteric conformational control (17, 18). ADEP additionally triggers a closed- to open-gate structural transition of the N-terminal segments of ClpP that opens the substrate entrance pore to the proteolytic chamber (19, 20), which is otherwise tightly closed (21). As a result, nonnative polypeptides and protein substrates are now allowed to enter the proteolytic chamber of ClpP and are subsequently degraded in a Clp-ATPase-independent manner (1, 13).

Depending on the applied ADEP concentration, treated bacteria show distinct phenotypes. At high ADEP concentrations, several times the MIC, cells rapidly stop growing due to ceased biomass production (22, 23). This phenotype may be readily explained by the broad destructive capacity of ClpP activation, and we showed earlier that ADEP activates ClpP to degrade nascent protein chains during translation (13), likely causing a depletion of several essential bacterial proteins. In contrast, at concentrations very close to the MIC, ADEP exposure results in a more specific phenotype, namely, bacterial cells retain considerable biosynthetic capacity, with macromolecular syntheses and biomass production proceeding for hours (22). However, cell size significantly increases, as indicated by the swelling of coccoid *S. aureus* and *Streptococcus pneumoniae* cells as well as an impressive filamentation of rod-shaped *B. subtilis*, eventually leading to cell death (22, 23). A strong ongoing biosynthetic capacity with blocked cytokinesis points to a preferential proteolytic target in bacterial cell division, and we reported earlier that this is due to the untimely degradation of the essential cell division protein FtsZ by ADEP-activated ClpP (22). This prominent phenotype clearly distinguishes FtsZ as being particularly susceptible to ADEP-ClpP. Intriguingly, the *B. subtilis* FtsZ protein was completely and easily degraded by ADEP-ClpP *in vitro*, while several other folded proteins were not (22). In exploring this enigma, it emerged that the short, hydrophobic N terminus of *B. subtilis* FtsZ is particularly prone to be targeted by ADEP-ClpP, leading to the unfolding of the FtsZ protein over the course of the degradation process, while degradation of the extended and flexible C terminus of FtsZ is only triggered at increased ADEP concentration. Thereby, our results allow new insight into the stability of the FtsZ protein, suggest extending the mechanistic capabilities of ADEP-ClpP toward ATP-independent protein unfolding, and provide a

molecular explanation for the different bacterial phenotypes observed at low versus high ADEP concentrations.

RESULTS

ADEP-activated ClpP preferentially targets the short N terminus of FtsZ. In this study, we set out to determine the molecular basis for the observed sensitivity of *B. subtilis* FtsZ toward ADEP-ClpP. To validate FtsZ as a preferred target for ADEP-ClpP, we first compared the abundance of the fructose-bisphosphate aldolase (FbaA) in relation to FtsZ in *B. subtilis* and *S. aureus* cells that were exposed to ADEP concentrations close to the MIC (2× to 3× MIC, i.e., 0.25 μg/ml ADEP2 for *B. subtilis* 168 and 1 μg/ml ADEP2 for *S. aureus* NCTC 8325) (Fig. 1A). Fragments of FbaA (as well as of elongation factor Tu [EF-Tu] and pyruvate kinase [Pyk]) were detected in notable amounts in a previous proteomics study of *S. aureus* cells exposed to ADEP at elevated concentrations (10× MIC) for an extended time period (3). Therefore, FbaA was assumed to be a target for ADEP-activated ClpP in this previous study. Using immunodetection of FtsZ and FbaA proteins, our results confirmed the rapid and complete degradation of FtsZ after 120 min in ADEP-treated cells; however, the protein concentration of FbaA remained unaltered under these conditions (Fig. 1A). To study this aspect in more detail, we proceeded to test the degradation of *B. subtilis* FbaA, EF-Tu, and Pyk (BsFbaA, BsEF-Tu, and BsPyk, respectively) by ADEP-ClpP using purified proteins *in vitro*. Here, BsFbaA, BsEF-Tu, BsPyk were not notably degraded by ADEP-ClpP under the same conditions *in vitro*, in contrast to FtsZ (Fig. 1B), thereby clearly corroborating a preferential degradation of FtsZ by ADEP-ClpP.

Next, we looked into the published crystal structure of FtsZ to identify structural features that may be potentially prone to degradation. *B. subtilis* FtsZ (BsFtsZ; Protein Data Bank entry 2RHO) (Fig. 1C) comprises an overall globular core protein with two independently folding domains (24–26), the N-terminal and the C-terminal domain, which are connected via the central core helix H7 followed by the T7 loop. The N-terminal domain harbors the nucleotide binding site which interacts with the T7 loop of a second FtsZ monomer to form the GTPase catalytic site (27). The long flexible C terminus (amino acids 316 to 382), which contains the interaction interface for other cell division proteins, as well as the short N terminus (amino acids 1 to 10), are not resolved in the crystal structure due to their inherent flexibility. *In silico* disorder predictions visualized the overall structural disorder of the C terminus (Fig. 1D), making it a structural feature likely to be attacked by ADEP-ClpP, as this flexible amino acid tail may easily diffuse through the opened entrance pores into the degradation chamber of ADEP-ClpP. To test this hypothesis, we constructed several mutant proteins of BsFtsZ and tested them in *in vitro* ADEP-ClpP degradation assays (Fig. 1E and F; see Fig. S1 in the supplemental material). Surprisingly, FtsZ mutants with deleted C termini, either short truncations omitting the last 18 amino acids containing the interaction interface (BsFtsZ$_{1\text{-}364}$) as well as longer truncations deleting the complete flexible C terminus (BsFtsZ$_{1\text{-}315}$), were still degraded similarly to full-length BsFtsZ$_{1\text{-}382}$. However, degradation was significantly impaired when we deleted the short N terminus of FtsZ (BsFtsZ$_{11\text{-}382}$, BsFtsZ$_{11\text{-}364}$, and BsFtsZ$_{11\text{-}315}$), identifying this structural feature as the preferred target site for ADEP-ClpP. Of note, all tested FtsZ protein variants were functional as shown in GTPase assays (see Fig. S2 in the supplemental material). We selected the synthetic derivative ADEP2 for all degradation assays in this study because, among a small series of ADEP congeners tested, it proved particularly effective at activating *B. subtilis* ClpP (BsClpP) for the degradation of BsFtsZ (see Fig. S3 in the supplemental material) and we had also used ADEP2 for degradation assays in our previous studies (14, 22). We further incubated FtsZ either alone or with ADEP (both in the absence of ClpP) for 60 min at 37°C, which did not affect FtsZ protein stability or functionality (see Fig. S4 in the supplemental material), ruling out off-target effects of ADEP on FtsZ or denaturing of FtsZ over the course of the *in vitro* assay.

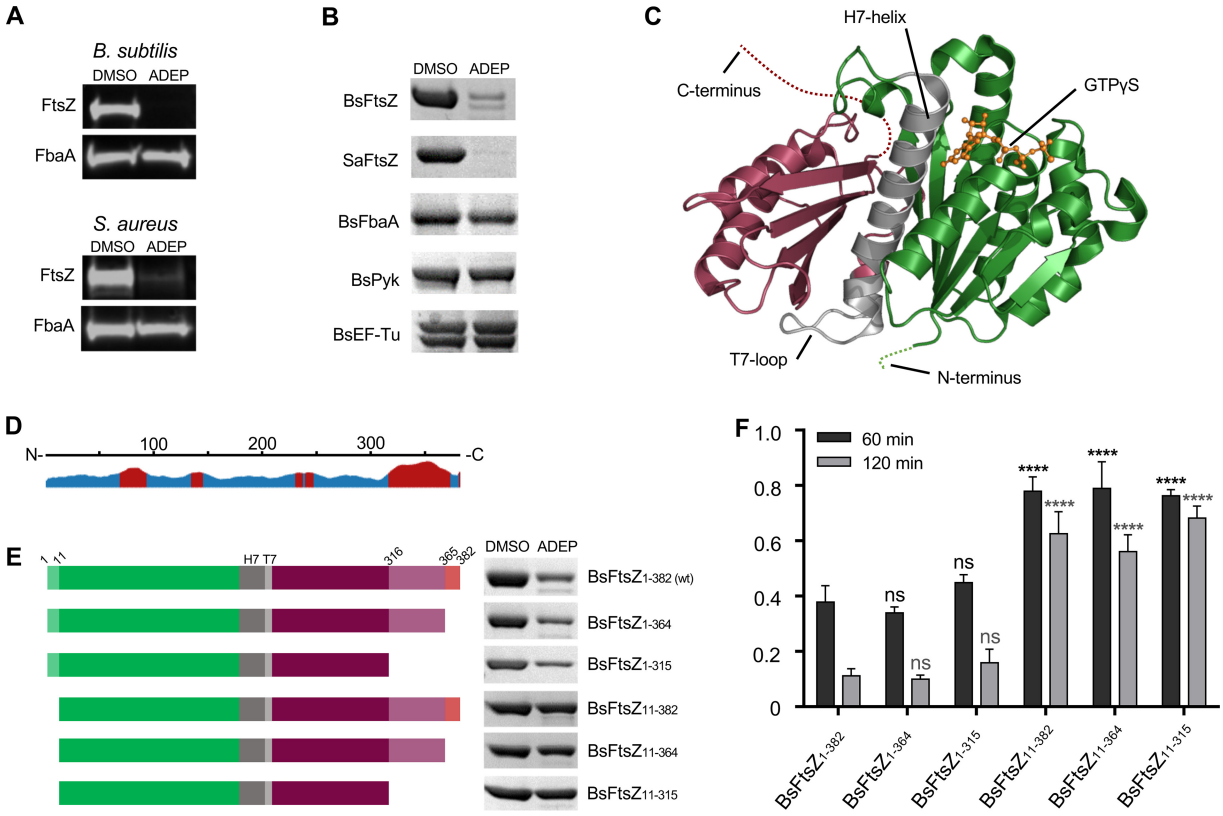

FIG 1 ADEP-activated ClpP preferentially targets the N terminus of FtsZ. (A) Immunoblotting of *B. subtilis* 168 and *S. aureus* NCTC8325 cells that were treated with ADEP concentrations close to the MIC (0.25 μg/ml ADEP2 for *B. subtilis* 168 and 1 μg/ml ADEP2 for *S. aureus* NCTC 8325), a concentration that leads to a pronounced filamentation phenotype of *B. subtilis* and swelling of *S. aureus*. Here, immunoblots show the rapid degradation of FtsZ compared with the untreated control (DMSO). In contrast, the abundance of FbaA was unaltered under the same conditions. Immunodetection of FtsZ and FbaA was performed using specific anti-FtsZ and anti-FbaA antibodies, respectively. Samples were taken after 120 min. DMSO was used as a control. (B) *In vitro* degradation assays using BsFtsZ and *S. aureus* FtsZ (SaFtsZ) as well as *B. subtilis* FbaA (BsFbaA), elongation factor Tu (BsEF-Tu), and pyruvate kinase (BsPyk) as purified protein substrates for ADEP-activated ClpP. In these assays, low concentrations of ADEP and ClpP were applied (1.5 μM ClpP; 1.5 μM ADEP). Samples were taken after 60 min. DMSO was used as a control. Of note, phosphorylation of BsEF-Tu often produces a doublet visible in SDS-PAGE, most probably resulting from partial phosphorylation of the multiply phosphorylated substrate (65). All experiments were performed at least in triplicate; representative images are depicted. (C) The crystal structure of *B. subtilis* FtsZ (BsFtsZ; Protein Data Bank entry 2RHO) bound to the nonhydrolyzable GTP-analog GTPγS shows two independently folding domains (24–26), the N-terminal domain harboring the nucleotide binding site (in green) as well as the C-terminal domain (in currant red). GTPγS is indicated in orange. Both domains are connected via the central H7 helix and the T7 loop (in gray). The short N terminus (amino acids 1 to 10) and the flexible C terminus (amino acids 316 to 382) are indicated by dotted lines. (D) Disorder prediction of BsFtsZ was computed with JRONN software (66) (Protein Data Bank entry 2RHO; https://www.rcsb.org). Predicted disordered regions (in red) and ordered regions (in blue) are indicated. (E) The left image panel provides a schematic representation of N- and C-terminal protein truncations of FtsZ used in degradation assays aligned to the disorder plot in D. The uppermost protein represents full-length FtsZ. The right image panel shows ADEP-ClpP degradation assays of full-length and truncated BsFtsZ proteins (aligned to the corresponding schematic on the left). In these assays, low concentrations of ADEP and ClpP were used (1.5 μM ClpP; 1.5 μM ADEP). Samples were taken after 60 min; DMSO was used as a control. (F) Densitometry of protein bands from SDS-PAGE was performed to compare FtsZ protein amounts in ADEP-treated samples with the corresponding DMSO control reactions after 60 min (black bars) and 120 min (gray bars). The respective DMSO control was set to 1.0 (100%). For each FtsZ variant, the data were collected from three different degradation assays and SDS-PAGE analyses using a standard curve. Protein amounts were calculated using a standard FtsZ concentration series that was applied on each SDS-PAGE. The plotted data depict the corresponding mean values, with standard deviations indicated by error bars. Compared with $BsFtsZ_{1-382}$, there was no significant (ns) difference regarding the remaining protein amount of the C-terminally truncated FtsZ mutant proteins $BsFtsZ_{1-364}$ and $_{Bs}FtsZ_{1-315}$ after 60 or 120 min of incubation with ADEP-ClpP. Contrariwise, the N-terminally truncated FtsZ proteins $BsFtsZ_{11-382}$, $BsFtsZ_{11-364}$, and $BsFtsZ_{11-315}$ were characterized by significantly less degradation of the FtsZ protein by ADEP-ClpP (****, $P < 0.0001$) than $BsFtsZ_{1-382}$. For all assays with substrates originating from *B. subtilis* or *S. aureus*, we used the corresponding BsClpP or *S. aureus* ClpP (SaClpP) proteins, respectively, with the according activity buffers (see Materials and Methods section). All results were confirmed by at least three independent experiments, and images of representative experiments are depicted.

Hydrophobicity of the FtsZ N terminus is important for degradation. The observation that ADEP-ClpP starts degradation at the N terminus of FtsZ was rather unexpected, raising the question of why the short N terminus should be preferred over the extended, flexible C terminus. To address this question, we analyzed the physicochemical properties of the N terminus of FtsZ *in silico*, and it emerged that it is overall hydrophobic in nature, in contrast to the C terminus of FtsZ (Fig. 2A). We thus

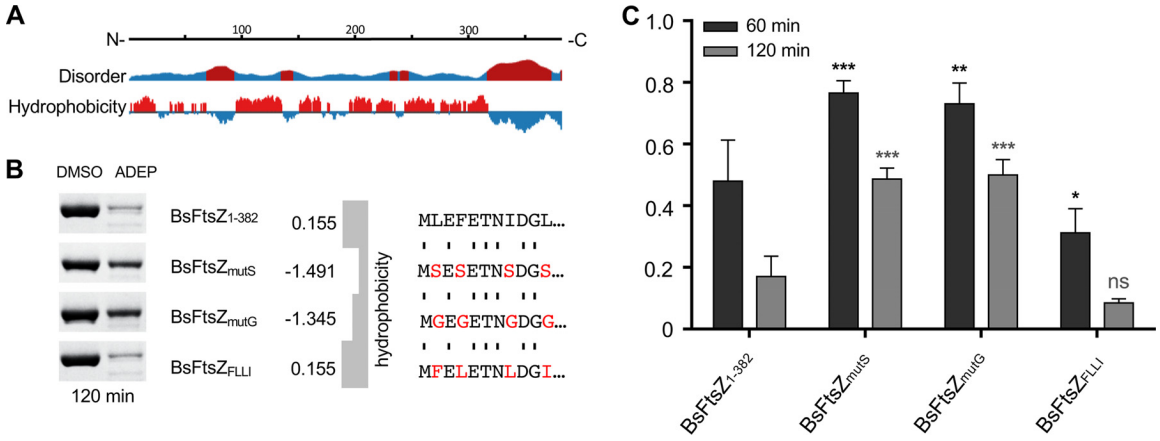

FIG 2 Hydrophobicity of the N terminus promotes FtsZ degradation. (A) Disorder prediction (top) and hydrophobicity prediction of FtsZ (bottom) were computed with JRONN software (66) (Protein Data Bank entry 2RHO; https://www.rcsb.org). Predicted disordered or hydrophobic regions are in red; ordered or hydrophilic regions are in blue. (B) ADEP-ClpP degradation assays of full-length, wild-type BsFtsZ$_{1-382}$ as well as of BsFtsZ$_{mutS}$ and BsFtsZ$_{mutG}$ mutant proteins (left image), which carry mutations that change the hydrophobicity of their N termini (right image). In addition, a BsFtsZ$_{FLLI}$ mutant protein was tested in which N-terminal hydrophobic amino acids were flipped, while overall hydrophobicity remained unchanged to wild-type FtsZ. The grand average of hydropathicity (GRAVY) of the mutated N termini was calculated according to the Kyte-Doolittle scale (67) using online software (https://web.expasy.org/protparam/). In these assays, low concentrations of ADEP and ClpP were used (1.5 μM ClpP; 1.5 μM ADEP). Samples were taken after a 120-min incubation; DMSO was used as a control. (C) Densitometry of protein bands from SDS-PAGE was performed to compare FtsZ protein amounts in ADEP-treated samples with the corresponding DMSO control reactions after 60 min (black bars) and 120 min (gray bars). The respective DMSO control was set to 1.0 (100%). For each FtsZ variant, the data were collected from three different degradation assays and SDS-PAGE analyses using a standard curve. The plotted data depict the corresponding mean values, with standard deviations indicated by error bars. Compared with BsFtsZ$_{1-382}$, BsFtsZ$_{mutS}$ and BsFtsZ$_{mutG}$ were significantly less degraded by ADEP-ClpP after incubation for 60 or 120 min. In contrast, FtsZ$_{FLLI}$ was similarly or slightly better degraded than BsFtsZ$_{1-382}$. *, $P < 0.05$; **, $P < 0.01$; ***, $P < 0.001$.

hypothesized that hydrophobicity may play a role in determining FtsZ as a target for ADEP-ClpP at low antibiotic concentrations and constructed functional mutant proteins with varied hydrophobicity of the N terminus. And indeed, the less hydrophobic mutant proteins BsFtsZ$_{mutG}$ and BsFtsZ$_{mutS}$, for which all hydrophobic amino acids of the N terminus were replaced by either glycine or serine, respectively, were clearly less prone to degradation by ADEP-ClpP (Fig. 2B and C), while retaining functionality in control GTPase assays (Fig. S2). When we exchanged the positions of the individual hydrophobic amino acids in BsFtsZ$_{FLLI}$ while keeping the overall hydrophobicity of this region unchanged, the mutant protein remained functional (Fig. S2) and was degraded similarly to full-length, wild-type BsFtsZ (Fig. 2B and C). This finding indicates that degradation of FtsZ does not depend on a certain amino acid sequence but that it is triggered by the hydrophobic nature of the N terminus.

The N terminus of FtsZ does not act as a universal degradation tag for ADEP-ClpP. We next wondered whether the hydrophobic N terminus of FtsZ may serve as a general degradation tag and would render proteins susceptible to ADEP-ClpP that otherwise resist degradation. To test this, we fused the N terminus of FtsZ (FtsZ$_{1-10}$) to enhanced green fluorescent protein (eGFP), a common model substrate for joint ClpP/Clp-ATPase complexes. However, neither attaching FtsZ$_{1-10}$ to the N terminus nor to the C terminus of eGFP resulted in its degradation by ADEP-ClpP (Fig. 3A). eGFP is known as a very stably folded protein that usually resists degradation by ClpP/Clp-ATPase complexes unless it is fused to a specific degron, which is recognized by the corresponding Clp-ATPase partner (28). Therefore, we also tested a fusion of FtsZ$_{1-10}$ to the Clp substrate Spx, but again, we did not observe degradation even after prolonged incubation with ADEP-ClpP (Fig. 3A), demonstrating that FtsZ$_{1-10}$ is not a degradation tag by itself that generally labels protein substrates for proteolysis by ADEP-ClpP. We then explored whether attaching the full-length FtsZ protein would trigger the degradation of eGFP by ADEP-ClpP. To this end, we constructed and purified a chimeric protein where eGFP is fused to the C terminus of full-length FtsZ, i.e., FtsZ-eGFP, which we then used in *in vitro* ADEP-ClpP degradation assays (Fig. 3B). As a control, we used

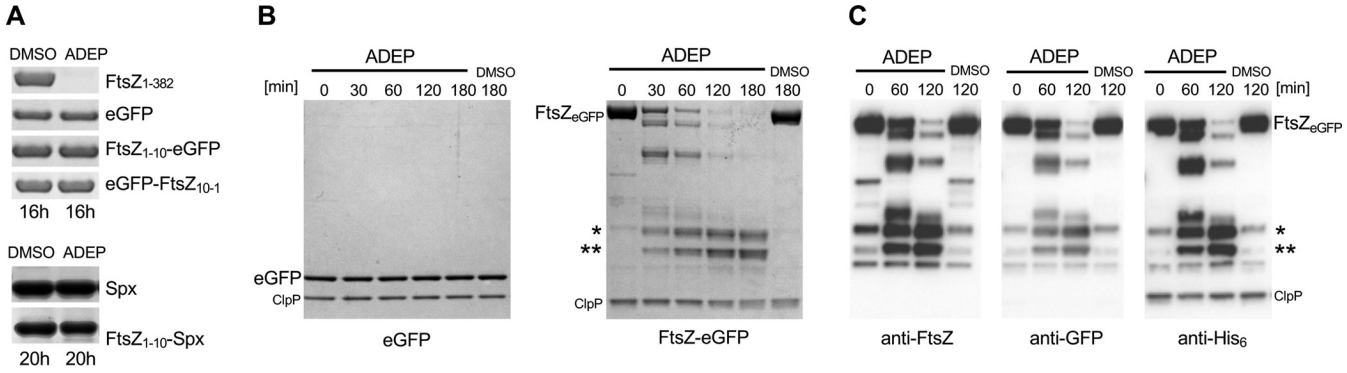

FIG 3 The N terminus of FtsZ is not sufficient to render proteins vulnerable to ADEP-ClpP. (A) *In vitro* ADEP-ClpP degradation assays of $FtsZ_{1-10}$ fused to either eGFP or Spx. For the fusion of $FtsZ_{1-10}$ to the C terminus of eGFP, the order of the N-terminal amino acids was inverted, which is indicated by $FtsZ_{10-1}$. (B) *In vitro* ADEP-ClpP degradation assays using eGFP alone as well as a fusion of eGFP to the C terminus of full-length FtsZ (FtsZ-eGFP). Here, eGFP alone resisted degradation, while FtsZ-eGFP was rapidly degraded, generating two accumulating degradation fragments over time (indicated by asterisks). (C) Immunoblotting of FtsZ-eGFP samples from ADEP-ClpP degradation assays using anti-FtsZ, anti-eGFP, and anti-His_6 antibodies. Of note, anti-FtsZ and anti-His_6 antibodies can be used to prove the integrity of the eGFP protein, as these antibodies recognize the C terminus of FtsZ and eGFP, respectively. The two accumulating degradation fragments of FtsZ-eGFP (indicated by asterisks) could be detected with all three antibodies, indicating an intact eGFP protein. In all assays, high concentrations of ClpP and ADEP2 were used (2.5 μM ClpP, 6.25 μM ADEP2). Samples were taken at indicated time points. DMSO was used as a control. All experiments were performed at least in triplicate; representative SDS-PAGE (A, B) or Western blot (C) images are depicted.

eGFP without FtsZ fusion, which resisted degradation by ADEP-ClpP. In our assay, FtsZ-eGFP was rapidly degraded, with two distinct degradation fragments accumulating over time. We further characterized these two fragments by immunoblotting using anti-His_6, anti-eGFP, and anti-FtsZ antibodies (Fig. 3C). Of note, the anti-FtsZ antibody used here recognizes the extreme C terminus of FtsZ, and the anti-His_6 antibody binds to the C-terminal His_6 tag of eGFP. Thus, anti-FtsZ and anti-His_6 antibodies can be used to confirm the integrity of the N and C terminus of eGFP, respectively, in this construct. Here, immunoblots showed that both accumulating fragments comprised full-length eGFP, since corresponding signals could be detected via all three antibodies. Corroborating the degradation of FtsZ from the N terminus, here ADEP-ClpP degraded the FtsZ part of the fusion protein FtsZ-eGFP, but it did not succeed in degrading eGFP even when fused to FtsZ. Obviously, FtsZ possesses additional inherent characteristics that only in combination with the hydrophobic N terminus permit degradation by ADEP-ClpP.

FtsZ cleavage extends into the folded N-terminal domain. FtsZ is efficiently degraded into smaller fragments, with a preferred degradation start at its N terminus (Fig. S1). However, one would expect that such degradation would require unfolding of the FtsZ protein in the absence of Clp-ATPases since the protein is presumably too large to access the proteolytic chamber in its folded form. One could speculate that the removal of the flexible N terminus (i.e., amino acids 1 to 10) might destabilize FtsZ such that it consequently unfolds on its own. However, our data demonstrate that the deletion of the flexible N-terminal portion leaves FtsZ folding intact. $BsFtsZ_{11-382}$ is functionally active in GTP hydrolysis (Fig. S2), and the truncated mutant is more stable than $BsFtsZ_{1-382}$ against degradation by ADEP-ClpP, making self-unfolding of the mutant protein highly unlikely. Furthermore, circular dichroism (CD) spectra of $BsFtsZ_{1-382}$, $BsFtsZ_{11-382}$ as well as untagged BsFtsZ in the absence or presence of the nonhydrolyzable GTP analogue guanosine-5′-*O*-(3-thiotriphosphate) (GTPγS) were superimposable. All spectra revealed the characteristic ellipticity of alpha-helical folds with two minima at 208 nm and 222 nm, indicating the presence of folded FtsZ proteins (without nucleotides as well as in the GTPγS-bound form) with similar average secondary structures under conditions that allow for the efficient degradation of full-length BsFtsZ (Fig. 4A). Therefore, we investigated whether ADEP-ClpP may be capable of destabilizing the fold of FtsZ during N-terminal attack to allow for further protein degradation.

To address this aspect of FtsZ proteolysis in more detail, we performed orienting analyses via label-free mass spectrometry (electrospray ionization-tandem mass spec-

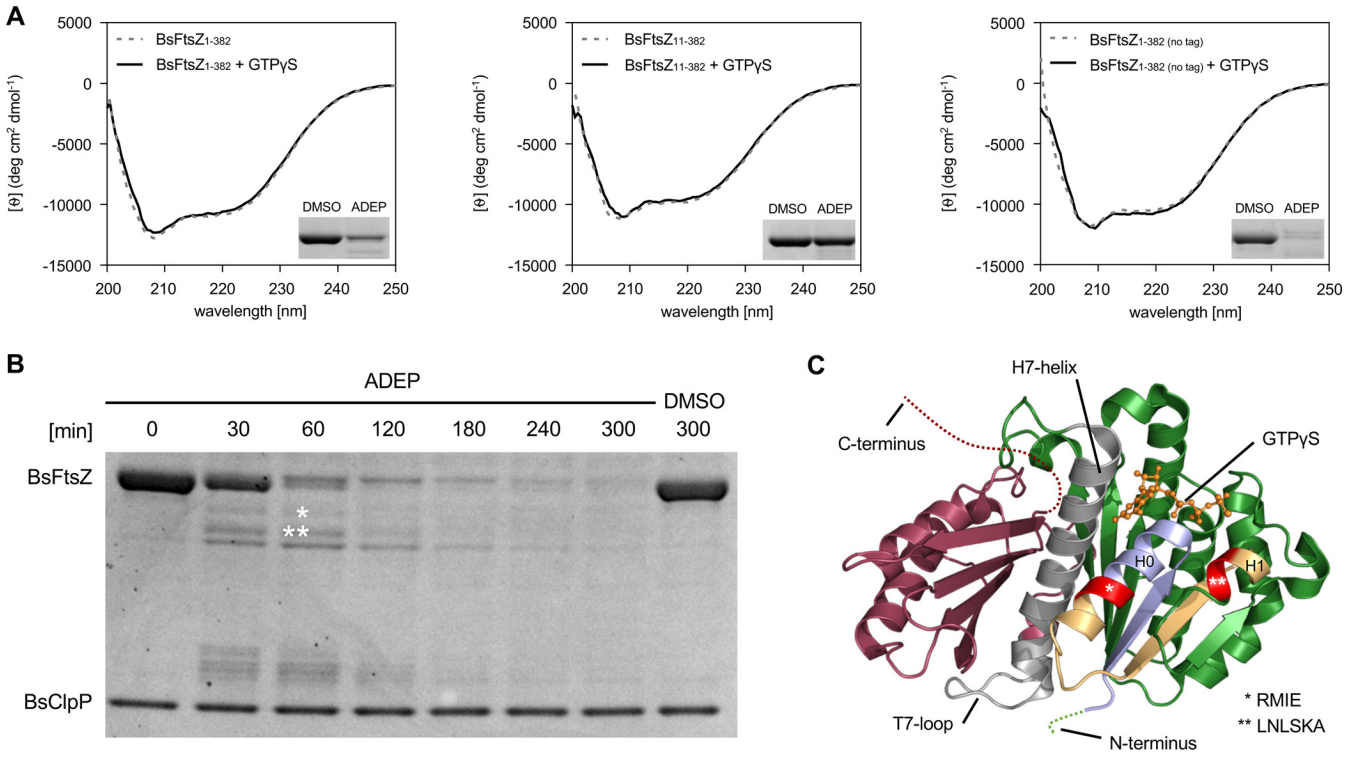

FIG 4 FtsZ folding and identification of early fragments of FtsZ degradation. (A) CD spectra of $BsFtsZ_{1-382}$ and $BsFtsZ_{11-382}$ (both C-terminally His_6 tagged) as well as $BsFtsZ_{1-382\ (no\ tag)}$ in the absence (gray dashed line) or presence of GTPγS (black line). All samples show the characteristic ellipticity spectra for an alpha-helical fold with two minima at 208 nm and 222 nm, indicating a folded state of the FtsZ protein under these conditions. As a control, *in vitro* degradation of the corresponding BsFtsZ proteins (without GTPγS) was performed using the CD buffer conditions (i.e., activity buffer CD) and low concentrations of ADEP and ClpP (1.5 μM ClpP, 1.5 μM ADEP, and 4 μM FtsZ). Samples were taken after 60 min; DMSO was used as a control. Representative images of duplicates are depicted. (B) Time course of $BsFtsZ_{1-382}$ degradation by ADEP-ClpP, indicating the generation of distinct degradation products. In these assays, low concentrations of ADEP and ClpP were used (1.5 μM ClpP, 1.5 μM ADEP, and 4 μM FtsZ). Samples were taken at indicated time points; DMSO was used as a control. Of note, when degradation reactions were allowed to continue, all depicted bands disappeared, indicating the capacity of ADEP-ClpP to fully digest FtsZ. The two largest of the emerging bands were excised (corresponding protein fragments are indicated by asterisks) and analyzed by Edman N-terminal protein sequencing. (C) Edman sequencing identified cleavage up to amino acid position 28 at the end of alpha-helix H0 (*RMIE) for the first fragment and up to position 49 of alpha helix H1 (**LNLSKA) for the second fragment (as indicated), which revealed that cleavage extends into the folded N-terminal domain of FtsZ. The crystal structure of GTPγS-bound BsFtsZ (Protein Data Bank entry 2RHO) highlights the first identified amino acid of both early fragments in red (the associated degradation product is indicated by asterisks) as well as the corresponding structural elements that are cleaved off by ADEP-ClpP (* in light blue, ** in light blue and yellow). GTPγS is indicated as the orange stick model.

trometry [ESI-MS]) of full-length and high-molecular-weight fragments of FtsZ, which indicated N-terminal truncations following degradation by ADEP-ClpP (see Fig. S5 in the supplemental material). To further corroborate this result, we next performed N-terminal protein sequencing by Edman degradation to identify early degradation fragments of wild-type FtsZ. Edman sequencing of the two largest degradation bands visible by SDS-PAGE (Fig. 4B) identified cleavage up to amino acid position 28 at the end of alpha-helix H0 (N-terminal amino acids determined by sequencing, RMIE) as well as up to position 49 of alpha helix H1 (N-terminal amino acids, LNLSKA). Thus, the data confirmed N-terminal degradation by ADEP-ClpP that extends into the folded region of the N-terminal domain of FtsZ (Fig. 4C).

Nucleotide binding prevents N-terminal degradation by stabilizing FtsZ. During the course of cell division, FtsZ assembles into protofilaments to form the "Z-ring" at the prospective division site, providing the scaffold for the assembly of the bacterial cytokinetic machinery. The formation of single-stranded protofilaments depends on GTP binding to FtsZ, which results in a dynamic head-to-tail association of individual FtsZ subunits (27, 29–33). The short hydrophobic N terminus of FtsZ can be assumed to be largely buried inside the binding interface between two subunits of an FtsZ protofilament (Fig. 5A). Therefore, we wondered whether the addition of GTP would have an impact on FtsZ degradation by rendering the N terminus less accessible to

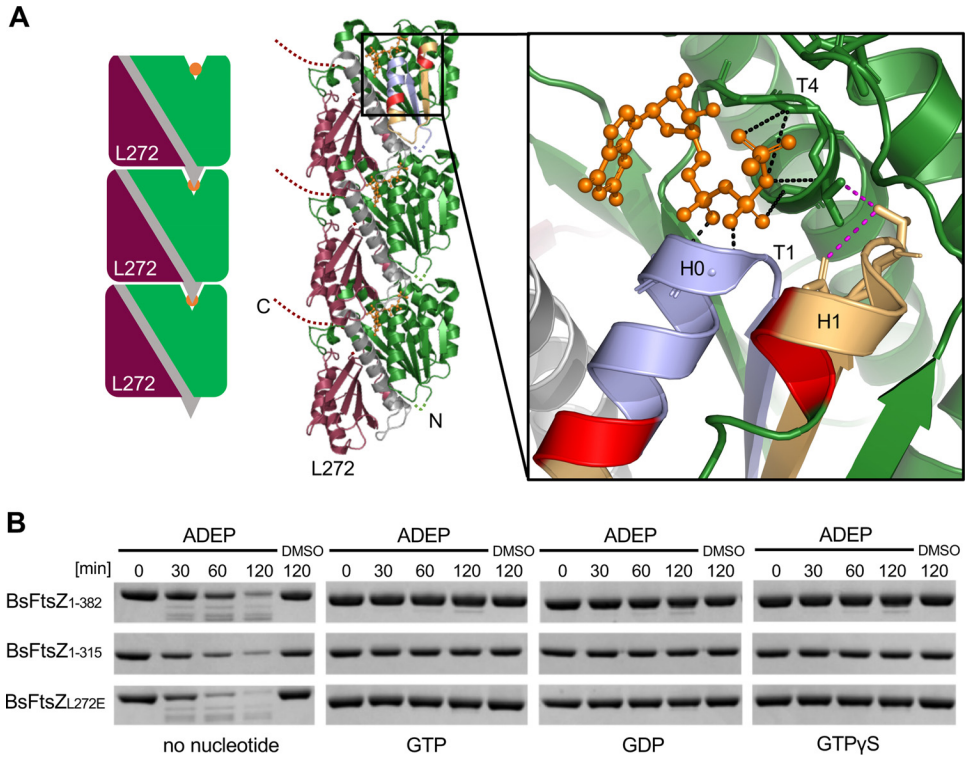

FIG 5 Nucleotide binding stabilizes FtsZ and inhibits degradation by ADEP-ClpP. (A) Head-to-tail association of individual FtsZ subunits result in single-stranded FtsZ protofilaments. The schematic shows the N-terminal domain (in green), the C-terminal domain (in currant red), and the central H7 helix with the T7 loop (in gray) as well as GTPγS (in orange). Also, the position of amino acid L272 inside the subunit interface is indicated. Note that in polymerized FtsZ, the short N terminus (N, green dotted line) is most probably largely buried in between two FtsZ monomers and may not be accessible to ADEP-ClpP. Zoom window shows established direct noncovalent contacts of GTPγS (in orange, Protein Data Bank entry 2RHO) with the T1 loop (Gly21-Gly22) and the T4 loop (Gly108-Gly110) (contacts in black) (37); the latter stabilizes helix H1 (contacts in magenta). The first amino acids of early FtsZ fragments, as identified by Edman sequencing (see Fig. 4), are indicated in red, cleaved off regions of the first and second degradation products in light blue and yellow, respectively. (B) ADEP-ClpP degradation assays of full-length $BsFtsZ_{1-382}$ as well as of $BsFtsZ_{1-315}$ and $BsFtsZ_{L272E}$ in the absence or presence of either GTP, GDP, or GTPγS. In these assays, low concentrations of ADEP and ClpP were used (1.5 μM ClpP; 1.5 μM ADEP). Samples were taken at indicated time points, DMSO was used as a control. All results were confirmed by at least three independent experiments, and images of representative experiments are depicted.

ADEP-ClpP. To test this, we preincubated FtsZ with GTP prior to ADEP-ClpP degradation and, indeed, preincubated FtsZ ($BsFtsZ_{1-382}$ and $BsFtsZ_{1-315}$) clearly resisted degradation, in contrast to the control which showed substantial proteolytic degradation in the absence of GTP (Fig. 5B). Also, preincubation with GDP, which mostly generates dimers or shorter, curved filaments of FtsZ (34–36), clearly inhibited the degradation of FtsZ. As a simple explanation for the observed protection from degradation, it might be speculated that the N terminus of FtsZ is hidden inside the protofilament and may, thus, be inaccessible to ADEP-ClpP (Fig. 5A, middle image).

Intriguingly, the N-terminal cuts detected by Edman sequencing require helices H0 and H1 to be pulled out of FtsZ, and these helices are located in the vicinity of the nucleotide binding site (Fig. 5A, right). Noteworthy, bound nucleotides establish direct noncovalent contacts with the T1 loop (Gly21-Gly22) and T4 loop (Gly108-Gly110) (37), the latter being part of the tubulin signature motif (GGGTGTG) which stabilizes helix H1 (Fig. 5A, right). As we hypothesized that FtsZ has to undergo unfolding during N-terminal degradation by ADEP-ClpP, we wondered if the sole binding of a guanosine nucleotide, regardless of protofilament formation, may already stabilize helices H0 and H1, thereby preventing FtsZ unfolding and subsequent degradation. To approach this hypothesis, we explored the impact of GTPγS that does not support protofilament formation. FtsZ polymerization cannot be induced by GTPγS that, however, still binds

to FtsZ (29, 38–41). And indeed, when we incubated FtsZ with GTPγS before the addition of ADEP-ClpP, thereby generating monomeric FtsZ bound to GTPγS, degradation was inhibited to the same extent as with GTP or GDP (Fig. 5B). To follow this route further, we employed a mutant FtsZ protein, $BsFtsZ_{L272E}$, which is capable of nucleotide binding but is impaired in GTP hydrolysis (Fig. S2). Accordingly, an *Escherichia coli* $FtsZ_{L272E}$ mutant had previously been described to exist only in the monomeric, nonpolymerized form, as L272 is located inside the biologically relevant intersubunit interface (42). In accordance with the results obtained for monomeric wild-type FtsZ bound to GTPγS, $BsFtsZ_{L272E}$ resisted degradation by ADEP-ClpP when preincubated with either GTP, GDP, or GTPγS (Fig. 5B). Although FtsZ (without the addition of nucleotides) appears to be in a folded state with similar average secondary structures under conditions allowing FtsZ degradation *in vitro* (Fig. 4A), nucleotide binding alone is sufficient, without the need of protofilament formation, to further stabilize the overall fold of the N-terminal domain of FtsZ and to prevent degradation of FtsZ from the N terminus.

The C terminus of FtsZ is increasingly degraded at higher concentrations of ADEP-ClpP. As detailed above, degradation of FtsZ by ADEP-ClpP preferentially starts from the N terminus, and low ADEP/ClpP concentrations (1.5 μM ClpP; 1.5 μM ADEP) were sufficient for efficient degradation of the entire protein into small fragments. FtsZ mutants lacking the short flexible N terminus remained largely intact when exposed to ADEP at these low concentrations. Nonetheless, in degradation assays using N-terminally truncated $BsFtsZ_{11\text{-}382}$ (Fig. 1E) or nucleotide-bound $FtsZ_{1\text{-}382}$ (Fig. 5B), a single faint band appeared slightly below the band of the full-length protein after prolonged incubation with ADEP-ClpP. The slow appearance of this band, its large size, and the fact that it was not readily degraded further oppose an origin from a fraction of residual unfolded or nucleotide-free FtsZ. Rather, these findings pointed toward a second target site within FtsZ to be degraded with considerably lower efficiency. We thus increased the concentration of ADEP and ClpP in our *in vitro* assay system (1.5 μM ClpP, 3.75 μM ADEP2 as well as 2.5 μM ClpP, 6.25 μM ADEP2; both correspond to 2.5 molar surplus of ADEP) and tested if we could also trigger degradation of nucleotide-bound FtsZ. And indeed, nucleotide-bound FtsZ was increasingly degraded at higher concentrations of ADEP/ClpP indicated by the appearance of more pronounced degradation fragments (Fig. 6A). Of note, degradation was also observed when using GTP, GDP, or GTPγS with $FtsZ_{L272E}$. Since the N terminus is stabilized in nucleotide-bound FtsZ, we hypothesized that the C terminus might serve as a secondary target site at higher concentrations of ADEP/ClpP. To further explore this, we tested the degradation of nucleotide-bound $BsFtsZ_{1\text{-}315}$ which lacks the flexible C terminus. In fact, the addition of nucleotides prevented the truncation of $BsFtsZ_{1\text{-}315}$, and no degradation bands appeared even at higher concentrations of ADEP/ClpP (Fig. 6A; see Fig. S6A in the supplemental material). C-terminal attack was also confirmed *in vitro* by immunoblotting using a His_6 tag fused to the C terminus of FtsZ (Fig. S6B). Likewise in whole cells, ADEP-ClpP truncated the C terminus of FtsZ when the N terminus was blocked with GFP, generating a stable degradation product only slightly smaller than FtsZ itself (see Fig. S7A in the supplemental material). In contrast, when GFP blocked the C terminus of FtsZ, FtsZ appeared fully degraded by ADEP-ClpP. Interestingly, we did not detect an accumulation of GFP fragments in the whole-cell situation that should have derived from an FtsZ-only degradation of the FtsZ-GFP fusion protein (Fig. S7B), as seen in our *in vitro* assays (Fig. 3C). Thus, we cannot exclude that FtsZ-GFP or fragments thereof may be fully degraded by ADEP-ClpP alone or with the help of other proteases in the bacterial cell, including degradation of GFP under these conditions.

We then gradually increased the ADEP concentration in our *in vitro* degradation assay, while keeping the ClpP concentration constant at 1.5 μM, and analyzed the degradation of the proteins $BsFtsZ_{1\text{-}382}$, $BsFtsZ_{11\text{-}382}$, and $BsFtsZ_{1\text{-}315}$ (Fig. 6B). Here, the degradation of $BsFtsZ_{1\text{-}382}$ was clearly increased at more than 2-fold the molar con-

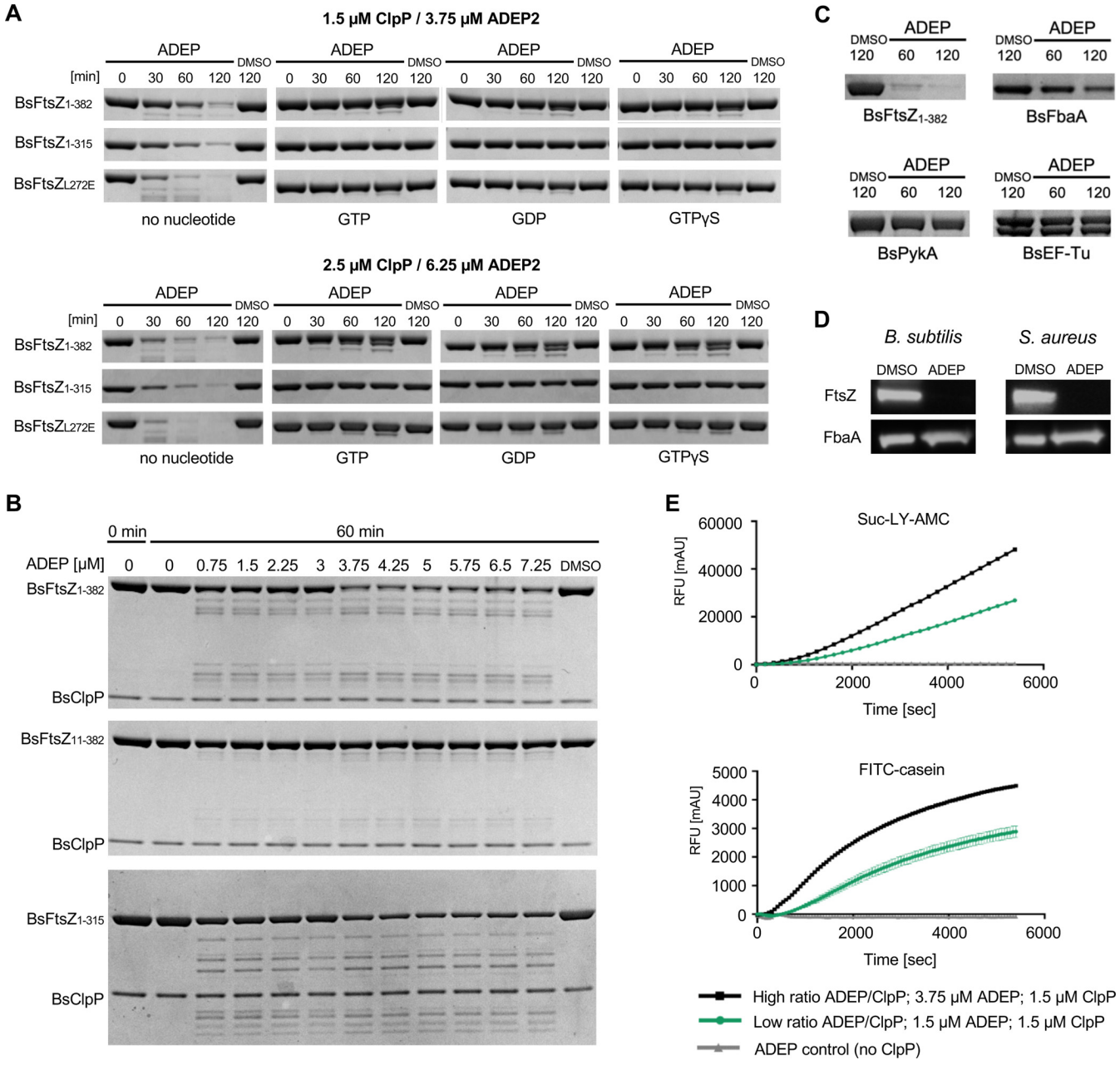

FIG 6 High concentrations of ADEP over ClpP lead to the degradation of the C terminus of FtsZ. (A) ADEP-ClpP degradation assays of $BsFtsZ_{1-382}$, $BsFtsZ_{1-315}$, or $BsFtsZ_{L272E}$ in the absence or presence of guanosine nucleotides using increased concentrations of ADEP over ClpP (top, 1.5 μM ClpP and 3.75 μM ADEP2; bottom, 2.5 μM ClpP and 6.25 μM ADEP2). DMSO was used as a control. Results were confirmed by at least three independent experiments, and images of representative experiments are depicted. (B) Degradation of $BsFtsZ_{1-382}$, $BsFtsZ_{11-382}$, or $BsFtsZ_{1-315}$ in the presence of 1.5 μM ClpP and increasing concentrations of ADEP2 (0 to 7.25 μM). Samples were taken after 60 min. DMSO was used as a control. Results were confirmed by at least three independent experiments, and images of representative experiments are depicted. (C) ADEP-ClpP degradation assays using $BsFtsZ_{1-382}$, BsFbaA, BsEF-Tu, or BsPyk as substrates for ADEP-activated ClpP at a high concentration of ADEP over ClpP (2.5 μM ClpP; 6.25 μM ADEP). Samples were taken at indicated time points. DMSO was used as a control. Of note, phosphorylation of BsEF-Tu produces a doublet band resulting from partial phosphorylation of a multiply phosphorylated substrate (65). All experiments were performed at least in triplicate; representative images are depicted. (D) Immunoblotting of *B. subtilis* 168 or *S. aureus* NCTC8325 cells that were treated with high ADEP concentrations (3 μg/ml ADEP2 for *B. subtilis* 168 and 8 μg/ml ADEP2 for *S. aureus* NCTC 8325, i.e., 10× MIC), leading to growth arrest due to ceased biomass production. Here, immunoblots indicated the rapid degradation of FtsZ compared with the untreated control (DMSO). In contrast and despite the increased ADEP concentration, the abundance of FbaA remained unaltered in both species over time. Immunodetection of FtsZ or FbaA was performed using specific anti-FtsZ or anti-FbaA antibodies, respectively. Samples were taken after 120 min. (E) Effects of low and high concentrations of ADEP on peptidase activity using the fluorogenic peptide substrate Suc-LY-AMC (top) or on protease activity using the fluorogenic protein substrate FITC-casein (bottom), respectively. Quenched 7-amino-4-methylcoumarin (AMC) fluorescence is released upon peptide hydrolysis (top). Quenched FITC fluorescence is released upon proteolysis (bottom). Reaction rates per 1.5 μM BsClpP in relative fluorescence units (RFUs) during the linear phase of substrate degradation. DMSO was used in control reactions and was subtracted from corresponding ADEP values. The reaction in the absence of ClpP was used as an additional control. Assays were confirmed in at least three independent experiments. Error bars for Suc-LY-AMC and FITC-casein assays indicate standard deviations.

centration of ADEP (starting at 3.75 μM ADEP2) over the ClpP monomer concentration. In accordance with our data described above, the degradation of $BsFtsZ_{11-382}$ was mostly prevented at lower ADEP/ClpP ratios but was triggered at higher ADEP concentrations, indicated by the appearance of pronounced degradation fragments, as a result of increased C-terminal degradation of FtsZ under these conditions. Also, N-terminal degradation of FtsZ was reproducibly accelerated at higher ADEP/ClpP ratios since $BsFtsZ_{1-315}$ was also increasingly degraded. To further test an ADEP/ClpP concentration-dependent degradation of other proteins, we attempted the degradation of BsEF-Tu, BsPyk, and BsFbaA using high ADEP/ClpP concentrations in our *in vitro* assays (Fig. 6C). While BsEF-Tu and BsPyk still resisted degradation under these conditions, the amount of BsFbaA slightly decreased over time, suggesting its degradation by ADEP-ClpP. However, when we employed immunoblotting to test the abundance of FbaA in *B. subtilis* and *S. aureus* cells that had been treated with high ADEP concentrations (>10× MIC), the protein concentration of BsFbaA still remained unaltered under these conditions, in contrast to BsFtsZ (Fig. 6D). Thus, it cannot be excluded that either a portion of the FbaA protein batch used in our *in vitro* assay may not have been properly folded, which may lead to its degradation, or that FbaA is sufficiently replenished by protein expression or its fold may be stabilized in the bacterial cytoplasm, impeding its degradation.

Our data consistently indicate that the flexible C terminus of FtsZ is targeted at higher concentrations of ADEP/ClpP in addition to the N terminus. To explore the molecular rationale for this observation, we tested the peptidase and protease activity of ADEP-ClpP under the same assay conditions (low versus high concentration of ADEP/ClpP). By studying the degradation of the peptide substrate Suc-Leu-Tyr-7-amino-4-methylcoumarin (Suc-LY-AMC) (Fig. 6E, top graph) or the loosely folded protein model substrate fluorescein isothiocyanate-casein (FITC-casein) (Fig. 6E, bottom graph), both the peptidolytic and proteolytic degradation rate of ADEP-activated ClpP were notably increased when the concentration of ADEP was raised. However, it is a matter not only of degradation velocity but also of selection capability, as a further target structure (the C-terminal end in addition to the N terminus of FtsZ) is addressed under these conditions. Hence, our data indicate that the destructive quality of ClpP increases with rising concentrations of ADEP, i.e., the spectrum of efficiently degraded substrates by ADEP-ClpP is widened. In the treated cell, this probably reflects the degradation of additional target structures, of which the C terminus of FtsZ is only but one example. Our results on FtsZ thus show that the fate of a protein, when targeted by ADEP-ClpP, depends not only on the capabilities of the deregulated protease but also on protein-intrinsic fragile or stabilizing substructures as well as physiochemical properties.

DISCUSSION

ADEP antibiotics have a dual mechanism of antibacterial action that is based on the multilayered deregulation of bacterial protease Clp; by binding to ClpP, ADEP inhibits all Clp functions in the bacterial cell (13, 14), and at the same time, it activates ClpP for the proteolysis of nonnative substrates in the absence of regulatory Clp-ATPases (1, 13, 17, 22). Depending on the bacterial species, ADEP uses either one or the other mechanisms for bacterial killing (1, 14). With regard to ClpP activation for the Clp-ATPase-independent degradation of nonnative substrates, we previously observed the following two concentration-dependent phenotypes in *B. subtilis*: (i) at ADEP concentrations several times the MIC, biomass increase ceased early (22, 23) and treated cells remained small, suggesting a depletion of essential proteins in various processes of the bacterial metabolism; and (ii) in contrast, at ADEP concentrations close to the MIC, treated cells were characterized by a phenotype of extensive filamentation, clearly marking an inhibition of cell division as the major antibiotic effect at these antibiotic concentrations. This filamentation phenotype is due to the untimely degradation of FtsZ (22), the pacemaker protein of cell division in most bacteria (30, 31). In fact, our new data show that the FtsZ protein seems especially prone to degradation compared

with other proteins, such as FbaA, EF-Tu, or Pyk, although FtsZ is most probably not the only cellular protein substrate of ADEP-ClpP, and nascent polypeptides at the ribosome are ADEP-ClpP targets as well (1, 13). In this context, it is further noteworthy that ADEP-activated BsClpP is even capable of degrading FtsZ from different species, including *Mycobacterium tuberculosis* (14). However, the reason for such a preferential degradation of FtsZ at low inhibitory ADEP concentrations has remained elusive so far.

In the current report, we now provide insight into the mechanism of FtsZ degradation by ADEP-ClpP which emerged to occur stepwise at different structural sites of FtsZ, depending on the applied concentration of ADEP and ClpP. At low concentrations of ADEP/ClpP, our results show that degradation by ADEP-ClpP preferably starts at the short N terminus of FtsZ. This finding was rather unexpected because the N-terminal region of FtsZ, which extends beyond the globular protein structure, is too short to reach the secluded catalytic sites of the ADEP-activated ClpP tetradecamer without the need of unfolding FtsZ. Assuming that the accessible part of the FtsZ N terminus is an extended peptide chain without secondary structure, its calculated length according to the Pauling model would be 36 Å (10 amino acids, 3.6 Å each for an extended peptide chain) (43, 44). However, a polypeptide chain would need to cover a distance of at least 40 Å from the entrance pore of the ADEP-ClpP tetradecamer (Glu53) to the active site serine (S97) of the catalytic triads (19). In contrast, the extended, flexible C terminus of FtsZ with a theoretical length of more than 200 Å would be long enough by far to easily diffuse through the opened pores of a ClpP tetradecamer to reach the catalytic triad and be degraded. Although the entrance pore diameter changes from ~1.8 nm in apo-BsClpP to ~2.7 nm in ADEP-bound BsClpP (19), it is still not wide enough to allow for entry of the N-terminal domain of FtsZ in its folded state (diameter, ~4 nm) into the degradation chamber, which implies that the N terminus of FtsZ needs to unfold during attack by ADEP-ClpP. A mechanism of protein unfolding is further supported by our observation that nucleotide binding to FtsZ prevents degradation at the N terminus, most probably by stabilizing the overall fold of the N-terminal domain of FtsZ. To our best knowledge, ClpP has not been described before to lead to protein unfolding in the absence of an associated Clp-ATPase, which usually unfolds Clp target proteins in an energy-dependent manner and upon recognition of a specific degron, such as SsrA (28). In *Escherichia coli*, for example, ClpX identifies FtsZ as a Clp target via two recognition signals located near the C terminus of FtsZ (45, 46). In this context, we have previously attempted the degradation of native Clp protease substrates using ADEP-ClpP, including MecA, McsB, and ComK from *B. subtilis* or DnaK, TigA, or GroEL from *E. coli*, as well as SsrA-tagged GFP, which all resisted degradation by ADEP-ClpP in our *in vitro* assays (22). On the other hand, FtsZ appears not to be degraded by ClpXP in *B. subtilis* (47, 48), indicating that the recognition of substrates by the Clp protease fundamentally differs from the substrate preference of ADEP-ClpP.

FtsZ has not principally been regarded as intrinsically unstable or loosely folded (25, 26, 30, 31). However, as FtsZ is a preferential target of ADEP-ClpP, which implies special inherent characteristics of the FtsZ protein, it may well be that the stability of the N-terminal domain of FtsZ (when devoid of nucleotides) is lower than that of other cytoplasmic proteins (49). Several studies reported on the presence of an unfolding intermediate of FtsZ and suggested that intradomain stabilization is important for overall protein stability (49–52). Since the N- and C-terminal domains of FtsZ represent independent folding domains (24), one could envision that partial unfolding of FtsZ, where the N-terminal half becomes unfolded and unbound from the C-terminal half of the polymerization domain, would allow for the exposure of a region smaller than the 2.7-nm diameter of the ADEP-bound BsClpP pore. Very recently, it has been reported that under certain *in vitro* conditions *S. aureus* FtsZ would occur in an unfolded state and requires nucleotide binding for proper folding (53). Although FtsZ was not intrinsically unfolded in our *in vitro* conditions, as shown by our CD data that indicate a normal FtsZ secondary structure fold with no difference in the absence or presence of nucleotides, this finding is very intriguing regarding the general stability of the FtsZ protein. Our data on the preferred degradation of FtsZ by ADEP-ClpP further support

the notion of a rather fragile fold of the FtsZ protein (under *in vitro* conditions as well as in the living cell) compared with other tested cellular proteins, including natural Clp substrates or eGFP. We therefore suggest that upon direct binding, ADEP-ClpP exploits such intrinsic conformational flexibility of the folded FtsZ protein (or at least of its N-terminal domain), leading to protein unfolding and subsequent digestion. Such intrinsic flexibility of a protein's fold may be a prerequisite for protein substrates of ADEP-ClpP, a degradative machine not supported by protein unfolding via energy-dependent Clp-ATPases.

Our data show that hydrophobic interactions play a pivotal role in the degradation of the N-terminal region of FtsZ by ADEP-ClpP, which may provide an explanation for the observed phenomenon. Hydrophobic residues also cluster around the rim of the ClpP entrance pore (54), and the inner surface of the degradation chamber is largely hydrophobic as well (55). Since the hydrophobic effect is considered the major driving force for the folding of proteins, strong enough to trigger supramolecular assemblies (56), establishing new hydrophobic contacts between FtsZ and ADEP-ClpP might weaken intrinsic contacts within FtsZ itself and lead to its unfolding. We therefore propose that the N terminus of FtsZ establishes hydrophobic contacts with the entrance pore of ClpP and beyond within the degradation chamber and that the sum of such interactions might be sufficient to allow the N terminus of FtsZ to partially unfold and stretch further into the degradation chamber of ClpP, leading to a destabilization of the N-terminal protein fold of nucleotide-free FtsZ (Fig. 7).

At higher concentrations of ADEP/ClpP, our data show that the spectrum of effectively degraded substrates by ADEP-ClpP is broadened, as we observed the additional degradation of the C terminus of FtsZ when using excess ADEP over ClpP, a substructure which mostly resisted degradation at lower concentrations of ADEP/ClpP. The molecular reason for such a broadening of the ADEP-ClpP substrate spectrum remains currently unclear and deserves further study. However, although equimolar concentrations of ADEP and ClpP were used for the condition of "low concentration of ADEP/ClpP" in our assays, it is feasible that the ClpP tetradecamer may not be saturated with ADEP molecules under these conditions. In all available crystal structures of ADEP-ClpP, all hydrophobic pockets of ClpP were fully occupied (2, 19, 20, 57, 58), the entrance pores were widened to the extent described above, and all catalytic sites were captured in the active conformation. However, crystal structures present a static endpoint generated at very high protein and compound concentrations. In a dynamic constellation, lower versus higher concentrations of ADEP may well influence ClpP occupancy, pore dynamics, and active site activity, which may lead to a preference for certain targets, such as the N terminus of FtsZ, over others. In our study, we observed a two-step activation mechanism of ClpP regarding FtsZ degradation, where degradation efficiency visibly increased at more than 2-fold the molar excess of ADEP over ClpP (Fig. 6B), that may therefore reflect unsaturated and saturated states of the ClpP tetradecamer with respect to ADEP binding.

FtsZ assembles into protofilaments to eventually form the Z-ring at midcell and initiate cell division. FtsZ protofilament formation is characterized by a continuous binding and consumption of GTP, which is then released as GDP from FtsZ to allow the binding of a new GTP molecule. This constant exchange of nucleotides is accompanied by the dynamic exchange of FtsZ subunits between the Z-ring and the cytoplasmic pool (27, 29–33). Importantly, a certain critical concentration of FtsZ is required for protofilament formation (29, 59). Our data show that nucleotide-bound FtsZ resists proteolytic attack at lower ADEP concentrations. In the context of bacterial cell division, it may therefore be hypothesized that ADEP-ClpP will predominantly deplete the cytoplasmic pool of apo-FtsZ when low inhibitory ADEP concentrations are used. This may consequently lead to a reduction of the cytoplasmic FtsZ level below the critical concentration required for filamentation, which will inevitably result in an inhibition of cell division and eventually cell death. At higher ADEP concentrations, we showed that nucleotide binding does not prevent FtsZ degradation by ADEP-ClpP since the C terminus becomes an additional target independent of the presence of bound

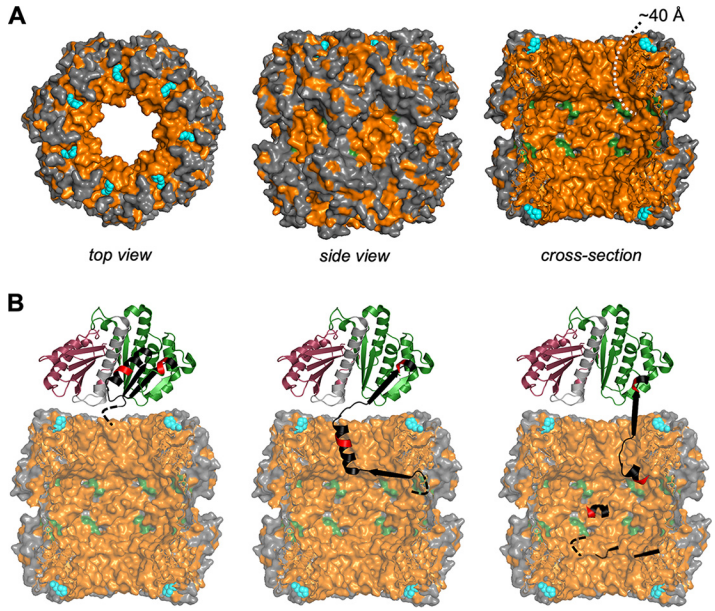

FIG 7 Proposed model for the N-terminal degradation of FtsZ by ADEP-ClpP. (A) Crystal structure of a *B. subtilis* ClpP tetradecamer (BsClpP; Protein Data Bank entry 3KTK; in gray with overall hydrophobic regions in orange) with ADEP2 bound to the hydrophobic pockets (cyan). Catalytic triads are highlighted in green. The cross-section of a BsClpP tetradecamer (right) models the inside of the proteolytic chamber, illustrating the overall hydrophobic nature of the ClpP entrance pore (54) and the inner surface of the degradation chamber (55). Noteworthy, in the available BsClpP crystal structure, the outermost N-terminal amino acids lining the entrance pore are not visible due to inherent flexibility. Thus, the actual situation regarding the hydrophobic surface interacting with an unfolded FtsZ N terminus or any unfolded protein will slightly deviate from what is shown here. To reach the catalytic triads within the proteolytic chamber, a peptide chain has to span a length of approximately 40 Å. (B) Hydrophobic interactions appear to be important for the attack of ADEP-ClpP on the N-terminal region of FtsZ since the hydrophobicity of the FtsZ N terminus supports its degradation. We propose that the hydrophobic N terminus of FtsZ (black dashed line) engages with ClpP via manifold hydrophobic interactions that occur within the entrance pore of ClpP and beyond within the degradation chamber. A sum of interactions that is, in total, stronger than the binding forces within the FtsZ N-terminal domain itself, supported by a nonstatic nature of the ClpP pore surface, might trigger an unfolding process that allows the N terminus of FtsZ to extend further and yet further into the catalytic chamber. Although ClpP alone might not "pull" by force, as the Clp-ATPases can do during their ATP-fueled power stroke, it might still be perfectly capable of "holding tight" long enough to destabilize the secondary structure within the potentially rather flexible N-terminal domain of nucleotide-free FtsZ (in black and green). Nucleotide binding, however, prevents FtsZ unfolding by stabilizing the N-terminal domain and thus inhibits degradation of the N terminus.

nucleotides. Here, the grappling hook peptide (GHP) (60) located at the extreme C terminus of FtsZ is degraded, which represents the interaction interface of FtsZ with other divisome proteins. Hence, C-terminal degradation will further contribute to a depletion of intact FtsZ available for Z-ring formation, thus accelerating the detrimental effects on cell division.

In conclusion, our data identify the hydrophobic N terminus of FtsZ as a preferred target at low levels of ADEP/ClpP, although it cannot be excluded that further proteins are also degraded at filamentation concentrations but show a less prominent phenotype. A stepwise degradation of distinct target structures by ADEP-ClpP as indicated here provides a rationale for the series of events that lead to the strikingly different phenotypes at low versus high ADEP concentrations (prolonged filamentation versus rapid cessation of biomass production, respectively) (23). This suicide-like mechanism of protease activation with its broad destructive capacity is distinct from all clinically applied antibiotics and makes ADEPs a promising starting point for the development of novel strategies for antibacterial attack.

MATERIALS AND METHODS

Bacterial strains and growth conditions. Bacterial strains and plasmids used in this study are listed in Table S1 in the supplemental material. Bacteria were grown in lysogeny broth (LB) at 37°C, which was

supplemented with appropriate antibiotics or inducing compounds when required. ADEP2 was added to early-exponential-phase *B. subtilis* or *S. aureus* cultures unless otherwise stated. For low (2× to 3× MIC) or high (>10× MIC) ADEP2 concentrations, 0.25 μg/ml or 3 μg/ml ADEP2 was used for *B. subtilis* and 1 μg/ml or 8 μg/ml ADEP2 for *S. aureus*, respectively. Of note, the ADEP per ClpP (ADEP/ClpP) molar ratios occurring in bacterial cells when exposed to the low and high ADEP concentrations in our whole-cell assays may, of course, differ from the ADEP/ClpP ratios adjusted in our *in vitro* assays. The actual ADEP concentrations in the two distinct settings were chosen for the following reasons: *in vitro*, the low and high concentrations were selected to clearly differentiate between the N-terminally focused degradation and the combined N-/C-terminal attack. In the whole-cell context, the low concentration leads to a strong filamentation phenotype in *B. subtilis* (respective swelling in *S. aureus*) and thus a phenotype dominated by FtsZ degradation, whereas under the high concentration, biomass increase and metabolism in general are severely inhibited, demonstrating degradation of a wider range of substrates. MICs were determine according to the guidelines of the Clinical and Laboratory Standards Institute (CLSI) except for using LB.

Cloning experiments. Primers that were used for cloning experiments in this study are listed in Table S2 in the supplemental material. Polymerase, T4 ligase, and antarctic phosphatase as well as restriction enzymes that were used for cloning experiments were obtained from New England BioLabs (NEB). Genes were amplified from genomic DNA of *B. subtilis* 168 (*clpP*, *ftsZ*, *fbaA*, *pyk*, and *tufA*) or *S. aureus* NCTC 8325 (*clpP* and *ftsZ*) (Table S1 and S2). The sequence of *egfp* was amplified using the plasmid pDest007-eGFP-(Ec)-ssrA (17). For ligation, a vector:insert ratio of 1:5 was employed using 70 ng of the double digested and dephosphorylated vector. PCR products were purified and digested with respective enzymes and ligated into expression vector pET22b or pET11a as indicated. For attaching purification tags or the N terminus of FtsZ, corresponding DNA fragments were amplified from template plasmids (indicated in Table S2) using either 5′-phosphorylated oligonucleotides or oligonucleotides with the same restriction site. The plasmids pET11a-bsPyk and pETftsZbs-egfp$_{H6}$ were cloned using the Gibson assembly master mix (NEB). For plasmid pETftsZbs-egfp$_{H6}$, a linker comprising 24 bp was inserted between the sequence of *ftsZ* and *egfp* to support correct protein folding and to allow sufficient flexibility of the protein fusion (the linker region is highlighted in gray in Table S2). Plasmid pETftsZbs$_{L272E}$ was generated using the QuikChange II site-directed mutagenesis kit (Agilent Technologies). Primers were constructed as described according to the manufacturer's manual.

Protein purification of ClpP and FtsZ. Native FtsZ of *B. subtilis* 168 was expressed in *E. coli* strain W3110 (pBS58) (pCXZ), as described earlier (22, 61). His$_6$-tagged FtsZ and ClpP proteins (originating from *B. subtilis* 168 or *S. aureus* NCTC8325) were expressed in *E. coli* BL21(DE3) harboring the respective expression plasmid (Table S1) and were purified as previously described (62). The quality and quantity of purified proteins were verified by SDS-PAGE, Bradford assay (using bovine serum albumin as the control), and spectrophotometry (Nanodrop Technologies). All tested FtsZ mutant proteins in this study were catalytically active, as shown by GTPase activity assays (GTPase-Glo assay; Promega) (Fig. S2), and the use of purification tags had no effect on degradation preference (see Fig. S8 in the supplemental material).

GTPase activity assays. The functionality of wild-type and mutant FtsZ proteins was analyzed using the GTPase-Glo assay (Promega) according to the manufacturer's instructions (Fig. S2). The assay measures the amount of residual GTP after a GTPase reaction by converting remaining GTP into ATP that is then detected using a luciferin/luciferase reaction. Different FtsZ concentrations were incubated in a white 384-well microtiter plate (Brand) for 1 h at 25°C in the presence of 5 μM GTP and 1 mM DTT in GTPase/GAP buffer (volume, 10 μl). An equal volume of GTPase/Glo buffer was then added, and the reaction mixture was incubated for 30 min at 25°C while shaking. For the luciferin/luciferase reaction, 20 μl of the detection reagent was added to each well, and the luminescence was measured in a microplate reader (Tecan Infinite M200) after 10 min.

Circular dichroism. FtsZ proteins were used at a concentration of 3.5 μM in activity buffer CD (50 mM Tris/HCl [pH 8], 25 mM $MgCl_2$, and 100 mM KCl) in the absence or presence of 40 μM GTPγS. To allow nucleotide binding by FtsZ, samples were preincubated for 10 min at room temperature before the start of the measurement. CD spectra were recorded from 200 to 250 nm (1-nm bandwidth, 20-nm min^{-1} scanning speed) with a Jasco J-720 spectropolarimeter using a 1-mm cuvette. The spectra were recorded 10 times for each protein sample, averaged, and corrected for the buffer system (with or without GTPγS, respectively). Spectra were only shown in the range of 200 nm to 250 nm since the activity buffer CD contains ions that strongly absorb at lower wavelengths.

***In vitro* nucleotide binding and degradation assays.** For *in vitro* guanosine nucleotide binding, FtsZ proteins (4 μM) were incubated in activity buffer BS (50 mM Tris/HCl [pH 8], 25 mM $MgCl_2$, and 100 mM KCl, 2 mM DTT) for *B. subtilis* proteins or activity buffer SA (20 mM HEPES [pH 7], 100 mM NaCl) for *S. aureus* proteins. Desired guanosine nucleotides were added to the reaction mixture to a final concentration of 1 mM according to a method described previously (63). For *in vitro* degradation, target proteins (4 μM BsPyk, BsEF-Tu, BsFbaA, eGFP, BsFtsZ-eGFP, and nucleotide-free or nucleotide-bound FtsZ) were incubated at 37°C in activity buffer BS (for *B. subtilis* proteins), activity buffer SA (for *S. aureus* proteins), or activity buffer CD (for CD spectroscopy control assays) in the presence of either low (1.5 μM ClpP; 1.5 μM ADEP) or high (1.5 μM ClpP; 3.75 μM ADEP, or 2.5 μM ClpP; 6.25 μM ADEP) concentrations of ADEP2 and ClpP monomer as indicated. Samples were taken at indicated time points and were analyzed via SDS-PAGE and immunodetection techniques (64). Where appropriate, protein amounts were calculated from SDS-PAGE band intensities measured via densitometry using Image Lab software (Bio-Rad). For quantitative/comparative analyses, a standard curve was generated representing 1 μg, 2 μg, 3 μg, 4 μg, and 5 μg of the control protein BsFtsZ$_{1-382}$, which was loaded on the same SDS-PAGE

as the protein samples derived from degradation experiments. Remaining FtsZ protein amounts in the ADEP-treated samples were then compared and normalized to the respective DMSO control reaction which was set to 100%. The data were plotted using mean values collected from three different degradation experiments and SDS-PAGE analyses for each FtsZ variant, with corresponding standard deviations indicated by error bars.

Suc-LY-AMC and FITC-casein degradation assays. For the degradation of the fluorescent peptide substrate Suc-LY-AMC, concentrations of ADEP2 and ClpP (monomer) were used as indicated. Peptidase assays were performed in activity buffer BS using 1.5 μM of purified ClpP protein and 400 μM of Suc-LY-AMC (dissolved in DMSO) in 100-μl reaction volumes. For the degradation of the fluorogenic protein fluorescein isothiocyanate-casein (FITC-casein; Sigma), concentrations of ADEP2 and ClpP (monomer) were used as indicated. Protease assays were performed in activity buffer BS using 1.5 μM of purified ClpP protein and 20 μM FITC-casein in 100-μl reaction volumes. In both peptidase and protease assays, an equal volume of DMSO compared to ADEP was used as a control. Corresponding DMSO samples were used as the baseline control and were subtracted from ADEP values. Hydrolysis of the peptide or protein substrates (indicated by fluorescence emission) was monitored in black, flat-bottom 96-well microplates (Sarstedt) at 37°C via measuring the release of either AMC or FITC, respectively, in a spectrofluorometer (Tecan Infinite M200) at an excitation wavelength (λex) of 380 nm and an emission wavelength (λem) of 460 nm (for Suc-LY-AMC) or at an λex of 490 nm and an λem of 525 nm (for FITC-casein).

Immunoblotting of FtsZ, GFP, and FbaA. To analyze the degradation of GFP-fused FtsZ in whole cells, *B. subtilis* strains 2014 and 2020 were cultivated in LB medium containing 1 mM isopropyl-β-D-thiogalactopyranoside (IPTG) and 0.5% xylose. Degradation of FtsZ and FbaA was further investigated using *B. subtilis* strain 168 as well as *S. aureus* strain NCTC 8325. Overnight cultures of all strains were diluted 1:200 in fresh LB (with or without appropriate inducers) and grown to an optical density at 600 nm (OD_{600}) of 0.1 to 0.25 at 37°C while shaking. Then, cultures were split, adding either ADEP2 or DMSO as a negative control. For *B. subtilis* strains 2014 and 2020, 0.5 μg/ml ADEP2 was used. For *B. subtilis* 168 and *S. aureus* NCTC 8325, 0.25 μg/ml or 3 μg/ml and 1 μg/ml or 8 μg/ml ADEP2 were used for low or high concentrations, respectively. Cultures were further shaken at 37°C for 60 or 120 minutes (as indicated). Cells were then harvested, suspended in 0.5 to 1 ml lysis buffer (50 mM NaH_2PO_4 and 300 mM NaCl [pH 8], with added EDTA-free mini protease inhibitor; Roche), and lysed via cell disruption in a PreCellys homogenizer (6,800 rpm, 3 times for 20 s) using a mixture of 0.1-μm and 0.5-μm glass beads in 0.5-ml PreCellys tubes. The protein content of the cell lysates was measured by Nanodrop spectrophotometry and adjusted accordingly. Immunoblotting of whole-cell extracts or purified proteins was performed by standard techniques (64) using anti-FtsZ, anti-GFP, anti-His_6, anti-FbaA, or anti-Div4A antibodies as indicated. A Coomassie blue-stained SDS-PAGE was additionally used to control the applied protein amount.

Protein identification by mass spectrometry. For orienting analyses, a partially truncated FtsZ protein was analyzed by label-free mass spectrometry (MS) using a Synapt G2-S HDMS time of flight (TOF) mass spectrometer equipped with an ESI NanoLockSpray source coupled online to a nanoAcquity ultraperformance liquid chromatography (UPLC) system and operated with MassLynx software (version V4.1 SCN932; Waters). Proteins were excised from the gel and destained twice in washing solution (20 mM ammonium bicarbonate, 30% acetonitrile). For reduction of disulfide bonds, gel pieces were incubated with 10 mM DTT in washing solution at 60°C for 45 min. Alkylation of cysteines was then performed with 50 mM iodoacetamide (IAA) in washing solution for 25 min at room temperature in the dark. Gel pieces were washed again twice with washing solution for 5 min at room temperature and dried using a vacuum centrifuge at 40°C prior to tryptic digestion with 6.25 ng/μl trypsin (Promega) in washing solution for 16 h at 37°C. Tryptic peptides were eluted using 20 μl of 0.1% trifluoroacetic acid and an ultrasonic bath for 15 min. Tryptic peptides were purified using a nanoAcquity UPLC trap symmetry C_{18} column (pore size, 100 Å; particle size, 5 μm; length, 20 mm; Waters) with a flow of 10 μl/min in 0.5% buffer B for 4 min. Tryptic peptides were then eluted from a nanoAcquity UPLC CSH130 C_{18} column (pore size, 130 Å; particle size, 1.7 μm; length, 100 mm; Waters) with a flow of 0.35 μl/min at 40°C using the following gradient: initial, 0.5% eluent B; 22 min, 60% eluent B; 24 min, 90% eluent B; 26 min, 99% eluent B; 27 min, 0.5% eluent B; and 30 min, 0.5% eluent B. Continuous MS^E spectra were recorded in a mass range from 50 to 1800 *m/z* and with a scan time of 1 s in positive resolution mode with the following settings: capillary voltage, 2.1 kV; cone voltage, 30 V; source temperature, 100°C; cone gas flow, 50 liters/h; desolvation gas flow, 550 liters/h; and desolvation temperature, 150°C. Collision energy was ramped from 14 to 45 eV. Serving as mass reference, leucine-encephalin was injected with a capillary voltage of 3 kV every 60 s. The mass spectra were processed with ProteinLynx Global Server (version 2.5.2; Waters). Processing parameters were adjusted as follows: chromatographic peak width, automatic; MS TOF resolution, automatic; lock mass for charge 1, 556.2771 Da/e; lock mass window, 0.25 Da; low energy threshold, 2,000 counts; elevated energy threshold, 500 counts; and intensity threshold, 10,000 counts. For protein identification, a data bank containing 4,156 proteins of *E. coli* BL21 (Uniprot reference sequence UP000002032, added manually; *B. subtilis* FtsZ and ClpP, trypsin, and keratin) was used. The following settings were used: peptide tolerance, automatic; fragment tolerance, automatic; min fragment ion matches per peptide, 5; min fragment ion matches per protein, 5; min peptide matches per protein, 1; maximum protein mass, 400,000; primary digest reagent, trypsin; secondary digest reagent, none; missed cleavages, 1; fixed modifications, carbamidomethyl C; variable modifications, deamidation N, deamidation Q, oxidation M; and false-positive rate, 4.

Edman protein sequencing. Edman protein sequencing was used to further characterize early fragments of native FtsZ degradation. To this end, 5 μM FtsZ protein was digested by ADEP2-ClpP as

described above and subsequently separated by SDS-PAGE (12%), followed by semidry electroblotting on a polyvinylidene difluoride (PVDF) membrane (blot buffer was 50 mM sodium borate [pH 9.0], 0.1% SDS, and 20% methanol) for 4 h at 4°C. Transferred proteins were stained with Ponceau S solution (0.5% Ponceau S and 1% acetic acid in deionized water) for 6 min, and desired bands were excised. Automated Edman protein sequencing was performed by Genaxxon (Germany) using a Procise capillary-liquid chromatography (cLC) Edman sequencer (Applied Biosystems), including N-terminal degradation steps 1 to 5 with amino acid identification and verification.

SUPPLEMENTAL MATERIAL

Supplemental material is available online only.

FIG S1, PDF file, 0.6 MB.

FIG S2, PDF file, 0.05 MB.

FIG S3, PDF file, 0.7 MB.

FIG S4, PDF file, 0.2 MB.

FIG S5, PDF file, 2.1 MB.

FIG S6, PDF file, 1 MB.

FIG S7, PDF file, 0.5 MB.

FIG S8, PDF file, 0.3 MB.

TABLE S1, PDF file, 0.1 MB.

TABLE S2, PDF file, 0.04 MB.

ACKNOWLEDGMENTS

We gratefully thank L. Hamoen, J. Errington, F. Götz, S. Sieber, and K. Turgay for the kind gift of strains, plasmids, or antibodies; and we acknowledge the technical support of A. Wochele, J. Alford, and L. Alfter, as well as advice by N. Bartlick and T. Stehle regarding CD spectroscopy. We further thank A. Berscheid, D. Thomy, I. Malik, J. Bandow, and H.-G. Sahl for critical discussions.

N.S. and P.S. designed the experiments. N.S., S.P., S.S., C.M., and P.S. performed the experiments. N.S., S.S., and P.S. analyzed the data. N.S. and P.S. prepared figures. P.S. drafted the manuscript. All authors discussed data and edited the manuscript. H.B.-O. and P.S. conceived and supervised the study. H.B.-O. and P.S. acquired funding.

We declare that no competing interests exist.

We appreciate funding by the Deutsche Forschungsgemeinschaft (DFG, German Research Foundation), including project ID 398967434 (TRR 261, TPs A01 and A02), project ID 32152271 (SFB766, TP A17), and project ID 33421847 (FOR854, TP 1), as well as support by infrastructural funding from Cluster of Excellence EXC 2124 Controlling Microbes to Fight Infections.

REFERENCES

1. Brötz-Oesterhelt H, Beyer D, Kroll HP, Endermann R, Ladel C, Schroeder W, Hinzen B, Raddatz S, Paulsen H, Henninger K, Bandow JE, Sahl HG, Labischinski H. 2005. Dysregulation of bacterial proteolytic machinery by a new class of antibiotics. Nat Med 11:1082–1087. https://doi.org/10.1038/nm1306.
2. Brown Gandt A, Griffith EC, Lister IM, Billings LL, Han A, Tangallapally R, Zhao Y, Singh AP, Lee RE, LaFleur MD. 2018. *In vivo* and *in vitro* effects of a ClpP-activating antibiotic against vancomycin-resistant enterococci. Antimicrob Agents Chemother 62:e00424-18. https://doi.org/10.1128/AAC.00424-18.
3. Conlon BP, Nakayasu ES, Fleck LE, LaFleur MD, Isabella VM, Coleman K, Leonard SN, Smith RD, Adkins JN, Lewis K. 2013. Activated ClpP kills persisters and eradicates a chronic biofilm infection. Nature 503:365–370. https://doi.org/10.1038/nature12790.
4. Thomy D, Culp E, Adamek M, Cheng EY, Ziemert N, Wright GD, Sass P, Brötz-Oesterhelt H. 2019. The ADEP biosynthetic gene cluster in *Streptomyces hawaiiensis* NRRL 15010 reveals an accessory *clpP* gene as a novel antibiotic resistance factor. Appl Environ Microbiol 85:e01292-19. https://doi.org/10.1128/AEM.01292-19.
5. Bukau B, Weissman J, Horwich A. 2006. Molecular chaperones and protein quality control. Cell 125:443–451. https://doi.org/10.1016/j.cell.2006.04.014.
6. Frees D, Gerth U, Ingmer H. 2014. Clp chaperones and proteases are central in stress survival, virulence and antibiotic resistance of *Staphylococcus aureus*. Int J Med Microbiol 304:142–149. https://doi.org/10.1016/j.ijmm.2013.11.009.
7. Brötz-Oesterhelt H, Sass P. 2014. Bacterial caseinolytic proteases as novel targets for antibacterial treatment. Int J Med Microbiol 304:23–30. https://doi.org/10.1016/j.ijmm.2013.09.001.
8. Baker TA, Sauer RT. 2012. ClpXP, an ATP-powered unfolding and protein-degradation machine. Biochim Biophys Acta 1823:15–28. https://doi.org/10.1016/j.bbamcr.2011.06.007.
9. Raju RM, Goldberg AL, Rubin EJ. 2012. Bacterial proteolytic complexes as therapeutic targets. Nat Rev Drug Discov 11:777–789. https://doi.org/10.1038/nrd3846.
10. Kirstein J, Moliere N, Dougan DA, Turgay K. 2009. Adapting the machine: adaptor proteins for Hsp100/Clp and AAA+ proteases. Nat Rev Microbiol 7:589–599. https://doi.org/10.1038/nrmicro2185.
11. Kim YI, Levchenko I, Fraczkowska K, Woodruff RV, Sauer RT, Baker TA. 2001. Molecular determinants of complex formation between Clp/Hsp100 ATPases and the ClpP peptidase. Nat Struct Biol 8:230–233. https://doi.org/10.1038/84967.
12. Olivares AO, Baker TA, Sauer RT. 2016. Mechanistic insights into bacterial AAA+ proteases and protein-remodelling machines. Nat Rev Microbiol 14:33–44. https://doi.org/10.1038/nrmicro.2015.4.
13. Kirstein J, Hoffmann A, Lilie H, Schmidt R, Rübsamen-Waigmann H,

Brötz-Oesterhelt H, Mogk A, Turgay K. 2009. The antibiotic ADEP reprogrammes ClpP, switching it from a regulated to an uncontrolled protease. EMBO Mol Med 1:37–49. https://doi.org/10.1002/emmm.200900002.

14. Famulla K, Sass P, Malik I, Akopian T, Kandror O, Alber M, Hinzen B, Ruebsamen-Schaeff H, Kalscheuer R, Goldberg AL, Brötz-Oesterhelt H. 2016. Acyldepsipeptide antibiotics kill mycobacteria by preventing the physiological functions of the ClpP1P2 protease. Mol Microbiol 101:194–209. https://doi.org/10.1111/mmi.13362.
15. Leodolter J, Warweg J, Weber-Ban E. 2015. The *Mycobacterium tuberculosis* ClpP1P2 protease interacts asymmetrically with its ATPase partners ClpX and ClpC1. PLoS One 10:e0125345. https://doi.org/10.1371/journal.pone.0125345.
16. Raju RM, Unnikrishnan M, Rubin DH, Krishnamoorthy V, Kandror O, Akopian TN, Goldberg AL, Rubin EJ. 2012. *Mycobacterium tuberculosis* ClpP1 and ClpP2 function together in protein degradation and are required for viability *in vitro* and during infection. PLoS Pathog 8:e1002511. https://doi.org/10.1371/journal.ppat.1002511.
17. Gersch M, Famulla K, Dahmen M, Göbl C, Malik I, Richter K, Korotkov VS, Sass P, Rübsamen-Schaeff H, Madl T, Brötz-Oesterhelt H, Sieber SA. 2015. AAA+ chaperones and acyldepsipeptides activate the ClpP protease via conformational control. Nat Commun 6:6320. https://doi.org/10.1038/ncomms7320.
18. Malik IT, Brötz-Oesterhelt H. 2017. Conformational control of the bacterial Clp protease by natural product antibiotics. Nat Prod Rep 34:815–831. https://doi.org/10.1039/c6np00125d.
19. Lee B-G, Park EY, Lee K-E, Jeon H, Sung KH, Paulsen H, Rübsamen-Schaeff H, Brötz-Oesterhelt H, Song HK. 2010. Structures of ClpP in complex with a novel class of antibiotics reveal its activation mechanism. Nat Struct Mol Biol 17:471–478. https://doi.org/10.1038/nsmb.1787.
20. Li DH, Chung YS, Gloyd M, Joseph E, Ghirlando R, Wright GD, Cheng YQ, Maurizi MR, Guarne A, Ortega J. 2010. Acyldepsipeptide antibiotics induce the formation of a structured axial channel in ClpP: a model for the ClpX/ClpA-bound state of ClpP. Chem Biol 17:959–969. https://doi.org/10.1016/j.chembiol.2010.07.008.
21. Malik IT, Pereira R, Vielberg MT, Mayer C, Straetener J, Thomy D, Famulla K, Castro H, Sass P, Groll M, Brötz-Oesterhelt H. 2020. Functional characterisation of ClpP mutations conferring resistance to acyldepsipeptide antibiotics in Firmicutes. Chembiochem https://doi.org/10.1002/cbic.201900787.
22. Sass P, Josten M, Famulla K, Schiffer G, Sahl HG, Hamoen L, Brötz-Oesterhelt H. 2011. Antibiotic acyldepsipeptides activate ClpP peptidase to degrade the cell division protein FtsZ. Proc Natl Acad Sci U S A 108:17474–17479. https://doi.org/10.1073/pnas.1110385108.
23. Mayer C, Sass P, Brötz-Oesterhelt H. 2019. Consequences of dosing and timing on the antibacterial effects of ADEP antibiotics. Int J Med Microbiol 309:151329. https://doi.org/10.1016/j.ijmm.2019.151329:151329.
24. Oliva MA, Cordell SC, Löwe J. 2004. Structural insights into FtsZ protofilament formation. Nat Struct Mol Biol 11:1243–1250. https://doi.org/10.1038/nsmb855.
25. Löwe J, Amos LA. 1998. Crystal structure of the bacterial cell-division protein FtsZ. Nature 391:203–206. https://doi.org/10.1038/34472.
26. Nogales E, Downing KH, Amos LA, Löwe J. 1998. Tubulin and FtsZ form a distinct family of GTPases. Nat Struct Biol 5:451–458. https://doi.org/10.1038/nsb0698-451.
27. Scheffers DJ, de Wit JG, den Blaauwen T, Driessen AJ. 2002. GTP hydrolysis of cell division protein FtsZ: evidence that the active site is formed by the association of monomers. Biochemistry 41:521–529. https://doi.org/10.1021/bi011370i.
28. Flynn JM, Levchenko I, Seidel M, Wickner SH, Sauer RT, Baker TA. 2001. Overlapping recognition determinants within the ssrA degradation tag allow modulation of proteolysis. Proc Natl Acad Sci U S A 98:10584–10589. https://doi.org/10.1073/pnas.191375298.
29. Mukherjee A, Lutkenhaus J. 1998. Dynamic assembly of FtsZ regulated by GTP hydrolysis. EMBO J 17:462–469. https://doi.org/10.1093/emboj/17.2.462.
30. Erickson HP, Anderson DE, Osawa M. 2010. FtsZ in bacterial cytokinesis: cytoskeleton and force generator all in one. Microbiol Mol Biol Rev 74:504–528. https://doi.org/10.1128/MMBR.00021-10.
31. Adams DW, Errington J. 2009. Bacterial cell division: assembly, maintenance and disassembly of the Z-ring. Nat Rev Microbiol 7:642–653. https://doi.org/10.1038/nrmicro2198.
32. Sundararajan K, Goley ED. 2017. The intrinsically disordered C-terminal linker of FtsZ regulates protofilament dynamics and superstructure in vitro. J Biol Chem 292:20509–20527. https://doi.org/10.1074/jbc.M117.809939.
33. Scheffers DJ, Driessen AJ. 2002. Immediate GTP hydrolysis upon FtsZ polymerization. Mol Microbiol 43:1517–1521. https://doi.org/10.1046/j.1365-2958.2002.02828.x.
34. Huecas S, Andreu JM. 2004. Polymerization of nucleotide-free, GDP- and GTP-bound cell division protein FtsZ: GDP makes the difference. FEBS Lett 569:43–48. https://doi.org/10.1016/j.febslet.2004.05.048.
35. Romberg L, Simon M, Erickson HP. 2001. Polymerization of Ftsz, a bacterial homolog of tubulin. Is assembly cooperative? J Biol Chem 276:11743–11753. https://doi.org/10.1074/jbc.M009033200.
36. Hsin J, Gopinathan A, Huang KC. 2012. Nucleotide-dependent conformations of FtsZ dimers and force generation observed through molecular dynamics simulations. Proc Natl Acad Sci U S A 109:9432–9437. https://doi.org/10.1073/pnas.1120761109.
37. Raymond A, Lovell S, Lorimer D, Walchli J, Mixon M, Wallace E, Thompkins K, Archer K, Burgin A, Stewart L. 2009. Combined protein construct and synthetic gene engineering for heterologous protein expression and crystallization using Gene Composer. BMC Biotechnol 9:37. https://doi.org/10.1186/1472-6750-9-37.
38. Mukherjee A, Lutkenhaus J. 1999. Analysis of FtsZ assembly by light scattering and determination of the role of divalent metal cations. J Bacteriol 181:823–832. https://doi.org/10.1128/JB.181.3.823-832.1999.
39. Bramhill D, Thompson CM. 1994. GTP-dependent polymerization of *Escherichia coli* FtsZ protein to form tubules. Proc Natl Acad Sci U S A 91:5813–5817. https://doi.org/10.1073/pnas.91.13.5813.
40. Yu XC, Margolin W. 1997. Ca2+-mediated GTP-dependent dynamic assembly of bacterial cell division protein FtsZ into asters and polymer networks in vitro. EMBO J 16:5455–5463. https://doi.org/10.1093/emboj/16.17.5455.
41. Scheffers DJ, den Blaauwen T, Driessen AJ. 2000. Non-hydrolysable GTP-gamma-S stabilizes the FtsZ polymer in a GDP-bound state. Mol Microbiol 35:1211–1219. https://doi.org/10.1046/j.1365-2958.2000.01791.x.
42. Li Y, Hsin J, Zhao L, Cheng Y, Shang W, Huang KC, Wang HW, Ye S. 2013. FtsZ protofilaments use a hinge-opening mechanism for constrictive force generation. Science 341:392–395. https://doi.org/10.1126/science.1239248.
43. Pauling L, Corey RB, Branson HR. 1951. The structure of proteins; two hydrogen-bonded helical configurations of the polypeptide chain. Proc Natl Acad Sci U S A 37:205–211. https://doi.org/10.1073/pnas.37.4.205.
44. Eisenberg D. 2003. The discovery of the alpha-helix and beta-sheet, the principal structural features of proteins. Proc Natl Acad Sci U S A 100:11207–11210. https://doi.org/10.1073/pnas.2034522100.
45. Camberg JL, Hoskins JR, Wickner S. 2009. ClpXP protease degrades the cytoskeletal protein, FtsZ, and modulates FtsZ polymer dynamics. Proc Natl Acad Sci U S A 106:10614–10619. https://doi.org/10.1073/pnas.0904886106.
46. Camberg JL, Viola MG, Rea L, Hoskins JR, Wickner S. 2014. Location of dual sites in *E. coli* FtsZ important for degradation by ClpXP; one at the C-terminus and one in the disordered linker. PLoS One 9:e94964. https://doi.org/10.1371/journal.pone.0094964.
47. Weart RB, Nakano S, Lane BE, Zuber P, Levin PA. 2005. The ClpX chaperone modulates assembly of the tubulin-like protein FtsZ. Mol Microbiol 57:238–249. https://doi.org/10.1111/j.1365-2958.2005.04673.x.
48. Haeusser DP, Lee AH, Weart RB, Levin PA. 2009. ClpX inhibits FtsZ assembly in a manner that does not require its ATP hydrolysis-dependent chaperone activity. J Bacteriol 191:1986–1991. https://doi.org/10.1128/JB.01606-07.
49. Andreu JM, Oliva MA, Monasterio O. 2002. Reversible unfolding of FtsZ cell division proteins from archaea and bacteria. Comparison with eukaryotic tubulin folding and assembly. J Biol Chem 277:43262–43270. https://doi.org/10.1074/jbc.M206723200.
50. Diaz-Espinoza R, Garces AP, Arbildua JJ, Montecinos F, Brunet JE, Lagos R, Monasterio O. 2007. Domain folding and flexibility of *Escherichia coli* FtsZ determined by tryptophan site-directed mutagenesis. Protein Sci 16:1543–1556. https://doi.org/10.1110/ps.072807607.
51. Santra MK, Panda D. 2003. Detection of an intermediate during unfolding of bacterial cell division protein FtsZ: loss of functional properties precedes the global unfolding of FtsZ. J Biol Chem 278:21336–21343. https://doi.org/10.1074/jbc.M301303200.
52. Montecinos-Franjola F, Ross JA, Sanchez SA, Brunet JE, Lagos R, Jameson DM, Monasterio O. 2012. Studies on the dissociation and urea-induced unfolding of FtsZ support the dimer nucleus polymerization mechanism. Biophys J 102:2176–2185. https://doi.org/10.1016/j.bpj.2012.03.064.

53. Huecas S, Canosa-Valls AJ, Araújo-Bazán L, Ruiz FM, Laurents DV, Fernández-Tornero C, Andreu JM. 2020. Nucleotide-induced folding of cell division protein FtsZ from *Staphylococcus aureus*. FEBS J https://doi.org/10.1111/febs.15235.
54. Sowole MA, Alexopoulos JA, Cheng YQ, Ortega J, Konermann L. 2013. Activation of ClpP protease by ADEP antibiotics: insights from hydrogen exchange mass spectrometry. J Mol Biol 425:4508–4519. https://doi.org/10.1016/j.jmb.2013.08.005.
55. Wang J, Hartling JA, Flanagan JM. 1997. The structure of ClpP at 2.3 A resolution suggests a model for ATP-dependent proteolysis. Cell 91:447–456. https://doi.org/10.1016/S0092-8674(00)80431-6.
56. Garcia-Seisdedos H, Empereur-Mot C, Elad N, Levy ED. 2017. Proteins evolve on the edge of supramolecular self-assembly. Nature 548:244–247. https://doi.org/10.1038/nature23320.
57. Wong KS, Mabanglo MF, Seraphim TV, Mollica A, Mao YQ, Rizzolo K, Leung E, Moutaoufik MT, Hoell L, Phanse S, Goodreid J, Barbosa LRS, Ramos CHI, Babu M, Mennella V, Batey RA, Schimmer AD, Houry WA. 2018. Acyldepsipeptide analogs dysregulate human mitochondrial ClpP protease activity and cause apoptotic cell death. Cell Chem Biol 25:1017–1030.e9. https://doi.org/10.1016/j.chembiol.2018.05.014.
58. Schmitz KR, Carney DW, Sello JK, Sauer RT. 2014. Crystal structure of *Mycobacterium tuberculosis* ClpP1P2 suggests a model for peptidase activation by AAA+ partner binding and substrate delivery. Proc Natl Acad Sci U S A 111:E4587–E4595. https://doi.org/10.1073/pnas.1417120111.
59. Huecas S, Llorca O, Boskovic J, Martin-Benito J, Valpuesta JM, Andreu JM. 2008. Energetics and geometry of FtsZ polymers: nucleated self-assembly of single protofilaments. Biophys J 94:1796–1806. https://doi.org/10.1529/biophysj.107.115493.
60. Buske PJ, Levin PA. 2013. A flexible C-terminal linker is required for proper FtsZ assembly *in vitro* and cytokinetic ring formation *in vivo*. Mol Microbiol 89:249–263. https://doi.org/10.1111/mmi.12272.
61. Wang X, Lutkenhaus J. 1993. The FtsZ protein of *Bacillus subtilis* is localized at the division site and has GTPase activity that is dependent upon FtsZ concentration. Mol Microbiol 9:435–442. https://doi.org/10.1111/j.1365-2958.1993.tb01705.x.
62. Sass P, Bierbaum G. 2007. Lytic activity of recombinant bacteriophage phi11 and phi12 endolysins on whole cells and biofilms of *Staphylococcus aureus*. Appl Environ Microbiol 73:347–352. https://doi.org/10.1128/AEM.01616-06.
63. Krol E, Scheffers DJ. 2013. FtsZ polymerization assays: simple protocols and considerations. J Vis Exp e50844. https://doi.org/10.3791/50844.
64. Sambrook J, Fritsch EF, Maniatis T. 1989. Molecular cloning: a laboratory manual, 2nd edition. Cold Spring Harbor Laboratory Press, Cold Spring Harbor, NY.
65. Pereira SF, Gonzalez RL, Jr, Dworkin J. 2015. Protein synthesis during cellular quiescence is inhibited by phosphorylation of a translational elongation factor. Proc Natl Acad Sci U S A 112:E3274–E3281. https://doi.org/10.1073/pnas.1505297112.
66. Yang ZR, Thomson R, McNeil P, Esnouf RM. 2005. RONN: the bio-basis function neural network technique applied to the detection of natively disordered regions in proteins. Bioinformatics 21:3369–3376. https://doi.org/10.1093/bioinformatics/bti534.
67. Kyte J, Doolittle RF. 1982. A simple method for displaying the hydropathic character of a protein. J Mol Biol 157:105–132. https://doi.org/10.1016/0022-2836(82)90515-0.

6.1.1 Supplemental Information

Supporting information
Cell division protein FtsZ is unfolded for N-terminal degradation by antibiotic-activated ClpP
Nadine Silber, Stefan Pan, Sina Schäkermann, Christian Mayer, Heike Brötz-Oesterhelt, Peter Sass

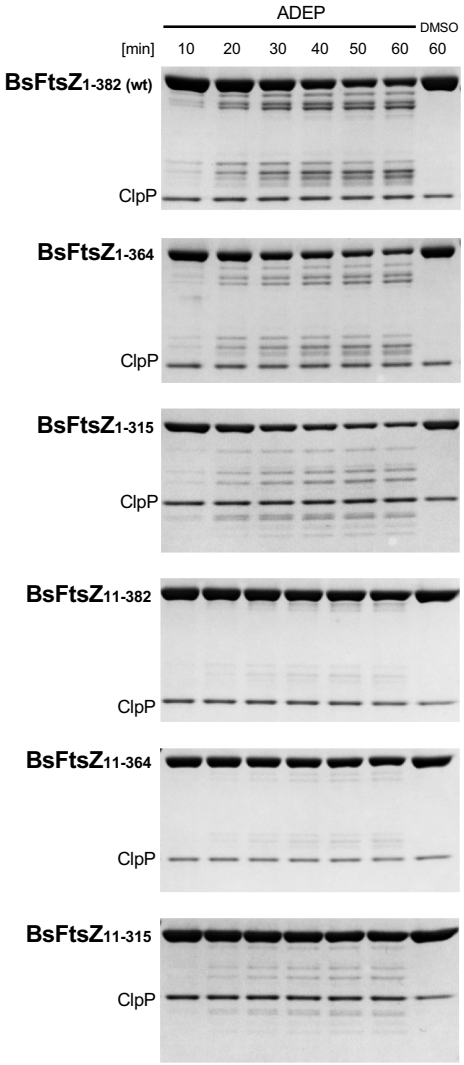

Figure S1:
Time-course of the degradation of FtsZ wild-type and mutant proteins by ADEP-ClpP.

Degradation of FtsZ wild-type and mutant proteins using low concentrations of ADEP and ClpP (1.5 µM ClpP; 1.5 µM ADEP) was followed over time. Samples were taken every 10 min over a time period of 60 min. DMSO was used as a control. The intensity of the ClpP protein band also serves as a loading control.

Supporting information
Cell division protein FtsZ is unfolded for N-terminal degradation by antibiotic-activated ClpP
Nadine Silber, Stefan Pan, Sina Schäkermann, Christian Mayer, Heike Brötz-Oesterhelt, Peter Sass

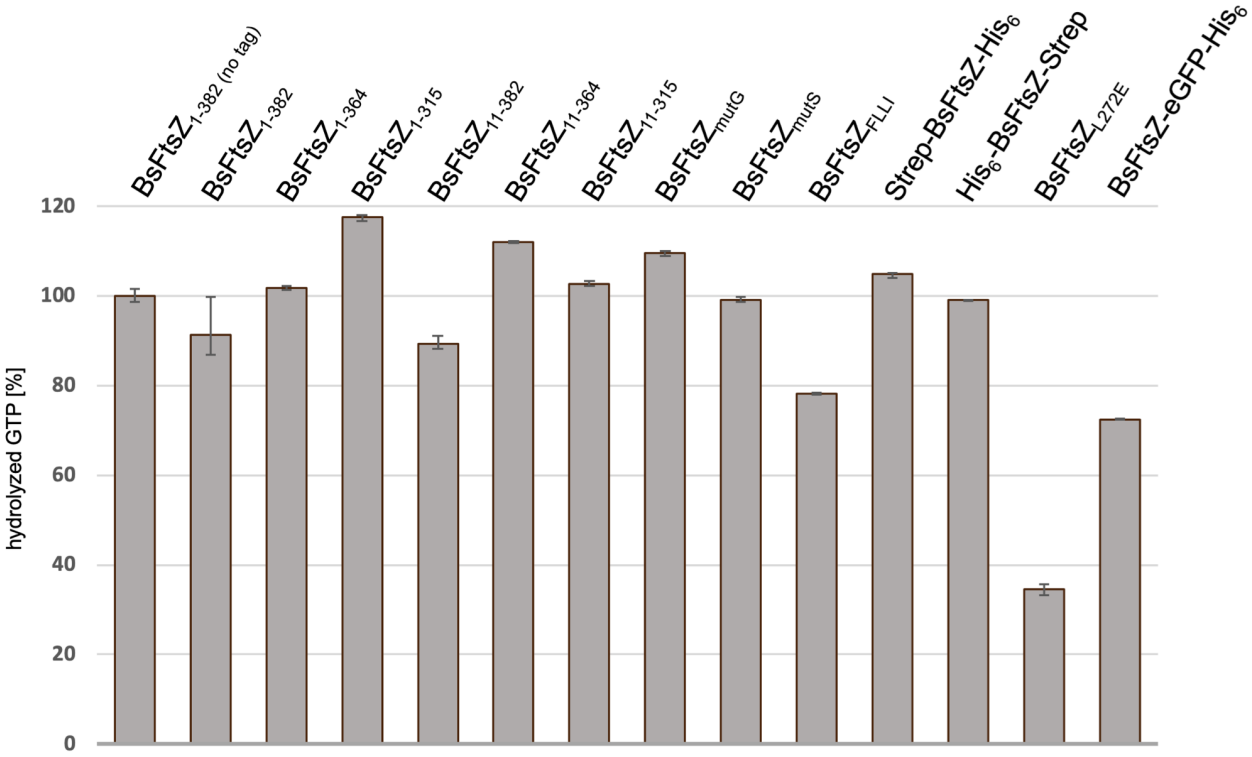

Figure S2:
GTPase activity assays of FtsZ wild-type and mutant proteins indicate their functionality.

Functionality of FtsZ was tested by comparing GTPase activities of full-length, wild-type proteins ($BsFtsZ_{1\text{-}382\ (no\ tag)}$ and $BsFtsZ_{1\text{-}382}$) and individual mutants. With the exception of $BsFtsZ_{1\text{-}382\ (no\ tag)}$, depicted proteins were expressed with a C-terminal His-6 tag. All mutants, except for $BsFtsZ_{L272E}$ as expected, retained GTPase activity mostly similar to wild-type level. Accordingly, an *E. coli* $FtsZ_{L272E}$ mutant was shown to bind nucleotides but was incapable to polymerize. Also for the BsFtsZ-eGFP fusion, GTPase activity of FtsZ was slightly reduced, which may be due to a disturbance by the eGFP fusion partner. In all assays, 10 µM of protein was used and GTP turnover was measured after 10 min. The mean of three biological replicates is indicated, error bars show highest and lowest values of the replicates. Wild-type, untagged BsFtsZ ($BsFtsZ_{1\text{-}382\ (no\ tag)}$) was set to 100%.

Supporting information
Cell division protein FtsZ is unfolded for N-terminal degradation by antibiotic-activated ClpP
Nadine Silber, Stefan Pan, Sina Schäkermann, Christian Mayer, Heike Brötz-Oesterhelt, Peter Sass

A

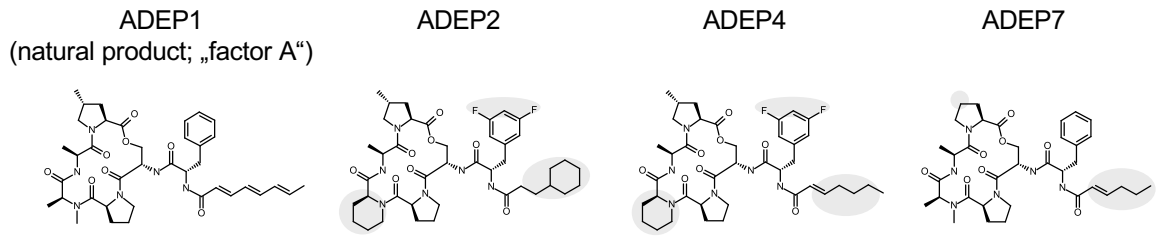

B

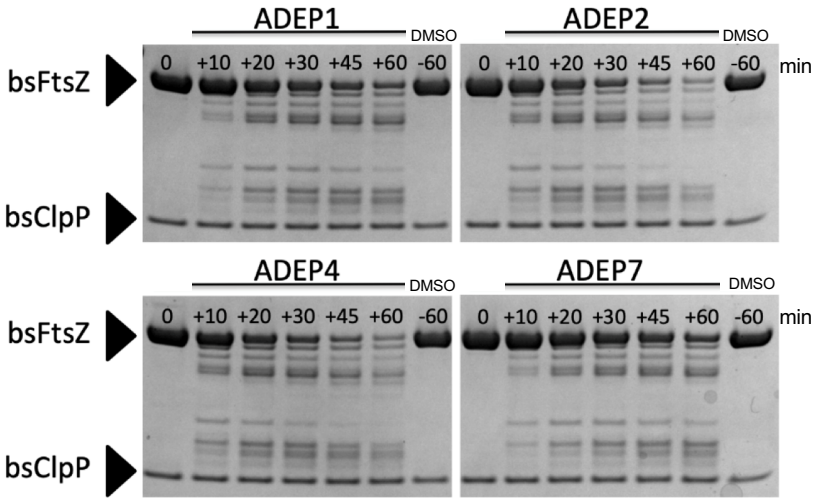

Figure S3:
ADEP derivatives differ in activating ClpP for the degradation of FtsZ.

(A) Structure of the natural product ADEP1 and its synthetic congeners ADEP2, 4, and 7. ADEP1 (“factor A”) is a natural product of *Streptomyces hawaiiensis* NRRL 15010 (4). The synthetic congeners have been reported previously (1). Highlighted regions indicate where the synthetic congeners deviate from the natural product ADEP1.
(B) SDS-PAGE analyses of *in vitro* ADEP-ClpP degradation assays using full-length $BsFtsZ_{1\text{-}382}$ and BsClpP proteins in combination with different ADEP derivatives. Here, ADEP2 and ADEP4 were most effective in activating BsClpP. DMSO was used as a control (“-60 min”). ADEP2 was selected for all subsequent experiments. All experiments were performed at least in triplicate, representative images are depicted.

Supporting information
Cell division protein FtsZ is unfolded for N-terminal degradation by antibiotic-activated ClpP
Nadine Silber, Stefan Pan, Sina Schäkermann, Christian Mayer, Heike Brötz-Oesterhelt, Peter Sass

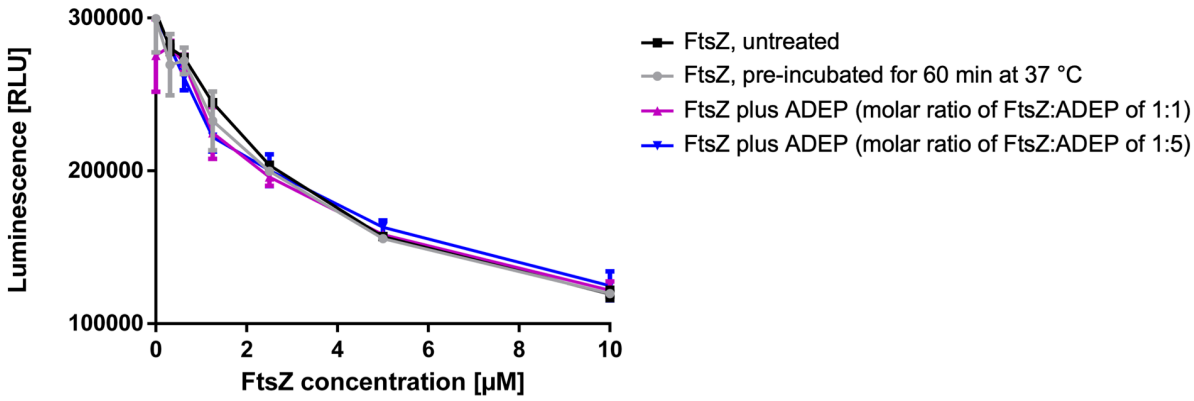

Figure S4:
ADEP does not interfere with FtsZ GTPase activity.

The target of ADEP is ClpP. To further exclude self-unfolding of FtsZ during incubation at 37 °C as well as off-target effects of ADEP on FtsZ activity in our *in vitro* assays, we tested the functionality of FtsZ under these conditions via GTPase activity assays. Non-hydrolysed GTP was read-out by conversion to ATP to fuel a luciferase reaction. Here, GTPase activity of FtsZ remained unaffected upon 60 min incubation at 37 °C. Hence, FtsZ does not turn unstable or functionally inactive during our *in vitro* assays. Furthermore, low or high concentrations of ADEP (molar ratio of FtsZ:ADEP2 of 1:1 or 1:5, respectively) did not affect GTPase activity, indicating that there are no off-target effects of ADEP on FtsZ to be expected. Of note, in the *in vitro* degradation assays of this study, the ADEP concentration never surpassed the molar ratio for FtsZ:ADEP2 of 1:1.6.

Supporting information
Cell division protein FtsZ is unfolded for N-terminal degradation by antibiotic-activated ClpP
Nadine Silber, Stefan Pan, Sina Schäkermann, Christian Mayer, Heike Brötz-Oesterhelt, Peter Sass

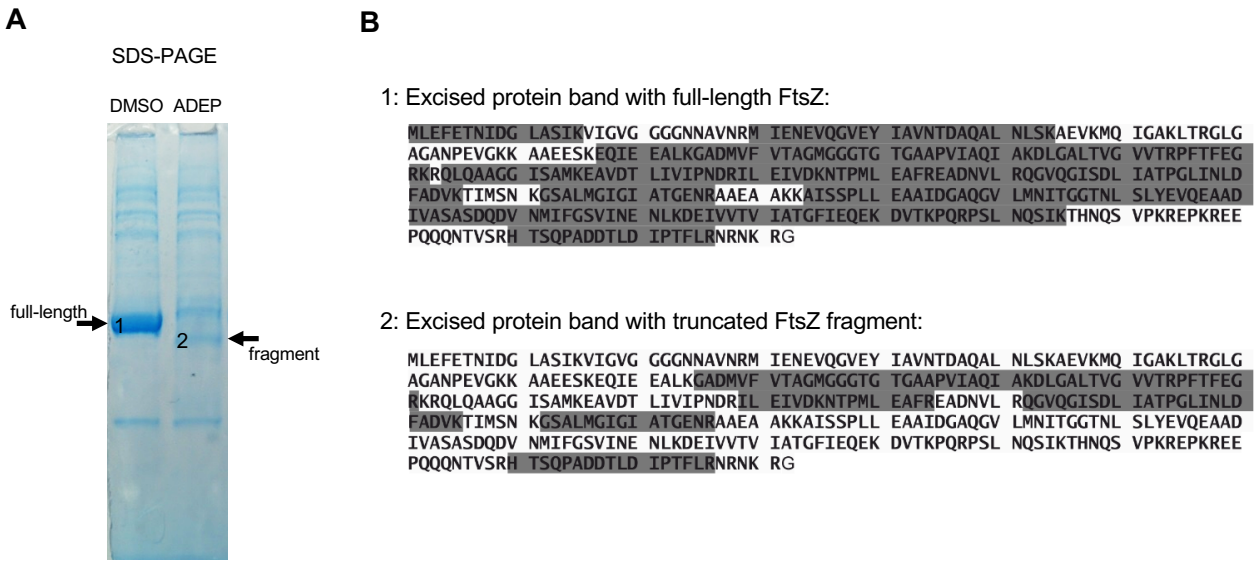

Figure S5:
ESI-MS of full-length and high-molecular weight fragments of FtsZ indicate N-terminal truncations following degradation by ADEP-ClpP.

(A) FtsZ was purified and incubated with ClpP in the presence of ADEP2 or DMSO (negative control) and subsequently separated by SDS-PAGE. Protein bands corresponding to FtsZ full-length protein in the control (1) and a fragment thereof appearing in the ADEP-treated sample (2) were excised from the gel, tryptically digested and subjected to orienting LC-ESI-MS studies. Low concentrations of ADEP/ClpP (1.5 µM ClpP monomer; 1.5 µM ADEP) were used.
(B) ESI-MS sequence coverages of FtsZ are highlighted in gray and show that the FtsZ fragment generated no N-terminal tryptic peptides compared to the full-length protein. Amino acid identification of the N-termini was then achieved using Edman protein sequencing (Fig. 4, main text).

Supporting information
Cell division protein FtsZ is unfolded for N-terminal degradation by antibiotic-activated ClpP
Nadine Silber, Stefan Pan, Sina Schäkermann, Christian Mayer, Heike Brötz-Oesterhelt, Peter Sass

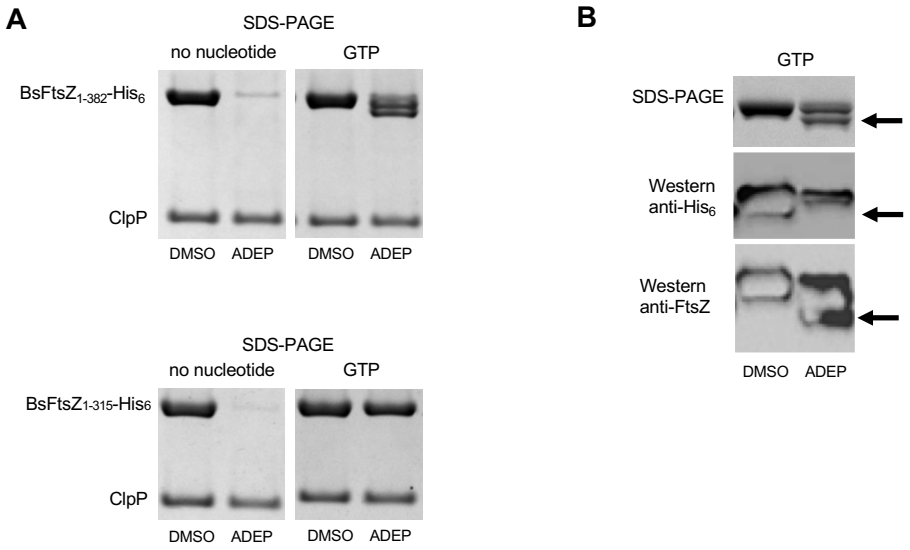

Figure S6:
The C-terminus of FtsZ is an additional target site at high concentrations of ADEP/ClpP.

(A) $FtsZ_{1\text{-}382}$ or $FtsZ_{1\text{-}315}$, both with attached C-terminal His_6-tags, were pre-incubated with or without GTP and subsequently used in ADEP-ClpP degradation assays with a high concentration of ADEP/ClpP (2.5 µM ClpP; 6.25 µM ADEP2). SDS-PAGE images show two distinct degradation products for $FtsZ_{1\text{-}382}$ after 120 min in the presence of ADEP-ClpP and GTP. Of note, no degradation bands were detected for $FtsZ_{1\text{-}315}$ in the presence of ADEP-ClpP and GTP. DMSO was used as a control.
(B) SDS-PAGE and corresponding Western blots using either anti-His_6 or anti-FtsZ antibodies show that the degradation products of $FtsZ_{1\text{-}382}$ lack the C-terminal His_6-tag, proving C-terminal attack by ADEP-ClpP.
Signals for anti-His_6 and anti-FtsZ antibodies were intentionally overexposed (resulting in white regions within the protein band) to also allow detection of weaker signals. Arrows mark the position of a C-terminal degradation product that could be detected by SDS-PAGE and with an anti-FtsZ antibody, but not with an anti-His6 antibody. DMSO was used as a control. All experiments were performed at least in triplicate, representative images are depicted.

Supporting information
Cell division protein FtsZ is unfolded for N-terminal degradation by antibiotic-activated ClpP
Nadine Silber, Stefan Pan, Sina Schäkermann, Christian Mayer, Heike Brötz-Oesterhelt, Peter Sass

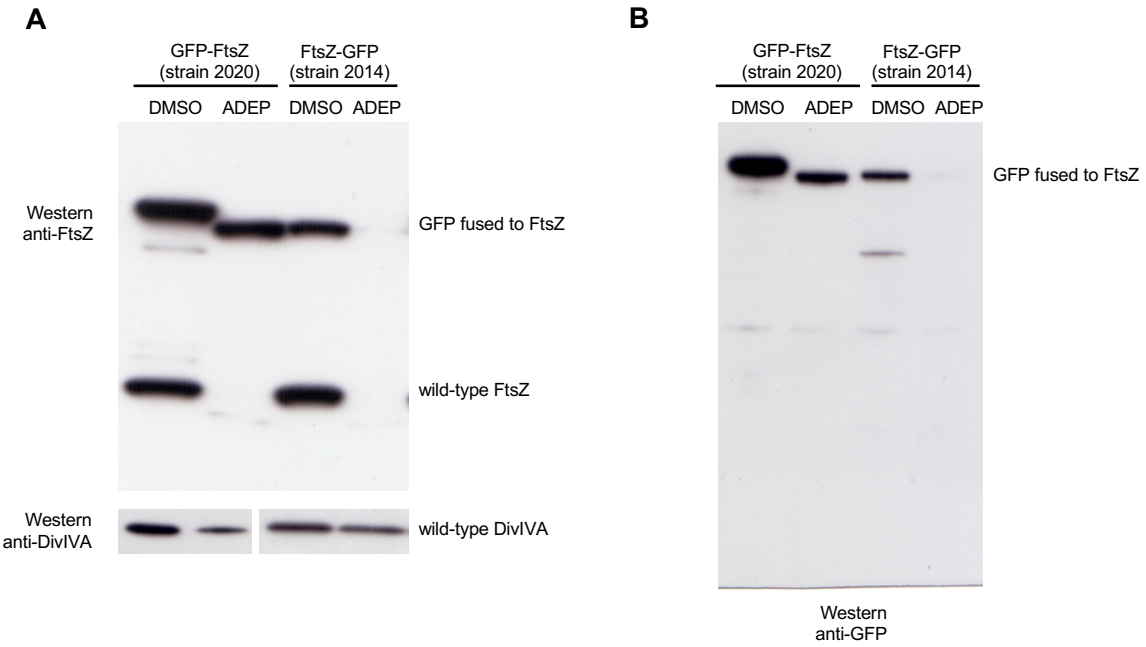

Figure S7:
ADEP-ClpP targets both termini of FtsZ at increased ADEP concentrations in whole cells.

Exponentially growing *B. subtilis* strains, which expressed both wild-type FtsZ as well as FtsZ mutant proteins attached to GFP (either fused to the N- or to the C-terminus of FtsZ) were treated for 60 minutes with either DMSO (negative control) or 0.5 µg/ml ADEP2, an antibiotic concentration that is well above the optimal filamentation concentration. Protein extracts were prepared and analysed via immunoblotting using anti-FtsZ (A) and anti-GFP antibodies (B). In accordance with our *in vitro* data of nucleotide-bound FtsZ, blocking the hydrophobic N-terminus of FtsZ with GFP only led to the truncation of the flexible C-terminus of FtsZ thereby generating a stable degradation product. On the contrary, when the C-terminus of FtsZ was blocked by GFP and the N-terminus remained accessible, FtsZ was fully degraded similar to wild-type FtsZ. Noteworthy, FtsZ-GFP runs sightly lower on SDS-PAGE than GFP-FtsZ which may be the result of the fusion of GFP to the long flexible C-terminus of FtsZ, probably providing more flexibility to the protein while running on SDS-PAGE compared to an N-terminal fusion. Detection of DivIVA protein using an anti-DivIVA antibody (A) served as a loading control. Further noteworty, we did not detect accumulating GFP fragments upon ADEP treatment of strain 2014 expressing the FtsZ-GFP fusion. Thus, we cannot exclude that GFP fragments of FtsZ-GFP may be further processed by either ADEP-ClpP or other proteases in the bacterial cell under these conditions. Images are representative of at least three independent experiments.

S1 Table. Bacterial strains and plasmids

Strain /plasmid	Relevant characteristic(s) /genotype	Ref. /Source
Strains		
B. subtilis		
168	*trpC2*; wild type strain	(1)
2014	*trpC2 chrI::pJSIZΔpble (Pspac-ftsZ ble) Ω(Pxyl-ftsZ-gfpmut1 cat)*	(2)
2020	*trpC2 spc amyE::Pxyl-gfp-ftsZ*	(3)
S. aureus		
NCTC 8325	*rsbU, tcaR;* wild-type strain	NARSA
E. coli		
K-12 JM109	subcloning host	(4)
Bl21(DE3)	λDE3 lysogen; expression host	(5)
W3110 (pBS58)(pCXZ)	Strain W3110 carrying the plasmids pCXZ(Ptac-*ftsZ*bs, Amp^R) and pBS58 (*ftsQAZ*ec, Spc^R)	(6)
Plasmids		
pClpP11	pQE70 (Qiagen) + ORF BSU34540 (*clpP*)	(7)
pET22b	vector for the expression of C-terminal His_6 fusion proteins	Novagen
pET11a	vector for the expression of native proteins	Novagen
pET22BΔ*pelB*	pET22b without *pelB*-leader tag, for the expression of C-terminal His_6 fusion proteins	(8)
pNP90	pET21d (Novagen) + ORF BSU15290 (*B. subtilis ftsZ*)	Hamoen lab
pETftsZsa	pET22BΔ*pelB* + ORF SAOUHSC_01150 (*S. aureus ftsZ*)	this study
pETclpPsa	pET22BΔ*pelB* + ORF SAOUHSC_00790 (*S. aureus clpP*)	this study
pETftsZbs$_{1-315}$	pET22BΔ*pelB* + ORF BSU15290 (*B. subtilis ftsZ*) comprising aa 1-315	this study
pETftsZbs$_{1-364}$	pET22BΔ*pelB* + ORF BSU15290 (*B. subtilis ftsZ*) comprising aa 1-364	this study
pETftsZbs$_{11-382}$	pET22BΔ*pelB* + ORF BSU15290 (*B. subtilis ftsZ*) comprising aa 11-382	this study
pETftsZbs$_{11-315}$	pET22b + ORF BSU15290 (*B. subtilis ftsZ*) comprising aa 11-315	this study
pETftsZbs$_{11-364}$	pET22b + ORF BSU15290 (*B. subtilis ftsZ*) comprising aa 11-364	this study
pETftsZbs$_{mutG}$	pET22b + ORF BSU15290 (*B. subtilis ftsZ*) carrying aa mutations L2G, F4G, I8G, L11G	this study
pETftsZbs$_{mutS}$	pET22b + ORF BSU15290 (*B. subtilis ftsZ*) carrying aa mutations L2S, F4S, I8S, L11S	this study
pETftsZbs$_{FLLI}$	pET22b + ORF BSU15290 (*B. subtilis ftsZ*) carrying aa mutations L2F, F4L, I8L, L11I	this study
pETftsZbs$_{L272E}$	pNP90 carrying aa mutation L272E in the *B. subtilis ftsZ* gene	this study
pETftsZbs-strep	pET11a + ORF BSU15290 (*B. subtilis ftsZ*) with C-terminal Strep-tag II	
pETstrep-ftsZ-his$_6$	pNP90 with additional N-terminal Strep-tag II	this study
pEThis$_6$-ftsZ-strep	pET11a + ORF BSU15290 (*B. subtilis ftsZ*) with attached N-terminal His_6-tag and C-terminal Strep-tag II	this study
pET22b-egfp	pET22b + *egfp* gene (UniProtKB ID C5MKY7)	this study
pET22b-NZ-egfp	pET22b + *egfp* gene (UniProtKB ID C5MKY7) carrying aa 1-10 of ORF BSU15290 (*B. subtilis* FtsZ$_{1-10}$) attached to the N-terminus of eGFP	this study
pDEST007 -strep-egfp	pDest007-eGFP-(Ec)-ssrA with deleted ssrA tag	(9), this study
pDEST007 -strep-egfp-NZ	pDEST007-strep-gfp carrying aa 1-10 of ORF BSU15290 (FtsZ$_{10-1}$) attached to the C-terminus of eGFP	this study
pETftsZbs-egfp$_{H6}$	pET22b + *egfp* gene (UniProtKB ID C5MKY7) with an His_6-tag fused to the C-terminus of *B. subtilis ftsZ* (ORF BSU15290)	this study
pET$_{H6}$egfp$_{H6}$	pET22b + *egfp* gene (UniProtKB ID C5MKY7) with an N- and C-terminal His_6-tag	this study
pSpx	pQE-60 (Qiagen) + ORF BSU11500 (*B. subtilis yjbD*)	(7)
pQE-NZ-Spx	pSpx carrying aa 1-10 of ORF BSU15290 (*B. subtilis* FtsZ$_{1-10}$) attached to the N-terminus of Spx	this study
pET11a-bsEF-Tu	pET11a + ORF BSU01130 (*B. subtilis tufA*)	this study
pET11a-bsPyk	pET11a + ORF BSU29180 (*B. subtilis pyk*)	this study
pET11a-bsFbaA	pET11a + ORF BSU37120 (*B. subtilis fbaA*)	this study

Abbreviations: aa, amino acids; ORF BSU, open reading frame of *Bacillus subtilis* 168 (genome accession number NC_000964), N-terminus, amino-terminus; C-terminus, carboxy-terminus; eGFP, enhanced green fluorescent protein; NZ, amino-acids 1-10 of BSU15290 (FtsZ$_{1-10}$); NARSA, Network on Antimicrobial Resistance in *Staphylococcus aureus*.

Table S1 references

1. Anagnostopoulos C, Spizizen J. 1961. Requirements for transformation of *Bacillus subtilis*. J Bacteriol 81:741-746.
2. Sievers J, Errington J. 2000. The *Bacillus subtilis* cell division protein FtsL localizes to sites of septation and interacts with DivIC. Mol Microbiol 36:846-855.
3. Stokes NR, Sievers J, Barker S, Bennett JM, Brown DR, Collins I, Errington VM, Foulger D, Hall M, Halsey R, Johnson H, Rose V, Thomaides HB, Haydon DJ, Czaplewski LG, Errington J. 2005. Novel inhibitors of bacterial cytokinesis identified by a cell-based antibiotic screening assay. J Biol Chem 280:39709-39715.
4. Yanisch-Perron C, Vieira J, Messing J. 1985. Improved M13 phage cloning vectors and host strains: nucleotide sequences of the M13mp18 and pUC19 vectors. Gene 33:103-119.
5. Studier FW, Moffatt BA. 1986. Use of bacteriophage T7 RNA polymerase to direct selective high-level expression of cloned genes. J Mol Biol 189:113-130.
6. Wang X, Lutkenhaus J. 1993. The FtsZ protein of *Bacillus subtilis* is localized at the division site and has GTPase activity that is dependent upon FtsZ concentration. Mol Microbiol 9:435-442.
7. Turgay K, Hahn J, Burghoorn J, Dubnau D. 1998. Competence in *Bacillus subtilis* is controlled by regulated proteolysis of a transcription factor. EMBO J 17:6730-6738.
8. Sass P, Bierbaum G. 2007. Lytic activity of recombinant bacteriophage phi11 and phi12 endolysins on whole cells and biofilms of *Staphylococcus aureus*. Appl Environ Microbiol 73:347-352.
9. Gersch M, Famulla K, Dahmen M, Gobl C, Malik I, Richter K, Korotkov VS, Sass P, Ruebsamen-Schaeff H, Madl T, Brötz-Oesterhelt H, Sieber SA. 2015. AAA+ chaperones and acyldepsipeptides activate the ClpP protease via conformational control. Nat Commun 6:6320.

Supporting information
Cell division protein FtsZ is unfolded for N-terminal degradation by antibiotic-activated ClpP
Nadine Silber, Stefan Pan, Sina Schäkermann, Christian Mayer, Heike Brötz-Oesterhelt, Peter Sass

S2 Table. Primer used in this study.

Plasmid	Forward (F) / Reverse (R) oligo (5'-3' direction)	Template
pETftsZsa	F: tttccatggtagaatttgaacaaggatttaatc R: aaactcgagacgtcttgttcttcttgaacg	*S. aureus* gDNA
pETclpPsa	F: Ttccatggatttaattcctacagttattgaaac R: aaactcgagttttgtttcaggtaccatcacttc	*S. aureus* gDNA
pETftsZbs$_{1-315}$	F: tttccatggtggagttcgaaacaaacatagac R: aaactcgagaaagccggttgcaatcactg	*B. subtilis* gDNA
pETftsZbs$_{1-364}$	F: tttccatggtggagttcgaaacaaacatagac R: aaactcgagcggctgtgaagtatgacgg	*B. subtilis* gDNA
pETftsZbs$_{11-382}$	F: tttccatggcatcaattaaagtaatcggagtag R: aaactcgaggccgcgtttattacggtttc	*B. subtilis* gDNA
pETftsZbs$_{11-315}$	F: tttccatggcatcaattaaagtaatcggagtag R: aaactcgagaaagccggttgcaatcactg	*B. subtilis* gDNA
pETftsZbs$_{11-364}$	F: tttccatggcatcaattaaagtaatcggagtag R: aaactcgagcggctgtgaagtatgacgg	*B. subtilis* gDNA
pETftsZbs$_{mutG}$	F: tttcatatgggagagggagaaacaaacggagacggcggagcatcaattaaagtaatcggagtag R: aaactcgaggccgcgtttattacggtttc	*B. subtilis* gDNA
pETftsZbs$_{mutS}$	F: tttcatatgagcgagagcgaaacaaacagcgacggcagcgcatcaattaaagtaatcggagtag R: aaactcgaggccgcgtttattacggtttc	*B. subtilis* gDNA
pETftsZbs$_{FLLI}$	F: tttcatatgttcgagttggaaacaaacttagacg gcatagcatcaattaaagtaatcggagtag R: aaactcgaggccgcgtttattacggtttc	*B. subtilis* gDNA
pETftsZbs$_{L272E}$	F: gaacaaacctcagcgaatatgaggttcag R: ctgaacctcatattcgctgaggtttgttc	pNP90
pETstrep-ftsZ-his$_6$	F: P-tggagccacccgcagttcgaaaaggtggagttcga aacaaacatag R: P-catggtatatctccttcttaaag	pNP90
pETftsZbs-strep	F: aaacatatgttggagttcgaaacaaac R: aaaggatcccttttcgaactgcgggtggctccactcgaggccgcgtttattacg	*B. subtilis* gDNA
pEThis$_6$-ftsZ-strep	F: P-gtggtggtgcatatgtatatctccttcttaaagttaaac R: P-caccaccacttggagttcgaaacaaacatagac	pETftsZbs-strep
pET22b-egfp	F: aaacatatggtgagcaagggcgaggag R: aaactcgaggctgcccagctcgtcc	pDest007-eGFP-(Ec)-ssrA
pET22b-NZ-egfp	F: P-tttcgaactccaacatatgtatatctccttcttaaagttaaac R: P-caaacatagacggcttagtgagcaagggcgagg	pET22b-egfp
pDEST007 -strep-egfp-NZ	F: P-acagagttcgagttgtaacacccagctttcttgtacaaagtgg R: P-attgatgtctccaagcttgtacagctcgtccatgccgag	pDest007-eGFP-(Ec)-ssrA
pDEST007 -strep-egfp	F: tttgaattccacccagctttcttgtacaaagtgg R: tttgaattcttacttgtacagctcgtccatgcc	pDEST007-strep-egfp-NZ
pETftsZbs-egfp$_{H6}$	F: ggctcaggaagcggctcaggctccgtgagcaagggcgaggag R: atgtatatctccttcttaaagttaaacaaaattatttctagagg F: tttaagaaggagatatacatatgttggagttcgaaacaaac R: ggagcctgagccgcttcctgagccgccgcgtttattacggtttc	*B. subtilis* gDNA/ pET22b-egfp, Gibson assembly
pET22b$_{H6}$egfp$_{H6}$	F: ttttcat**atg**caccaccaccaccaccacgtgagcaagggcgagg R: aaaacatatgtatatctccttcttaaagttaaac	pET22b-egfp
pQE-NZ-Spx	F: P-caaacatagacggcttagttacactatacacatcaccaagc R: P-tttcgaactccaacatggttaatttctcctctttaatgaattc	pSpx
pET11a-bsEF-Tu	F: aaacatatggctaaagaaaaattcgacc R: aaaggatcccttactcagtgattgtagaaacaacg	*B. subtilis* gDNA
pET11a-bsPyk	F: tcgggctttgttagcagccgttaaagaacgctcgcacg R: taagaaggagatatacatatgagaaaaattgtttgtacc F: atatgtatatctccttcttaaagttaaac R: cggctgctaacaaagccc	*B. subtilis* gDNA Gibson assembly
pET11a-bsFbaA	F: aaacatatgcctttagtttctatgacgg R: aaaggatcccttaagcttggtttgaagaacc	*B. subtilis* gDNA

Restriction sites are underlined. Linker regions, which were inserted between FtsZ and eGFP protein fusions, are highlighted in grey. Abbreviations: gDNA, genomic DNA; P-, 5' phosphorylated; eGFP, enhanced green fluorescent protein; NZ, amino-acids 1-10 of BSU15290 (FtsZ$_{1-10}$).

6.2 Publication 2

Review

For reprint orders, please contact: reprints@futuremedicine.com

Future MICROBIOLOGY

Cell division protein FtsZ: from structure and mechanism to antibiotic target

Nadine Silber[‡,1], Cruz L Matos de Opitz[‡,1], Christian Mayer[‡,1] & Peter Sass*[,1,2]

[1]Department of Microbial Bioactive Compounds, Interfaculty Institute of Microbiology & Infection Medicine, University of Tübingen, Auf der Morgenstelle 28, Tübingen 72076, Germany

[2]German Center for Infection Research (DZIF), partner site Tübingen, Tübingen 72076, Germany

*Author for correspondence: peter.sass@uni-tuebingen.de

[‡]Authors contributed equally

Antimicrobial resistance to virtually all clinically applied antibiotic classes severely limits the available options to treat bacterial infections. Hence, there is an urgent need to develop and evaluate new antibiotics and targets with resistance-breaking properties. Bacterial cell division has emerged as a new antibiotic target pathway to counteract multidrug-resistant pathogens. New approaches in antibiotic discovery and bacterial cell biology helped to identify compounds that either directly interact with the major cell division protein FtsZ, thereby perturbing the function and dynamics of the cell division machinery, or affect the structural integrity of FtsZ by inducing its degradation. The impressive antimicrobial activities and resistance-breaking properties of certain compounds validate the inhibition of bacterial cell division as a promising strategy for antibiotic intervention.

First draft submitted: 30 December 2019; Accepted for publication: 22 April 2020; Published online: 21 July 2020

Keywords: ADEP • antimicrobials • cytokinesis • divisome • drug discovery • MRSA • PC190723 • VRE

Cell division is a central and vital process for almost all living organisms. In bacteria, the generation of progeny commonly relies on binary fission of a parent cell into identical daughter cells. To assure the correct execution of cell division, and thus viability of the offspring, parent cells have to coordinate a plethora of cellular processes in time and space, such as overall biomass increase, chromosome duplication, membrane syntheses, production of cell wall with septum formation as well as timely segregation of daughter cells to complete cytokinesis. In principle, bacterial cell division is orchestrated by a macromolecular complex of proteins, the so-called divisome, which mediates the individual and distinct steps during cell division. Here, FtsZ acts as a pacemaker of divisome formation and cytokinesis, as it assembles into protofilaments to form a ring-like structure, the FtsZ-ring (or Z-ring), at the prospective division site where it functions as a scaffold for further members of the divisome. As the cell cycle proceeds, the divisome constricts and synthesizes septal peptidoglycan to allow for septum formation and eventually cytokinesis.

Considering the global spread of multidrug-resistant bacteria, which pose an increasing threat to the public healthcare system and the community, intensified research on new antibacterial targets is urgently needed. In recent years, bacterial cell division has been recognized as a promising new target pathway for antibiotic attack, and new antibiotics have been described, which interfere with this central process by different means. We here review the structural and biochemical features of the central division protein FtsZ as well as its role in the course of division, and we address current approaches to deregulate FtsZ by antibiotic action.

Crystal structure & abundance of FtsZ

Filamenting temperature sensitive mutant Z (FtsZ) was first described for *Escherichia coli* in 1980 [1], based on the finding that various isolated mutants of *E. coli* were not able to divide but grew into long filaments at a nonpermissive temperature of 42°C [2]. A decade later in a breakthrough study, Bi and Lutkenhaus could show that FtsZ self-assembles into a ring-like structure at the future site of division [3], which depended on the binding and

Future Medicine

subsequent hydrolysis of the nucleotide guanosine-5′-triphosphate (GTP) [3–6]. The likely presence of cytoskeletal elements in bacterial cells, probably functionally analogous to the roles of actin or tubulin during cytokinesis in eukaryotic cells, challenged the view regarding bacteria at that time and supported the emerging awareness that bacteria are more than just a bag full of enzymes, thereby triggering a multitude of further investigations on FtsZ.

In 1998, Löwe and Amos reported the first crystal structure of FtsZ, which was refined later at a resolution of 1.7 Å (PDB: 1FSZ and 2VAP, respectively; protein data bank, https://www.rcsb.org) [7–9]. Resolving amino acid residues 23-356 of FtsZ from the hyper-thermophilic methanogen *Methanocaldococcus jannaschii* (MjFtsZ, formerly *Methanococcus jannaschii*; total protein length: 364 amino acids), the first crystal structure revealed two major protein domains, in particular an N-terminal GTP-binding domain and a C-terminal domain, and it proved structural homology to the eukaryotic cytoskeletal protein tubulin (Figure 1A & B). In both β-tubulin and FtsZ, the N-terminal domain is composed of six β-sheets arranged in parallel and surrounded by α-helices H1-H6. The C-terminal domain consists of four parallel arranged β-sheets (S7–S10), which are surrounded by α-helices H8-H10, and it is connected with the N-terminal domain via the central α-helix H7. MjFtsZ carries an additional α-helix H0 at the N-terminus, which is absent in tubulin and FtsZ from other described organisms. Moreover, tubulin carries two additional long α-helices at the C-terminus (H11 + H12), while MjFtsZ is characterized by a small β-hairpin region (S11 + S12) at this position [7,10]. Noteworthy, MjFtsZ additionally features an elongated, more than 30 amino acids long N-terminal tail that protrudes the globular core protein [7], which is significantly shorter in other bacteria including *E. coli, Pseudomonas aeruginosa, Bacillus subtilis, Streptococcus pneumoniae, Staphylococcus aureus* and *Mycobacterium tuberculosis*.

Although the topology of the GTP-binding domains of FtsZ and tubulin are analogous to the ones found in classical GTPases such as EF-Tu (elongation factor thermo unstable; PDB: 1TUI) [15,16], the structural data showed that the mechanism of nucleotide binding is different [10]. FtsZ and tubulin involve seven segments for nucleotide binding, whereas only five segments are involved in classical GTPases. In tubulin and FtsZ, phosphate binding is sustained by loops T1–T4, of which loop T4 carries the highly conserved glycine-rich tubulin signature motif with the sequence pattern GGGTG[S/T]G, while loop T5 is involved in ribose binding and loop T6 as well as helix H7 are in contact with the guanine base. In fact, nucleotide binding by FtsZ and tubulin is more similar to the protein GAPDH, even though GAPDH binds a different nucleotide, namely NAD^+. These observations led to the categorization of FtsZ and tubulin as a distinct family of GTP-hydrolyzing enzymes [10], thus further supporting a homologous relationship between bacterial FtsZ and eukaryotic tubulin.

With the genomic era, it emerged that FtsZ is indeed largely conserved across the domains Bacteria and Archaea [17] with only a few exceptions including the phyla Crenarchaeota, Planctomycetes, Chlamydiae [18–20], or the strains *Carsonella ruddii* [21], *Ureaplasma urealyticum* [22] and *Mycoplasma mobile* [23]. Moreover, homologous proteins of FtsZ also mediate the division of plastids in algae and plants [24,25]. Accordingly, the tubulin signature motif is conserved in various sequences from bacteria, archaea, eukarya and even bacteriophages as listed in the PROSITE database (PS00227, PDOC00199; https://prosite.expasy.org). Interestingly, even though FtsZ and tubulin share a high structural similarity, their conserved N-terminal domains reveal an amino acid sequence identity of only 10%. Here, conserved residues are mostly located in regions that are involved in nucleotide binding such as the T4 loop [10]. On the contrary, primary structure analyses of FtsZ from *S. aureus*, *B. subtilis*, *M. tuberculosis*, *S. pneumoniae* and *E. coli* revealed at least 42% amino acid sequence identity with the highest identity of 68% observed between FtsZ from *B. subtilis* (BsFtsZ) and *S. aureus* (SaFtsZ). Nonetheless, due to its structural and functional homology with eukaryotic tubulin, and together with the ubiquitous abundance in bacteria and even eukaryotic plastids, FtsZ is consequently assumed to be the ancestral progenitor of eukaryotic tubulin [26]. In an evolutionary context, it is further noteworthy that the N- and C-terminal domains of FtsZ fold independently, in other words, they can be expressed separately and still show GTPase activity when joined (as shown for *Thermotoga maritima* FtsZ) [11], suggesting that both domains may have evolved from two independent proteins.

Functional regions of the FtsZ protein

In principle, FtsZ may be subdivided into the following five distinct functional regions: a poorly conserved N-terminal peptide (NTP); a globular, highly conserved core region including the major parts of the N- and C-terminal domains as well as the GTP-binding pocket; an unstructured C-terminal linker (CTL); a short, conserved C-terminal tail (CTT); and a C-terminal variable region (CTV) (Figure 1B) [17,27].

The NTP region is poorly conserved and can have a length of a few to more than 60 amino acids. The NTP region ends with the conserved isoleucine at the beginning of the 'Rossmann fold' [28], the defined start of the FtsZ

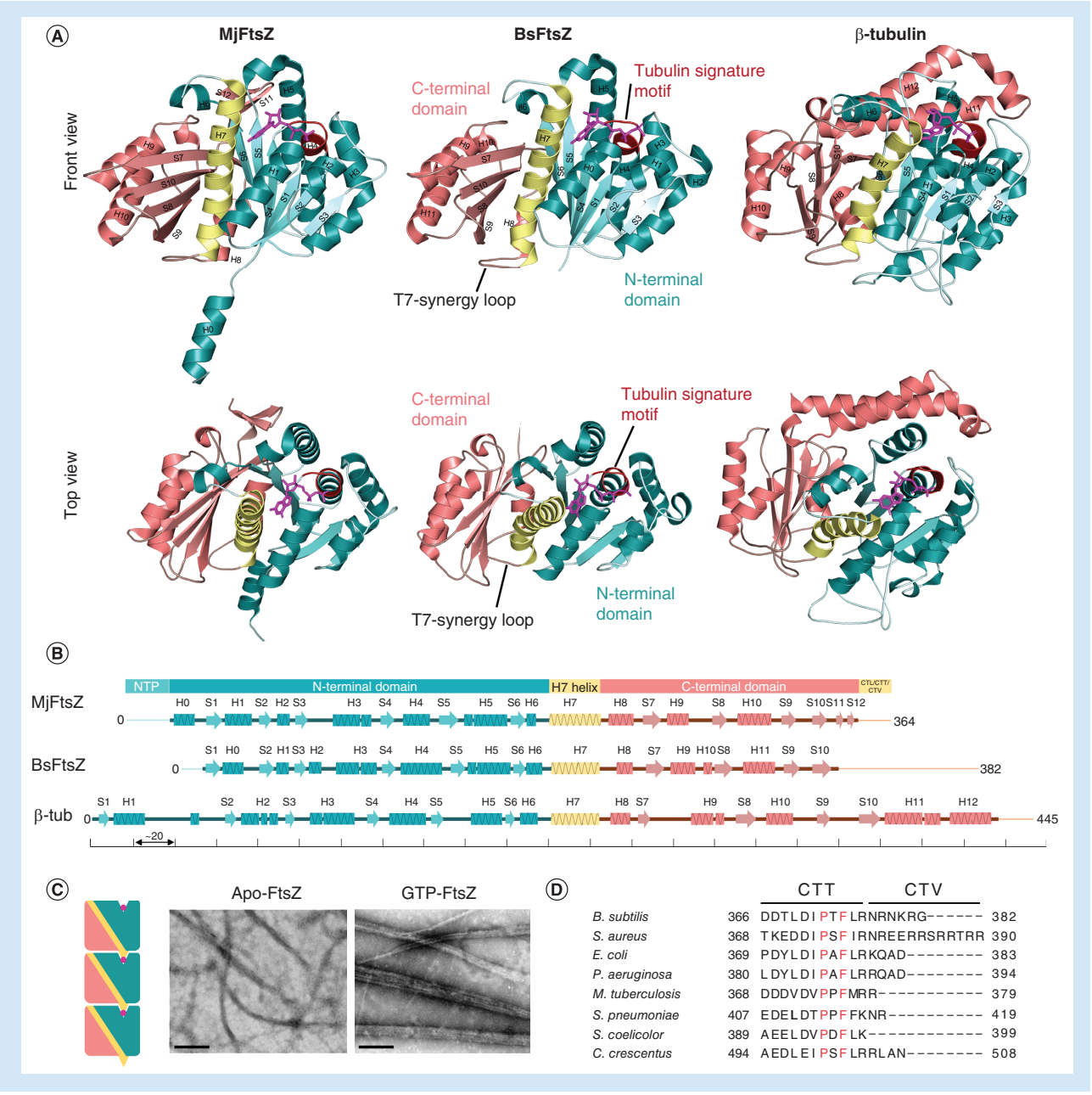

Figure 1. Crystal structure and functional regions of FtsZ. (A) Crystal structure of FtsZ from *Methanocaldococcus jannaschii* and *Bacillus subtilis* as well as of tubulin. The crystal structures of GDP-bound *M. jannaschii* FtsZ (MjFtsZ; residues 20-354, PDB: 2VAP, [11]), GTPγS-bound *B. subtilis* FtsZ (BsFtsZ; residues 12-316, PDB: 2RHO, [12]) and GDP-bound β-tubulin (residues 2-437, PDB: 1JFF, [13]) are depicted as front and top view as indicated. The N-terminal domain including the GTP-binding site is colored in cyan and the C-terminal domain in salmon with the connecting α-helix H7 in yellow. The conserved tubulin signature motif GGGTG[S/T]G is marked in red. Bound nucleotides are colored in magenta. α-helices (H) and β-sheets (S) are numbered in the crystal structures. **(B)** Functional regions of MjFtsZ and secondary structure of MjFtsZ, BsFtsZ and β-tubulin. FtsZ comprises five distinct functional regions: i) a short, unstructured and poorly conserved N-terminal peptide (NTP); ii) a globular, highly conserved core region including major parts of the N- and C-terminal domains with the GTP-binding pocket and the connecting α-helix H7; iii) an unstructured C-terminal linker (CTL); iv) a short, conserved C-terminal tail (CTT); as well as v) a C-terminal variable region (CTV). α-helices (H) and β-sheets (S) are numbered and illustrated as boxes and arrows, respectively. The unsolved NTP region is marked in light blue, the unsolved CTL and CTT/CTV regions are depicted as a salmon-colored line. **(C)** Head-to-tail polymerization of FtsZ and protofilament formation. Left image: Schematic of the head-to-tail association of individual FtsZ monomers that polymerize into protofilaments. Here, the active site of the GTPase is formed at the interface of two adjacent FtsZ subunits by the T7 synergy loop of the 'upper' and the GTP-bound nucleotide-binding pocket of the 'lower' FtsZ monomer. The N-terminal domain is depicted in cyan, the C-terminal domain in salmon and the connecting α-helix H7 with the T7 synergy loop in yellow (the latter indicated as bottom face triangle). GTP is indicated as a pink dot. Right image: Electron micrographs of polymers formed by apo-FtsZ or GTP-bound FtsZ. Scale bars indicate 200 nm. **(D)** Amino acid sequence alignment of the CTT and CTV regions of FtsZ from different organisms. Highly conserved residues are marked in red.
Electron micrographs were reproduced with permission from [14] and reprinted with permission from Wiley.

core domain [17]. Accordingly, the NTP regions of BsFtsZ (PDB: 2RHO) and MjFtsZ (PDB: 2VAP) comprise 13 and 39 amino acids [7,8,12], respectively, while in the phylum of cyanobacteria the NTP reaches a length of up to 68 amino acids [17]. In most bacteria including Firmicutes and Proteobacteria, the NTP has not yet been assigned a decided function; however, in cyanobacteria, it is highly conserved and recent data demonstrated its importance for Z-ring formation in these bacteria. Here, efforts were directed to delete the amino acids 2–51 of FtsZ in *Anabaena* sp. PCC 7120, which repeatedly failed, suggesting a more important role for the extended NTP in cyanobacteria [29]. Subsequent co-expression of N-terminally truncated FtsZ together with wild-type FtsZ led to an increased cell size of *Anabaena* accompanied by hampered cell division. Results obtained from bacterial two-hybrid assays revealed an interaction of the NTP of FtsZ with the cell division protein SepF [29], which has been previously shown to be an essential, FtsZ-interacting septal protein in *Synechocystis* PCC 6803 [30].

The globular, highly conserved core region of FtsZ comprises the main parts of the N-terminal domain with the GTP-binding site as well as the C-terminal domain. To build the Z-ring, the core region provides the interface for a head-to-tail polymerization of individual FtsZ monomers into protofilaments (Figure 1C), thereby triggering GTPase activity. During polymerization, the active site of the GTPase is formed at the interface of two adjacent subunits of FtsZ. Here, the 'upper' subunit inserts its C-terminal T7 synergy loop into the GTP-bound nucleotide-binding pocket of the 'lower' subunit, thereby inducing GTP hydrolysis [4,10,31]. Crystal structures of nucleotide-bound *M. tuberculosis* FtsZ (MtbFtsZ), harboring either guanosine-5′-diphosphate (GDP) or the nonhydrolyzable GTP analog guanosine-5′-O-3-thiotriphosphate (GTPγS), suggested a switch mechanism of the FtsZ core during GTP hydrolysis (PDB: 1RQ7, 1RLU) [32]. Here, the GTP γ-phosphate appears to stabilize the T3 loop in a compact tension state (T-state), while in a GDP-bound crystal in the absence of the γ-phosphate, the T3 loop is in a relaxed conformation (R-state) [33,34]. It was therefore assumed that hydrolysis of the nucleotide may trigger a switch from the T-state to the R-state of the T3 loop, thus weakening the longitudinal interaction between loops T3 and T7 of two adjacent FtsZ subunits. Such a switch could lead to a hinge-opening around the pivot point and bending of the filament, thereby generating mechanical work, which causes an inward force on the membrane that is needed for Z-ring constriction during cytokinesis [33,34]. Similarly, a structural switch of the T3 loop from the T- to the R-state may also be caused by interactions of GTP with the T7 loop of the next subunit [35]. On the contrary, different MjFtsZ structures showed only negligible differences in the T3 loop region when bound to either GDP or GTP compared with apo-MjFtsZ (PDB: 1W58, 1W5B, 1W59, 1FSZ) [7,11]. Nucleotide-dependent conformational changes were also not observed for *Aquifex aeolicus* FtsZ (AaFtsZ) comparing crystal structures of AaFtsZ:GDP and AaFtsZ:8-morpholino-GTP [9,36]. Further, the crystal structure of SaFtsZ bound to either GTP or GDP did not show a conformational switch of the T3 loop, but revealed an opened and a closed conformation of the FtsZ core [37]. When compared with the closed conformation of SaFtsZ (PDB: 5MN8), the open conformation showed a rotation between the N- and C-terminal domains, thereby opening a cleft between the two domains while shifting the central α-helix H7 downward (PDB: 5MN4). The opened conformation seems to be established upon FtsZ polymerization, whereas the closed conformation is adopted in the monomeric state of FtsZ, suggesting that the conformational switch of FtsZ depends on polymerization rather than nucleotide binding alone. Here, categorizing previous FtsZ crystal structures from different organisms revealed a higher similarity of most FtsZ structures to the closed conformation of SaFtsZ [37].

Regarding the interaction between the core regions of different FtsZ subunits, crystal structures of polymeric MtbFtsZ bound to GDP revealed a series of hydrogen bonds as well as hydrophobic interactions at the interface of two FtsZ monomers that are intimately involved in assembly. To confirm the importance of the observed intersubunit contacts, the identified hydrophobic amino acids with acidic residues were mutated in *E. coli* FtsZ (EcFtsZ; i.e., F137E, G139E, L178E, A181E, L205E, L272E, V292E, M206E and I294E). Here, the mutations abrogated GTPase activity *in vitro*, and *in vivo* complementation approaches with these mutants failed [34]. Furthermore, lateral interactions between FtsZ protofilaments are promoted by the widely conserved residues Glu_{83} and Arg_{85} that are both located within α-helix H3. In *E. coli*, mutations at these two positions led to decreased viability, and mutant proteins were impaired in polymerization and GTPase activity *in vitro*, suggesting a major role of these residues in longitudinal and lateral interactions [38]. It is further suggested that lateral contacts are mostly ascribed to van der Waals interactions, which are weaker compared with hydrophobic interactions at the longitudinal interface, and it seems that such lateral interactions between FtsZ protofilaments play an important role for correct cytokinesis, as substitutions at the lateral site of FtsZ strongly affect cell division [39].

Only a few modulatory proteins have yet been reported to interact with the core region of FtsZ, such as the SOS cell division inhibitor SulA [40], which is induced upon DNA damage and binds to the T7 loop surface of FtsZ.

A crystal structure of FtsZ bound to SulA from *P. aeruginosa* showed that SulA entirely covers the T7 loop, and by doing so prevents polymerization of FtsZ (PDB: 1OFU) [41]. MinC is a further inhibitor of cell division that interacts with residues in the C-terminal core region of BsFtsZ. More precisely, interaction with the core region occurs via amino acids within as well as in close proximity to α-helices H9 and H10 (i.e., T232I, K243R, I245F, D255V, V260A, A285T, D287V, I293T and V310A) [42]. The region around H9 and H10 is characterized by a negatively charged surface that was suggested to be important for the binding of MinC [42], which matches the finding that the MinC–FtsZ interaction is pH dependent [43]. In *E. coli*, the same regions of FtsZ (H10 and the CTT) are involved in MinC binding, but the residues differ from those observed for BsFtsZ [44,45].

The unstructured CTL (or spacer) spans the region between the globular core of FtsZ and the extreme CTT/CTV region, and it is highly variable regarding its length and amino acid sequence. Depending on the organism, the CTL comprises up to 330 residues [17] and it is predicted to be mostly disordered, thus explaining why this region is commonly not resolved in crystal structures. Deletion of the CTL region results in impaired protofilament formation *in vitro*, indicating an important role in establishing lateral interactions between protofilaments. Also, deletion of CTL leads to a decreased GTPase activity with a concomitant increase of the critical concentration of FtsZ required for filamentation, revealing a decline in cooperative assembly [46]. In *B. subtilis*, CTL deletion mutants are also incapable of developing an intact Z-ring and show a delocalization of FtsZ, leading to a filamentous cell shape. Intriguingly, deletion of only 50% of the CTL region, scrambling of the CTL sequence or exchanging the entire CTL region by an unrelated, intrinsically disordered peptide sequence restores normal cell division. However, extending the CTL region significantly beyond the normal number of residues (here: >249 in *B. subtilis*) or replacing it with helical repeats (i.e., residues 398–455 from human beta-catenin) results in filamentous cells that are unable to divide [46]. While the amino acid sequence and length (to a certain extent) appears less critical, the CTL region obviously functions as a flexible tether that provides a defined distance from the membrane, where FtsZ is anchored via modulatory proteins that interact with the conserved CTT region of FtsZ [46,47]. In addition, cryo-electron microscopy (cryo-EM) and small-angle x-ray scattering (SAXS) experiments showed that the distance between individual FtsZ protofilaments is reduced from 70 Å to approximately 55 Å when the CTL region is deleted, indicating a role of the CTL region for the correct spacing between protofilaments in higher-ordered FtsZ bundles, thereby providing a certain flexibility that is needed for FtsZ dynamics [48]. Hence, the CTL region is important for protofilament formation and correct assembly of the Z-ring.

The extreme CTT region comprises approximately 11 amino acid residues (Figure 1D), which together with the CTV region is designated the 'grappling hook peptide' (GHP) that acts as a central hub for FtsZ-interacting proteins [46]. During the last decades, several modulatory proteins related to the division machinery have been identified to interact with the CTT region, including negative regulators of Z-ring assembly, such as EzrA [49,50], MinC [42,51,52] or SlmA [53–55], as well as positive regulators, including FtsA [56–58], ZipA [56,59–62], SepF [63], or ZapC and ZapD [64,65]. A more detailed description of these regulatory proteins and their roles in the course of cell division is addressed in a later section of this review.

The CTV region is highly variable and comprises only a few amino acid residues (Figure 1D). The CTV region of BsFtsZ (NRNKRG) is highly positively charged and is important for lateral interactions between FtsZ protofilaments. In contrast, the CTV region of EcFtsZ (KQAD) is neutrally charged. Intriguingly, EcFtsZ primarily forms single-stranded filaments *in vitro* with a length of approximately 200 nm, whereas BsFtsZ assembles into stable, large protofilament bundles that are composed of rings and sheets of single-stranded filaments (approximately 130 nm in length) under the same conditions [27]. Truncation of the CTT-CTV region in BsFtsZ leads to defects in lateral interactions, while the same truncations do not affect the polymerization behavior of EcFtsZ with protofilaments that are only slightly shorter in length. Chimeric proteins were generated by swapping the CTV regions of BsFtsZ and EcFtsZ. Here, chimeric EcFtsZ now assembles into thick filaments, whereas chimeric BsFtsZ only polymerizes into straight protofilaments, indicating that the CTV region of FtsZ is crucial for lateral interactions *in vitro*. *In vivo*, the importance of the CTV region was further emphasized by the inability of the chimeric proteins to support normal cell division in the respective bacterial species [27].

Z-ring assembly & force generation

In most bacteria, FtsZ is regarded as the central player and pace-making protein of cell division. To build the Z-ring, the scaffold that further proteins of the cytokinetic apparatus adhere to, FtsZ self-polymerizes in a GTP-dependent manner to form protofilaments and larger bundles thereof, eventually assembling into a discontinuous ring-like structure at the inner side of the cytoplasmic membrane [3,66,67], marking the prospective site of division.

Here, the protein concentration of FtsZ plays a critical role during protofilament and Z-ring assembly. *In vitro*, nucleotide-dependent polymerization of EcFtsZ occurs only above a critical concentration (1–2 μM depending on the buffer conditions) [68,69], which results in different types of protofilament structures. Addition of GTP leads to single-stranded straight protofilaments (Figure 1C) that in the presence of the crowding agent DEAE-dextran assemble into sheets of straight filaments. Contrariwise, GDP induces the formation of shorter and curved filaments as well as minirings with a diameter of approximately 23 nm that form tubes in DEAE-dextran [70]. Further, increasing the concentration of EcFtsZ above the critical concentration leads to a higher proportion of double-stranded filaments *in vitro* (~9 nm wide), in contrast to mainly single-stranded filaments (~4 nm wide) observed close to the critical concentration [68]. Accordingly, overexpression of FtsZ in whole cells perturbs Z-ring assembly and results in minicell formation [71].

Once assembling, the Z-ring continues to be a highly dynamic structure that is treadmilling around the division plane, constantly exchanging FtsZ subunits with the cytoplasmic pool (with a half-time of ~10–30 s), the latter comprising approximately 70% of the overall cellular pool of FtsZ [72–75]. *In vitro* experiments with Cy5- and Alexa Fluor 488-labeled FtsZ showed that filaments grow at one end while depolymerization takes place at the opposite end [76]. A study investigating top- ($FtsZ_{L178E}$) and bottom- ($FtsZ_{L272E}$) face mutant proteins of FtsZ showed that FtsZ filaments, in contrast to microtubules, are characterized by bottom-end growth [34,77]. Furthermore, the bottom face mutant $FtsZ_{L272E}$ inhibits cell division *in vivo* corroborating polymerization at the bottom end [77]. In *B. subtilis*, the rate of FtsZ treadmilling was reported to control both the rate of cell division and peptidoglycan synthesis [73]. In contrast, a recent study by Monteiro and colleagues proposed an alternative model for *S. aureus* that involves two sequential steps as the driving force for septum constriction: a first slow step that is dependent on FtsZ treadmilling, and a second faster step that is driven by peptidoglycan synthesis [78]. Similarly, in *S. pneumoniae*, the movement of peptidoglycan synthesis enzymes was demonstrated to be independent of FtsZ treadmilling, suggesting that septal FtsZ rings organize the peptidoglycan synthesis complex of the divisome dependent on peptidoglycan substrate availability [79].

In the course of cytokinesis, the divisome constricts to finalize septum formation and cell division. The presence of a membrane-tethered ring-like structure, which is formed by dynamic protofilaments of GTP-consuming FtsZ, promoted the idea that the Z-ring may generate a mechanical force on the bacterial membrane sufficient to allow for the constriction of the division apparatus. In this context, a mathematical model suggested that the minimal force needed for constriction, which the Z-ring has to create in an *E. coli* cell, would be about 8 pN [80]. By attempting *in vitro* reconstitution of the Z-ring in liposomes, an FtsZ mutant protein carrying an amphipathic helix for membrane anchoring (instead of the FtsA/ZipA-binding site) assembled into ring-like structures and indeed led to a constriction of the liposome in presence of GTP [81]. An alternative hypothesis argues that inward growth may provide the driving force for constriction, while the role of FtsZ might be that of simply serving as a scaffold [82]. However, *in silico* simulations indicated that cell wall growth alone is not sufficient for cell division to occur without an initial constriction force provided by the Z-ring [83,84].

Positioning of the Z-ring & division site selection

The correct placement of the future division site is crucial and needs to be coordinated with other cellular processes, such as chromosome segregation. In *B. subtilis* and *E. coli*, division site selection occurs in a stunningly precise fashion with approximately 2% deviation off-center midcell [85,86]. To achieve such precision, Z-ring positioning is controlled by distinct regulatory mechanisms. In *B. subtilis*, spatial regulation is primarily achieved by two negatively-acting regulatory systems, the nucleoid occlusion (NO) and the minicell (Min) systems (Figure 2A). The NO system, driven by the ParB-family protein Noc, prevents premature division events over unsegregated nucleoids [87–89]. To this end, Noc binds to about 70 distinct Noc-binding sites on the chromosome to form nucleoprotein complexes that associate with the cell membrane via an N-terminal amphipathic α-helix of the Noc protein [90]. Since the Noc-binding sites are distributed only in the origin-proximal 2/3 of the chromosome and are absent in the terminus region [91], these membrane-bound nucleoprotein complexes are assumed to physically prevent the assembly of the divisome over insufficiently segregated nucleoids [90]. In *E. coli*, NO is conferred by the SlmA protein [53], which alike Noc in *B. subtilis* recognizes specific SlmA-binding sites that are distributed all over the chromosome except for the terminus region [92,93]. However, in contrast to Noc in *B. subtilis*, which does not seem to act directly on FtsZ [91], SlmA has been reported to antagonize Z-ring assembly by directly binding to the CTT region of FtsZ [54,92,94,95]. Thus, although SlmA and Noc do not share considerable amino acid sequence identity or structural homology, they fulfill the same function in the bacterial cell yet by different mechanisms [53,89].

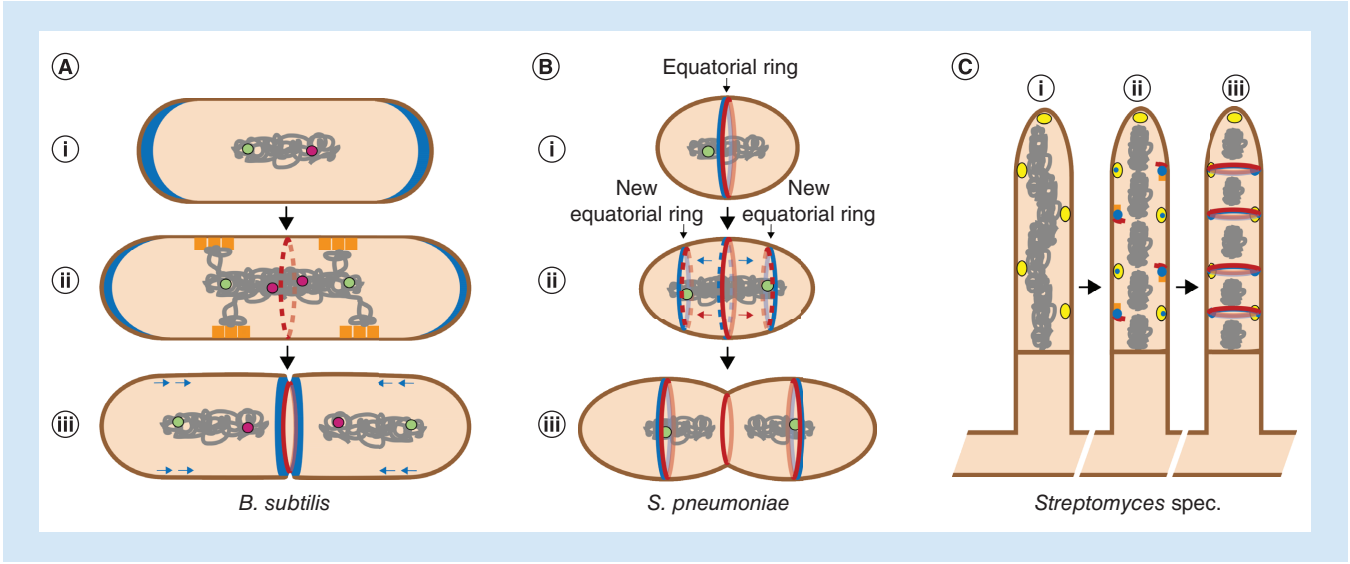

Figure 2. Division site selection in bacteria. (A) Negative regulation of division site selection in *Bacillus subtilis*. (i) DivIVA localizes to the cell poles and recruits MinCDJ to form the DivIVA-MinCDJ regulatory complex (in blue), inhibiting Z-ring formation at the old cell poles. (ii) The nucleoid occlusion factor Noc (orange rectangles) binds to the membrane as well as to specific Noc-binding sites on the nucleoid, thereby forming large membrane-associated nucleoprotein complexes that prevent the formation of the Z-ring over the chromosome (indicated by red dotted ring). The origin region of the nucleoid is depicted in green, the terminus-region in pink. (iii) After nucleoids have segregated, a Noc- and Min-free zone is established at mid-cell that allows for Z-ring and subsequent divisome formation (indicated by the continuous red ring). Later, the DivIVA-MinCDJ complex is recruited from the old poles to the current division site, thus preventing the assembly of additional Z-rings close to the new septum (blue arrows indicate the dynamic movement of DivIVA-MinCDJ from the old cell poles to the new/current division site). **(B)** Positive regulation of division site selection in *Streptococcus pneumoniae*. (i) In cells undergoing early division, MapZ-rings (in blue) and FtsZ-rings (in red) are localized at the equatorial ring, the current division site. (ii) After initiation of peripheral peptidoglycan synthesis, MapZ bifurcates into two rings that migrate to the future division sites (movement indicated by blue arrows), following the origin of replication (in green). Subsequently, FtsZ, EzrA and FtsA continuously move out from mature septal rings at mid-cell toward the new equatorial MapZ-rings in the prospective daughter cells (depicted as red dashed rings). (iii) Later, MapZ proteins have moved to the new equatorial rings, while the FtsZ-ring and further divisome members remain at the constricting old septum, finalizing cell division. **(C)** Division site selection in sporogenic cells of streptomycetes. (i) SsgA (yellow circles) localizes in distinct foci along young sporogenic aerial hyphae. At this stage, SsgB is still localized more or less diffusively while FtsZ assembles into spiral-like filaments throughout the sporogenic cell prior to division (not depicted). (ii) SsgA then recruits SsgB (blue circles) to the sporulation-specific cell division site and both proteins co-localize temporarily at the early division stage. In addition, correct localization of SsgB is supported by the membrane protein SepG (orange rectangles). SsgB, in turn, is involved in recruiting FtsZ to the division site and supports FtsZ polymerization. (iii) Regularly spaced Z-rings are then formed at the decided division sites that direct synchronous sporulation septation. While SsgAB and FtsZ remain at the division site, SepG dissociates and re-localizes to the spore periphery (not depicted).

The Min system of *B. subtilis*, which is characterized by the proteins DivIVA, MinD, MinJ and MinC, prevents the formation of new Z-rings in the regions near the cell poles. Here, DivIVA recognizes the negative curvature of the cell membrane that is generated upon constriction of the divisome in the course of septum formation, thus marking the former division site/the new cell pole [96]. Via the adaptor protein MinJ, DivIVA then directs the membrane-associated Walker-type ATPase MinD to the cell pole [97,98], which again recruits MinC, the actual negative regulator of FtsZ. To inhibit Z-ring formation, MinC directly interacts with the bottom face of the α-helix H10 as well as the CTT region of FtsZ [42], thereby preventing lateral interactions between individual protofilaments of FtsZ, leading to the formation of shorter and curved filaments [43,51,52]. In *E. coli*, the Min system consists of the proteins MinC, MinD and MinE [99], of which MinC directly interacts with FtsZ, similar to previous observations in *B. subtilis* [44]. However, unlike in *B. subtilis*, the Min system of *E. coli* has an oscillating nature. Here, MinD forms a membrane-bound complex with MinC that is spatially controlled by MinE. MinE oscillates with MinD from one pole of the cell to the other, providing a time-averaged gradient concentration of MinC with higher concentrations at the cell poles and lower concentrations at midcell, thus permitting FtsZ polymerization and Z-ring formation only at midcell [100–105]. Hence, homologous Min proteins fulfill the same function, but yet again, by different mechanisms, thus illustrating the different ways evolution has used to fine-tune the NO and

Min systems in *B. subtilis* and *E. coli*, thereby underlining their importance for division site selection. However, it is noteworthy that individual Min and Noc/SlmA proteins are not essential in *B. subtilis* or *E. coli* [53,89], and independent studies in both species revealed that Z-rings may still be positioned at midcell even in the absence of both Min and NO, suggesting additional, yet unknown factors to be involved in division site selection in these species [106,107].

In this context, for example, *Caulobacter crescentus* lacks both Min and NO systems, but employs a further negatively regulating mechanism mediated by the ParA-like ATPase MipZ. MipZ interacts with the chromosome-partitioning protein ParB to form a bipolar gradient in the predivisional cell, leading to higher concentrations of MipZ at the cell tips. Then, ParB promotes dimerization of MipZ, which in turn prevents polymerization of FtsZ and thus Z-ring formation at the cell poles [108,109]. Noteworthy, ParA-like proteins can also act as positive regulators for division site selection, such as PomZ in *Myxococcus xanthus*, an organism that is also devoid of other known factors for the positioning of the Z-ring. Here, PomZ localizes to the future division site prior to and independent of FtsZ, and then recruits FtsZ [110]. Similarly, correct Z-ring placement in *S. pneumoniae* depends on positive regulation by the chromosomal origin of replication [111] as well as the MapZ (or LocZ) protein [112,113], the latter localizes to the future division site prior to the arrival of FtsZ (Figure 2B). Here, MapZ is important for establishing the correct division plane, while the *oriC* region is crucial for the assembly and positioning of the cytokinetic machinery [111]. Another example of positive regulation of Z-ring positioning in the absence of Min and NO systems can be observed in the actinomycete *Streptomyces coelicolor*, where the SsgAB proteins mark the position for Z-ring assembly and recruit FtsZ to the division site (Figure 2C) [114]. *S. aureus* lacks a complete Min system but encodes for DivIVA and Noc [115,116]. Here, Noc has a conserved function in spatially regulating Z-ring formation by inhibiting divisome assembly over the nucleoid, consistent with the role of Noc in other bacteria, but interestingly, it is also involved in controlling the initiation of DNA replication in *S. aureus* [117]. In this context, there is also strong evidence for a role of DNA replication in division site selection in *B. subtilis* [118–120] and *E. coli* [106,121–123]. Thus, the multiplicity and the joint functions of such inventive regulatory mechanisms, which lead to a tight control of Z-ring positioning, emphasize the central importance of division site selection.

Modulation of the Z-ring by divisome proteins

The Z-ring is assembled by individual protofilaments of FtsZ and, in principle, appears to be sufficient to generate the constrictive force required for cytokinesis [81,83,84]. However, for correct cell division, a plethora of further divisome proteins have to be recruited to the Z-ring, which interact with FtsZ, tethering the Z-ring to the membrane and modulating its dynamics (Figure 3). In total, more than 35 proteins have been identified to be involved in cell division so far [124]. As shown for the two model organisms *B. subtilis* and *E. coli*, divisome assembly may be separated into two temporally distinct steps. First, the Z-ring is formed on the inner side of the cytoplasmic membrane by the aid of early-stage cell division proteins that are important for membrane-tethering or fulfill other regulatory functions during Z-ring maturation. Second, late-stage cell division proteins including peptidoglycan synthesis enzymes arrive at the future division site, which allow for the synthesis of septal peptidoglycan and finally cytokinesis [125,126]. In *C. crescentus*, assembly of the cytokinetic apparatus occurs in at least seven distinct steps, nonetheless, the time difference between the recruitment of early- and late-division proteins to the division site is comparable with the observations made for *E. coli* and *B. subtilis* [127]. The early-stage division proteins commonly arrive at the division site at approximately 25% progression of the cell cycle, which members differ depending on the bacterial species. For example, early-cell division proteins in *B. subtilis* include FtsZ, FtsA, SepF, ZapA and EzrA [126], while these are represented by FtsA, ZipA, ZapA, FtsE and FtsX in *E. coli* [125]. *C. crescentus* mostly encodes for the same early-division proteins found in *E. coli*, except for ZipA, but also involves further proteins such as FzlA, FzlC and DipI [127–129].

FtsA, an ATPase of the actin/Hsc70/hexokinase superfamily, is conserved among most bacterial species including *E. coli*, *B. subtilis* and *S. aureus* [130–132], emphasizing its central role in regulating the Z-ring. FtsA acts as a membrane anchor for FtsZ, as it interacts with the CTT region of FtsZ and concomitantly binds to the lipid bilayer via its C-terminal amphipathic helix [133–135]. Furthermore, FtsA forms actin-like protofilaments in an ATP-dependent manner [136–138] that can assemble into lipid-bound minirings and antagonize lateral interactions between FtsZ protofilaments [139–141]. It is hypothesized that FtsA minirings may guide FtsZ to form long, often parallel, but unbundled protofilaments, thereby influencing the higher order structure of FtsZ and divisome function [139]. Recent data suggest that by consuming ATP, FtsA may even reorganize liposome architecture upon the binding of ATP to recruit FtsZ [142]. Inactivation of FtsA in rod-shaped *B. subtilis* and *E. coli* causes filamentation of the

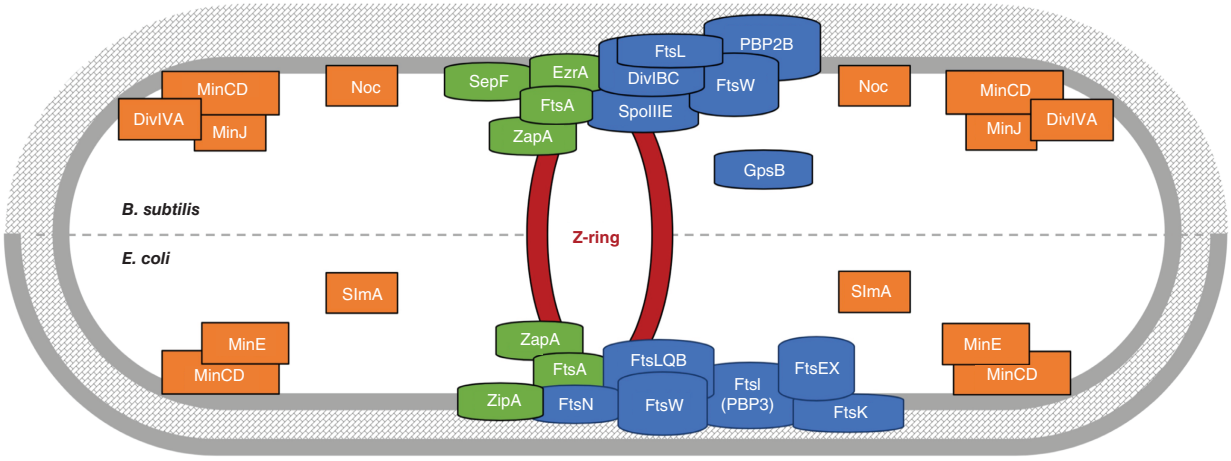

B. subtilis	*E. coli*	Function
Divisome proteins		
FtsZ	FtsZ	Forms the division site ring that is a scaffold for further downstream division proteins
FtsA	FtsA	Tethers FtsZ to the membrane and stabilizes Z-rings at the membrane
ZapA	ZapA	Promotes FtsZ polymerization and protofilament bundling
–	ZipA	Involved in tethering FtsZ to the membrane and modulates ClpXP-mediated degradation of FtsZ
EzrA	–	Spectrin-like regulator that negatively affects FtsZ protofilament bundling and promotes septal localization of PBP1
SepF	–	Supports anchoring the Z-ring to the membrane and promotes FtsZ bundling
–	FtsE, FtsX	ABC transporter recruiting other division proteins to the Z-ring; coordination of septal PG synthesis with PG hydrolysis
SpoIIIE	FtsK	ATP-dependent dsDNA translocase involved in translocation of double-stranded DNA during cell division
GpsB	–	Functions as an adaptor for cell wall enzymes in the course of the bacterial cell cycle
FtsL, DivIB, DivIC	FtsL, FtsQ, FtsB	Membrane proteins which serve as a scaffold in late steps of divisome assembly; potential role in regulating divisome activity
FtsW	FtsW	SEDS protein, proposed PG polymerase (glycosyltransferase)
PBP2B	FtsI (PBP3)	Class B PBP with D-D-transpeptidase activity, involved in synthesis of septal PG together with its partner SEDS protein
–	FtsN	Arrival of FtsN triggers the activation of septal PG synthesis, e.g. via FtsW/FtsI
Regulators of divisome assembly		
MinC	MinC	Binds to the C-terminal core region of FtsZ to inhibit FtsZ polymerization
MinD	MinD	Walker-type ATPase, tethers MinC to membrane via MinJ in *B. subtilis* or MinE in *E. coli*
–	MinE	Binds to MinD and stimulates ATPase activity of MinD, leading to the release of MinD from the membrane
MinJ	–	Binds to the N-terminal lipid-binding domain of DivIVA and directs MinD to the cell pole
DivIVA	–	Curvature sensitive membrane protein that recruits MinCD via MinJ
Noc	SlmA	Effector of nucleoid occlusion (NO)

Figure 3. Divisome proteins of *Bacillus subtilis* and *Escherichia coli*. In *B. subtilis* and *E. coli*, cell division is initiated by the midcell localization of FtsZ and the formation of the Z-ring (in red), which is followed by the recruitment of early divisome proteins such as FtsA, EzrA, ZapA, SepF and ZipA (in green) that contribute to Z-ring dynamics and membrane tethering. Late-phase divisome proteins (in blue), including the penicillin-binding proteins (PBPs) and FtsW, contribute to septum formation by redirecting peptidoglycan (PG) synthesis toward cross-wall growth. Regulators of Z-ring positioning (in orange), such as the Min and NO systems, act to prevent the initiation of extra Z-rings at the newly formed cell pole or over the nucleoid, respectively.

bacterial cells [143–145]. Moreover, in the coccoid *S. pneumoniae*, depletion of FtsA results in swelling and eventually cell lysis that is accompanied by the dispersion of peptidoglycan synthesis, thus suggesting a dual role for *S. pneumoniae* FtsA in divisome assembly as well as peptidoglycan synthesis [146].

ZipA, which appears to be specific to γ-proteobacteria such as *E. coli*, tethers dynamic polymers of FtsZ to the cytoplasmic membrane by interacting with the CTT region of FtsZ [59,62,134,147]. ZipA has been assumed to regulate FtsZ dynamics by supporting the bundling of FtsZ protofilaments to stabilize the Z-ring. However, a recent report suggests that ZipA does not directly stimulate lateral interactions between FtsZ protofilaments, but acts via passive membrane attachment for FtsZ filaments as they treadmill [148]. Interestingly, gain of function mutants of FtsA, which are impaired for self-interaction, bypass the loss of the essential ZipA protein in *E. coli*, suggesting that self-interaction of FtsA competes with the ability of FtsA to recruit further downstream division proteins [149,150]. In this context, it has recently been confirmed that ZipA directly interacts with FtsA [151]. Also noteworthy, in addition

to supporting Z-ring assembly via direct interaction with FtsZ, ZipA is assumed to prevent degradation of FtsZ by the bacterial protease ClpXP in *E. coli* via occupying the recognition signal for the unfoldase ClpX in the last 18 amino acid residues of FtsZ [59,152]. By doing so ZipA indirectly modulates the assembly/disassembly dynamics of the Z-ring via ClpXP in *E. coli*. In *B. subtilis*, which lacks a ZipA homolog, SepF acts as an additional membrane anchor that binds to the C-terminus of FtsZ resulting in stabilization of FtsZ protofilaments [63,153,154]. *In vitro*, SepF polymerizes into large rings that support the bundling of FtsZ protofilaments [155]. SepF is not essential for survival under normal growth conditions, but it is synthetically lethal when combined with either *ezrA* or *ftsA* deletion mutants [153,154,156]. In *S. pneumoniae*, a deletion of *sepF* results in elongated cells with septation defects and unconstricted Z-rings, indicating a role in the later steps of cell division rather than for anchoring FtsZ to the membrane [146]. *C. crescentus* also lacks a ZipA homolog, instead FzlC is assumed to anchor the Z-ring to the inner side of the cytoplasmic membrane, since it is capable to recruit FtsZ to membranes *in vitro* [157].

In addition to FtsA, SepF and ZipA, further early-stage division proteins modulate the dynamics of FtsZ protofilaments and Z-ring formation, such as ZapA, ZapB, ZapC, ZapD and EzrA. The widely conserved small coiled-coil protein ZapA binds to FtsZ to affect GTPase activity *in vitro* and to promote bundling of FtsZ protofilaments [158–160], and by doing so even reverses the inhibitory effects of the FtsZ polymerization antagonist SulA in *E. coli* [161]. Noteworthy, the cellular concentration of ZapA roughly equals that of FtsZ, and *in vitro* pelleting assays revealed an equal stoichiometry between both proteins as well [162,163], which may suggest a more intimate relationship between both proteins. In this context, overproduction of ZapA rescues the defects of an FtsZ mutant in *B. subtilis*, which is impaired in lateral interactions between protofilaments [67], supporting a role for ZapA as a cross-linking and bundling factor for FtsZ. In *E. coli*, ZapA further recruits ZapB to form FtsZ-independent structures at the division site that are assumed to link Z-ring assembly to the terminus region of the chromosome [106,164]. In addition, ZapC and ZapD interact with FtsZ to promote bundling between FtsZ polymers. To do so, ZapD binds to the CTT region of FtsZ [64,165], whereas ZapC interacts with the GTPase core region [65]. In *C. crescentus*, however, ZapA did not show any effects on FtsZ bundling or GTPase activity, but appears to interact with ZauP to stabilize Z-ring formation at midcell via a mechanism that is independent of FtsZ polymer bundling [166]. Of note, Zap proteins are nonessential in their respective organisms under normal growth conditions, but the depletion of multiple Zap proteins or their deletion in combination with other divisome proteins, may cause severe cell division defects or are synthetically lethal [64,158,167,168].

In *E. coli* and *C. crescentus*, the ATP-binding cassette transporter-like complex FtsEX represents early divisome proteins, which aid in recruiting further downstream division proteins. Additionally, FtsEX play a role in activating both the divisome via FtsA to allow for septal peptidoglycan synthesis [169], as well as peptidoglycan hydrolases to regulate cell wall hydrolysis at the division site [169–171]. In contrast, FtsEX in *B. subtilis* appear to control peptidoglycan hydrolases involved in cell elongation, while both proteins are not involved in cell wall hydrolysis at the septum [172,173].

In *B. subtilis*, the integral membrane protein EzrA, which is conserved among low G/C Gram-positive bacteria, comprises an N-terminal transmembrane spanning helix as well as a large cytoplasmic domain that is assumed to connect bacterial cytoskeletal elements with membrane-associated proteins analogous to the function of eukaryotic spectrins [174]. EzrA interacts with FtsZ via the CTT/CTV regions [50], as well as with other cell division proteins such as PBP1 and GpsB [175,176] to exert both negative as well as positive effects on the individual divisome proteins. On the one hand, EzrA negatively affects FtsZ protofilament bundling and the deletion of *ezrA* results in extra Z-rings that localize at the future division plane and at the polar regions of the cell [49,177]. On the other hand, EzrA promotes the septal localization of PBP1 (or PonA), a bi-functional glycosyltransferase-transpeptidase peptidoglycan synthase that contributes to cell wall synthesis at the septum [175]. In addition, the deletion of *ezrA* results in a delay of Z-ring constriction and cells are significantly longer compared with wild-type cells. Moreover, combining an *ezrA* deletion with single deletions of other divisome proteins, such as ZapA or SepF, which individually do not significantly affect growth, results in severe growth defects [153,158]. In *S. aureus*, EzrA is essential and it was shown to interact with FtsZ, SepF as well as with GpsB, PBP2 and RodA to coordinate cell division with peptidoglycan synthesis [178].

In the context of antibiotic action, it is further noteworthy that the deletion of *ezrA* in *B. subtilis* leads to tetracycline hypersensitivity even in the presence of the tetracycline efflux pump TetA [179], indicating an effect that appears to be unrelated to the protein translation inhibiting activity of tetracycline. While the explicit reason for the tetracycline hypersensitivity has remained unclear so far, it is hypothesized that an accumulation of tetracycline

molecules into the lipid bilayer destabilizes certain membrane proteins [179], which may be synthetically lethal in combination with a deletion of *ezrA*.

After a temporal delay, late-stage divisome proteins are recruited to the Z-ring, which among others include FtsK, FtsQ, FtsL, FtsB, FtsW, FtsI (or PBP3) and FtsN in *E. coli* [124,180] or PBP2b, FtsL, DivIB, DivIC, GpsB, FtsW and DivIVA in *B. subtilis* [126]. These proteins either function in peptidoglycan synthesis or in the coordination of cytokinesis with other cellular processes. In *E. coli* for example, the membrane-bound DNA-translocase FtsK consists of two functionally distinct domains that work together to coordinate the divisome with the late stages of chromosome segregation [124,181,182]. Similarly, DivIVA may play a role in linking chromosome segregation and cell division in *S. aureus*, since an increased number of anucleate cells has been observed in mutants with double deletions of *divIVA* and either *dnaK* or *smc* [183]. Regarding peptidoglycan synthesis, a ternary complex of the bitopic integral membrane proteins FtsQ, FtsL and FtsB in *E. coli* (as well as their homologs DivIB, FtsL and DivIC in *B. subtilis*) acts as a scaffold for the recruitment of other cell division proteins to regulate the activity of the divisome [184–186], thereby connecting the developing divisome with components of the peptidoglycan synthesis machinery (e.g., FtsW, FtsI/PBP3, PBP2b, GpsB) [126,187–194]. To complete cytokinesis, late-stage division proteins further trigger the constriction of the divisome, such as DipI in *C. crescentus* [129] or FtsN in *E. coli* [185,195,196], with the latter organized in large, discrete macromolecular assemblies, representing distinct FtsZ-rings and FtsN-rings, rather than one super-complex [197].

Targeting FtsZ with antimicrobial agents

The previous sections highlighted the complexity of cell division, a central and vital process to many bacteria, which emerges to be tightly regulated by conserved and often interacting effectors. Nonetheless, most cell division inhibitors described to date act via FtsZ, either by interfering with its GTPase activity or the assembly/disassembly dynamics of the Z-ring, as well as by destabilizing the structural integrity of FtsZ leading to its degradation (Table 1).

The vast majority of cell division inhibitors bind to the core region of FtsZ and modulate its GTPase activity, which is crucial for the assembly and constriction of the Z-ring. For example, *in silico* analyses of potential competitors of GTP led to the discovery of **gallates** and derivatives thereof, such as compound 28, with antimicrobial activity against methicillin-resistant *S. aureus* (MRSA) and *Listeria monocytogenes* in the low μM range. To do so, the compounds bind to FtsZ with a dissociation constant (K_d) of 0.5 μM without cross-targeting eukaryotic tubulin (K_d >100 μM). As a consequence, gallates induce filamentation of *B. subtilis* cells, which is characterized by impaired Z-ring dynamics [198]. Similarly, alkyl gallates inhibit cell division via direct targeting of FtsZ and additionally permeabilize the bacterial membrane, thus exhibiting a dual mode of action [199]. **Curcumin**, a natural polyphenolic compound from *Curcuma longa*, exerts only moderate antimicrobial activity against *B. subtilis* and *E. coli* with MICs of about 100 μM [200]. However, curcumin bioconjugates showed improved activity against several pathogens including staphylococci, streptococci and enterococci in the range of 2.5–20 μM [201]. Curcumin induces filamentation of rod-shaped bacteria and prevents Z-ring formation. By interacting with the GTP-binding pocket of FtsZ, curcumin increases FtsZ GTPase activity and blocks the assembly and bundling of FtsZ protofilaments. The latter may be explained by an increased GTP hydrolysis that favors the reconversion of FtsZ protofilaments into monomers [200,202]. Although derivatization of curcumin led to the identification of promising analogs regarding antimicrobial activity against clinically relevant enterobacteria [203], several hurdles prevent the use of curcumin as a therapeutic agent [204] such as restricted bioavailability [205] as well as potential cytotoxicity, since curcumin binds to eukaryotic tubulin at concentrations of 0.1 μM (physiological) or higher, and results in the depolymerization of microtubules [206]. It is therefore not surprising that curcumin is known to act as an anticancer and anti-inflammatory agent as well [201]. However, further derivatization and computational docking studies might help to explore structural mimetics and more potent derivatives with selective antibacterial activity. **Chrysophaentins** comprise eight macrocyclic natural products, designated chrysophaentin A–H that are produced by the chrysophyte marine alga *Chrysophaeum taylorii*, of which chrysophaentin A exhibits antibacterial activity against MRSA and vancomycin-resistant enterococci (VRE) [207]. Chrysophaentin A induces mislocalization of FtsZ in *B. subtilis* and in permeabilized *E. coli* cells, which is most probably due to a decreased level of FtsZ GTPase activity (IC_{50} SaFtsZ, 67 μM; IC_{50} EcFtsZ, 10 μM) [208]. Computational docking studies identified the binding region of chrysophaentins at the GTP-binding site, explaining its mode of action by direct competition with GTP for the binding to FtsZ. Noteworthy, chrysophaentin A appears to have a higher specificity for FtsZ over tubulin, potentially allowing a more selective use of these compounds as antimicrobial agents [207]. **Vanillin** is appreciated for its antimicrobial properties as a food preservative [209]. Derivatives of vanillin are active against *E.*

Table 1. Chemical structures, modes of action and antibacterial activities of FtsZ inhibitors.

Compound/source	Chemical structure	Cell division effects/binding sites	Antibacterial activity
3-MBA, synthetic	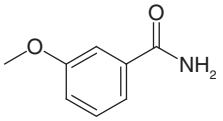	• Filamentation of *Bacillus subtilis* • Unknown binding site	• MIC: *B. subtilis*, 26.5 μM
3-MBA analog **PC190723**, synthetic	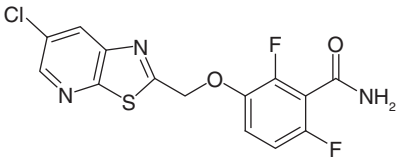	• Potent inhibition of FtsZ GTPase activity (IC_{50}, 160 nM) • Stabilizes FtsZ polymers • Filamentation of *B. subtilis*, and volume increase of *Staphylococcus aureus* cells • Binds to the cleft between H7 helix and T7 loop of FtsZ	• MIC: MRSA/MDRSA, 1.4–2.8 μM • Effective treatment of mice in an *S. aureus* model for septicemia • Re-sensitizes MRSA to β-lactams
3-phenyl-isoquinoline, synthetic	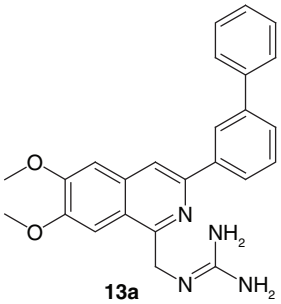 **13a**	• Stabilizes FtsZ polymers • Reduces FtsZ-GTPase activity • Interacts with eukaryotic tubulin • Unknown binding site	• MIC: MRSA/MSSA, 5 μM; VRE/VSE, 19 μM
ADEP, natural products (e.g., ADEP1) and synthetic derivatives (e.g., ADEP4)	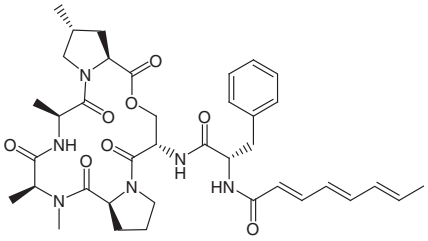 **ADEP1** 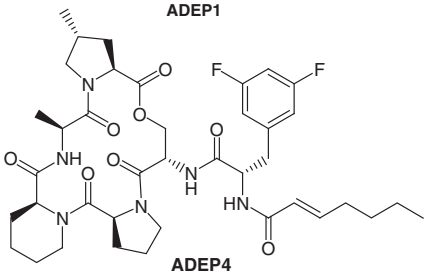 **ADEP4**	• Binds to and dysregulates bacterial ClpP peptidase • ADEP-activated ClpP degrades polypeptides and proteins; FtsZ is a preferred degradation target • Strong filamentation of *B. subtilis* and swelling of *S. aureus* • Inhibition of Z-ring formation/cell division	• MIC: G+ species including MRSA, VRE and PRSP, 0.3–0.9 μM • Combination of ADEP4 and rifampicin eradicates MRSA persister cells and biofilms
B10, synthetic pyridinium derivative	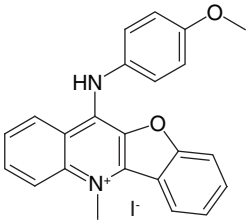	• Inhibits GTPase activity and polymerization of FtsZ • Leads to short and thicker polymers and reduced bundling • Filamentation of *B. subtilis* cells • Binds to the interdomain cleft between T7 loop, H7 helix and the four-stranded β-sheet of FtsZ	• MIC: *B. subtilis*, MRSA/MSSA, VRE/VSE, 4 μM; *Escherichia coli*, 12 μM; *Klebsiella pneumoniae* and *Pseudomonas aeruginosa*, 100 μM
trisubstituted **benzimidazoles**, synthetic	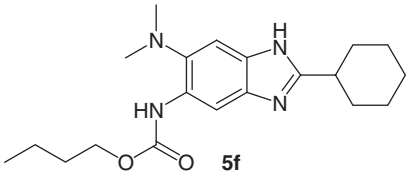 **5f**	• Reduces FtsZ polymerization • Increases GTPase hydrolysis rate • Cytokinesis defects • Unknown binding site	• MIC: *Mycobacterium tuberculosis*, 0.2 μM • Active against dormant cells and murine models of tuberculosis infection

G+: Gram-positive bacteria; G-: Gram-negative bacteria; MDR: multidrug-resistant; MIC_{50}: Lowest concentration of the antibiotic at which 50% of the bacteria are inhibited; MRSA: Methicillin-resistant *S. aureus*; MSSA: Methicillin-susceptible *S. aureus*; PRSP: Penicillin-resistant *S. pneumoniae*; VRE: Vancomycin-resistant enterococci; VSE: Vancomycin-susceptible enterococci.

Table 1. Chemical structures, modes of action and antibacterial activities of FtsZ inhibitors (cont.).

Compound/source	Chemical structure	Cell division effects/binding sites	Antibacterial activity
berberine, plant natural product	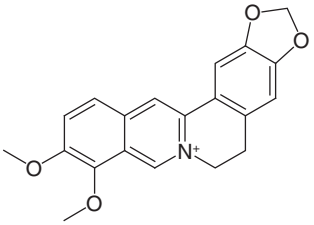	• Inhibits FtsZ polymerization (IC_{50}): *E. coli*, 10 μM; *S. aureus*, 200 μM; and *B. anthracis*, 63 μM • Reduces GTPase activity • Leads to filamentation and impairment of Z-ring formation • Binds to the hydrophobic pocket in the GTP binding region of FtsZ	• MIC: G+ and G- species, >190 μM
berberine analog **dibenzo[a,g]quinolizin-7-ium**, synthetic	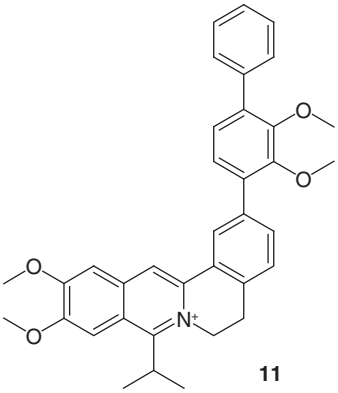 **11**	• Stimulates FtsZ polymerization • Unknown binding site	• MIC: MRSA/MRSA, 0.9 μM; VRE/VSE, 3.7 μM
BT-benzo-29, synthetic phenolic compound	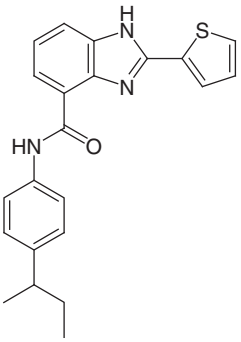	• Filamentation of *B. subtilis* at sublethal concentrations (1 μM) • Perturbs Z-ring dynamics • Delocalization of divisome proteins such as FtsZ, FtsA, ZapA and SepF • Inhibits BsFtsZ polymerization (IC_{50}, 26 ± 3 μM) • Reduces FtsZ GTPase activity (IC_{50}, 15.3 ± 3.2 μM) • Binds to the C-terminal domain in the vicinity of the T7 loop	• MIC: *B. subtilis*, 4.2 ± 0.7 μM; *Mycobacterium smegmatis*, 1.6 ± 0.4 μM
CCR-11, synthetic phenolic compound	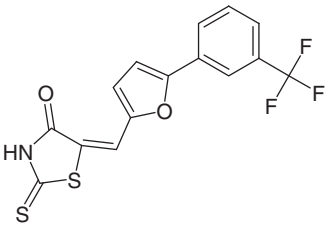	• Inhibits BsFtsZ polymerization • Reduces FtsZ GTPase activity • Filamentation of *B. subtilis* at 2.5 μM • Binds to a cleft near the T7 loop	• MIC: *B. subtilis*, 3 μM; *M. smegmatis*, 4 μM (determined by agar dilution method)
chrysophaentin A, natural product	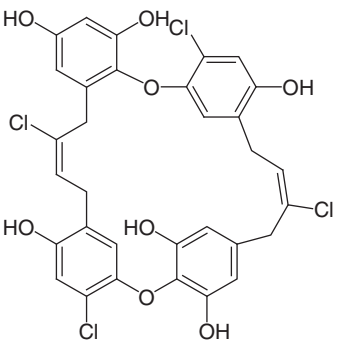	• Inhibits FtsZ GTPase activity (EcFtsZ IC_{50}, 9.9 ± 2.5 μM; SaFtsZ IC_{50}, 67 ± 13 μM) • Mislocalization of FtsZ in *B. subtilis* and permeabilized *E. coli* cells • Binds to the GTP-binding site	• MIC_{50}: *S. aureus*, 2.2 ± 1.0 μM; MDR *S. aureus*, 1.9 ± 0.6 μM; VRE, 4.3 ± 1.2 μM

G+: Gram-positive bacteria; G-: Gram-negative bacteria; MDR: multidrug-resistant; MIC_{50}: Lowest concentration of the antibiotic at which 50% of the bacteria are inhibited; MRSA: Methicillin-resistant *S. aureus*; MSSA: Methicillin-susceptible *S. aureus*; PRSP: Penicillin-resistant *S. pneumoniae*; VRE: Vancomycin-resistant enterococci; VSE: Vancomycin-susceptible enterococci.

Table 1. Chemical structures, modes of action and antibacterial activities of FtsZ inhibitors (cont.).

Compound/source	Chemical structure	Cell division effects/binding sites	Antibacterial activity
compound 28, synthetic gallate	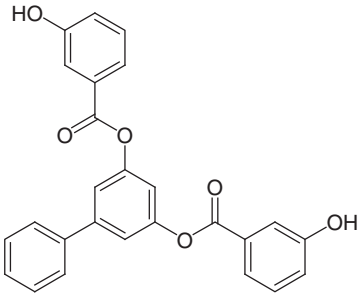	• Inhibits FtsZ GTPase activity (K_d, 0.5 μM) • Strong filamentation of *B. subtilis* cells • Impairs Z-ring formation • Permeabilizes the cell membrane • Unknown binding site	• MIC: MRSA and *Listeria monocytogenes*, 7 μM
curcumin, plant natural product	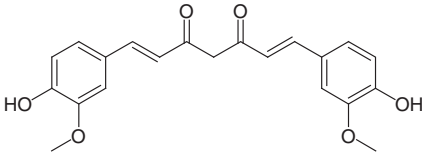	• Decreases FtsZ polymerization and increases protofilament disassembly • Increases GTPase activity • Leads to filamentation of *B. subtilis* cells and inhibition of Z-rings formation • Binds to the GTP-binding region	• MIC: G+ and G- species incl. *S. aureus*, 100 μM (2.5–20 μM for related bioconjugates)
taxanes, synthetic	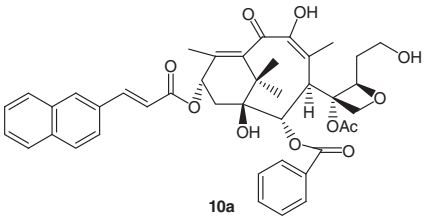 10a	• Increases FtsZ polymerization and stabilizes polymers • Reduces GTPase activity • Filamentation of *M. tuberculosis* and *B. subtilis* cells • Disturbs Z-ring dynamics • Binds to the interdomain cleft between the C-terminal region and the H7 helix	• MIC 10a: *M. tuberculosis*, 1.25–2.5 μM; • MIC SB-RA-2001: *B. subtilis*, 38 μM; *M. smegmatis*, 60 μM
vanillin, plant natural product	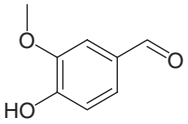	• Inhibits FtsZ polymerization (IC_{50}, 2.1–7.6 μM) • Binds to the GTP-binding site	• MIC: G+ and G- species, 0.28–45.67 μg/ml
zantrins, synthetic polyphenols	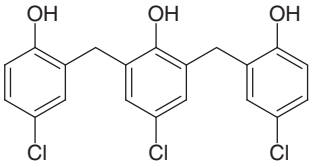	• Inhibits GTPase activity (IC_{50}, 4–100 μM) • Stabilize lateral interactions of FtsZ or destabilize protofilaments • Reduce frequency of Z-rings • Unknown binding site	• MIC: *S. aureus* and *Streptococcus pneumoniae*, 5–10 μM; *E. coli* and *P. aeruginosa*, >80 μM

G+: Gram-positive bacteria; G-: Gram-negative bacteria; MDR: multidrug-resistant; MIC_{50}: Lowest concentration of the antibiotic at which 50% of the bacteria are inhibited; MRSA: Methicillin-resistant *S. aureus*; MSSA: Methicillin-susceptible *S. aureus*; PRSP: Penicillin-resistant *S. pneumoniae*; VRE: Vancomycin-resistant enterococci; VSE: Vancomycin-susceptible enterococci.

coli in the sub-μg/ml range and inhibit GTPase activity of FtsZ with an IC_{50} of 2.1 μM [210]. **Amikacin**, a broad-spectrum semi-synthetic aminoglycoside antibiotic, which is known to inhibit protein biosynthesis by preventing the translocation of peptidyl-tRNA, shows a second mode of action at sublethal concentrations (6.8 μM) by inhibiting cell division without affecting chromosome dynamics. Here, amikacin causes a reduction of Z-rings accompanied by an elongation of *E. coli* cells [211], which is most probably due to the binding of amikacin to the GTP-binding site of FtsZ [212]. **Zantrins** represent a group of five diverse phenolic compounds that affect the GTPase activity of FtsZ (IC_{50} 4–100 μM) and either destabilize FtsZ protofilaments (zantrins Z1, Z2 and Z4) or lead to hyperstability of FtsZ protofilaments by supporting lateral interactions (zantrins Z3 and Z5). *In vivo*, zantrins reduce the frequency of Z-ring formation in *E. coli* but do not induce filamentation in cells, except for Z5. Due to their rather weak antimicrobial activity with MICs in the range of 66–98 μM for zantrins Z1–Z4 against Gram-positive bacteria, zantrins require further optimization to yield more promising lead compounds [213]. **Taxanes** are well-known therapeutic anticancer agents that act on eukaryotic tubulin, which hampers their immediate use as antimicrobial agents. However, derivatization of taxanes produced noncytotoxic and more potent antitubercular compounds with MICs in the range of 1.25–2.5 μM against multidrug-resistant *M. tuberculosis*, such as compound 10a that stabilizes FtsZ polymerization and induces filamentation of *M. tuberculosis* cells [214]. *In silico* data suggest that taxanes bind

to the interdomain cleft between the C-terminal region and the α-helix H7 of FtsZ [215]. **Berberine**, a natural isoquinoline-type alkaloid obtained from the widely distributed Berberidaceae and other plant families [216], perturbs Z-ring dynamics, decreases the number of Z-rings per cell unit and induces filamentation of *E. coli* cells [217,218]. Berberine binds to a hydrophobic pocket of FtsZ, which overlaps the GTP region, with a K_d of 0.023 μM [218], reduces GTPase activity, and disrupts the protofilament architecture of FtsZ *in vitro*, thereby preventing FtsZ polymerization [218–220]. Due to its anti-FtsZ activity, berberine has been the subject of various derivatization programs, some of which yielded improved derivatives that inhibit the growth of MRSA and VRE with MICs in the range of 0.5–2 μg/ml, respectively [221,222]. Berberine and the benzophenanthridine alkaloid sanguinarine share a pyridinium core from which synthetic quaternary pyridinium and 5-methylphenantridium derivatives were designed [223,224]. For example, derivative B10 displays broad-spectrum antimicrobial activity against important pathogens including MRSA, VRE, *Klebsiella pneumoniae*, *P. aeruginosa* and *E. coli* with MICs in the range of 2–48 μg/ml (4–100 μM) [223]. Moreover, combination of the ring cores of berberine and sanguinarine led to the design and synthesis of 3-phenyl-isoquinoline derivatives, which reduce the GTPase activity of SaFtsZ and stabilize polymers *in vitro*. Some of the synthetic derivatives were effective against MRSA and VRE (MIC of 1–8 μg/ml) and showed only low cytotoxicity against mammalian cells [225]. Interestingly, addition of an aryl group in either position two or 12 improved the antimicrobial activity of the synthetic berberine analog dibenzo[a,g]quinolizin-7-ium, which in contrast to its natural counterpart, stimulates SaFtsZ polymerization [221]. Noteworthy, antimicrobial activity of berberine could also be increased in combination with 5′-methoxyhydnocarpin, a natural compound that inhibits the NorA eflux pump of *S. aureus* [226]. Furthermore, there are reports on synergistic effects of berberine in combination with penicillin, oxacillin, erythromycin, azithromycin, cefazolin, levofloxacin and clindamycin against Gram-positive bacteria including MRSA [227,228]. Also noteworthy, berberine inhibits the GTPase activity of FtsZ from *Wolbachia*, an obligate bacterial endosymbiont of filarial nematode parasites, and reduces the motility and reproduction of the filarial nematode *Brugia malayi in vitro* [229], thus validating FtsZ inhibition as a new approach to control and treat filarial infections.

The compounds described so far bind to or at least near the GTP-binding site of FtsZ. However, targeting the conserved GTP-binding site may principally bear a higher risk for cross-targeting eukaryotic tubulin and thus provoke cytotoxicity in human cells, a notion that is supported by numerous compounds with known pharmacological side effects, such as plumbagin [230,231], viriditoxin [232,233], sanguinarine [234–236] or doxorubicin [235,237,238]. Thus, compounds with binding sites other than the conserved GTP-binding region may be favorable. In this context, screening a library of rhodanine compounds for a filamentation phenotype of *B. subtilis* identified compound **CCR-11**, which binds to FtsZ with a K_d of 1.5 μM and inhibits FtsZ polymerization as well as GTPase activity *in vitro* [239]. Furthermore, CCR-11 inhibits the growth of *B. subtilis* and *Mycobacterium smegmatis* with MICs of 3 and 4 μM, respectively, disturbs Z-ring formation, and causes delocalization of FtsZ in whole cells. Notably, CCR-11 showed no cytotoxic activity against HeLa cells in that study. According to *in silico* docking simulations, interestingly, CCR-11 rather binds to a cleft near the T7 loop of FtsZ than to the GTP-binding site [239]. **Trisubstituted benzimidazoles** represent a group of promising antitubercular lead compounds, which inhibit the growth of several clinical isolates with MICs in the range of 0.39–6.1 μg/ml. *In vitro*, these compounds inhibit the polymerization of MtbFtsZ by stimulating the GTPase activity of FtsZ in a dose-dependent manner [240]. Structure–activity relationship (SAR) analyses and drug development programs led to the discovery of derivatives with improved antibacterial activity *in vitro* (e.g., compound 5f with an MIC of 0.06 μg/ml) [241] as well as in dormant cells and in murine models of tuberculosis infection [242,243]. The benzimidazole derivative BT-benzo-29 binds to FtsZ with a K_d of 24 μM (tubulin, K_d 152 μM) and reduces GTPase activity of BsFtsZ with an IC_{50} of 15 μM. In whole cells, BT-benzo-29 induces filamentation of *B. subtilis* at rather low concentrations (1 μM) and inhibits growth with an MIC_{50} (MIC to inhibit proliferation by 50%) of 4.2 μM for *B. subtilis* and 1.6 μM for *M. smegmatis*. Colocalization studies indicated perturbed Z-ring dynamics and a concomitant delocalization of other divisome proteins, such as FtsA, ZapA and SepF. Noteworthy, *in silico* analysis also proposed binding of BT-benzo-29 in the vicinity of the T7 loop of the C-terminal domain [244]. In this context, further effectors of FtsZ have been predicted to bind in the T7 loop region, thereby interfering with FtsZ function and preventing cell division, such as cinnamaldehyde, coumarins and phenylpropanoids [245–249], which may thus represent a promising strategy to avoid cross-targeting of tubulin and reduce cytotoxic effects in eukaryotic cells.

Thinking along these lines, a group of synthetic benzamide derivatives (including 3-methoxybenzamide, 3-MBA) induces filamentation and cell death in *B. subtilis*, which is abrogated in *ftsZ*-deficient mutants [250]. SAR-based derivatization of 3-MBA yielded more than 500 analogs, among them **PC190723** with strong antibacterial

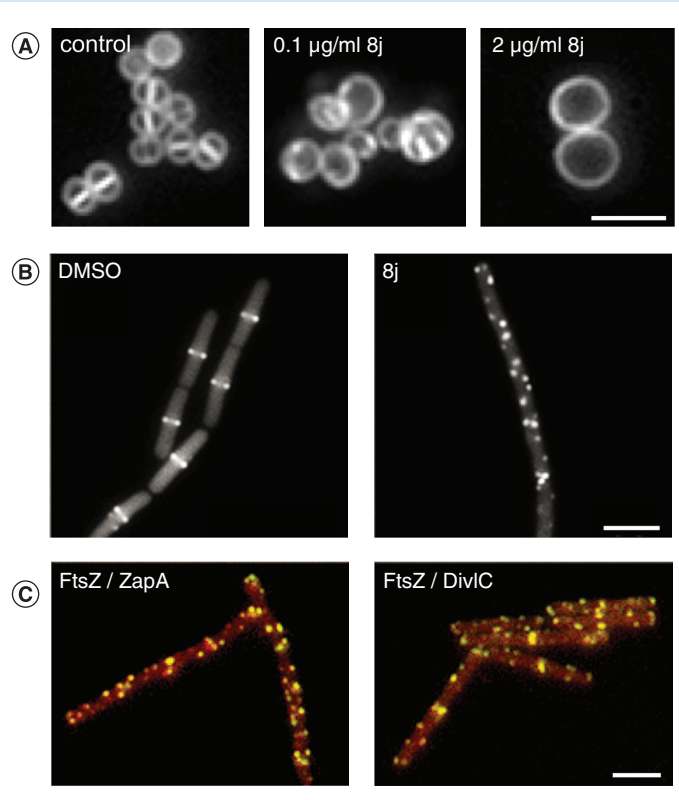

Figure 4. Deregulation of Z-ring formation by the PC190723-analog 8j. (A) 8j treatment leads to abnormal cell division in *Staphylococcus aureus* cells. *S. aureus* strain RN4220 was grown in the absence and presence of 0.1 or 2 μg/ml 8j. Cell membranes were stained with FM5-95. Scale bar, 3 μm. **(B)** Mislocalization of FtsZ in 8j-treated *Bacillus subtilis* cells. Fluorescence microscopy images of *B. subtilis* strain 2020 (GFP-FtsZ) show that 8j inhibits FtsZ localization and results in the formation of abnormal discrete foci throughout the cell, thereby preventing regular cell division. Scale bar, 3 μm. **(C)** Colocalization of FtsZ–CFP with either YFP–ZapA (left image) or YFP–DivIC (right image), indicated by yellow color, shows that downstream division proteins assemble at FtsZ foci in 8j-treated *B. subtilis* cells. Scale bar, 3 μm.
(A) Images adapted from [256], reprinted with permission from Wiley.
(B) Images adapted from [256], reprinted with permission from Wiley.
(C) Images adapted from [256], reprinted with permission from Wiley.

activity against *S. aureus* including MRSA with MICs in the range of 0.5–1 μg/ml (1.4–2.8 μM) as well as in *in vivo* murine models of *S. aureus* septicemia [251,252]. PC190723 significantly reduces the GTPase activity of FtsZ in a dose-dependent manner (IC_{50} value of 0.16 μM). To do so, PC190723 binds to a cleft that is formed by the α-helix H7, the T7 loop and the C-terminal four-stranded β-sheets of FtsZ, and importantly, no interference with eukaryotic tubulin has been observed *in vitro* [252]. Follow-up studies revealed an interesting nature of PC190723, as unlike most other FtsZ inhibitors, the effect of PC190723 involves stabilization of FtsZ polymers rather than destabilization, which consecutively halts the dynamics and functionality of FtsZ [253,254]. Accordingly, PC190723 and derivatives thereof, such as compound 8j, lead to the formation of multiple rings and arcs of FtsZ in *S. aureus* (Figure 4A) as well as twisted septa and abnormal discrete foci of FtsZ at the cell poles and over the nucleoid in *B. subtilis* cells (Figure 4B) [252,255,256]. Noteworthy, such foci of FtsZ remain active and dynamic in terms of FtsZ turnover and still recruit further cell division proteins that interact with FtsZ (Figure 4C) [256]. Of note, fluorescent probes of PC190723 have been shown to change the fluorescence anisotropy after binding to previously polymerized FtsZ [257]. This finding supports the idea of an open conformation of FtsZ in the polymerized state as discussed above, while monomeric FtsZ adopts a closed conformation to which PC190723 appears unable to bind, thus demonstrating that antibiotics, in addition to their antimicrobial activity, may also function as tools to unravel

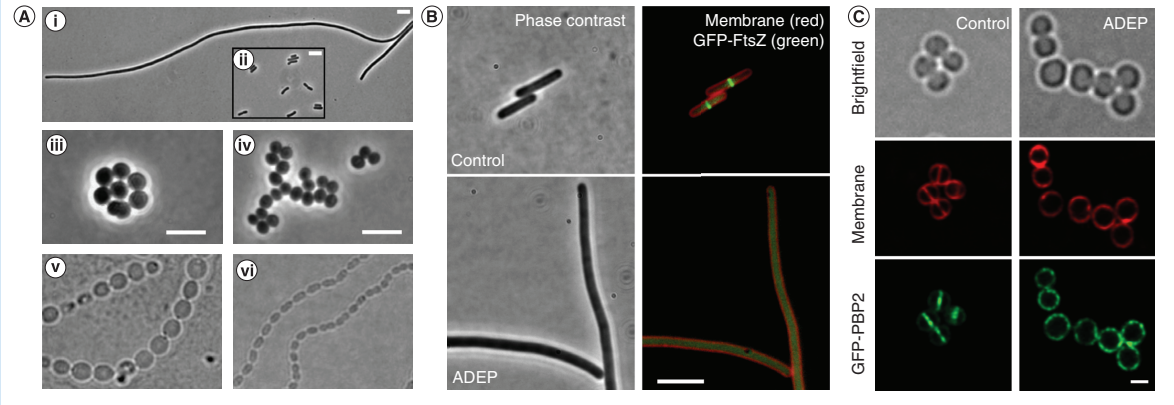

Figure 5. ADEP antibiotics inhibit cell division by activating bacterial ClpP peptidase to degrade FtsZ. (A) ADEP treatment results in an impressive filamentation of rod-shaped *Bacillus subtilis* 168 cells (i) as well as swelling of coccoid *Staphylococcus aureus* HG001 (iii) and *Streptococcus pneumoniae* G9A cells (v) compared with untreated control cells (ii, iv, and vi, respectively), thus indicating an inhibition of cell division. Scale bars, 5 μm. **(B)** Delocalization of GFP-FtsZ in ADEP-treated *B. subtilis* 2020 cells (lower panel), in contrast to normal Z-ring assembly in untreated cells (upper panel), leads to an inhibition of Z-ring/septum formation and finally cell division as indicated by the filamentous growth after prolonged ADEP treatment. Scale bar, 5 μm. **(C)** Fluorescence microscopy images show the delocalization of the divisome member PBP2 away from the septum to the cell periphery of *S. aureus* as a consequence of FtsZ degradation. Scale bar, 1 μm.
(A) Images reprinted from [265].
(B) Images reprinted from [265].
(C) Images adapted from [266] reprinted with permission from Elsevier.

general principles of bacterial cell biology. Further optimization of PC190723 yielded 'compound 1' and its succinate prodrug 'compound 2', which exhibit improved pharmacokinetic properties and superior antimicrobial activities toward pathogenic bacteria [258]. Novel derivatives of PC190723, such as TXY541, TXA709 or compound 9, resolve low bioavailability, are effective in animal models of severe staphylococcal infection and exert low cytotoxicity in mammalian cell lines [259–261]. Also, these derivatives exhibit superior metabolic and pharmacokinetic properties, improved *in vivo* antibacterial activity against MRSA [260], as well as an extended antibacterial spectrum regarding mycobacteria [261]. Moreover, PC190723 and derivatives thereof synergize with imipenem, cefdinir or cefuroxime by re-sensitizing MRSA to β-lactam antibiotics [255,262,263], for example, leading to a threefold reduction of the TXA709 oral dose required for efficacy. Since the septal localization of PBP2, which function is essential in MRSA, depends on FtsZ, the observed synergistic activity is most probably based on the concomitant delocalization of both drug targets. Resistance to PC190723 and TXA707 was reported to occur via mutations in the *ftsZ* gene with residues G196 and G193 being among the most prevalent [255,262]. Although several PC190723-resistant MRSA *ftsZ* mutants were also characterized by attenuated virulence [255], the use of PC190723/imipenem and TXA707/cefdinir combinations further proved beneficial in terms of resistance development as it markedly reduced the spontaneous frequency of PC190723- and TXA707-resistant mutants in MRSA, thereby addressing emerging issues related to suboptimal frequency of resistance associated with FtsZ-targeting benzamide antibiotics [255,262]. Recently, derivative TXA6101 has been described to even retain activity against MRSA that carry either G196S or G193D mutations in *ftsZ*, which is assumed to result from the greater structural flexibility of TXA6101 relative to other PC190723 derivatives, thereby avoiding steric clashes with Ser196 and Asp193 [264]. Such potent synergistic action of PC190723 and derivatives with β-lactam antibiotics validates FtsZ inhibition as a promising strategy for antibiotic combination therapy.

The antibiotic compounds mentioned so far all directly interact with FtsZ, albeit using different binding sites to modulate FtsZ function and finally inhibit cell division. However, in recent years, studies on a new class of antibiotic acyldepsipeptides, designated **ADEP**, revealed a new and unprecedented way of interfering with bacterial cell division by leading to the untimely degradation of FtsZ. At low inhibitory concentrations of ADEP, rod-shaped *B. subtilis* cells grow into impressively long filaments, whereas coccoid *S. aureus* and *S. pneumoniae* cells start swelling (Figure 5A) [265,266]. Furthermore, septum formation and Z-ring assembly is rapidly inhibited in treated cells, leading to the mislocalization of central divisome proteins (Figure 5B & C). Under these conditions,

biomass production and major cellular biosynthetic processes proceed unaffected [265], thus pointing at a potential target that is intimately involved in cell division. However, quite the contrary, ADEP was identified to bind to and deregulate the function of the bacterial caseinolytic protease Clp [267–273]. Here, ADEP binding leads to an inhibition of all natural Clp functions by abrogating the interaction of the proteolytic core ClpP with regulatory Clp-ATPases, such as ClpX or ClpC [270,271,273]. At the same time, ADEP activates the core ClpP for uncontrolled proteolysis of non-native protein substrates [270,271,274]. For further details on the deregulation of Clp protease by ADEP and other compounds, we kindly refer the reader to a recent comprehensive review on this topic [275]. In fact, ClpP activation by ADEP leads to the preferred and rapid degradation of FtsZ in ADEP-treated cells as well as *in vitro* [265], thereby explaining the observed phenotype of cell division inhibition that eventually leads to bacterial cell death. Noteworthy, at higher ADEP concentrations, ADEP-treated cells remain shorter and biomass production ceases, indicating an increased degradation of additional targets by ADEP-ClpP in the bacterial cell [266,276], which finally leads to suicide of the bacteria via self-digestion. Very recent data revealed the molecular basis for the preferred degradation of FtsZ by ADEP-ClpP. It emerged that ADEP-ClpP preferably attacks the N-terminus of FtsZ, which leads to the unfolding and subsequent degradation of the FtsZ N-terminal domain, thus indicating that the protein fold of FtsZ appears to be more flexible than previously expected [276]. The natural product ADEP1 is produced by *Streptomyces hawaiiensis* NRRL 15010 and already shows promising antibiotic activity against Gram-positive bacteria (*S. aureus* MIC of 6.3 μg/ml, 8.8 μM) [267,277] which was significantly improved by chemical engineering and total synthesis of new synthetic derivatives, such as ADEP4, with enhanced chemical and metabolic stability [278–281]. For example, ADEP4 is exceptionally potent to kill Gram-positive pathogens with MICs in the sub-μg/ml range, including MRSA (MIC = 0.05 μg/ml, 0.065 μM) and vancomycin-resistant enterococci (VRE; MIC = ≤0.01 μg/ml, 0.013 μM) [267,282]. Furthermore, ADEP4 shows impressive efficacy in rodent models of staphylococcal infections, which was superior to that of the marketed antibiotic linezolid [267]. In combination with rifampicin, ADEP4 even eradicates persister cells in a chronic biofilm infection [283]. In addition, ADEPs are antibacterially active against streptococci [267], clostridia [284], mycobacteria [273,285], *Wolbachia* endobacteria [286] and even against Gram-negative *Neisseria meningitidis* [280]. However, due to the molecular size of ADEP, it is commonly too large to cross the outer membrane of Gram-negative bacteria, which mostly limits the use of ADEP to Gram-positives. Furthermore, its unprecedented mechanism of action combined with an impressive antibacterial activity in murine models of infection, ADEPs further proved noncytotoxic to eukaryotic cells in the concentration range that inhibits bacterial growth. Although ADEPs were shown to deregulate human mitochondrial ClpP *in vitro* [272], cytotoxicity did only occur at compound levels 100–1000-fold higher than the bacterial MIC [267,287,288], validating ADEP antibiotics as a promising new route for antibacterial intervention.

Future perspective

Bacterial cell division, coordinated by the central pacemaker protein FtsZ, may be compared with a well-adjusted clockwork with a defined set of gears to control and drive the division machine, in other words, parent cells have to coordinate a plethora of biosynthetic processes with the help of diverse divisome proteins to eventually divide and produce viable daughter cells. Due to its complexity and cross-regulative nature, further divisome proteins other than FtsZ may be envisioned as targets for antimicrobial or also antivirulence intervention, for example, since the deletion of *minD* in enterohemorrhagic *E. coli* (EHEC) caused reduced adherence to human epithelioid cervical carcinoma [289]. In recent years, especially the advances in fluorescence light microscopy, increasing both real and effective optical resolution, boosted the research in the field of bacterial cell biology and enabled vast progress to gain unprecedented insights into structures and complex dynamics of cellular systems. A profound understanding of the spatial dimensions and the dynamics of bacterial cell biology provides a basis for antibacterial drug development and thus aids in the discovery of new antibiotics that perturb such tightly regulated systems, potentially breaking the resistance of important human pathogens. This review summarized the mode of bacterial cell division along with a structurally diverse collection of cell division inhibitors, among which PC190723 and ADEP stand out as most promising leads for further exploration and the development of novel antimicrobials. Both compounds share resistance-breaking potential, suitable *in vitro* pharmaceutical properties and *in vivo* pharmacokinetic profiles, as well as substantial antibacterial activities in murine models of infection. Despite these promising assets, a major future task will be to explore suitable strategies to overcome the resistance problems that both antibiotic classes suffer from, since resistance may be conferred by mutations in FtsZ (for PC190723 [254,255]) or in ClpP (for ADEPs [267]). However, the synergistic activities of either PC190723 and derivatives with β-lactam antibiotics to combat MRSA or ADEP4 with rifampicin to eradicate staphylococcal persister cells represent promising approaches

to tackle the resistance problem. Although resistance development may restrict their potential use to combination therapy against some pathogens, at least ADEP proved active against *M. tuberculosis*, an important human pathogen that strictly depends on ClpP for survival and expression of virulence factors during host infection [290], making inactivating mutations of ClpP in this pathogen at least unlikely. Thus, further compound optimization approaches to improve antibacterial activities against such pathogens are encouraged to develop both compound classes as antibiotic agents, which share promising mechanisms of action that impressively illustrate the broad and innovative repertoire that nature has invented to prevent bacterial growth by interfering with bacterial cell division.

Executive summary

Crystal structure, abundance & functional regions of FtsZ

- FtsZ is the structural homolog of the eukaryotic cytoskeletal protein tubulin and consists of two major, self-folding protein domains, an N-terminal GTP-binding domain and a C-terminal domain.
- FtsZ and tubulin represent a distinct family of GTP-hydrolyzing enzymes.
- FtsZ is largely conserved across the domains Bacteria and Archaea, and it is assumed to be the ancestral progenitor of eukaryotic tubulin.
- The poorly conserved N-terminal peptide plays a role in cell division of cyanobacteria; however, it has not yet been assigned a function in Firmicutes and Proteobacteria.
- The highly conserved globular core region comprises the GTPase active site, functions as an interface for the head-to-tail association of FtsZ monomers into protofilaments, and it is involved in supporting lateral interactions of FtsZ protofilaments.
- The unstructured C-terminal linker (CTL) acts as a flexible tether to provide a defined distance from the bacterial membrane, where FtsZ is anchored via modulatory proteins.
- The short, conserved C-terminal tail (CTT) is the central hub for FtsZ-interacting divisome proteins.
- The C-terminal variable region (CTV) plays a role in lateral interactions of FtsZ protofilaments.

Positioning, assembly & modulation of the Z-ring

- The Z-ring is a highly dynamic structure that is treadmilling around the division plane by bottom-end growth, constantly exchanging FtsZ subunits with the cytoplasmic pool.
- Z-ring positioning is controlled by negatively-acting factors, such as the NO- and Min-systems in *Bacillus subtilis* and *Escherichia coli* that prevent extra Z-rings over unsegregated nucleoids and at the cell pole region, respectively, or by positively-acting factors such as SsgAB in streptomycetes or MapZ/*oriC* in streptococci that mark the prospective division site.
- More than 35 divisome members have been identified so far, including early-stage proteins for membrane-tethering and Z-ring maturation as well as late-stage proteins involved in the synthesis of septal peptidoglycan and finally cytokinesis.

Targeting FtsZ with antimicrobial agents

- PC190723 and ADEP are among the most promising leads with resistance-breaking potential, suitable *in vitro* pharmaceutical properties and *in vivo* pharmacokinetic profiles, as well as substantial antibacterial activities in murine models of infection.
- PC190723 stabilizes FtsZ polymers and halts the dynamics and functionality of FtsZ, leading to the formation of multiple rings and arcs of FtsZ or abnormal discrete foci at the cell poles and over the nucleoid.
- ADEP antibiotics activate the bacterial peptidase ClpP for the untimely proteolytic digestion of FtsZ, thereby preventing Z-ring formation and thus cell division.

Author contributions

N Silber, CL Matos de Opitz and C Mayer drafted the manuscript; all authors prepared figures and tables; P Sass outlined, edited and finalized the manuscript.

Acknowledgments

We gratefully thank all team members of our department for their support and critical discussions.

Financial & competing interests disclosure

The authors declare no competing interests. The authors appreciate funding by the Deutsche Forschungsgemeinschaft (DFG, German Research Foundation): Project-ID 398967434 (TRR 261, TP A02), Project-ID 32152271 (SFB766, TP A17), and support by infrastructural funding from Cluster of Excellence EXC 2124 Controlling Microbes to Fight Infections. PS further appreciates funding by the German Center for Infection Research (DZIF; TTU 09.815). The authors have no other relevant affiliations or financial

involvement with any organization or entity with a financial interest in or financial conflict with the subject matter or materials discussed in the manuscript apart from those disclosed.

No writing assistance was utilized in the production of this manuscript.

References

Papers of special note have been highlighted as: • of interest; •• of considerable interest

1. Lutkenhaus JF, Wolf-Watz H, Donachie WD. Organization of genes in the *ftsA-envA* region of the *Escherichia coli* genetic map and identification of a new *fts* locus (*ftsZ*). *J. Bacteriol.* 142(2), 615–620 (1980).
2. Van De Putte P, Van Dillewijn J, Rörsch A. The selection of mutants of *Escherichia coli* with impaired cell division at elevated temperature. *Mutat. Res. Fund. Mol. M.* 1, 121–128 (1964).
3. Bi E, Lutkenhaus J. FtsZ ring structure associated with division in *Escherichia coli*. *Nature* 354, 161–164 (1991).

•• **Breakthrough study shows that FtsZ forms a ring-like structure at the prospective division site, thereby boosting research in the field of bacterial cell biology.**

4. De Boer P, Crossley R, Rothfield L. The essential bacterial cell division protein FtsZ is a GTPase. *Nature* 359(6392), 254–256 (1992).
5. Raychaudhuri D, Park JT. *Escherichia coli* cell-division gene *ftsZ* encodes a novel GTP-binding protein. *Nature* 359(6392), 251–254 (1992).
6. Mukherjee A, Dai K, Lutkenhaus J. *Escherichia coli* cell division protein FtsZ is a guanine nucleotide binding protein. *Proc. Natl Acad. Sci. USA* 90(3), 1053–1057 (1993).
7. Löwe J, Amos LA. Crystal structure of the bacterial cell-division protein FtsZ. *Nature* 391, 203–206 (1998).

•• **Describes the first crystal structure of FtsZ, revealing its homology to eukaryotic tubulin.**

8. Löwe J. Crystal structure determination of FtsZ from *Methanococcus jannaschii*. *J. Struct. Biol.* 124(2–3), 235–243 (1998).
9. Oliva MA, Trambaiolo D, Löwe J. Structural insights into the conformational variability of FtsZ. *J. Mol. Biol.* 373, 1229–1242 (2007).
10. Nogales E, Downing KH, Amos LA, Löwe J. Tubulin and FtsZ form a distinct family of GTPases. *Nat. Struct. Mol. Biol.* 5(6), 451–458 (1998).
11. Oliva MA, Cordell SC, Löwe J. Structural insights into FtsZ protofilament formation. *Nat. Struct. Mol. Biol.* 11, 1243–1250 (2004).
12. Raymond A, Lovell S, Lorimer D *et al.* Combined protein construct and synthetic gene engineering for heterologous protein expression and crystallization using Gene Composer. *BMC Biotechnol.* 9, 37 (2009).
13. Löwe J, Li H, Downing KH, Nogales E. Refined structure of alpha beta-tubulin at 3.5 A resolution. *J. Mol. Biol.* 313(5), 1045–1057 (2001).
14. Huecas S, Andreu JM. Polymerization of nucleotide-free, GDP- and GTP-bound cell division protein FtsZ: GDP makes the difference. *FEBS Lett.* 569(1–3), 43–48 (2004).
15. Bourne HR, Sanders DA, Mccormick F. The GTPase superfamily: conserved structure and molecular mechanism. *Nature* 349, 117–127 (1991).
16. Polekhina G, Thirup S, Kjeldgaard M, Nissen P, Lippmann C, Nyborg J. Helix unwinding in the effector region of elongation factor EF-Tu-GDP. *Structure* 4(10), 1141–1151 (1996).
17. Vaughan S, Wickstead B, Gull K, Addinall SG. Molecular evolution of FtsZ protein sequences encoded within the genomes of Archaea, Bacteria, and Eukaryota. *J. Mol. Evol.* 58, 19–39 (2004).
18. Kalman S, Mitchell W, Marathe R *et al.* Comparative genomes of *Chlamydia pneumoniae* and *C. trachomatis*. *Nat. Genet.* 21, 385–389 (1999).
19. Pilhofer M, Rappl K, Eckl C *et al.* Characterization and evolution of cell division and cell wall synthesis genes in the bacterial phyla Verrucomicrobia, Lentisphaerae, Chlamydiae, and Planctomycetes and phylogenetic comparison with rRNA genes. *J. Bacteriol.* 190, 3192–3202 (2008).
20. Stephens RS, Kalman S, Lammel C *et al.* Genome sequence of an obligate intracellular pathogen of humans: *Chlamydia trachomatis*. *Science* 282(5389), 754–759 (1998).
21. Nakabachi A, Yamashita A, Toh H *et al.* The 160-kilobase genome of the bacterial endosymbiont *Carsonella*. *Science* 314(5797), 267 (2006).
22. Glass JI, Lefkowitz EJ, Glass JS, Heiner CR, Chen EY, Cassell GH. The complete sequence of the mucosal pathogen *Ureaplasma urealyticum*. *Nature* 407, 757–762 (2000).

23. Jaffe JD, Stange-Thomann N, Smith C *et al.* The complete genome and proteome of *Mycoplasma mobile*. *Genome Res.* 14, 1447–1461 (2004).
24. Grosche C, Rensing SA. Three rings for the evolution of plastid shape: a tale of land plant FtsZ. *Protoplasma* 254, 1879–1885 (2017).
25. Terbush AD, Maccready JS, Chen C, Ducat DC, Osteryoung KW. Conserved dynamics of chloroplast cytoskeletal FtsZ proteins across photosynthetic lineages. *Plant Physiol.* 176(1), 295–306 (2018).
26. Van Den Ent F, Amos LA, Löwe J. Bacterial ancestry of actin and tubulin. *Curr. Opin. Microbiol.* 4, 634–638 (2001).
27. Buske PJ, Levin PA. Extreme C terminus of bacterial cytoskeletal protein FtsZ plays fundamental role in assembly independent of modulatory proteins. *J. Biol. Chem.* 287, 10945–10957 (2012).
28. Rossmann MG, Moras D, Olsen KW. Chemical and biological evolution of nucleotide-binding protein. *Nature* 250(463), 194–199 (1974).
29. Corrales-Guerrero L, Camargo S, Valladares A *et al.* FtsZ of filamentous, heterocyst-forming cyanobacteria has a conserved N-terminal peptide required for normal FtsZ polymerization and cell division. *Front. Microbiol.* 9, 2260 (2018).
30. Marbouty M, Saguez C, Cassier-Chauvat C, Chauvat F. Characterization of the FtsZ-interacting septal proteins SepF and Ftn6 in the spherical-celled cyanobacterium *Synechocystis* strain PCC 6803. *J. Bacteriol.* 191(19), 6178–6185 (2009).
31. Scheffers D-J, De Wit JG, Den Blaauwen T, Driessen AJM. GTP hydrolysis of cell division protein FtsZ: evidence that the active site is formed by the association of monomers. *Biochemistry* 41, 521–529 (2002).
32. Leung AKW, Lucile White E, Ross LJ, Reynolds RC, Devito JA, Borhani DW. Structure of *Mycobacterium tuberculosis* FtsZ reveals unexpected, G protein-like conformational switches. *J. Mol. Biol.* 342, 953–970 (2004).
33. Diaz JF, Kralicek A, Mingorance J, Palacios JM, Vicente M, Andreu JM. Activation of cell division protein FtsZ. Control of switch loop T3 conformation by the nucleotide gamma-phosphate. *J. Biol. Chem.* 276, 17307–17315 (2001).
34. Li Y, Hsin J, Zhao L *et al.* FtsZ protofilaments use a hinge-opening mechanism for constrictive force generation. *Science* 341, 392–395 (2013).
35. Matsui T, Han X, Yu J, Yao M, Tanaka I. Structural change in FtsZ induced by intermolecular interactions between bound GTP and the T7 loop. *J. Biol. Chem.* 289, 3501–3509 (2014).
36. Läppchen T, Pinas VA, Hartog AF *et al.* Probing FtsZ and tubulin with C8-substituted GTP analogs reveals differences in their nucleotide binding sites. *Chem. Biol.* 15(2), 189–199 (2008).
37. Wagstaff JM, Tsim M, Oliva MA *et al.* A polymerization-associated structural switch in FtsZ that enables treadmilling of model filaments. *mBio* 8(3), e00254–00217 (2017).
38. Shin JY, Vollmer W, Lagos R, Monasterio O. Glutamate 83 and arginine 85 of helix H3 bend are key residues for FtsZ polymerization, GTPase activity and cellular viability of *Escherichia coli*: lateral mutations affect FtsZ polymerization and *E. coli* viability. *BMC Microbiol.* 13, 26 (2013).
39. Guan F, Yu J, Yu J *et al.* Lateral interactions between protofilaments of the bacterial tubulin homolog FtsZ are essential for cell division. *Elife* 7, e35578 (2018).
40. Huang J, Cao C, Lutkenhaus J. Interaction between FtsZ and inhibitors of cell division. *J. Bacteriol.* 178(17), 5080–5085 (1996).
41. Cordell SC, Robinson EJH, Löwe J. Crystal structure of the SOS cell division inhibitor SulA and in complex with FtsZ. *Proc. Natl Acad. Sci. USA* 100(13), 7889–7894 (2003).
42. Blasios V, Bisson-Filho AW, Castellen P *et al.* Genetic and biochemical characterization of the MinC-FtsZ interaction in *Bacillus subtilis*. *PLoS ONE* 8(4), e60690 (2013).
43. Scheffers D-J. The effect of MinC on FtsZ polymerization is pH dependent and can be counteracted by ZapA. *FEBS Lett.* 582, 2601–2608 (2008).
44. Shen B, Lutkenhaus J. The conserved C-terminal tail of FtsZ is required for the septal localization and division inhibitory activity of MinC(C)/MinD. *Mol. Microbiol.* 72(2), 410–424 (2009).
45. Shen B, Lutkenhaus J. Examination of the interaction between FtsZ and MinCN in *E. coli* suggests how MinC disrupts Z rings. *Mol. Microbiol.* 75(5), 1285–1298 (2010).
46. Buske PJ, Levin PA. A flexible C-terminal linker is required for proper FtsZ assembly *in vitro* and cytokinetic ring formation *in vivo*. *Mol. Microbiol.* 89, 249–263 (2013).
47. Gardner KA, Moore DA, Erickson HP. The C-terminal linker of *Escherichia coli* FtsZ functions as an intrinsically disordered peptide. *Mol. Microbiol.* 89(2), 264–275 (2013).
48. Huecas S, Ramirez-Aportela E, Vergonos A *et al.* Self-organization of FtsZ polymers in solution reveals spacer role of the disordered C-terminal tail. *Biophys. J.* 113(8), 1831–1844 (2017).
49. Levin PA, Kurtser IG, Grossman AD. Identification and characterization of a negative regulator of FtsZ ring formation in *Bacillus subtilis*. *Proc. Natl Acad. Sci. USA* 96, 9642–9647 (1999).

50. Singh JK, Makde RD, Kumar V, Panda D. A membrane protein, EzrA, regulates assembly dynamics of FtsZ by interacting with the C-terminal tail of FtsZ. *Biochemistry* 46, 11013–11022 (2007).
51. Hu Z, Mukherjee A, Pichoff S, Lutkenhaus J. The MinC component of the division site selection system in *Escherichia coli* interacts with FtsZ to prevent polymerization. *Proc. Natl Acad. Sci. USA* 96, 14819–14824 (1999).
52. Dajkovic A, Lan G, Sun SX, Wirtz D, Lutkenhaus J. MinC spatially controls bacterial cytokinesis by antagonizing the scaffolding function of FtsZ. *Curr. Biol.* 18, 235–244 (2008).
53. Bernhardt TG, De Boer PA. SlmA, a nucleoid-associated, FtsZ binding protein required for blocking septal ring assembly over chromosomes in *E. coli*. *Mol. Cell* 18, 555–564 (2005).
54. Du S, Lutkenhaus J. SlmA antagonism of FtsZ assembly employs a two-pronged mechanism like MinCD. *PLoS Genet.* 10, e1004460 (2014).
55. Schumacher MA, Zeng W. Structures of the nucleoid occlusion protein SlmA bound to DNA and the C-terminal domain of the cytoskeletal protein FtsZ. *Proc. Natl Acad. Sci. USA* 113, 4988–4993 (2016).
56. Ma X, Margolin W. Genetic and functional analyses of the conserved C-terminal core domain of *Escherichia coli* FtsZ. *J. Bacteriol.* 181, 7531–7544 (1999).
57. Wang XD, Huang JA, Mukherjee A, Cao C, Lutkenhaus J. Analysis of the interaction of FtsZ with itself, GTP, and FtsA. *J. Bacteriol.* 179(17), 5551–5559 (1997).
58. Yan K, Pearce KH, Payne DJ. A conserved residue at the extreme C-terminus of FtsZ is critical for the FtsA-FtsZ interaction in *Staphylococcus aureus*. *Biochem. Biophys. Res. Commun.* 270(2), 387–392 (2000).
59. Pazos M, Natale P, Vicente M. A specific role for the ZipA protein in cell division: stabilization of the FtsZ protein. *J. Biol. Chem.* 288, 3219–3226 (2013).
60. Hale CA, De Boer PA. Direct binding of FtsZ to ZipA, an essential component of the septal ring structure that mediates cell division in *E. coli*. *Cell* 88, 175–185 (1997).
61. Hale CA, Rhee ZC, De Boer PA. ZipA-induced bundling of FtsZ polymers mediated by an interaction between C-terminal domains. *J. Bacteriol.* 182(18), 5153–5166 (2000).
62. Mosyak L, Zhang Y, Glasfeld E *et al.* The bacterial cell-division protein ZipA and its interaction with an FtsZ fragment revealed by X-ray crystallography. *EMBO J.* 19(13), 3179–3191 (2000).
63. Król E, Van Kessel SP, Van Bezouwen LS, Kumar N, Boekema EJ, Scheffers DJ. *Bacillus subtilis* SepF binds to the C-terminus of FtsZ. *PLoS ONE* 7, e43293 (2012).
64. Durand-Heredia J, Rivkin E, Fan G, Morales J, Janakiraman A. Identification of ZapD as a cell division factor that promotes the assembly of FtsZ in *Escherichia coli*. *J. Bacteriol.* 194, 3189–3198 (2012).
65. Durand-Heredia JM, Yu HH, De Carlo S, Lesser CF, Janakiraman A. Identification and characterization of ZapC, a stabilizer of the FtsZ ring in *Escherichia coli*. *J. Bacteriol.* 193, 1405–1413 (2011).
66. Addinall SG, Bi E, Lutkenhaus J. FtsZ ring formation in *fts* mutants. *J. Bacteriol.* 178(13), 3877–3884 (1996).
67. Monahan LG, Robinson A, Harry EJ. Lateral FtsZ association and the assembly of the cytokinetic Z ring in bacteria. *Mol. Microbiol.* 74, 1004–1017 (2009).
68. Huecas S, Llorca O, Boskovic J, Martin-Benito J, Valpuesta JM, Andreu JM. Energetics and geometry of FtsZ polymers: nucleated self-assembly of single protofilaments. *Biophys. J.* 94, 1796–1806 (2008).
69. Mukherjee A, Lutkenhaus J. Dynamic assembly of FtsZ regulated by GTP hydrolysis. *EMBO J.* 17(2), 462–469 (1998).
70. Lu CL, Reedy M, Erickson HP. Straight and curved conformations of FtsZ are regulated by GTP hydrolysis. *J. Bacteriol.* 182, 164–170 (2000).
71. Ward JEJ, Lutkenhaus J. Overproduction of FtsZ induces minicell formation in *E. coli*. *Cell* 42, 941–949 (1985).
72. Anderson DE, Gueiros-Filho FJ, Erickson HP. Assembly dynamics of FtsZ rings in *Bacillus subtilis* and *Escherichia coli* and effects of FtsZ-regulating proteins. *J. Bacteriol.* 186, 5775–5781 (2004).
73. Bisson-Filho AW, Hsu Y-P, Squyres GR *et al.* Treadmilling by FtsZ filaments drives peptidoglycan synthesis and bacterial cell division. *Science* 355, 739–743 (2017).

•• **Reports on the mechanisms that trigger divisome constriction and septal peptidoglycan synthesis during cell division in *Bacillus subtilis*.**

74. Stricker J, Maddox P, Salmon ED, Erickson HP. Rapid assembly dynamics of the *Escherichia coli* FtsZ-ring demonstrated by fluorescence recovery after photobleaching. *Proc. Natl Acad. Sci. USA* 99, 3171–3175 (2002).
75. Yang X, Lyu Z, Miguel A, Mcquillen R, Huang KC, Xiao J. GTPase activity-coupled treadmilling of the bacterial tubulin FtsZ organizes septal cell wall synthesis. *Science* 355, 744–747 (2017).
76. Loose M, Mitchison TJ. The bacterial cell division proteins FtsA and FtsZ self-organize into dynamic cytoskeletal patterns. *Nat. Cell Biol.* 16, 38–46 (2014).

77. Du S, Pichoff S, Kruse K, Lutkenhaus J. FtsZ filaments have the opposite kinetic polarity of microtubules. *Proc. Natl Acad. Sci. USA* 115, 10768–10773 (2018).

78. Monteiro JM, Pereira AR, Reichmann NT *et al.* Peptidoglycan synthesis drives an FtsZ-treadmilling-independent step of cytokinesis. *Nature* 554, 528–532 (2018).

•• **Reports on the mechanisms that trigger divisome constriction and septal peptidoglycan synthesis during cell division in *Staphylococcus aureus*.**

79. Perez AJ, Cesbron Y, Shaw SL *et al.* Movement dynamics of divisome proteins and PBP2x: FtsW in cells of *Streptococcus pneumoniae*. *Proc. Natl Acad. Sci. USA* 116, 3211–3220 (2019).

80. Lan G, Wolgemuth CW, Sun SX. Z-ring force and cell shape during division in rod-like bacteria. *Proc. Natl Acad. Sci. USA* 104, 16110–16115 (2007).

81. Osawa M, Anderson DE, Erickson HP. Reconstitution of contractile FtsZ rings in liposomes. *Science* 320, 792–794 (2008).

82. Coltharp C, Buss J, Plumer TM, Xiao J. Defining the rate-limiting processes of bacterial cytokinesis. *Proc. Natl Acad. Sci. USA* 113(8), E1044–1053 (2016).

83. Nguyen LT, Oikonomou CM, Ding HJ *et al.* Simulations suggest a constrictive force is required for Gram-negative bacterial cell division. *Nat. Commun.* 10(1), 1259 (2019).

84. Osawa M, Erickson HP. Turgor pressure and possible constriction mechanisms in bacterial division. *Front. Microbiol.* 9, 111 (2018).

85. Migocki MD, Freeman MK, Wake RG, Harry EJ. The Min system is not required for precise placement of the midcell Z ring in *Bacillus subtilis*. *EMBO Rep.* 3, 1163–1167 (2002).

86. Yu XC, Margolin W. FtsZ ring clusters in *min* and partition mutants: role of both the Min system and the nucleoid in regulating FtsZ ring localization. *Mol. Microbiol.* 32, 315–326 (1999).

87. Mulder E, Woldringh CL. Actively replicating nucleoids influence positioning of division sites in *Escherichia coli* filaments forming cells lacking DNA. *J. Bacteriol.* 171, 4303–4314 (1989).

88. Woldringh CL, Mulder E, Valkenburg JaC, Wientjes FB, Zaritsky A, Nanninga N. Role of the nucleoid in the toporegulation of division. *Res. Microbiol.* 141, 39–49 (1990).

89. Wu LJ, Errington J. Coordination of cell division and chromosome segregation by a nucleoid occlusion protein in *Bacillus subtilis*. *Cell* 117, 915–925 (2004).

90. Adams DW, Wu LJ, Errington J. Nucleoid occlusion protein Noc recruits DNA to the bacterial cell membrane. *EMBO J.* 34(4), 491–501 (2015).

91. Wu LJ, Ishikawa S, Kawai Y, Oshima T, Ogasawara N, Errington J. Noc protein binds to specific DNA sequences to coordinate cell division with chromosome segregation. *EMBO J.* 28(13), 1940–1952 (2009).

92. Cho H, Mcmanus HR, Dove SL, Bernhardt TG. Nucleoid occlusion factor SlmA is a DNA-activated FtsZ polymerization antagonist. *Proc. Natl Acad. Sci. USA* 108(9), 3773–3778 (2011).

93. Cho H, Bernhardt TG. Identification of the SlmA active site responsible for blocking bacterial cytokinetic ring assembly over the chromosome. *PLoS Genet.* 9, e1003304 (2013).

94. Du S, Park KT, Lutkenhaus J. Oligomerization of FtsZ converts the FtsZ tail motif (conserved carboxy-terminal peptide) into a multivalent ligand with high avidity for partners ZipA and SlmA. *Mol. Microbiol.* 95(2), 173–188 (2015).

95. Tonthat NK, Milam SL, Chinnam N, Whitfill T, Margolin W, Schumacher MA. SlmA forms a higher-order structure on DNA that inhibits cytokinetic Z-ring formation over the nucleoid. *Proc. Natl Acad. Sci. USA* 110(26), 10586–10591 (2013).

96. Lenarcic R, Halbedel S, Shaw M *et al.* Localisation of DivIVA by targeting to negatively curved membranes. *EMBO J.* 28(15), 2272–2282 (2009).

97. Bramkamp M, Emmins R, Weston L, Donovan C, Daniel RA, Errington J. A novel component of the division-site selection system of *Bacillus subtilis* and a new mode of action for the division inhibitor MinCD. *Mol. Microbiol.* 70(6), 1556–1569 (2008).

98. Patrick JE, Kearns DB. MinJ (YvjD) is a topological determinant of cell division in *Bacillus subtilis*. *Mol. Microbiol.* 70, 1166–1179 (2008).

99. De Boer PA, Crossley RE, Rothfield LI. A division inhibitor and a topological specificity factor coded for by the minicell locus determine proper placement of the division septum in *E. coli*. *Cell* 56(4), 641–649 (1989).

100. Fu X, Shih Y-L, Zhang Y, Rothfield LI. The MinE ring required for proper placement of the division site is a mobile structure that changes its cellular location during the *Escherichia coli* division cycle. *Proc. Natl Acad. Sci. USA* 98(3), 980–985 (2001).

101. Hu Z, Saez C, Lutkenhaus J. Recruitment of MinC, an inhibitor of Z-Ring formation, to the membrane in *Escherichia coli*: role of MinD and MinE. *J. Bacteriol.* 185(1), 196–203 (2003).

102. Hu Z, Lutkenhaus J. Topological regulation of cell division in *Escherichia coli* involves rapid pole to pole oscillation of the division inhibitor MinC under the control of MinD and MinE. *Mol. Microbiol.* 34(1), 82–90 (1999).

103. Raskin DM, De Boer PA. MinDE-dependent pole-to-pole oscillation of division inhibitor MinC in *Escherichia coli*. *J. Bacteriol.* 181(20), 6419–6424 (1999).

104. Raskin DM, De Boer PA. Rapid pole-to-pole oscillation of a protein required for directing division to the middle of *Escherichia coli*. *Proc. Natl Acad. Sci. USA* 96(9), 4971–4976 (1999).

105. Hale CA, Meinhardt H, De Boer PA. Dynamic localization cycle of the cell division regulator MinE in *Escherichia coli*. *EMBO J.* 20(7), 1563–1572 (2001).

106. Bailey MW, Bisicchia P, Warren BT, Sherratt DJ, Männik J. Evidence for divisome localization mechanisms independent of the Min system and SlmA in *Escherichia coli*. *PLoS Genet.* 10(8), e1004504 (2014).

107. Rodrigues CDA, Harry EJ. The Min system and nucleoid occlusion are not required for identifying the division site in *Bacillus subtilis* but ensure its efficient utilization. *PLoS Genet.* 8, e1002561 (2012).

108. Kiekebusch D, Michie KA, Essen LO, Löwe J, Thanbichler M. Localized dimerization and nucleoid binding drive gradient formation by the bacterial cell division inhibitor MipZ. *Mol. Cell.* 46(3), 245–259 (2012).

109. Thanbichler M, Shapiro L. MipZ, a spatial regulator coordinating chromosome segregation with cell division in *Caulobacter*. *Cell* 126(1), 147–162 (2006).

110. Treuner-Lange A, Aguiluz K, Van Der Does C *et al.* PomZ, a ParA-like protein, regulates Z-ring formation and cell division in *Myxococcus xanthus*. *Mol. Microbiol.* 87(2), 235–253 (2013).

111. Van Raaphorst R, Kjos M, Veening JW. Chromosome segregation drives division site selection in *Streptococcus pneumoniae*. *Proc. Natl Acad. Sci. USA* 114, E5959–E5968 (2017).

112. Fleurie A, Lesterlin C, Manuse S *et al.* MapZ marks the division sites and positions FtsZ rings in *Streptococcus pneumoniae*. *Nature* 516(7530), 259 (2014).

113. Holečková N, Doubravová L, Massidda O *et al.* LocZ is a new cell division protein involved in proper septum placement in *Streptococcus pneumoniae*. *mBio* 6, e01700–01714 (2014).

114. Willemse J, Borst JW, De Waal E, Bisseling T, Van Wezel GP. Positive control of cell division: FtsZ is recruited by SsgB during sporulation of *Streptomyces*. *Genes Dev.* 25(1), 89–99 (2011).

115. Pinho MG, Errington J. A *divIVA* null mutant of *Staphylococcus aureus* undergoes normal cell division. *FEMS Microbiol. Lett.* 240(2), 145–149 (2004).

116. Veiga H, Jorge AM, Pinho MG. Absence of nucleoid occlusion effector Noc impairs formation of orthogonal FtsZ rings during *Staphylococcus aureus* cell division. *Mol. Microbiol.* 80(5), 1366–1380 (2011).

117. Pang T, Wang X, Lim HC, Bernhardt TG, Rudner DZ. The nucleoid occlusion factor Noc controls DNA replication initiation in *Staphylococcus aureus*. *PLoS Genet.* 13, e1006908 (2017).

118. Hajduk IV, Rodrigues CDA, Harry EJ. Connecting the dots of the bacterial cell cycle: coordinating chromosome replication and segregation with cell division. *Semin. Cell Dev. Biol.* 53, 2–9 (2016).

119. Harry EJ, Rodwell J, Wake RG. Co-ordinating DNA replication with cell division in bacteria: a link between the early stages of a round of replication and mid-cell Z ring assembly. *Mol. Microbiol.* 33(1), 33–40 (1999).

120. Moriya S, Rashid RA, Rodrigues CDA, Harry EJ. Influence of the nucleoid and the early stages of DNA replication on positioning the division site in *Bacillus subtilis*. *Mol. Microbiol.* 76(3), 634–647 (2010).

121. Cambridge J, Blinkova A, Magnan D, Bates D, Walker JR. A replication-inhibited unsegregated nucleoid at mid-cell blocks Z-ring formation and cell division independently of SOS and the SlmA nucleoid occlusion protein in *Escherichia coli*. *J. Bacteriol.* 196(1), 36–49 (2014).

122. Männik J, Bailey MW. Spatial coordination between chromosomes and cell division proteins in *Escherichia coli*. *Front. Microbiol.* 6, 306 (2015).

123. Monterroso B, Zorrilla S, Sobrinos-Sanguino M *et al.* The bacterial DNA binding protein MatP involved in linking the nucleoid terminal domain to the divisome at midcell interacts with lipid membranes. *mBio* 10(3), e00376–00319 (2019).

124. Du S, Lutkenhaus J. Assembly and activation of the *Escherichia coli* divisome. *Mol. Microbiol.* 105(2), 177–187 (2017).

125. Aarsman MEG, Piette A, Fraipont C, Vinkenvleugel TMF, Nguyen-Distèche M, Den Blaauwen T. Maturation of the *Escherichia coli* divisome occurs in two steps. *Mol. Microbiol.* 55(6), 1631–1645 (2005).

126. Gamba P, Veening JW, Saunders NJ, Hamoen LW, Daniel RA. Two-step assembly dynamics of the *Bacillus subtilis* divisome. *J. Bacteriol.* 191(13), 4186–4194 (2009).

127. Goley ED, Yeh YC, Hong SH *et al.* Assembly of the *Caulobacter* cell division machine. *Mol. Microbiol.* 80(6), 1680–1698 (2011).

128. Goley ED, Dye NA, Werner JN, Gitai Z, Shapiro L. Imaging-based identification of a critical regulator of FtsZ protofilament curvature in *Caulobacter*. *Mol. Cell.* 39(6), 975–987 (2010).

129. Osorio A, Camarena L, Cevallos MA, Poggio S. A new essential cell division protein in *Caulobacter crescentus*. *J. Bacteriol.* 199(8), e00811–00816 (2017).

130. Busiek KK, Margolin W. Bacterial actin and tubulin homologs in cell growth and division. *Curr. Biol.* 25(6), R243–R254 (2015).

131. Van Den Ent F, Löwe J. Crystal structure of the cell division protein FtsA from *Thermotoga maritima*. *EMBO J.* 19(20), 5300–5307 (2000).

132. Bork P, Sander C, Valencia A. An ATPase domain common to prokaryotic cell cycle proteins, sugar kinases, actin, and hsp70 heat shock proteins. *Proc. Natl Acad. Sci. USA* 89(16), 7290–7294 (1992).

133. Pichoff S, Lutkenhaus J. Tethering the Z ring to the membrane through a conserved membrane targeting sequence in FtsA. *Mol. Microbiol.* 55(6), 1722–1734 (2005).

134. Haney SA, Glasfeld E, Hale C, Keeney D, He Z, De Boer P. Genetic analysis of the *Escherichia coli* FtsZ-ZipA interaction in the yeast two-hybrid system. Characterization of FtsZ residues essential for the interactions with ZipA and with FtsA. *J. Biol. Chem.* 276(15), 11980–11987 (2001).

135. Pichoff S, Lutkenhaus J. Identification of a region of FtsA required for interaction with FtsZ. *Mol. Microbiol.* 64(4), 1129–1138 (2007).

136. Szwedziak P, Wang Q, Freund SMV, Löwe J. FtsA forms actin-like protofilaments. *EMBO J.* 31(10), 2249–2260 (2012).

137. Lara B, Rico AI, Petruzzelli S *et al.* Cell division in cocci: localization and properties of the *Streptococcus pneumoniae* FtsA protein. *Mol. Microbiol.* 55(3), 699–711 (2005).

138. Krupka M, Cabre EJ, Jimenez M, Rivas G, Rico AI, Vicente M. Role of the FtsA C terminus as a switch for polymerization and membrane association. *mBio.* 5(6), e02221 (2014).

139. Krupka M, Rowlett VW, Morado D *et al. Escherichia coli* FtsA forms lipid-bound minirings that antagonize lateral interactions between FtsZ protofilaments. *Nat. Commun.* 8, 15957 (2017).

140. Krupka M, Margolin W. Unite to divide: oligomerization of tubulin and actin homologs regulates initiation of bacterial cell division. *F1000Res.* 7, 235 (2018).

141. Schoenemann KM, Krupka M, Rowlett VW, Distelhorst SL, Hu B, Margolin W. Gain-of-function variants of FtsA form diverse oligomeric structures on lipids and enhance FtsZ protofilament bundling. *Mol. Microbiol.* 109(5), 676–693 (2018).

142. Conti J, Viola MG, Camberg JL. FtsA reshapes membrane architecture and remodels the Z-ring in *Escherichia coli*. *Mol. Microbiol.* 107(4), 558–576 (2018).

143. Addinall SG, Lutkenhaus J. FtsA is localized to the septum in an FtsZ-dependent manner. *J. Bacteriol.* 178, 7167–7172 (1996).

144. Beall B, Lutkenhaus J. Impaired cell division and sporulation of a *Bacillus subtilis* strain with the *ftsA* gene deleted. *J. Bacteriol.* 174(7), 2398–2403 (1992).

145. Jensen SO, Thompson LS, Harry EJ. Cell division in *Bacillus subtilis*: FtsZ and FtsA association is Z-ring independent, and FtsA is required for efficient midcell Z-ring assembly. *J. Bacteriol.* 187(18), 6536–6544 (2005).

146. Mura A, Fadda D, Perez AJ *et al.* Roles of the essential protein FtsA in cell growth and division in *Streptococcus pneumoniae*. *J. Bacteriol.* 199, e00608–00616 (2017).

147. Haeusser DP, Rowlett VW, Margolin W. A mutation in *Escherichia coli* ftsZ bypasses the requirement for the essential division gene *zipA* and confers resistance to FtsZ assembly inhibitors by stabilizing protofilament bundling. *Mol. Microbiol.* 97, 988–1005 (2015).

148. Krupka M, Sobrinos-Sanguino M, Jiménez M, Rivas G, Margolin W. *Escherichia coli* ZipA organizes FtsZ polymers into dynamic ring-like protofilament structures. *mBio* 9, e01008–01018 (2018).

149. Geissler B, Elraheb D, Margolin W. A gain-of-function mutation in *ftsA* bypasses the requirement for the essential cell division gene *zipA* in *Escherichia coli*. *Proc. Natl Acad. Sci. USA* 100, 4197–4202 (2003).

150. Pichoff S, Shen B, Sullivan B, Lutkenhaus J. FtsA mutants impaired for self-interaction bypass ZipA suggesting a model in which FtsA's self-interaction competes with its ability to recruit downstream division proteins. *Mol. Microbiol.* 83, 151–167 (2012).

151. Vega DE, Margolin W. Direct interaction between the two Z ring membrane anchors FtsA and ZipA. *J. Bacteriol.* 5452, JB.00579-00518 (2018) (Epub ahead of print).

152. Camberg JL, Hoskins JR, Wickner S. ClpXP protease degrades the cytoskeletal protein, FtsZ, and modulates FtsZ polymer dynamics. *Proc. Natl Acad. Sci. USA* 106, 10614–10619 (2009).

153. Hamoen LW, Meile JC, De Jong W, Noirot P, Errington J. SepF, a novel FtsZ-interacting protein required for a late step in cell division. *Mol. Microbiol.* 59, 989–999 (2006).

154. Ishikawa S, Kawai Y, Hiramatsu K, Kuwano M, Ogasawara N. A new FtsZ-interacting protein, YlmF, complements the activity of FtsA during progression of cell division in *Bacillus subtilis*. *Mol. Microbiol.* 60, 1364–1380 (2006).

155. Gündoğdu ME, Kawai Y, Pavlendova N *et al.* Large ring polymers align FtsZ polymers for normal septum formation. *EMBO J.* 30, 617–626 (2011).

156. Duman R, Ishikawa S, Celik I *et al.* Structural and genetic analyses reveal the protein SepF as a new membrane anchor for the Z ring. *Proc. Natl Acad. Sci. USA* 110, E4601–4610 (2013).

157. Meier EL, Razavi S, Inoue T, Goley ED. A novel membrane anchor for FtsZ is linked to cell wall hydrolysis in *Caulobacter crescentus*. *Mol. Microbiol.* 101, 265–280 (2016).

158. Gueiros-Filho FJ, Losick R. A widely conserved bacterial cell division protein that promotes assembly of the tubulin-like protein FtsZ. *Genes Dev.* 16(19), 2544–2556 (2002).

159. Pacheco-Gómez R, Cheng X, Hicks MR *et al.* Tetramerization of ZapA is required for FtsZ bundling. *Biochem. J.* 449, 795–802 (2013).

160. Small E, Marrington R, Rodger A *et al.* FtsZ polymer-bundling by the *Escherichia coli* ZapA orthologue, YgfE, involves a conformational change in bound GTP. *J. Mol. Biol.* 369(1), 210–221 (2007).

161. Dajkovic A, Pichoff S, Lutkenhaus J, Wirtz D. Cross-linking FtsZ polymers into coherent Z rings. *Mol. Microbiol.* 78, 651–668 (2010).

162. Mohammadi T, Ploeger GE, Verheul J *et al.* The GTPase activity of *Escherichia coli* FtsZ determines the magnitude of the FtsZ polymer bundling by ZapA *in vitro*. *Biochemistry* 48(46), 11056–11066 (2009).

163. Galli E, Gerdes K. FtsZ-ZapA-ZapB interactome of *Escherichia coli*. *J. Bacteriol.* 194(2), 292–302 (2012).

164. Buss JA, Peters NT, Xiao J, Bernhardt TG. ZapA and ZapB form an FtsZ-independent structure at midcell. *Mol. Microbiol.* 104, 652–663 (2017).

165. Schumacher M, Huang K-H, Zeng W, Janakiraman A. Structure of the Z ring associated protein, ZapD, bound to the C-terminal domain of the tubulin-like protein, FtsZ, suggests mechanism of Z ring stabilization through FtsZ crosslinking. *J. Biol. Chem.* 292(9), 3740–3750 (2017).

166. Woldemeskel SA, Mcquillen R, Hessel AM, Xiao J, Goley ED. A conserved coiled-coil protein pair focuses the cytokinetic Z-ring in *Caulobacter crescentus*. *Mol. Microbiol.* 105, 721–740 (2017).

167. Buss J, Coltharp C, Huang T *et al. In vivo* organization of the FtsZ-ring by ZapA and ZapB revealed by quantitative super-resolution microscopy. *Mol. Microbiol.* 89, 1099–1120 (2013).

168. Hale CA, Shiomi D, Liu B *et al.* Identification of *Escherichia coli* ZapC (YcbW) as a component of the division apparatus that binds and bundles FtsZ polymers. *J. Bacteriol.* 193, 1393–1404 (2011).

169. Du S, Pichoff S, Lutkenhaus J. FtsEX acts on FtsA to regulate divisome assembly and activity. *Proc. Natl Acad. Sci. USA* 113, E5052–E5061 (2016).

170. Meier EL, Daitch AK, Qing Y, Bhargava A, Jensen GJ, Goley ED. FtsEX-mediated regulation of inner membrane fusion and cell separation reveals 2 morphogenetic plasticity in *Caulobacter crescentus*. *PLoS Genet.* 13, e1006999 (2017).

171. Pichoff S, Du S, Lutkenhaus J. Roles of FtsEX in cell division. *Res. Microbiol.* 170(8), 374–380 (2019).

172. Domínguez-Cuevas P, Porcelli I, Daniel RA, Errington J. Differentiated roles for MreB-actin isologues and autolytic enzymes in *Bacillus subtilis* morphogenesis. *Mol. Microbiol.* 89, 1084–1098 (2013).

173. Meisner J, Llopis PM, Sham L-T, Garner EC, Bernhardt TG, Rudner DZ. FtsEX is required for CwlO peptidoglycan hydrolase activity during cell wall elongation in *Bacillus subtilis*. *Mol. Microbiol.* 89, 1069–1083 (2014).

174. Cleverley RM, Barrett JR, Baslé A *et al.* Structure and function of a spectrin-like regulator of bacterial cytokinesis. *Nat. Commun.* 5, 5421 (2014).

175. Claessen D, Emmins R, Hamoen LW, Daniel RA, Errington J, Edwards DH. Control of the cell elongation-division cycle by shuttling of PBP1 protein in *Bacillus subtilis*. *Mol. Microbiol.* 68, 1029–1046 (2008).

176. Land AD, Luo Q, Levin PA. Functional domain analysis of the cell division inhibitor EzrA. *PLoS ONE* 9, e102616 (2014).

177. Haeusser DP, Schwartz RL, Smith AM, Oates ME, Levin PA. EzrA prevents aberrant cell division by modulating assembly of the cytoskeletal protein FtsZ. *Mol. Microbiol.* 52, 801–814 (2004).

178. Steele VR, Bottomley AL, Garcia-Lara J, Kasturiarachchi J, Foster SJ. Multiple essential roles for EzrA in cell division of *Staphylococcus aureus*. *Mol. Microbiol.* 80, 542–555 (2011).

179. Gamba P, Rietkötter E, Daniel RA, Hamoen LW. Tetracycline hypersensitivity of an *ezrA* mutant links GalE and TseB (YpmB) to cell division. *Front. Microbiol.* 6, 1–15 (2015).

180. Condon SGF, Mahbuba DA, Armstrong CR *et al.* The FtsLB subcomplex of the bacterial divisome is a tetramer with an uninterrupted FtsL helix linking the transmembrane and periplasmic regions. *J. Biol. Chem.* 293, 1623–1641 (2018).

181. Bisicchia P, Steel B, Debela MHM, Löwe J, Sherratt DJ. The N-terminal membrane-spanning domain of the *Escherichia coli* DNA translocase FtsK hexamerizes at midcell. *mBio* 4, 1–6 (2013).

182. Chen JC, Beckwith J. FtsQ, FtsL and Ftsl require FtsK, but not FtsN, for co-localization with FtsZ during *Escherichia coli* cell division. *Mol. Microbiol.* 42, 395–413 (2001).

183. Bottomley AL, Liew ATF, Kusuma KD *et al.* Coordination of chromosome segregation and cell division in *Staphylococcus aureus*. *Front. Microbiol.* 8, 1–13 (2017).

184. Daniel RA, Harry EJ, Errington J. Role of penicillin-binding protein PBP2B in assembly and functioning of the division machinery of *Bacillus subtilis*. *Mol. Microbiol.* 35, 299–311 (2000).

185. Liu B, Persons L, Lee L, De Boer PA. Roles for both FtsA and the FtsBLQ subcomplex in FtsN-stimulated cell constriction in *Escherichia coli*. *Mol. Microbiol.* 95, 945–970 (2015).

186. Rowland SL, Wadsworth KD, Robson SA, Robichon C, Beckwith J, King GF. Evidence from artificial septal targeting and site-directed mutagenesis that residues in the extracytoplasmic β domain of DivIB mediate its interaction with the divisomal transpeptidase PBP2B. *J. Bacteriol.* 192, 6116–6125 (2010).

187. Mohammadi T, Sijbrandi R, Lutters M *et al.* Specificity of the transport of lipid II by FtsW in *Escherichia coli*. *J. Biol. Chem.* 289, 14707–14718 (2014).

188. Meeske AJ, Eammon P, William P *et al.* SEDS proteins are a widespread family of bacterial cell wall polymerases. *Nature* 537, 634–638 (2016).

189. Taguchi A, Welsh MA, Marmont LS *et al.* FtsW is a peptidoglycan polymerase that is functional only in complex with its cognate penicillin-binding protein. *Nat. Microbiol.* 4, 587–594 (2019).

190. Mercer KLN, Weiss DS. The *Escherichia coli* cell division protein FtsW is required to recruit its cognate transpeptidase, FtsI (PBP3), to the division site. *J. Bacteriol.* 184, 904–912 (2002).

191. Fraipont C, Alexeeva S, Wolf B *et al.* The integral membrane FtsW protein and peptidoglycan synthase PBP3 form a subcomplex in *Escherichia coli*. *Microbiology* 157, 251–259 (2011).

192. Piette A, Fraipont C, Den Blaauwen T, Aarsman MEG, Pastoret S, Nguyen-Distèche M. Structural determinants required to target penicillin-binding protein 3 to the septum of *Escherichia coli*. *J. Bacteriol.* 186, 6110–6117 (2004).

193. Cleverley RM, Rutter ZJ, Rismondo J *et al.* The cell cylce regulator GpsB functions as cytosolic adaptor for multiple cell wall enzymes. *Nat. Commun.* 10, 1–17 (2019).

194. Tavares JR, De Souza RF, Meira GLS, Gueiros-Filho FJ. Cytological characterization of YpsB, a novel component of the *Bacillus subtilis* divisome. *J. Bacteriol.* 190, 7096–7107 (2008).

195. Pichoff S, Du S, Lutkenhaus J. Disruption of divisome assembly rescued by FtsN-FtsA interaction in *Escherichia coli*. *Proc. Natl Acad. Sci. USA* 115(29), E6855–e6862 (2018).

196. Gerding MA, Liu B, Bendezu FO, Hale CA, Bernhardt TG, De Boer PA. Self-enhanced accumulation of FtsN at division sites and roles for other proteins with a SPOR domain (DamX, DedD, and RlpA) in *Escherichia coli* cell constriction. *J. Bacteriol.* 191(24), 7383–7401 (2009).

197. Söderström B, Chan H, Shilling PJ, Skoglund U, Daley DO. Spatial separation of FtsZ and FtsN during cell division. *Mol. Microbiol.* 107, 387–401 (2018).

198. Artola M, Ruiz-Avila LB, Vergoñós A *et al.* Effective GTP-replacing FtsZ inhibitors and antibacterial mechanism of action. *ACS Chem. Biol.* 10, 834–843 (2015).

199. Król E, De Sousa Borges A, Da Silva I *et al.* Antibacterial activity of alkyl gallates is a combination of direct targeting of FtsZ and permeabilization of bacterial membranes. *Front. Microbiol.* 6, 390 (2015).

200. Rai D, Singh JK, Roy N, Panda D. Curcumin inhibits FtsZ assembly: an attractive mechanism for its antibacterial activity. *Biochem. J.* 410, 147–155 (2008).

201. Mishra S, Narain U, Mishra R, Misra K. Design, development and synthesis of mixed bioconjugates of piperic acid–glycine, curcumin–glycine/alanine and curcumin–glycine–piperic acid and their antibacterial and antifungal properties. *Bioorg. Med. Chem.* 13(5), 1477–1486 (2005).

202. Kaur S, Modi NH, Panda D, Roy N. Probing the binding site of curcumin in *Escherichia coli* and *Bacillus subtilis* FtsZ – A structural insight to unveil antibacterial activity of curcumin. *Eur. J. Med. Chem.* 45(9), 4209–4214 (2010).

203. Morão LG, Polaquini CR, Kopacz M *et al.* A simplified curcumin targets the membrane of *Bacillus subtilis*. *Microbiologyopen* e683, 8(4), 1–12 (2019).

204. Cheng AL, Hsu CH, Lin JK *et al.* Phase I clinical trial of curcumin, a chemopreventive agent, in patients with high-risk or pre-malignant lesions. *Anticancer Res.* 21, 2895–2900 (2001).

205. Anand P, Kunnumakkara AB, Newman RA, Aggarwal BB. Bioavailability of curcumin: problems and promises. *Mol. Pharm.* 4, 807–818 (2007).

206. Jackson SJT, Murphy LL, Venema RC, Singletary KW, Young AJ. Curcumin binds tubulin, induces mitotic catastrophe, and impedes normal endothelial cell proliferation. *Food Chem. Toxicol.* 60, 431–438 (2013).

207. Plaza A, Keffer JL, Bifulco G, Lloyd JR, Bewley CA. Chrysophaentins A−H, antibacterial bisdiarylbutene macrocycles that inhibit the bacterial cell division protein FtsZ. *J. Am. Chem. Soc.* 132, 9069–9077 (2010).

208. Keffer JL, Huecas S, Hammill JT, Wipf P, Andreu JM, Bewley CA. Chrysophaentins are competitive inhibitors of FtsZ and inhibit Z-ring formation in live bacteria. *Bioorg. Med. Chem.* 21(18), 5673–5678 (2013).

209. Cerrutti P, Alzamora SM, Vidales SL. Vanillin as an antimicrobial for producing shelf-stable strawberry puree. *J. Food Sci.* 62, 608–610 (2006).

210. Sun J, Li M-H, Wang X-Y *et al.* Vanillin derivatives as the selective small molecule inhibitors of FtsZ. *Med. Chem. Res.* 23, 2985–2994 (2014).

211. Possoz C, Newmark J, Sorto N, Sherratt DJ, Tolmasky ME. Sublethal concentrations of the aminoglycoside amikacin interfere with cell division without affecting chromosome dynamics. *Antimicrob. Agents Chemother.* 51, 252–256 (2007).

212. Schaffner-Barbero C, Martín-Fontecha M, Chacón P, Andreu JM. Targeting the assembly of bacterial cell division protein FtsZ with small molecules. *ACS Chem. Biol.* 7, 269–277 (2012).

213. Margalit DN, Romberg L, Mets RB *et al.* Targeting cell division: small-molecule inhibitors of FtsZ GTPase perturb cytokinetic ring assembly and induce bacterial lethality. *Proc. Natl Acad. Sci. USA* 101, 11821–11826 (2004).

214. Huang Q, Kirikae F, Kirikae T *et al.* Targeting FtsZ for antituberculosis drug discovery: noncytotoxic taxanes as novel antituberculosis agents. *J. Med. Chem.* 49, 463–466 (2006).

215. Singh D, Bhattacharya A, Rai A *et al.* SB-RA-2001 inhibits bacterial proliferation by targeting FtsZ assembly. *Biochemistry* 53, 2979–2992 (2014).

216. Grycová L, Dostál J, Marek R. Quaternary protoberberine alkaloids. *Phytochemistry* 68, 150–175 (2007).

217. Boberek JM, Stach J, Good L. Genetic evidence for inhibition of bacterial division protein FtsZ by berberine. *PLoS ONE* 5, e13745 (2010).

218. Domadia PN, Bhunia A, Sivaraman J, Swarup S, Dasgupta D. Berberine targets assembly of *Escherichia coli* cell division protein FtsZ. *Biochemistry* 47, 3225–3234 (2008).

219. Park H-C, Gedi V, Cho J-H *et al.* Characterization and *in vitro* inhibition studies of *Bacillus anthracis* FtsZ: a potential antibacterial target. *Appl. Biochem. Biotechnol.* 172, 3263–3270 (2014).

220. Sun N, Chan F-Y, Lu Y-J *et al.* Rational design of berberine-based FtsZ inhibitors with broad-spectrum antibacterial activity. *PLoS ONE* 9, e97514 (2014).

221. Parhi A, Lu S, Kelley C, Kaul M, Pilch DS, Lavoie EJ. Antibacterial activity of substituted dibenzo[a,g]quinolizin-7-ium derivatives. *Bioorg. Med. Chem. Lett.* 22, 6962–6966 (2012).

222. Wang J, Yang T, Chen H *et al.* The synthesis and antistaphylococcal activity of 9, 13-disubstituted berberine derivatives. *Eur. J. Med. Chem.* 127, 424–433 (2017).

223. Sun N, Du R-L, Zheng Y-Y *et al.* Antibacterial activity of N-methylbenzofuro[3,2-b]quinoline and N-methylbenzoindolo[3,2-b]-quinoline derivatives and study of their mode of action. *Eur. J. Med. Chem.* 135, 1–11 (2017).

224. Liu F, Venter H, Bi F *et al.* Synthesis and antibacterial activity of 5-methylphenanthridium derivatives as FtsZ inhibitors. *Bioorg. Med. Chem. Lett.* 27, 3399–3402 (2017).

225. Kelley C, Zhang Y, Parhi A, Kaul M, Pilch DS, Lavoie EJ. 3-phenyl substituted 6,7-dimethoxyisoquinoline derivatives as FtsZ-targeting antibacterial agents. *Bioorg. Med. Chem.* 20, 7012–7029 (2012).

226. Stermitz FR, Lorenz P, Tawara JN, Zenewicz LA, Lewis K. Synergy in a medicinal plant: antimicrobial action of berberine potentiated by 5-methoxyhydnocarpin, a multidrug pump inhibitor. *Proc. Natl Acad. Sci. USA* 97, 1433–1437 (2000).

227. Dziedzic A, Wojtyczka R, Kubina R. Inhibition of oral streptococci growth induced by the complementary action of berberine chloride and antibacterial compounds. *Molecules* 20, 13705–13724 (2015).

228. Zuo G-Y, Li Y, Han J, Wang G-C, Zhang Y-L, Bian Z-Q. Antibacterial and synergy of berberines with antibacterial agents against clinical multi-drug resistant isolates of methicillin-resistant *Staphylococcus aureus* (MRSA). *Molecules* 17, 10322–10330 (2012).

229. Li Z, Garner AL, Gloeckner C, Janda KD, Carlow CK. Targeting the *Wolbachia* cell division protein FtsZ as a new approach for antifilarial therapy. *PLoS Negl. Trop. Dis.* 5(11), e1411 (2011).

230. Acharya BR, Bhattacharya B, Chakrabarti G. The natural naphthoquinone plumbagin exhibits antiproliferative activity and disrupts the microtubule network through tubulin binding. *Biochemistry* 47, 7838–7845 (2008).

231. Aziz MH, Dreckschmidt NE, Verma AK. Plumbagin, a medicinal plant-derived naphthoquinone, is a novel inhibitor of the growth and invasion of hormone-refractory prostate cancer. *Cancer Res.* 68, 9024–9032 (2008).

232. Wang J, Galgoci A, Kodali S *et al.* Discovery of a small molecule that inhibits cell division by blocking FtsZ, a novel therapeutic target of antibiotics. *J. Biol. Chem.* 278, 44424–44428 (2003).

233. Noh TH, Sen L, Hong J, Lee J-H, Moon HR, Jung JH. Antibacterial activities of viriditoxin congeners and synthetic analogues against fish pathogens. *Bioorg. Med. Chem. Lett.* 27, 4970–4974 (2017).

234. Beuria TK, Santra MK, Panda D. Sanguinarine blocks cytokinesis in bacteria by inhibiting FtsZ assembly and bundling. *Biochemistry* 44, 16584–16593 (2005).

235. Croaker A, King GJ, Pyne JH, Anoopkumar-Dukie S, Simanek V, Liu L. Carcinogenic potential of sanguinarine, a phytochemical used in 'therapeutic' black salve and mouthwash. *Mutat. Res.* 774, 46–56 (2017).

236. Lopus M, Panda D. The benzophenanthridine alkaloid sanguinarine perturbs microtubule assembly dynamics through tubulin binding. *FEBS J.* 273, 2139–2150 (2006).

237. Panda P, Taviti AC, Satpati S, Kar MM, Dixit A, Beuria TK. Doxorubicin inhibits *E. coli* division by interacting at a novel site in FtsZ. *Biochem. J.* 471, 335–346 (2015).

238. Minotti G, Menna P, Salvatorelli E, Cairo G, Gianni L. Anthracyclines: molecular advances and pharmacologic developments in antitumor activity and cardiotoxicity. *Pharmacol. Rev.* 56, 185–229 (2004).

239. Singh P, Jindal B, Surolia A, Panda D. A rhodanine derivative CCR-11 inhibits bacterial proliferation by inhibiting the assembly and GTPase activity of FtsZ. *Biochemistry* 51, 5434–5442 (2012).

240. Kumar K, Awasthi D, Lee S-Y *et al.* Novel trisubstituted benzimidazoles, targeting Mtb FtsZ, as a new class of antitubercular agents. *J. Med. Chem.* 54, 374–381 (2011).

241. Awasthi D, Kumar K, Knudson SE, Slayden RA, Ojima I. SAR studies on trisubstituted benzimidazoles as inhibitors of Mtb FtsZ for the development of novel antitubercular agents. *J. Med. Chem.* 56, 9756–9770 (2013).

242. Knudson SE, Awasthi D, Kumar K *et al.* Cell division inhibitors with efficacy equivalent to isoniazid in the acute murine *Mycobacterium tuberculosis* infection model. *J. Antimicrob. Chemother.* 70, 3070–3073 (2015).

243. Knudson SE, Kumar K, Awasthi D, Ojima I, Slayden RA. *In vitro–in vivo* activity relationship of substituted benzimidazole cell division inhibitors with activity against *Mycobacterium tuberculosis*. *Tuberculosis* 94, 271–276 (2014).

244. Ray S, Jindal B, Kunal K, Surolia A, Panda D. BT-benzo-29 inhibits bacterial cell proliferation by perturbing FtsZ assembly. *FEBS J.* 282, 4015–4033 (2015).

245. Domadia P, Swarup S, Bhunia A, Sivaraman J, Dasgupta D. Inhibition of bacterial cell division protein FtsZ by cinnamaldehyde. *Biochem. Pharmacol.* 74, 831–840 (2007).

246. Li X, Sheng J, Huang G *et al.* Design, synthesis and antibacterial activity of cinnamaldehyde derivatives as inhibitors of the bacterial cell division protein FtsZ. *Eur. J. Med. Chem.* 97, 32–41 (2015).

247. Chiang C-C, Cheng M-J, Peng C-F, Huang H-Y, Chen I-S. A novel dimeric coumarin analog and antimycobacterial constituents from *Fatoua pilosa*. *Chem. Biodivers.* 7, 1728–1736 (2010).

248. Duggirala S, Nankar RP, Rajendran S, Doble M. Phytochemicals as inhibitors of bacterial cell division protein FtsZ: coumarins are promising candidates. *Appl. Biochem. Biotechnol.* 174, 283–296 (2014).

249. Hemaiswarya S, Soudaminikkutty R, Narasumani ML, Doble M. Phenylpropanoids inhibit protofilament formation of *Escherichia coli* cell division protein FtsZ. *J. Med. Microbiol.* 60, 1317–1325 (2011).

250. Ohashi Y, Chijiiwa Y, Suzuki K *et al.* The lethal effect of a benzamide derivative, 3-methoxybenzamide, can be suppressed by mutations within a cell division gene, *ftsZ*, in *Bacillus subtilis*. *J. Bacteriol.* 181, 1348–1351 (1999).

251. Czaplewski LG, Collins I, Boyd EA *et al.* Antibacterial alkoxybenzamide inhibitors of the essential bacterial cell division protein FtsZ. *Bioorg. Med. Chem. Lett.* 19, 524–527 (2009).

252. Haydon DJ, Stokes NR, Ure R *et al.* An inhibitor of FtsZ with potent and selective anti-staphylococcal activity. *Science* 321, 1673–1675 (2008).

•• **Reports on the FtsZ inhibitor PC190723, a promising anti-staphylococcal drug candidate that exerts potent antimicrobial activity in murine models of methicillin-resistant *Staphylococcus aureus* (MRSA) infections.**

253. Andreu JM, Schaffner-Barbero C, Huecas S *et al.* The antibacterial cell division inhibitor PC190723 is an FtsZ polymer-stabilizing agent that induces filament assembly and condensation. *J. Biol. Chem.* 285, 14239–14246 (2010).

254. Elsen NL, Lu J, Parthasarathy G *et al.* Mechanism of action of the cell-division inhibitor PC190723: modulation of FtsZ assembly cooperativity. *J. Am. Chem. Soc.* 134(30), 12342–12345 (2012).

255. Tan CM, Therien AG, Lu J *et al.* Restoring methicillin-resistant *Staphylococcus aureus* susceptibility to beta-lactam antibiotics. *Sci. Transl. Med.* 4(126), 126ra135 (2012).

•• **Here, the authors show that PC190723 re-sensitizes MRSA to β-lactam antibiotics, highlighting the potential of FtsZ inhibitors as combination partners for the treatment of staphylococcal infections.**

256. Adams DW, Wu LJ, Czaplewski LG, Errington J. Multiple effects of benzamide antibiotics on FtsZ function. *Mol. Microbiol.* 80(1), 68–84 (2011).

257. Artola M, Ruiz-Avila LB, Ramirez-Aportela E *et al.* The structural assembly switch of cell division protein FtsZ probed with fluorescent allosteric inhibitors. *Chem. Sci.* 8(2), 1525–1534 (2017).

258. Stokes NR, Baker N, Bennett JM *et al.* An improved small-molecule inhibitor of FtsZ with superior *in vitro* potency, drug-like properties, and *in vivo* efficacy. *Antimicrob. Agents Chemother.* 57, 317–325 (2013).

259. Kaul M, Mark L, Zhang Y, Parhi AK, Lavoie EJ, Pilch DS. Pharmacokinetics and *in vivo* antistaphylococcal efficacy of TXY541, a 1-methylpiperidine-4-carboxamide prodrug of PC190723. *Biochem. Pharmacol.* 86, 1699–1707 (2013).

260. Kaul M, Mark L, Zhang Y *et al.* TXA709, an FtsZ-targeting benzamide prodrug with improved pharmacokinetics and enhanced *in vivo* efficacy against methicillin-resistant *Staphylococcus aureus*. *Antimicrob. Agents Chemother.* 59, 4845–4855 (2015).

261. Hu Z, Zhang S, Zhou W, Ma X, Xiang G. Synthesis and antibacterial activity of 3-benzylamide derivatives as FtsZ inhibitors. *Bioorg. Med. Chem. Lett.* 27, 1854–1858 (2017).

262. Kaul M, Mark L, Parhi AK, Lavoie EJ, Pilch DS. Combining the FtsZ-targeting prodrug TXA709 and the cephalosporin cefdinir confers synergy and reduces the frequency of resistance in methicillin-resistant *Staphylococcus aureus*. *Antimicrob. Agents Chemother.* 60(7), 4290–4296 (2016).

263. Lui HK, Gao W, Cheung KC *et al.* Boosting the efficacy of anti-MRSA beta-lactam antibiotics via an easily accessible, non-cytotoxic and orally bioavailable FtsZ inhibitor. *Eur. J. Med. Chem.* 163, 95–115 (2019).

264. Fujita J, Maeda Y, Mizohata E *et al.* Structural flexibility of an inhibitor overcomes drug resistance mutations in *Staphylococcus aureus* FtsZ. *ACS Chem. Biol.* 12(7), 1947–1955 (2017).

265. Sass P, Josten M, Famulla K *et al.* Antibiotic acyldepsipeptides activate ClpP peptidase to degrade the cell division protein FtsZ. *Proc. Natl Acad. Sci. USA* 108, 17474–17479 (2011).

•• **Demonstrates that ADEP-antibiotics activate bacterial ClpP protease to degrade FtsZ, revealing an unprecedented strategy to target FtsZ and bacterial cell division.**

266. Mayer C, Sass P, Brötz-Oesterhelt H. Consequences of dosing and timing on the antibacterial effects of ADEP antibiotics. *Int. J. Med. Microbiol.* 309(7), 151329 (2019).

267. Brötz-Oesterhelt H, Beyer D, Kroll H-P *et al.* Dysregulation of bacterial proteolytic machinery by a new class of antibiotics. *Nat. Med.* 11, 1082–1087 (2005).

268. Lee B-G, Park EY, Lee K-E *et al.* Structures of ClpP in complex with acyldepsipeptide antibiotics reveal its activation mechanism. *Nat. Struct. Mol. Biol.* 17, 471–479 (2010).

269. Li DH, Chung YS, Gloyd M *et al.* Acyldepsipeptide antibiotics induce the formation of a structured axial channel in ClpP: a model for the ClpX/ClpA-bound state of ClpP. *Chem. Biol.* 17(9), 959–969 (2010).

270. Pan S, Malik IT, Thomy D, Henrichfreise B, Sass P. The functional ClpXP protease of *Chlamydia trachomatis* requires distinct *clpP* genes from separate genetic loci. *Sci. Rep.* 9(1), 14129 (2019).

271. Kirstein J, Hoffmann A, Lilie H *et al.* The antibiotic ADEP reprogrammes ClpP, switching it from a regulated to an uncontrolled protease. *EMBO Mol. Med.* 1, 37–49 (2009).

272. Lowth BR, Kirstein-Miles J, Saiyed T *et al.* Substrate recognition and processing by a Walker B mutant of the human mitochondrial AAA+ protein ClpX. *J. Struct. Biol.* 179(2), 193–201 (2012).

273. Famulla K, Sass P, Malik I *et al.* Acyldepsipeptide antibiotics kill mycobacteria by preventing the physiological functions of the ClpP1P2 protease. *Mol. Microbiol.* 101, 194–209 (2016).

274. Gersch M, Famulla K, Dahmen M *et al.* AAA+ chaperones and acyldepsipeptides activate the ClpP protease via conformational control. *Nat. Commun.* 6, 6320 (2015).

275. Malik IT, Brötz-Oesterhelt H. Conformational control of the bacterial Clp protease by natural product antibiotics. *Nat. Prod. Rep.* 34(7), 815–831 (2017).

276. Silber N, Pan S, Schäkermann S *et al.* Cell division protein FtsZ is unfolded for N-terminal degradation by antibiotic-activated ClpP. *mBio*11(3), e01006-20 (2020).

277. Thomy D, Culp E, Adamek M *et al.* The ADEP biosynthetic gene cluster in *Streptomyces hawaiiensis* NRRL 15010 reveals an accessory *clpP* gene as a novel antibiotic resistance factor. *Appl. Environ. Microbiol.* 85(20), e01292-19 (2019)

278. Hinzen B, Raddatz S, Paulsen H *et al.* Medicinal chemistry optimization of acyldepsipeptides of the enopeptin class antibiotics. *ChemMedChem* 1, 689–693 (2006).

279. Carney DW, Schmitz KR, Truong JV, Sauer RT, Sello JK. Restriction of the conformational dynamics of the cyclic acyldepsipeptide antibiotics improves their antibacterial activity. *J. Am. Chem. Soc.* 136(5), 1922–1929 (2014).

280. Goodreid JD, Janetzko J, Santa Maria JP Jr *et al.* Development and characterization of potent cyclic acyldepsipeptide analogues with increased antimicrobial activity. *J. Med. Chem.* 59(2), 624–646 (2016).

281. Griffith EC, Zhao Y, Singh AP *et al.* Ureadepsipeptides as ClpP Activators. *ACS Infect. Dis.* 5(11), 1915–1925 (2019).

282. Brown Gandt A, Griffith EC, Lister IM *et al. In vivo* and *in vitro* effects of a ClpP-activating antibiotic against vancomycin-resistant enterococci. *Antimicrob. Agents Chemother.* 62(8), pii:e00424–18 (2018).

283. Conlon BP, Nakayasu ES, Fleck LE *et al.* Activated ClpP kills persisters and eradicates a chronic biofilm infection. *Nature* 503, 365–370 (2013).

• **Reports on the synergistic activity of ADEP4 with rifampicin, an antibiotic combination that eradicates persisters, stationary and biofilm populations of MRSA *in vitro* and in a deep-seated murine infection.**

284. Gil F, Paredes-Sabja D. Acyldepsipeptide antibiotics as a potential therapeutic agent against *Clostridium difficile* recurrent infections. *Future Microbiol.* 11, 1179–1189 (2016).

285. Ollinger J, O'malley T, Kesicki EA, Odingo J, Parish T. Validation of the essential ClpP protease in *Mycobacterium tuberculosis* as a novel drug target. *J. Bacteriol.* 194(3), 663–668 (2012).

286. Schiefer A, Vollmer J, Lammer C *et al.* The ClpP peptidase of Wolbachia endobacteria is a novel target for drug development against filarial infections. *J. Antimicrob. Chemother.* 68(8), 1790–1800 (2013).

287. Arvanitis M, Li G, Li D-D *et al.* A conformationally constrained cyclic acyldepsipeptide is highly effective in mice infected with methicillin-susceptible and -resistant *Staphylococcus aureus*. *PLoS ONE* 11, e0153912 (2016).

288. Wong KS, Mabanglo MF, Seraphim TV *et al.* Acyldepsipeptide analogs dysregulate human mitochondrial ClpP protease activity and cause apoptotic cell death. *Cell Chem. Biol.* 25, 1017–1030.e1019 (2018).

289. Parti RP, Biswas D, Wang M, Liao M, Dillon JaR. A MinD mutant of enterohemorrhagic *E. coli* O157:H7 has reduced adherence to human epithelial cells. *Microb. Pathog.* 51, 378–383 (2011).

290. Raju RM, Unnikrishnan M, Rubin DH *et al. Mycobacterium tuberculosis* ClpP1 and ClpP2 function together in protein degradation and are required for viability *in vitro* and during infection. *PLoS. Pathog.* 8(2), e1002511 (2012).

6.3 Publication 3

communications biology

ARTICLE

https://doi.org/10.1038/s42003-021-01789-9 OPEN

Progression of the late-stage divisome is unaffected by the depletion of the cytoplasmic FtsZ pool

Nadine Silber [1,2,3], Christian Mayer[1,2,3], Cruz L. Matos de Opitz [1,2] & Peter Sass [1,2]✉

Cell division is a central and essential process in most bacteria, and also due to its complexity and highly coordinated nature, it has emerged as a promising new antibiotic target pathway in recent years. We have previously shown that ADEP antibiotics preferably induce the degradation of the major cell division protein FtsZ, thereby primarily leading to a depletion of the cytoplasmic FtsZ pool that is needed for treadmilling FtsZ rings. To further investigate the physiological consequences of ADEP treatment, we here studied the effect of ADEP on the different stages of the FtsZ ring in rod-shaped bacteria. Our data reveal the disintegration of early FtsZ rings during ADEP treatment in *Bacillus subtilis*, indicating an essential role of the cytoplasmic FtsZ pool and thus FtsZ ring dynamics during initiation and maturation of the divisome. However, progressed FtsZ rings finalized cytokinesis once the septal peptidoglycan synthase PBP2b, a late-stage cell division protein, colocalized at the division site, thus implying that the concentration of the cytoplasmic FtsZ pool and FtsZ ring dynamics are less critical during the late stages of divisome assembly and progression.

[1] Department of Microbial Bioactive Compounds, Interfaculty Institute of Microbiology and Infection Medicine, University of Tübingen, Auf der Morgenstelle, Tübingen, Germany. [2] Cluster of Excellence - Controlling Microbes to Fight Infections, University of Tübingen, Tübingen, Germany. [3] These authors contributed equally: Nadine Silber, Christian Mayer. ✉email: peter.sass@uni-tuebingen.de

Cell division is a vital process in most bacteria and ensures the generation of progeny, usually by yielding equal daughter cells. In rod-shaped bacteria, such as *Bacillus subtilis*, cell division occurs at midcell, driven by FtsZ and orchestrated by a diverse set of proteins together constituting the divisome[1,2]. As the pacemaker of cell division, FtsZ self-polymerizes into protofilaments, which are characterized by additional lateral interactions resulting in higher order polymer assemblies[3], to finally build the FtsZ ring at the future division site. Here, the FtsZ ring acts as the scaffold for other divisome members. During polymerization, the T7 loop of one FtsZ subunit inserts into the GTP binding site of the next subunit, thereby triggering hydrolysis of GTP to GDP and favoring the disassembly of FtsZ protofilaments[4,5]. Hence, there is a constant and rapid exchange of FtsZ subunits between the dynamic FtsZ ring and the cytoplasmic pool of FtsZ[6–8]. As the cell cycle proceeds, the divisome constricts and synthesizes septal peptidoglycan to allow for septum formation and eventually cytokinesis. Consequently, the process of divisome assembly and progression can be separated into different steps, for example, with regard to the attachment of the FtsZ ring to the membrane, the extent of FtsZ ring constriction, or the consecutive arrival of early and late cell division proteins[7,9,10]. Over the last years, principally two mechanisms have been discussed on how the force required for cytokinesis is generated, either by the chemical energy of FtsZ-dependent GTP hydrolysis[11,12], or alternatively by peptidoglycan synthesis[11,13]. Recently, FtsZ treadmilling, the GTP-dependent dynamic exchange of FtsZ from the cytoplasmic pool with the FtsZ ring, has been reported to drive divisome progression and constriction in rod-shaped bacteria[14,15]. In cocci such as *Staphylococcus aureus*, however, cell division mainly occurs in two steps in this context, an initial step involving FtsZ treadmilling and a second step that increasingly depends on peptidoglycan synthesis[16]. In this study, we set out to further investigate the role of the cytoplasmic FtsZ pool and FtsZ ring dynamics on the distinct steps of septum formation in rod-shaped bacteria.

Results and discussion

To examine the effect of the abundance of FtsZ on divisome assembly and progression, we employed antibiotics of the ADEP class as tools to rapidly modulate the cytoplasmic pool of FtsZ in the model organism *B. subtilis*. ADEP deregulates the bacterial caseinolytic protease, activating its dormant core ClpP for the untimely degradation of FtsZ[17,18]. ADEP incubation thus leads to an impressive filamentation phenotype of *B. subtilis* at concentrations close to the minimal inhibitory concentration (MIC)[18,19]. Very recently, we showed that ADEP-ClpP preferably targets the N terminus of monomeric FtsZ, leading to unfolding and degradation of the FtsZ N-terminal domain[20]. Intriguingly, N-terminal degradation was prevented upon nucleotide binding to FtsZ, most probably due to a stabilization of the FtsZ protein fold. Hence, at ADEP concentrations resulting in a filamentation phenotype, ADEP primarily leads to a depletion of the cytoplasmic pool of nucleotide-free FtsZ in the bacterial cell[20], thus reducing the FtsZ concentration below the critical level needed for FtsZ ring formation[21,22] and continuously removing available FtsZ required for FtsZ ring dynamics (Fig. 1a). In line with this, a recent model on cell-size homeostasis in rod-shaped bacteria described a direct correlation of FtsZ expression and accumulation on septal constriction initiation[23]. Therefore, ADEP was considered instrumental to investigate the role of the cytoplasmic FtsZ pool and FtsZ ring dynamics during divisome formation and progression. To do so, we first tested the effect of ADEP on polymerized FtsZ (in the presence of GTP) (Fig. 1b). Once assembled into protofilaments, FtsZ substantially resisted the degradation by ADEP-ClpP. It may thus be hypothesized that, if divisome assembly and constriction fully depend on the cytoplasmic FtsZ pool and FtsZ ring dynamics, ADEP treatment should result in the disintegration of early as well as late-stage divisomes, or at least, the progression of late-stage divisomes should be halted. To test this hypothesis, we conducted time-lapse and super-resolution fluorescence microscopy experiments with ADEP-treated *B. subtilis* strain 2020 using filamentation concentrations of the antibiotic. This strain additionally expresses

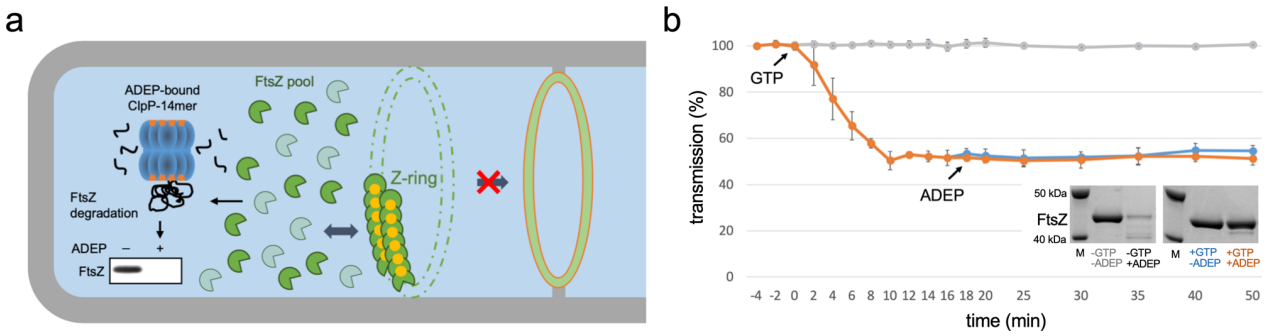

Fig. 1 ADEP antibiotics lead to a reduction of the cytoplasmic FtsZ pool. a Schematic of ADEP-dependent degradation of FtsZ. ADEP (orange) activates bacterial ClpP peptidase (blue) for untimely protein degradation, and nucleotide-free, monomeric FtsZ (dark green) represents a preferred protein substrate for ADEP-ClpP[18,20]. As a consequence, the cytoplasmic FtsZ pool is depleted (indicated by the shift from dark to light green), whereas GTP-bound FtsZ (GTP in yellow) is stabilized against proteolytic attack at antibiotic concentrations close to the MIC. FtsZ ring assembly relies on the dynamic exchange of FtsZ subunits between the FtsZ ring and the cytoplasmic FtsZ pool (indicated by dark blue arrow). In the presence of ADEP, the depletion of the FtsZ pool ultimately results in an inhibition of FtsZ ring formation and cell division, finally leading to bacterial cell death. However, it remained unresolved, whether only early or also later stages of the FtsZ ring/divisome are affected by ADEP treatment. **b** In vitro FtsZ polymerization and FtsZ degradation by ADEP-activated ClpP. Light transmission analysis of GTP-dependent FtsZ polymerization in vitro followed by incubation with a ClpP reaction mixture in the absence or presence of ADEP and/or GTP (−GTP/−ADEP, in gray; +GTP/−ADEP, in blue; +GTP/+ADEP, in orange). Here, polymerized FtsZ is not affected by incubation with ADEP-ClpP. The graphs show mean values of two independent experiments, bottom and top values of indicator bars show the individual data points of each respective replicate. Source data underlying the graphs is presented in Supplementary Table 1. As an independent control, we determined FtsZ protein amounts of samples that were incubated with or without GTP for 120 min in the absence or presence of ADEP. DMSO was used in untreated control reactions. Representative SDS-PAGE images of triplicates are depicted. Source data of the full, uncropped gel image is presented in Supplementary Fig. 4.

FtsZ fused to GFP from an ectopic locus. For microscopy, ADEP-treated bacteria were mounted and then further grown on microscopy slides coated with ADEP-supplemented agarose (approximate division time of bacteria on microscopy slides was 30–45 min). We have previously shown that ADEP leads to a depletion of the FtsZ pool within 15–20 min, i.e., the cellular concentration of FtsZ is reduced by more than half within 5 min of ADEP treatment, whereas biomass increase and metabolism in general remain unaltered[18,20]. Therefore, the elapsed time between the addition of ADEP to the cells and initial image acquisition was set to 15–20 min, ensuring that image acquisition was started under conditions of early FtsZ depletion. By monitoring FtsZ ring formation over time, we observed that ADEP inhibited the initiation of FtsZ ring assembly, and early FtsZ rings that had just been formed disintegrated. Of note, the presence of early FtsZ rings at the beginning of the experiment and their soon disintegration indicate that imaging started just before ADEP effects on FtsZ rings could visually be observed. In contrast to early FtsZ rings, more progressed FtsZ rings were apparently less sensitive to ADEP treatment and thus to a reduction of the cytoplasmic FtsZ pool, since progressed FtsZ rings further constricted and finished septum formation, finally yielding two separated daughter cells (Fig. 2a, b, Supplementary Figs. 1 and 2, Supplementary Movies 1–3).

Following up on this, we investigated whether the arrival of the late-stage cell division protein PBP2b[9], a septal peptidoglycan synthase, would coincide with a successful constriction of progressed FtsZ rings during ADEP treatment. By using *B. subtilis*

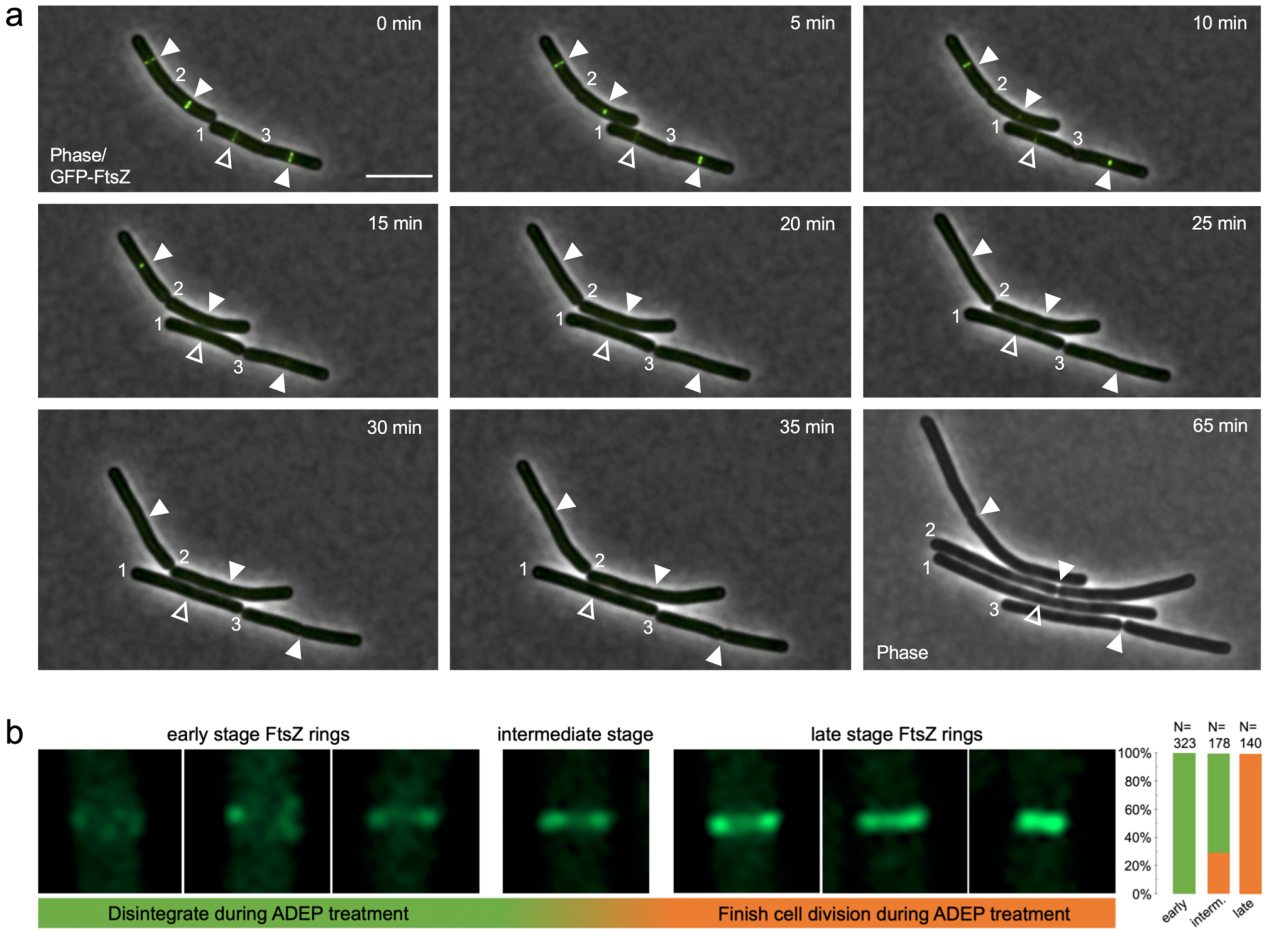

Fig. 2 Depletion of the FtsZ pool differently affects distinct stages of the FtsZ ring. a Time-lapse fluorescence microscopy of exponentially growing *B. subtilis* 2020 cells treated with 0.25 µg/ml ADEP2. Overlaid fluorescence and phase contrast images show the localization of GFP-tagged FtsZ (in green) and the progression of FtsZ rings over time. The micrographs indicate that early FtsZ rings (open triangles) disintegrate during ADEP treatment while more progressed FtsZ rings (closed triangles) constrict and finish septum formation to yield two separated daughter cells. Numbers indicate previously finished septa. For clarity, numbers remain positioned to the corresponding cell pole of the daughter cell on the right. A phase contrast image of bacterial cells after 65 min is included at the end of the series to prove failure or success of septum formation. Overlay (0–35 min) or single channel (65 min) images are provided. Scale bar, 5 µm. Images are representative of at least three biological replicate cultures of *B. subtilis* 2020 with >600 FtsZ rings analyzed over time. A time-lapse video is provided by Supplementary Movie 1. **b** Super-resolution fluorescence microscopy of different stages of FtsZ ring formation in *B. subtilis* 2020. While all of the early-stage FtsZ rings disintegrate upon ADEP treatment (100%, $N = 323$), all late-stage FtsZ rings further constrict and finalize septum formation (100%, $N = 140$). Intermediate-stage FtsZ rings, which were in transition from early to late stages, show a heterogeneous behavior with 71% of FtsZ rings abrogating division and 29% further constricting and finalizing septum formation ($N = 178$). Of note, we deliberately analyzed immediate daughter cells comprising both early and further progressed FtsZ rings, of which all late-stage FtsZ rings finalized division while all early FtsZ rings did not, thus making it unlikely that the cells with late-stage FtsZ rings may by chance happened to have considerably higher FtsZ levels compared to cells with early FtsZ rings. This is further supported by the fact that ADEP leads to a rapid depletion of the FtsZ pool within 15–20 min, where potential minor differences of the FtsZ level may be negligible in relation to the doubling time of the bacteria of ~30–45 min on microscopy slides. Images are representative of at least three biological replicate cultures. Source data underlying the graphs is presented in Supplementary Fig. 5.

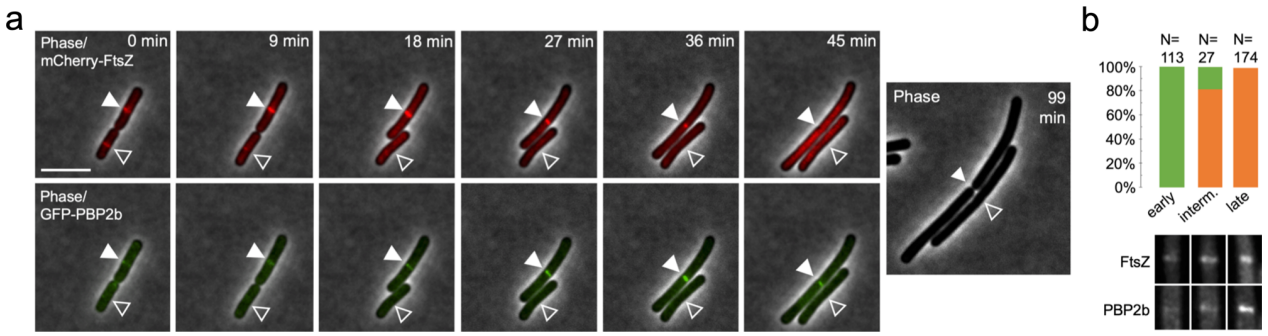

Fig. 3 The late-stage divisome progresses independent of the depletion of the FtsZ pool. a Time-lapse fluorescence microscopy of exponentially growing *B. subtilis* CM03 cells treated with 0.125 µg/ml ADEP2. Overlaid fluorescence and phase contrast images show the localization of mCherry-FtsZ or GFP-PBP2b, as indicated, during ADEP treatment over time. The micrographs show that the divisome succeeds to finalize cell division (closed triangles) in the presence of ADEP in situations when GFP-PBP2b is substantially detected at the septum area. In contrast, early-stage FtsZ rings, prior to the visible arrival of GFP-PBP2b at the septum, disintegrate during ADEP treatment (open triangles). For clarity, a phase contrast image of bacterial cells after 99 min is included at the end of the series to prove failure or success of septum formation. Scale bar, 5 µm. Images are representative of at least three biological replicate cultures of *B. subtilis* CM03 with >300 septa/FtsZ rings monitored over time. A time-lapse video is provided by Supplementary Movie 4. **b** Quantification analysis assessing divisome progression and success of cell division in cells with or without clear foci of PBP2b. In the absence of a substantial signal of GFP-PBP2b at the divisome, early-stage FtsZ rings disintegrate and cells fail to divide upon ADEP treatment (100%, $N = 113$), however, after substantial localization of GFP-PBP2b, the divisome progresses and cells finalize septum formation and division (100%, $N = 174$). In the transition phase of initial GFP-PBP2b localization, cells show a heterogeneous behavior with 18.5% of the divisomes abrogating division and 81.5% further constricting and finalizing division ($N = 27$). Bottom panels show representative fluorescence microscopy images of the different stages corresponding to the graphs in the upper panel. Images are representative of at least three biological replicate cultures of *B. subtilis* CM03. Source data underlying the graphs is presented in Supplementary Fig. 6.

strain CM03, which allows for the concomitant expression of mCherry-FtsZ and GFP-PBP2b, we observed that early FtsZ rings disintegrated prior to the arrival of PBP2b. On the contrary, the divisome consistently finalized cell division after PBP2b had substantially arrived at the septum area (Fig. 3a, b, Supplementary Fig. 3, and Supplementary Movie 4). It may therefore be hypothesized that the arrival or activity of late-stage cell division proteins, such as peptidoglycan synthases, may substantially support or even trigger divisome progression in rod-shaped bacteria similar as previously suggested for coccoid bacteria, such as *S. aureus*[16].

At the same time, Whitley and colleagues published a preprint reporting a related observation regarding the role of FtsZ treadmilling during cell division, however, using the antibiotic PC190723. In contrast to ADEP, PC190723 stabilizes FtsZ bundles and halts FtsZ dynamics instead of depleting FtsZ by fast degradation as occurs in ADEP-treated cells. In line with our observations, FtsZ treadmilling had a dispensable function in accelerating septal constriction rate in their study, while it was critical for assembling and initiating the bacterial divisome[24,25].

In conclusion, our data imply distinct stages during FtsZ ring initiation, maturation, and constriction in rod-shaped bacteria with regard to the role of the cytoplasmic FtsZ pool as well as the sensitivity to ADEP antibiotics. Clearly, during ADEP treatment it is distinguished between early and more progressed divisomes, thereby adding another level of complexity to the elaborate mechanism of ADEP action. Moreover, our data support a two-step model of cell division in *B. subtilis* (Fig. 4), in which the late-stage divisome is substantially less sensitive to a depletion of the cytoplasmic FtsZ pool, and thus less dependent on FtsZ ring dynamics, in contrast to initial assembly and early-stage FtsZ rings.

Methods

Protein purification. FtsZ and ClpP proteins were derived from *B. subtilis* 168 (*trpC2*; wild-type strain; NC_000964.3) and were expressed as C-terminally His_6-tagged proteins in *E. coli* BL21(DE3) harboring the respective expression plasmid[18,20]. Expression cultures were grown in lysogeny broth (LB) containing ampicillin (100 µg/ml) to an optical density at 600 nm (OD_{600}) of 0.6. Then protein expression was induced by the addition of isopropyl-β-D-thiogalactopyranoside (IPTG) to a final concentration of 1 mM. Expression cultures were harvested after 4 h followed by standard protein purification steps under native conditions using Ni-NTA affinity chromatography. Quantity and quality of the purified proteins were verified by Bradford assay (using bovine serum albumin as control), Nanodrop spectrophotometry (Nanodrop Technologies), and SDS-PAGE. We have shown previously that purification-tags have no effect on FtsZ degradation or enzyme activity of both proteins[20].

In vitro FtsZ polymerization and degradation assays. For GTP-dependent polymerization of FtsZ in vitro[26,27], purified *B. subtilis* 168 FtsZ (25 µM) was preincubated in polymerization buffer (50 mM MES/NaOH, pH 6.5, 50 mM KCl, 10 mM $MgCl_2$) for 10 min on ice. After initial incubation for 4 min at 37 °C allowing baseline correction, GTP was added to the respective reaction mixture to a final concentration of 1 mM. Then, reaction mixtures were transferred into a photometer cuvette for monitoring light transmission at 400 nm and 37 °C over time. For in vitro degradation of polymerized FtsZ, 12 µM ADEP2[17,28] (or equal volume of DMSO as a control) and 1.5 µM purified ClpP protein (monomer concentration) were added to the polymerization reaction after 16 min, as indicated, and light transmission was further monitored for 34 min. As an independent control, FtsZ (4 µM) was incubated with 1 mM GTP in activity buffer (50 mM Tris/HCl pH 8, 25 mM $MgCl_2$, 100 mM KCl, 2 mM DTT) at 37 °C for 30 min. Then 1.5 µM ClpP (monomer concentration) and 3.75 µM ADEP (or equal volume of DMSO as a control) were added to the reaction mixtures that were further incubated at 37 °C. Samples were taken after 120 min and were analyzed via SDS-PAGE using standard techniques[18,20].

Cloning strategy. For colocalization studies of FtsZ with PBP2b (mCherry-FtsZ/GFP-PBP2b), strain *B. subtilis* CM03 was constructed as follows. Plasmid pHJCM03 was generated using the coding sequence of *pbpB* that was amplified from chromosomal DNA of *B. subtilis* 168 (*trpC2*; wild-type strain; NC_000964.3) via PCR using the following primers: oCM07 5′-GGAAGCGGCTCAGGCTCCCG GATCCACATTCAAATGCCAAAAAAGAATAAATTTATG-3′, oCM08 5′-CGC GGCCGCTCTAGAACTAGAATTCTTAATCAGGATTTTTAAACTTAACCT TG-3′. The amplicon was then ligated into the linearized plasmid pHJCM01[19] by a Gibson isothermal reaction. The resulting plasmid was transformed into *B. subtilis* CM01 (*trpC2 cat aprE::Pspac-mcherry-ftsZ*)[19] to give strain CM03 (*trpC2 cat aprE::Pspac-mcherry-ftsZ; spc amyE::Pxyl-msfgfp-pbpB*).

Super-resolution and time-lapse fluorescence microscopy. Cells of *B. subtilis* 2020 (*trpC2 spc amyE::Pxyl-gfp-ftsZ*)[29] or *B. subtilis* CM03 (*trpC2 cat aprE::Pspac-mcherry-ftsZ; spc amyE::Pxyl-msfgfp-pbpB*) were grown at 37 °C to early-exponential phase (OD_{600} of 0.1). For the expression of GFP and mCherry fusion

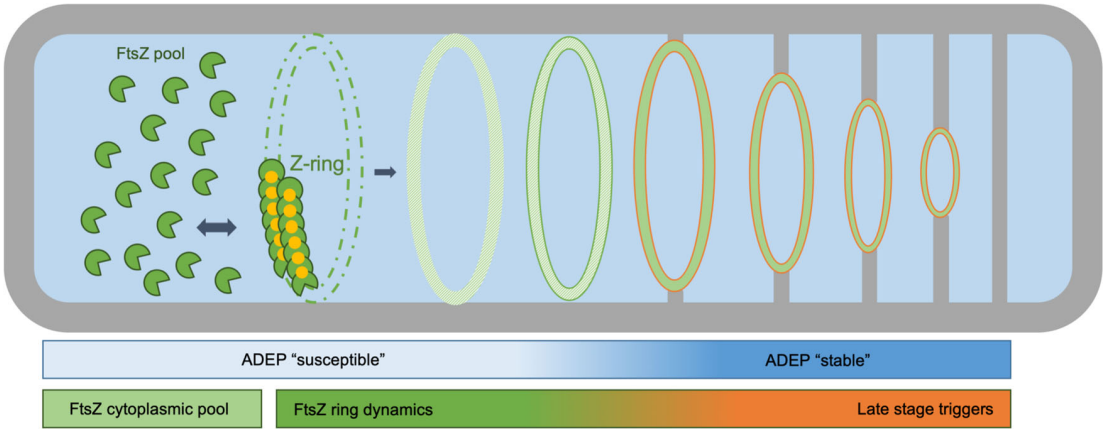

Fig. 4 Two-step model of FtsZ ring assembly and progression. At antibiotic concentrations close to the MIC, ADEP treatment essentially depletes the cytoplasmic pool of FtsZ[20], thereby continuously removing available FtsZ that is needed for FtsZ ring formation and dynamics[14]. Our data reveal that ADEP treatment leads to the disintegration of early FtsZ rings (framed green) in *B. subtilis*, while more progressed FtsZ rings (framed red) resist degradation and finish septum formation as well as daughter cell separation, suggesting distinct stages during FtsZ ring initiation and progression. Therefore, our results support a two-step model of FtsZ ring and divisome progression in *B. subtilis*. In the initial stage, FtsZ ring formation essentially relies on the cytoplasmic FtsZ pool and FtsZ ring dynamics, indicated by the disintegration of early FtsZ rings upon ADEP-dependent depletion of the cytoplasmic FtsZ pool. In the later stage, the more progressed divisome is considerably less sensitive to a depletion of the cytoplasmic FtsZ pool, implying that other triggers take over to drive divisome progression, for example, peptidoglycan synthases that arrive at the divisome during the later stages of cell division.

proteins, *Pxyl* and *Pspac* promoters were induced using 0.1–0.2% xylose and 0.1 mM IPTG, respectively. Then, cells were preincubated in LB supplemented with 0.125–0.25 µg/ml ADEP2 for 10 min or DMSO as a control. Bacteria were transferred onto microscopy slides using gene frames (Life Technologies) and a thin film of 1.5% agarose in 25% LB containing 0.125–0.25 µg/ml ADEP2 as well as according concentrations of the inducer compounds xylose and/or IPTG. Doubling times of bacteria on microscopy slides were in the range of 30–45 min. Phase contrast and fluorescence images were taken at distinct time points as indicated. Elapsed time between sampling and image acquisition was ~5–10 min. Of note, the ADEP2 concentration used here results in filamentation of *B. subtilis*, resembling a phenotype that is due to fast FtsZ degradation, i.e., the cellular amount of FtsZ is reduced by more than half within 5 min once ADEP-ClpP is fully engaged, whereas biomass increase and metabolism in general remain unaltered[18]. Since the addition of ADEP leads to an overall depletion of the FtsZ pool within 15–20 min[18,20], image acquisition was started at the assumed onset of detectable FtsZ pool reduction (correlating to approximately half the bacterial doubling time on microscopy slides), which is further indicated by the presence of early FtsZ rings at the start of imaging as well as their soon disintegration. For image analysis, we deliberately monitored bacterial cells or small cell clusters (i.e., immediate daughter cells) that showed both early as well as late FtsZ rings, thereby ensuring similar conditions of ADEP action on the distinct stages of the FtsZ ring and the divisome in the analyzed bacterial cells. Super-resolution images were recorded using a Zeiss Axio Observer Z1 LSM800 equipped with an Airyscan detector and a C Plan-Apo 63x/1.4 Oil DIC objective (Zeiss, Germany). Images were processed using the ZEN2.3 image analysis software package (Zeiss). Time-lapse micrographs were obtained using a Nikon Eclipse Ti automated microscope equipped with a Perfect Focus system (Nikon Instruments Europe BV, Netherlands), an Orca Flash 4.0 camera (Hamamatsu, Photonics, Japan), and CFI Plan-Apo DM 100x/1.45 Oil Ph3 objective (Nikon). Image acquisition and analysis were performed via the NIS elements AR software package (Nikon).

Statistics and reproducibility. Microscopy and in vitro FtsZ degradation results were each obtained from at least three independent experiments and biological samples. The results describing the effect of in vitro degradation of FtsZ polymers on light transmission (Fig. 1b) are based on two independent experiments. For experiments using samples of small sizes (Fig. 1b, $N = 2$) mean values were calculated and depicted, indicating individual data points via the bottom and top values of the respective indicator bars. For the evaluation of the fate of divisomes (localization of FtsZ and PBP2b) upon ADEP treatment, large numbers of divisomes (>950) from a total of 12 independent biological samples were examined. Total values and percentages are described (Supplementary Figs. 5 and 6).

Reporting Summary. Further information on research design is available in the Nature Research Reporting Summary linked to this article.

Data availability

Additional datasets generated and/or analyzed during the current study are available from the corresponding author on reasonable request.

Received: 21 August 2020; Accepted: 1 February 2021;
Published online: 01 March 2021

References

1. den Blaauwen, T., Hamoen, L. W. & Levin, P. A. The divisome at 25: the road ahead. *Curr. Opin. Microbiol.* **36**, 85–94 (2017).
2. Silber, N., Matos, C., Mayer, C. & Sass, P. Cell division protein FtsZ: from structure and mechanism to antibiotic target. *Fut. Microbiol.* **15**, 801–831 (2020).
3. Sundararajan, K. & Goley, E. D. The intrinsically disordered C-terminal linker of FtsZ regulates protofilament dynamics and superstructure in vitro. *J. Biol. Chem.* **292**, 20509–20527 (2017).
4. Scheffers, D. J., de Wit, J. G., den Blaauwen, T. & Driessen, A. J. GTP hydrolysis of cell division protein FtsZ: evidence that the active site is formed by the association of monomers. *Biochemistry* **41**, 521–529 (2002).
5. Scheffers, D. J. & Driessen, A. J. Immediate GTP hydrolysis upon FtsZ polymerization. *Mol. Microbiol.* **43**, 1517–1521 (2002).
6. Addinall, S. G., Cao, C. & Lutkenhaus, J. Temperature shift experiments with an *ftsZ*84(Ts) strain reveal rapid dynamics of FtsZ localization and indicate that the Z ring is required throughout septation and cannot reoccupy division sites once constriction has initiated. *J. Bacteriol.* **179**, 4277–4284 (1997).
7. Erickson, H. P., Anderson, D. E. & Osawa, M. FtsZ in bacterial cytokinesis: cytoskeleton and force generator all in one. *Microbiol. Mol. Biol. Rev.* **74**, 504–528 (2010).
8. Sun, Q. & Margolin, W. FtsZ dynamics during the division cycle of live *Escherichia coli* cells. *J. Bacteriol.* **180**, 2050–2056 (1998).
9. Gamba, P., Veening, J. W., Saunders, N. J., Hamoen, L. W. & Daniel, R. A. Two-step assembly dynamics of the *Bacillus subtilis* divisome. *J. Bacteriol.* **191**, 4186–4194 (2009).
10. Walker, B. E., Männik, J. & Männik, J. Transient membrane-linked FtsZ assemblies precede Z-Ring formation in *Escherichia coli*. *Curr. Biol.* **30**, 499–508 (2020). e6.
11. Coltharp, C. & Xiao, J. Beyond force generation: why is a dynamic ring of FtsZ polymers essential for bacterial cytokinesis? *Bioessays* **39**, 1–11 (2017).
12. Li, Z., Trimble, M. J., Brun, Y. V. & Jensen, G. J. The structure of FtsZ filaments in vivo suggests a force-generating role in cell division. *EMBO J.* **26**, 4694–4708 (2007).
13. Coltharp, C., Buss, J., Plumer, T. M. & Xiao, J. Defining the rate-limiting processes of bacterial cytokinesis. *Proc. Natl Acad. Sci. USA* **113**, E1044–E1053 (2016).
14. Bisson-Filho, A. W. et al. Treadmilling by FtsZ filaments drives peptidoglycan synthesis and bacterial cell division. *Science* **355**, 739–743 (2017).
15. Yang, X. et al. GTPase activity-coupled treadmilling of the bacterial tubulin FtsZ organizes septal cell wall synthesis. *Science* **355**, 744–747 (2017).
16. Monteiro, J. M. et al. Peptidoglycan synthesis drives an FtsZ-treadmilling-independent step of cytokinesis. *Nature* **554**, 528–532 (2018).

17. Brötz-Oesterhelt, H. et al. Dysregulation of bacterial proteolytic machinery by a new class of antibiotics. *Nat. Med.* **11**, 1082–1087 (2005).
18. Sass, P. et al. Antibiotic acyldepsipeptides activate ClpP peptidase to degrade the cell division protein FtsZ. *Proc. Natl Acad. Sci. USA* **108**, 17474–17479 (2011).
19. Mayer, C., Sass, P. & Brötz-Oesterhelt, H. Consequences of dosing and timing on the antibacterial effects of ADEP antibiotics. *Int. J. Med. Microbiol.* **309**, 151329 (2019).
20. Silber, N. et al. Cell division protein FtsZ is unfolded for N-terminal degradation by antibiotic-activated ClpP. *mBio* **11**, e01006–e01020 (2020).
21. Huecas, S. et al. Energetics and geometry of FtsZ polymers: nucleated self-assembly of single protofilaments. *Biophys. J.* **94**, 1796–1806 (2008).
22. Mukherjee, A. & Lutkenhaus, J. Dynamic assembly of FtsZ regulated by GTP hydrolysis. *EMBO J.* **17**, 462–469 (1998).
23. Si, F. et al. Mechanistic origin of cell-size control and homeostasis in bacteria. *Curr. Biol.* **29**, 1760–1770 (2019). e1767.
24. Whitley, K. D. et al. FtsZ treadmilling is essential for Z-ring condensation and septal constriction initiation in *Bacillus subtilis* cell division. Preprint at *bioRxiv* https://doi.org/10.1101/2020.07.01.182006 (2020).
25. Silber, N., Mayer, C., Matos, C. & Sass, P. Progression of the late-stage divisome is unaffected by the depletion of the cytoplasmic FtsZ pool. Preprint at *bioRxiv* https://doi.org/10.1101/2020.06.30.180018 (2020).
26. Krol, E. & Scheffers, D. J. FtsZ polymerization assays: simple protocols and considerations. *J. Vis. Exp.* **81**, e50844 (2013).
27. Scheffers, D. J., den Blaauwen, T. & Driessen, A. J. Non-hydrolysable GTP-gamma-S stabilizes the FtsZ polymer in a GDP-bound state. *Mol. Microbiol.* **35**, 1211–1219 (2000).
28. Hinzen, B. et al. Medicinal chemistry optimization of acyldepsipeptides of the enopeptin class antibiotics. *ChemMedChem.* **1**, 689–693 (2006).
29. Stokes, N. R. et al. Novel inhibitors of bacterial cytokinesis identified by a cell-based antibiotic screening assay. *J. Biol. Chem.* **280**, 39709–39715 (2005).

Acknowledgements

We thank Heike Brötz-Oesterhelt for providing ADEP2, as well as Leendert Hamoen, Jeff Errington and Kürşad Turgay for the kind gift of strains and plasmids. We also thank Anne Berscheid for critically reading and discussing the manuscript. The authors appreciate funding by the Deutsche Forschungsgemeinschaft (DFG, German Research Foundation): Project-ID 398967434 (TRR 261-A02), the German Center for Infection Research (DZIF; TTU 09.815), as well as support by infrastructural funding from the Cluster of Excellence EXC 2124 Controlling Microbes to Fight Infections. We further acknowledge support by the Open Access Publishing Fund of the University of Tübingen.

Author contributions

N.S., C.M., C.L.M.d.O., and P.S. designed and performed experiments, analyzed data, and prepared figures. P.S. conceived and supervised the study, wrote the manuscript, and raised funding. All authors discussed data and edited the manuscript.

Competing interests

The authors declare no competing interests.

Additional information

Supplementary information The online version contains supplementary material available at https://doi.org/10.1038/s42003-021-01789-9.

Correspondence and requests for materials should be addressed to P.S.

Reprints and permission information is available at http://www.nature.com/reprints

Publisher's note Springer Nature remains neutral with regard to jurisdictional claims in published maps and institutional affiliations.

6.3.1 Supplemental information

Supplementary information

Progression of the late-stage divisome is unaffected by the depletion of the cytoplasmic FtsZ pool

Nadine Silber[1,2§], Christian Mayer[1,2§], Cruz L Matos de Opitz[1,2], Peter Sass[1,2]*

[1]Department of Microbial Bioactive Compounds, Interfaculty Institute of Microbiology and Infection Medicine, University of Tübingen, Auf der Morgenstelle 28, 72076 Tübingen, Germany

[2]Cluster of Excellence - Controlling Microbes to Fight Infections, University of Tübingen, Germany

[§] These authors contributed equally

[*]Correspondence should be addressed to Peter Sass (peter.sass@uni-tuebingen.de)

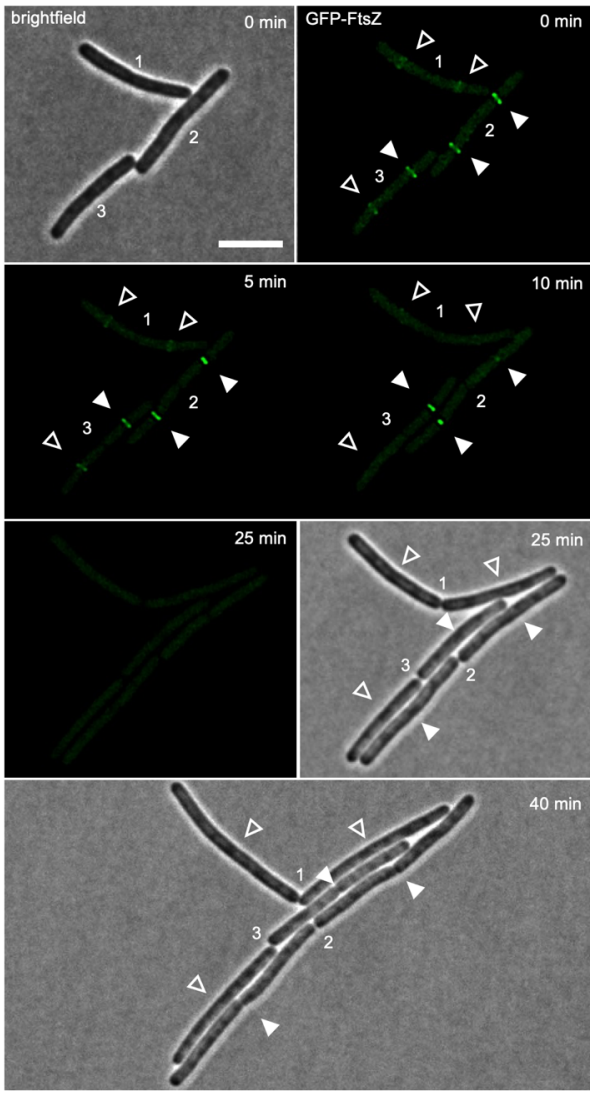

Supplementary Fig. 1:

ADEP-treatment leads to the disintegration of early, but not late stage FtsZ rings.

Super-resolution fluorescence microscopy of exponentially growing *B. subtilis* 2020 cells treated with 0.25 µg/ml ADEP2. Fluorescence images show the localization of GFP-tagged FtsZ and the progression of FtsZ rings (in green) over time. During ADEP treatment, early FtsZ rings disintegrate (open triangles), while mature FtsZ rings finish septum formation (closed triangles). Numbers indicate already finished, but undivided septa. Scale bar, 5 µm. Images are representative of at least three biological replicate cultures.

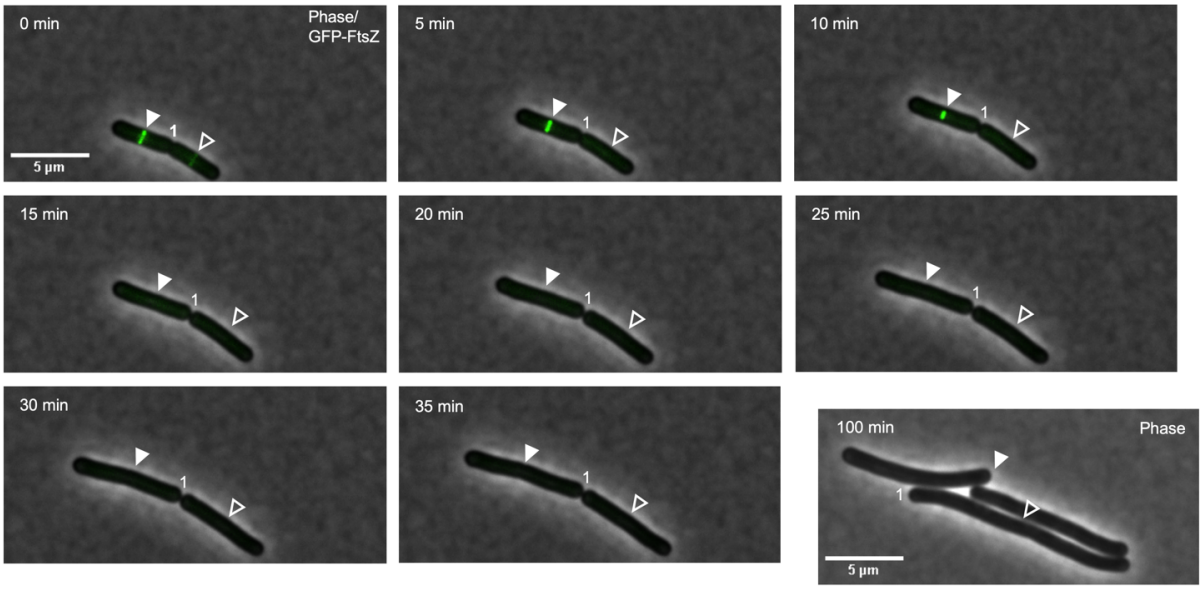

Supplementary Fig. 2:

Effect of ADEP treatment on FtsZ ring formation in *B. subtilis* cells visualized by time-lapse fluorescence microscopy.

Exponentially growing *B. subtilis* 2020 cells were treated with 0.25 µg/ml ADEP2 and FtsZ ring formation was followed over time. Micrographs show overlays of phase contrast images (greyscale) and GFP fluorescence images (green) indicating FtsZ ring formation at mid-cell. ADEP-treated cells show disintegration of early FtsZ rings (open triangles) while progressed FtsZ rings constrict and finalize septum formation to yield two separated daughter cells (closed triangles). Numbers indicate already finished, but undivided septa. For clarity, numbers remain positioned to the corresponding cell pole of the daughter cell on the right. An additional phase contrast image was acquired after prolonged incubation with ADEP (last image in the series) indicating failure or success of septum formation. Scale bars, 5 µm. Images are representative of at least three biological replicate cultures of *B. subtilis* with >600 FtsZ rings analyzed over time.

A time-lapse video of the image sequence is provided by Supplementary Movie 2.

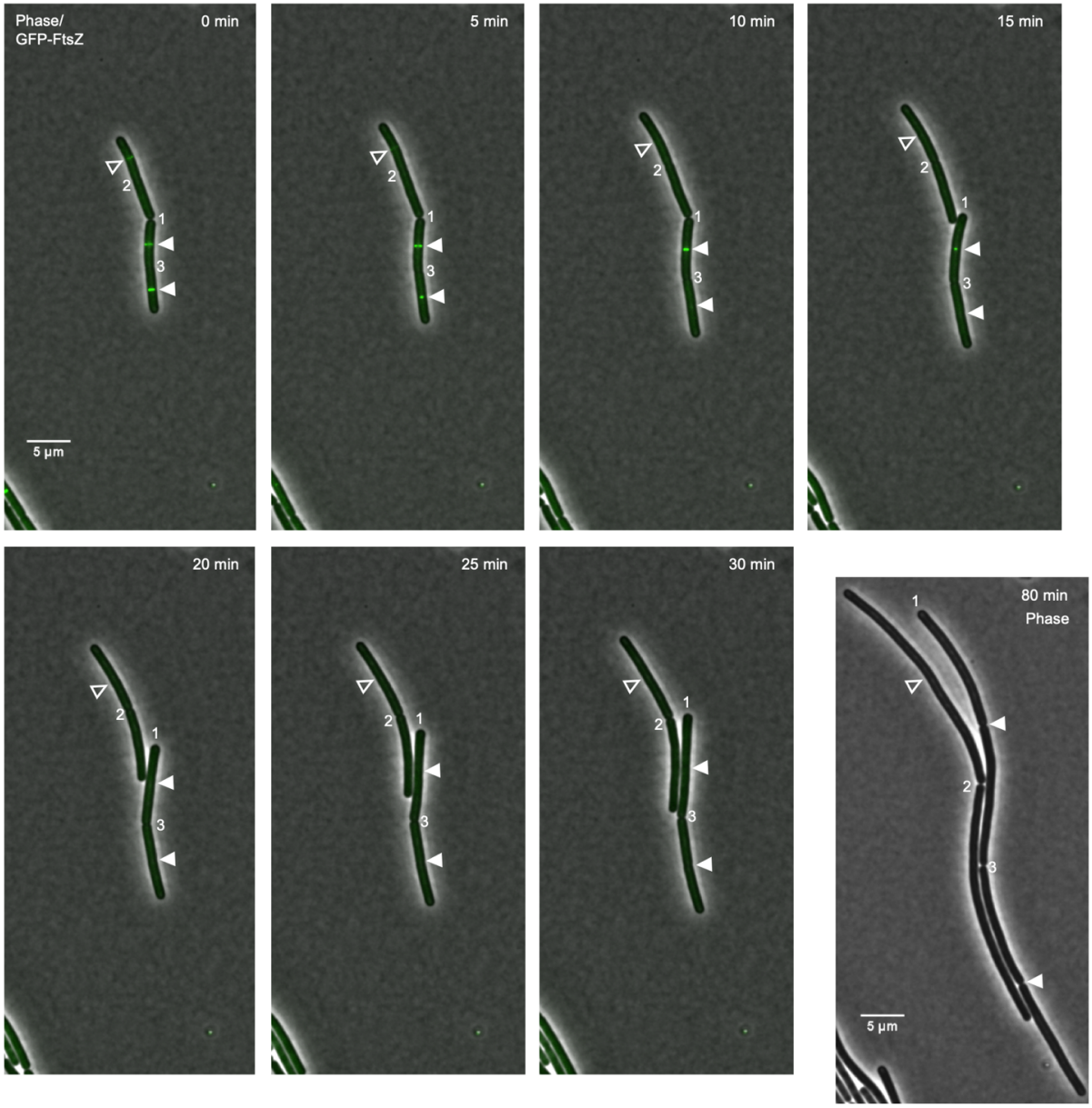

Supplementary Fig. 2 continued:

Effect of ADEP treatment on FtsZ ring formation in *B. subtilis* cells visualized by time-lapse fluorescence microscopy.

A time-lapse video of the image sequence is provided by Supplementary Movie 3.

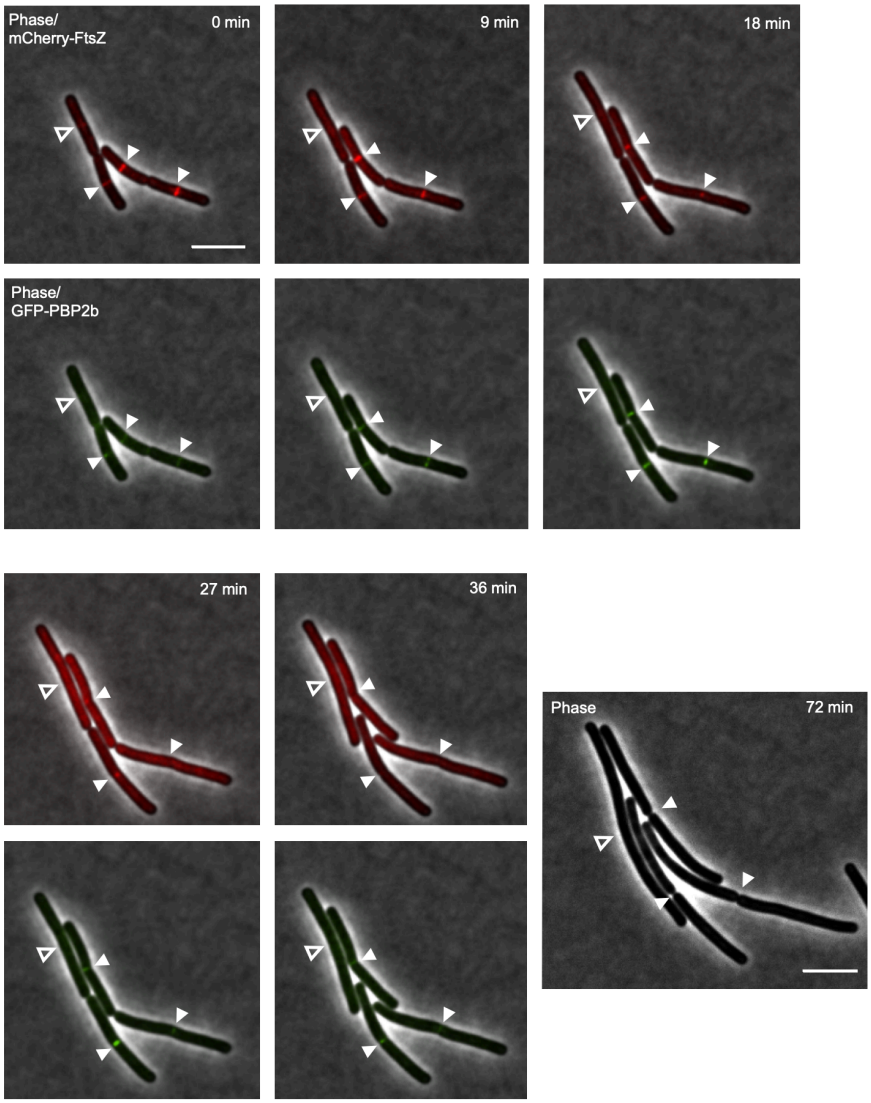

Supplementary Fig. 3:

Colocalization of mCherry-FtsZ and GFP-PBP2b during ADEP treatment of *B. subtilis* cells visualized by time-lapse fluorescence microscopy.

Overlaid fluorescence and phase contrast images are shown. During ADEP treatment (0.125 µg/ml ADEP2), early FtsZ rings disintegrate (open triangles), while mature FtsZ rings finish septum formation once PBP2b has substantially arrived at the septum (closed triangles). A phase contrast image of bacterial cells after 72 min is included at the end of the series to prove failure or success of septum formation. Scale bars, 5 µm. Images are representative of at least three biological replicate cultures of *B. subtilis* CM03 with >300 FtsZ rings analyzed over time.

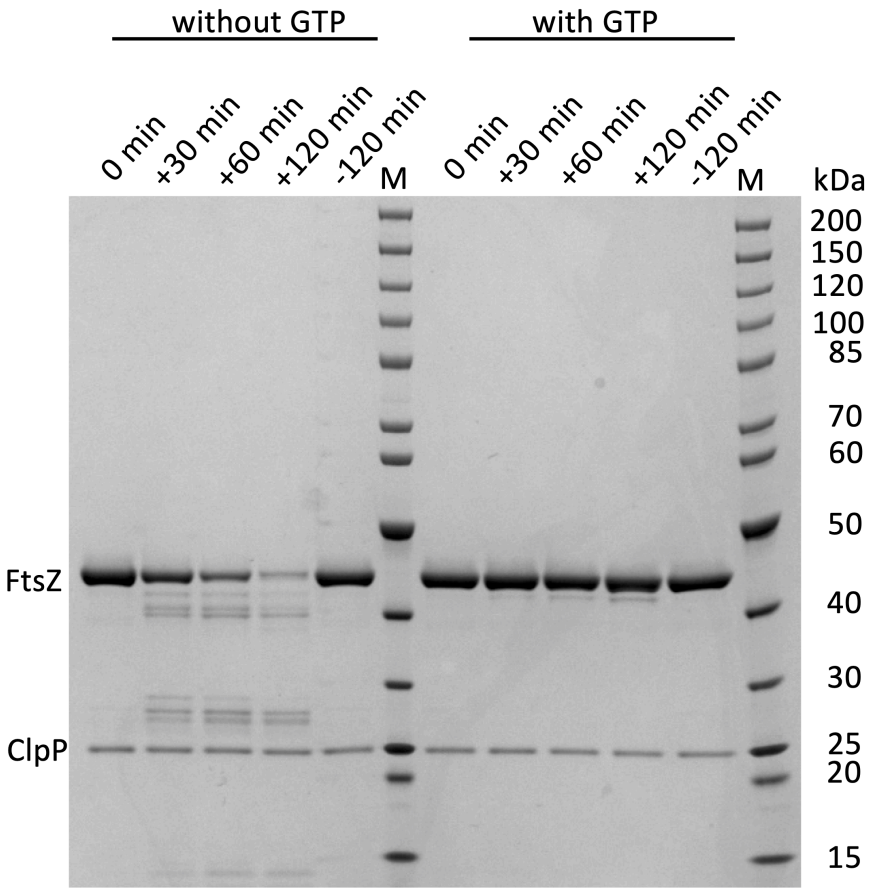

Supplementary Fig. 4:

Source data of the full, uncropped gel image according to Fig. 1b.

-, no ADEP; +, plus ADEP; M, molecular marker.

	early Z-rings		intermediate Z-rings		late Z-rings	
	disintegration	constriction	disintegration	constriction	disintegration	constriction
experiment 1	87	0	33	12	0	51
experiment 2	39	0	22	10	0	10
experiment 3	123	0	57	15	0	58
experiment 4	74	0	14	15	0	21
sum	323	0	126	52	0	140
sum (total)	**323**		**178**		**140**	
[%]	100	0	71	29	0	100

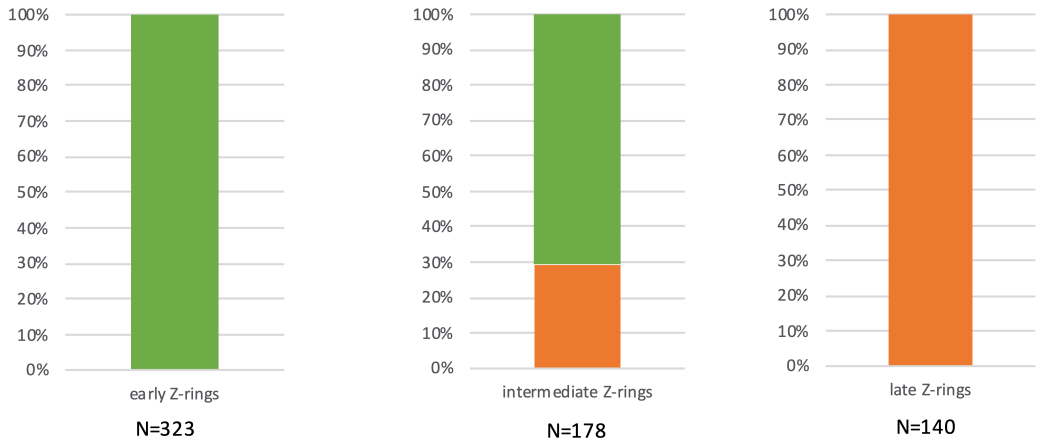

Supplementary Fig. 5:

Source data underlying the graphs in Fig. 2b showing the distribution of either success or failure of FtsZ ring/divisome progression among the cells counted.

	early Z-rings (no/weak PBP2b)		intermediate Z-rings (weak, but clear PBP2b)		late Z-rings (clear PBP2b signal)	
	disintegration	constriction	disintegration	constriction	disintegration	constriction
experiment 1	4	0	1	7	0	65
experiment 2	39	0	3	13	0	42
experiment 3	11	0	0	2	0	11
experiment 4	2	0	0	0	0	44
experiment 5	0	0	1	0	0	12
experiment 6	1	0	n.e.	n.e.	n.e.	n.e.
experiment 7	8	0	n.e.	n.e.	n.e.	n.e.
experiment 8	48	0	n.e.	n.e.	n.e.	n.e.
sum	113	0	5	22	0	174
sum (total)	**113**		**27**		**174**	
[%]	100	0	18.5	81.5	0	100

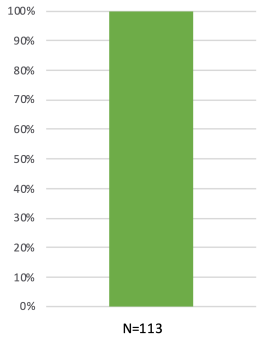

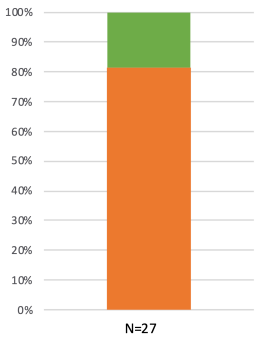

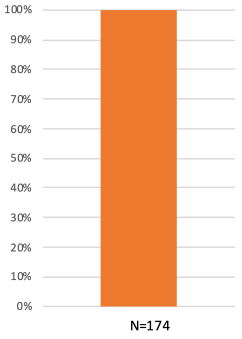

Supplementary Fig. 6:

Source data underlying the graphs in Fig. 3b showing the distribution of either success or failure of FtsZ ring/divisome progression among the cells counted. n.e., not evaluated.

Supplementary Table 1

Source data underlying the graphs of *in vitro* FtsZ polymerization according to Fig. 1b.

	no GTP, no ADEP			plus GTP, no ADEP			plus GTP, plus ADEP		
time (min)	replicate 1 (transmission %)	replicate 2 (transmission %)	mean (transmission %)	replicate 1 (transmission %)	replicate 2 (transmission %)	mean (transmission %)	replicate 1 (transmission %)	replicate 2 (transmission %)	mean (transmission %)
-4	100.0	100.0	100.0	100.0	100.0	100.0	100.0	100.0	100.0
-2	102.3	99.2	100.8	102.3	99.2	100.8	102.3	99.2	100.8
0	101.7	99.2	100.5	101.7*	98.1*	99.9	101.7*	98.1*	99.9
2	102.2	99.2	100.7	100.6	82.9	91.8	100.6	82.9	91.8
4	101.0	99.5	100.3	86.1	68	77.1	86.1	68	77.1
6	101.4	99.4	100.4	71.5	59.4	65.5	71.5	59.4	65.5
8	102.3	99.7	101.0	59.9	55.8	57.9	59.9	55.8	57.9
10	102.1	99.1	100.6	46.4	54.3	50.4	46.4	54.3	50.4
12	102.2	99.0	100.6	51.4	54.3	52.9	51.4	54.3	52.9
14	102.7	99.0	100.9	49.8	54.5	52.2	49.8	54.5	52.2
16	101.6	97.7	99.7	48.2	54.9	51.6	48.2	54.9	51.6
18	102.8	99.1	101.0	51	55.6	53.3	50.4**	52.8**	51.6
20	103.3	99.4	101.4	49.4	55.4	52.4	49.2	52.9	51.1
25	100.8	99.4	100.1	47.7	55.1	51.4	48	52.6	50.3
30	100.7	98.0	99.4	49.3	54.1	51.7	47.1	54.2	50.7
35	100.9	99.2	100.1	48.7	55.9	52.3	48.4	55.7	52.1
40	100.3	99.3	99.8	51.8	57.8	54.8	49.9	54.3	52.1
50	101.3	99.9	100.6	52.2	56.9	54.6	48.4	53.9	51.2

*addition of GTP, **addition of ADEP

Acknowledgements

An dieser Stelle möchte ich mich zuerst bedanken bei Herrn Dr. Peter Sass,
die Betreuung während meiner Masterarbeit und Promotion hast du gemeistert wie ein Ass!
Vielen Dank für das Überlassen des wohl besten Projektes weltweit
und auch für die stets gesicherte Finanzierung während meiner gesamten Zeit!
Danke für Diskussionen unter vier Augen, und den Austausch von Gedanken,
auch für das Korrekturlesen meiner Arbeit möchte ich mich bei dir bedanken.
Unterstützt hast du mich nicht nur in wissenschaftlicher Hinsicht,
du hast definitiv weit mehr getan als nur deine „Pflicht“!

Ebenso gilt mein Dank Prof. Dr. Heike Brötz-Oesterhelt an dieser Stelle,
für die Aufnahme in die Gruppe sowie die andauernde Sicherung der Finanzierungsquelle.
Danke für verschiedenste Feiern, AG-Ausflüge und den Retreat an den Bodensee,
auch die Cocktails an Weihnachtsfeiern waren eine herausragende Idee!
Prof. Dr. Friedrich Götz möchte ich für das Zweitgutachten meinen Dank ausdrücken,
das Bier ab vier mit deiner Gruppe am Freitag hab ich stets genossen mit Entzücken!

Ein großer Dank geht raus an die gesamte HBO Gruppe,
wie im Flug verging meine Promotion mit euch cooler Truppe!
Beim Raven mit lauter Musik im Labor hatten wir oft Spaß,
eine Richtig coole Zeit mit euch allen, das wars!

Doch der größte Dank geht wohl an die weltbeste Kollegin die man sich vorstellen kann.
Bei dem Gedanken, dass du nicht da gewesen wärst, liebe Dhana, wird mir ganz bang!
Mit dir wurden lange und anstrengende Tage im Labor zum Vergnügen -
und auch außerhalb der Arbeit hab ich die Zeit genossen auf verschiedensten Ausflügen.
Ob Urlaub mit dem Prinzen-Bruder oder Themenabende für verschiedener Länder,
du bist und bleibst eine meiner besten Freundinnen und ein Glückgefühlspender

Lieber Stefan, mich hats doch auch überrascht muss ich gestehen,
aber es hat sich herausgestellt, dass wir uns am Ende des Tages doch ganz gut verstehen.
Viele verrückte Diskussionen und auch Aktivitäten sind in meiner Erinnerung gespeichert.
Danke dir, du hast den Laboralltag und auch mein Leben in jeglicher Hinsicht bereichert!

Ein großer Dank geht an Katha und Daniel - meine Wanderfreunde und Leidensgenossen,
während unserer Promotionszeit sind nicht nur Tränen sondern auch Alkohol geflossen!
Ich freu mich darauf noch viele Berggipfeln mit euch zu besteigen,
natürlich mit Wassermelone - das sind Erinnerungen die werden für immer bleiben!
Besonders dir, liebe Katha, möchte ich danken aus tiefster Seele,
wenn ich an deine lieben und motivierenden Worte denke, schnürt es mir zu die Kehle.

Liebe Cruz auch dir möchte ich danken von Herzen,
die Zeit im Büro mit dir war immer schön und es gab stets was zu scherzen.
Mit dir zu arbeiten war immer entspannt und du warst stets hilfsbereit,
ganz romantisch durften wir dann auch noch Paris erkunden zu zweit…

Auch meine Studien-Girls-Gang gilt es hier zu nennen.
Inga, Cori und Alice ihr seid einmalige Spitze und ich bin so froh euch zu kennen!
Danke für Exkursionen, Ausflüge, Reisen und dass ihr immer für mich da gewesen seid,
ich freu mich auf alles was noch kommt – mit euch wird’s auf jeden Fall eine gute Zeit!

Auch außerhalb der Uni möchte ich so mancher Person meinen Dank entgegenbringen,
gern würd dich an dieser Stelle auch ein bisschen singen.
Yassine und Pauli, die Corona-Zeit hätt ich nicht überstanden ohne euch zwei,
es war eine schöne Zeit mit Workouts aber auch der ein oder anderen Fast-Food Leckerei.
Meinen neuen Mitbewohnern in der Vogtshaldenstr. danke ich für die Aufnahme ins Haus,
für eure offene und herzliche Art bekommt ihr von mir einen großen Applaus!

Lieber Nico, dir möchte ich danken, dass du da warst an diesem Abend,
als ich nur noch da saß jammernd und klagend.
Danke für die seelische Unterstützung und die Hilfe beim Formatieren -
LaTeX und Linux damit kann ich mich nur blamieren!

Außerdem möchte ich mich bei meinem Lacrosse-Team bedanken,
durch Training und Spieltage konnte ich Dampf ablassen und Akkus auftanken!
Liebe Birka, dir gilt mein Dank für Online-Working-Sessions in den letzten eineinhalb Jahren.
Ich hoffe wir können uns unsere Freundschaft und den Kontakt bewahren!

Lieber Markus, dir möchte ich danken für gute Gespräche und geile Pistentage.
Das Ghetto-Workout fehlt mir – frag mal meine Pralinentäschchen oder die Waage!

Bedanken möchte ich mich auch bei meine Freundinnen Erti und Nata aus Schulzeiten,
ich hab euch unglaublich lieb mit all euren Spinnereien und vor allem den verrückten Seiten!
Na ge schau her Erti, hier dank I dir für all die Urlaube, Abenteuer und Ausflüg‘
Ohne di wär i wohl nie zum Profisurfer gworden – des is fei koi Lüg!

Nicht zu vergessen ist, dass meinen Eltern ein besonderer Dank gilt an dieser Position,
Ihr habt mir das alles ermöglicht, mich stets unterstützt und wart da in jeder Situation.
Aber besonders meine Mama und Gerd waren stets für mich da!
Dem lieben Gerd hab ich vermutlich gekostet das letzte Haar!
Meinem großen Bruder Fabi danke ich für seine Unterstützung und Liebe
Du bist großartig und einzigartig - es wär schlimm wenn ich das hier verschwiege!